

Collective dynamics of dislocations

Citation for published version (APA):

Kooiman, M. (2015). *Collective dynamics of dislocations*. [Phd Thesis 1 (Research TU/e / Graduation TU/e), Mechanical Engineering]. Technische Universiteit Eindhoven.

Document status and date:

Published: 10/12/2015

Document Version:

Publisher's PDF, also known as Version of Record (includes final page, issue and volume numbers)

Please check the document version of this publication:

- A submitted manuscript is the version of the article upon submission and before peer-review. There can be important differences between the submitted version and the official published version of record. People interested in the research are advised to contact the author for the final version of the publication, or visit the DOI to the publisher's website.
- The final author version and the galley proof are versions of the publication after peer review.
- The final published version features the final layout of the paper including the volume, issue and page numbers.

[Link to publication](#)

General rights

Copyright and moral rights for the publications made accessible in the public portal are retained by the authors and/or other copyright owners and it is a condition of accessing publications that users recognise and abide by the legal requirements associated with these rights.

- Users may download and print one copy of any publication from the public portal for the purpose of private study or research.
- You may not further distribute the material or use it for any profit-making activity or commercial gain
- You may freely distribute the URL identifying the publication in the public portal.

If the publication is distributed under the terms of Article 25fa of the Dutch Copyright Act, indicated by the "Taverne" license above, please follow below link for the End User Agreement:

www.tue.nl/taverne

Take down policy

If you believe that this document breaches copyright please contact us at:

openaccess@tue.nl

providing details and we will investigate your claim.

Collective Dynamics of Dislocations



Marleen Kooiman



Collective Dynamics of Dislocations

Collective Dynamics of Dislocations
by Marleen Kooiman
Technische Universiteit Eindhoven, 2015 – Proefschrift.

A catalogue record is available from the Eindhoven University of Technology Library.
ISBN: 978-90-386-3977-2

Typeset by the author with the L^AT_EX documentation system.
Cover design: Marleen Kooiman, Roos van Swigchem en Wanno van Swigchem
Printed by: Ipskamp Drukkers

This work is part of the NWO Complexity programme, project CorFlux (nr. 10012310), which is financed by the Netherlands Organisation for Scientific Research (NWO).



© Copyright, 2015, Marleen Kooiman. All rights reserved.

Collective Dynamics of Dislocations

PROEFSCHRIFT

ter verkrijging van de graad van doctor aan de Technische
Universiteit Eindhoven, op gezag van de rector magnificus
prof.dr.ir. F.P.T. Baaijens, voor een commissie aangewezen door
het College voor Promoties, in het openbaar te verdedigen op
donderdag 10 december 2015 om 16:00 uur

door

Marleen Kooiman

geboren te Amsterdam

Dit proefschrift is goedgekeurd door de promotoren en de samenstelling van de promotiecommissie is als volgt:

voorzitter: prof.dr. L.P.H. de Goey
1^e promotor: prof.dr.ir. M.G.D. Geers
copromotor(en): dr.sc.nat. M. Hütter
leden: univ.-prof.dr.rer.nat. B. Svendsen (RWTH Aachen)
prof.dr. H.C. Öttinger (ETH Zurich)
prof.dr. M.A. Peletier
prof.dr.ir. P.P.A.M. van der Schoot (UU)
prof.dr. A. El-Azab (Purdue University)

Het onderzoek of ontwerp dat in dit proefschrift wordt beschreven is uitgevoerd in overeenstemming met de TU/e Gedragscode Wetenschapsbeoefening.

Contents

Summary	iii
1 Introduction	1
2 Collective behaviour of dislocations in a finite medium	7
3 Microscopically derived free energy of dislocations	33
4 Free energy of dislocations in a multi-slip geometry	65
5 Effective mobility of dislocations from systematic coarse-graining	73
6 Viscoplastic flow rule for dislocation-mediated plasticity from systematic coarse-graining	91
7 Conclusions and discussion	107
A Details about calculations in Chap. 2	115
B Details about calculations in Chap. 3	131
C Details about calculations in Chap. 5	137
D Details about calculations in Chap. 6	143
E Details about the complete set of evolution equations	147
Bibliography	149
Samenvatting voor algemeen publiek	158
Dankwoord	163
Curriculum Vitae	164

Summary

Collective Dynamics of Dislocations

The main carriers of plastic flow in metallic materials are dislocations, i.e. line-like defects in the crystal structure. Metals can contain up to 10^6 meters of dislocation lines per cubic millimeter. Therefore, the collective dynamical behavior of dislocation line segments is key in understanding the deformation behavior of metals.

For the dynamics of individual dislocations, it has been proven that linear response models work well in a realistic regime of parameters. In contrast, the viscoplastic flow rule in phenomenological, macroscopic models for crystal plasticity, which are based on the dynamics of dislocations, have a strongly non-linear stress-dependence. The central hypothesis of this thesis is:

“The collective, coarse-grained dynamics of dislocations reveals emergent phenomena that dominate the macroscopic system response. ”

To assess this hypothesis, systematic coarse-graining was applied to the dynamics of a model system of straight and parallel dislocations to obtain the dynamics of macroscopic density profiles of these dislocations under mechanical load. To this end, the framework of the General Equation for the Non-Equilibrium Reversible-Irreversible Coupling (GENERIC) was employed, together with its systematic coarse-graining procedure, based on statistical mechanics and projection-operator techniques.

To study the static behavior of the system, the free energy of the system was derived. The free energy is a functional of the dislocation density profile for each Burgers vector separately, of the mechanical load applied at the boundary, and of the configurational temperature. A finite system-size and the presence of glide planes have been accounted for. First, the grand-canonical partition function for this system is derived using an integral over all possible dislocation configurations and a path-integral over all possible strain fields. Then, a general expression was derived for the free energy by means of Legendre transformation. The free energy consists of a mean-field elastic contribution, a statistical contribution, and a many-body contribution that accounts for the screening of dislocation interactions. Moreover, an explicit expression was derived for the special cases of single- and multiple slip systems with edge dislocations.

Subsequently, evolution equations for the dislocation density profiles have been derived, following the GENERIC framework for the systematic coarse-graining. A two-temperature description was used to distinguish between the environmental temperature of the lattice and the configurational temperature that governs the distribution of dislocations. It was obtained that the transport of dislocations is not driven by the derivative of the previously obtained free energy, but by a modification thereof, such that diffusion of dislocations is governed by the environmental temperature, rather than by the configurational temperature. Moreover, an expression was obtained for the effective transport coefficient at the

macroscopic level in terms of correlations of the fluctuations in the dislocation velocity.

The dependence of both the driving force and the effective, macroscopic transport coefficient on the applied mechanical load were investigated using simplified Discrete Dislocation Dynamics simulations. The resulting macroscopic dislocation flux depends non-linearly on the applied mechanical load, which supports phenomenological flow rules currently used in Crystal Plasticity models.

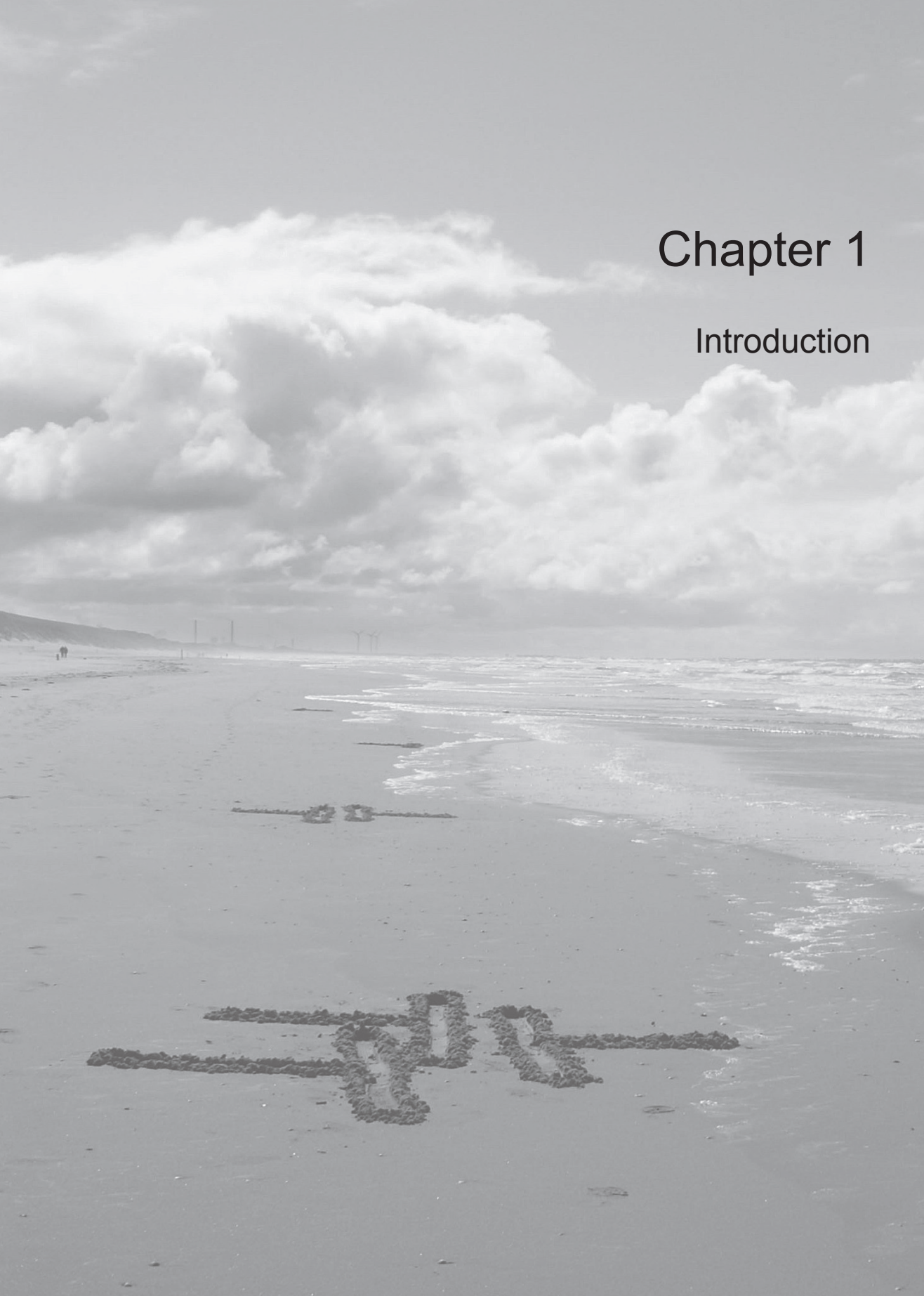
The overall conclusions of the thesis for a model system of straight and parallel dislocations are the following:

- The driving force for dislocation dynamics has, besides a long-range mean field contribution, a many-body contribution that depends on the total density of dislocations per slip plane. The latter implies that the system cannot be described by quantities based on the net dislocation content only, as was previously anticipated. For the many-body contribution, an explicit expression was obtained using a Local Density Approximation. Moreover, diffusion of dislocations is negligible compared to the other transport processes.
- The emergent contribution to the macroscopic transport coefficient is dominant over other contributions, and is load-dependent.
- The resulting macroscopic relation between applied mechanical load and dislocation flux is clearly non-linear. As the relation between applied mechanical load and dislocation velocity at the microscopic level is assumed to be linear, this thus constitutes an emergent phenomenon.

It is expected that also for more realistic dislocation models, emergent behavior dominates the dynamics of dislocation density profiles.

Chapter 1

Introduction



1.1 Background and motivation

Already back in 1943, it was proposed by Orowan, Polanyi and Taylor [55] that the main cause of plastic deformation in crystalline materials, such as metals, is caused by the dynamics of line-like defects in the crystal structure, i.e. dislocations.

Well-annealed metals contain about ten meters of dislocation line per cubic millimeter, while heavily cold-rolled metals can contain up to thousand kilometers of dislocation line in the same volume. The amount of dislocations can thus vary over several orders of magnitude, but is in any case large in realistic volumes.

Defects, such as dislocations, distort the lattice and thereby introduce stresses in the material. Yet, dislocations also move due to stresses in the material and influence each other via the varying stress field in the material. The stress field due to a dislocation segment only decays over long distances. Consequently, a single dislocation segment is influenced by the applied boundary conditions and by all other dislocation segments in the material. The strong and long-range interactions and the large amount of dislocations together imply that the plastic response of metals is determined by the collective behavior of dislocations, rather than by the dynamics of single, isolated dislocations. However, computer simulations of the dynamics of realistic amounts of dislocations are unfeasible because of the long-range nature of the interaction. The subject of this thesis is therefore the derivation of the collective dynamics of dislocations by means of systematic coarse-graining. This derivation might also explain the discrepancy in literature between the dynamics of individual dislocations and their collective behavior. Namely, the velocity of individual dislocations is generally assumed to be linearly proportional to the applied load, while the plastic flow at the macroscopic level depends on the applied load in a strongly non-linear manner.

Systematic coarse-graining techniques for dynamics have been applied to fluids, for example to obtain the viscosity of complex fluids, but only to a limited extent to solids under mechanical load, e.g. [56, 57]. They have been applied to (solid) glassy systems, but the dynamics of these systems on the smallest scale is not well-known. On the contrary, the dynamics of individual dislocations in metals is quite well-described in literature. The coarse-graining of dislocation dynamics could therefore be an ideal test case for applying these coarse-graining techniques to solids.

1.2 Hypothesis

The hypothesis in this thesis is that due to the strong and long-range interactions between dislocations, new phenomena emerge when the collective dynamics of large amounts of dislocations is considered. It is expected that the characteristic properties of the collective dynamics of dislocations are not equal to the properties of the dynamics of individual dislocations, and are therefore to be considered as emergent properties.

The central hypothesis of the thesis therefore reads:

“The collective, coarse-grained dynamics of dislocations reveals emergent phenomena that dominate the macroscopic system response. ”

1.3 Current approaches in literature

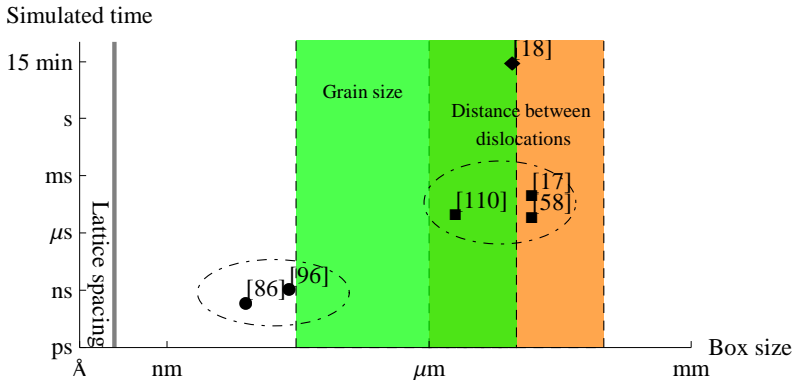


Figure 1.1: Overview of the different scales used in mechanical simulations. Circles are MD-simulations, squares are DDD-simulations and the rhombus is a mechanical test on single crystal ferrite experiment.

A vast amount of research has been done on the dynamics of dislocations and on dynamical coarse-graining. Here the results are summarized from literature on

- models at different scales capturing the mechanical properties of dislocations;
- 2D Coulomb particles, for which dislocations are a representative case;
- mathematical upscaling techniques applied to dislocations;
- dynamical coarse graining.

The mechanical properties of dislocations have been investigated on several length scales, see Fig. 1.1. The smallest length scale is considered in Molecular Dynamics (MD) simulations of the metal atoms in the crystal structure [86, 96]. These studies indicate that for edge dislocations in Aluminium and Nickel for realistic strain rates, the relation between dislocation velocity and applied mechanical load is nearly linear. The typical box size considered in these studies is 5 – 10 nm with fs timesteps.

A slightly larger scale is addressed when dislocations are considered as discrete line defects in a continuous elastic material. The motion of the dislocations is described by a linear drag law, and the Peach-Koehler force on dislocations results from both the externally applied load and the mutual interaction between dislocations. Using these evolution equations, simulations have been performed within the framework of Discrete Dislocation Dynamics (DDD), see e.g. [110]. For simplicity, these dislocations are sometimes assumed to be straight and parallel. DDD simulations have for example been used to study fatigue crack propagation [17] and the role of dislocations in hydrogen embrittlement of aluminium [58]. The typical box size considered in these simulations is around 10 μm with ns timesteps.

To obtain the evolution equations for the dislocation density from the dynamics of discrete dislocations, the BBGKY-hierarchy of equations with different closures on the two- or three-body-density [32, 120, 34, 73, 16], and several variational approaches [35, 36] have been proposed. Both approaches yield a linear relation between dislocation flux and applied mechanical load. To describe the randomness in the system, both approaches need a 'configurational' temperature to describe the dislocation distribution. This temperature is not equal to the temperature of the environment, as the environmental temperature is very low compared to the typical energy scale in the system, and hence it would hardly have any influence.

At the engineering scale, phenomenological evolution equations for the dislocation density have been developed. In the work of Gurtin [40, 43], a thermodynamically consistent higher-order gradient theory of crystal plasticity was derived from the principle of virtual power, supplemented by constitutive equations for the dislocation flow. The plastic flow in these models is either rate-independent, or it depends on the applied load in a strongly non-linear manner, usually such that the material is hardly rate-dependent. These formulations have been extended to account for grain boundaries as well [109]. Moreover, in the work of El-Azab [20], kinetic equations for the evolution of the dislocation density have been derived, which includes dislocation transport and reaction and multiplication of dislocations. However, an explicit flow rule for the dislocations was not further specified in this model.

Dislocations have been studied extensively in the context of the Kosterlitz-Thouless phase transition and the sine-Gordon model [63, 81, 82, 104], where straight and long dislocations can be considered as an example of two-dimensional Coulomb particles. This transition predicts the unbinding of dislocation pairs above the critical temperature, and hence explains dislocation-mediated melting of crystals. In the works of Mizushima [78], Ninomiya [84], Yamamoto [118] and Burakovskiy [11], this research has been extended to account for 3D effects, i.e. the core energy, the effect of the dislocation network and the non-overlapping condition for dislocations.

The disadvantage of these studies in a mechanical context is that the influence of externally applied loading and boundary conditions is not examined, and that the focus is on the behavior around the critical (melting) temperature. Moreover, the anisotropic nature of the interaction between edge dislocations is not accounted for.

Mathematicians have studied the behavior of large amounts of dislocations to investigate the relation between discrete and continuum descriptions of the system. The mathematical difficulties arise from the peculiar, non-convex interactions between dislocations. For instance, dislocation walls are considered, as these have shown to be a prototype for understanding the influence of the discrete nature of dislocations [98].

Techniques like Γ -convergence [99, 29, 112] and asymptotic analysis [45, 46, 47] have been used to study the structure of dislocation pile-ups against impenetrable objects in the limit of a large number of dislocations. These results have been extended to the evolution equations of dislocations [111], the next-order corrections to the minimizers [27], and the organization of dislocations in two dimensions [28].

The drawback of these works is that they all are performed in the absence of thermal noise, and that in several cases, strong assumptions are made on the arrangement of dislocations.

Collective dynamical behavior has been derived for other systems. The most well-known example of this are the Green-Kubo relations [66], which relate time-correlations of fluctuations in currents to transport coefficients close to equilibrium. These relations have for example been used to calculate the viscosity of liquids and gasses, see e.g. [52, 53, 103]. The Green-Kubo relations reflect that irreversibility is an emergent property that arises not only from averaging over phase space, but also from correlations in the fluctuating dynamical process.

Collective dynamics can be derived from the microscopic evolution equations in a more systematic manner within the framework of the General Equations for the Non-Equilibrium Reversible-Irreversible Coupling (GENERIC), see e.g. [31, 89, 88]. Within this framework, the dynamics is split additively into a reversible and an irreversible contribution. Subsequently, these two contributions can both be split multiplicatively in a derivative of a thermodynamic potential (energy or entropy) times a matrix that relates these derivatives to fluxes. The four ingredients on the fine level, two thermodynamic potentials and two matrices, can then be systematically coarse-grained to obtain the collective dynamics at the coarse level. The relation between the two levels of description is established by projection operators and non-equilibrium statistical mechanics. The coarse-graining is not only an average over phase space, but also entails a transition in timescale.

Dynamical coarse-graining within the GENERIC-framework has not been applied to solids, apart from some considerations on polymers [56, 57]. An extension of this framework to solids poses a challenge, as there is a strong influence of the boundary conditions, and the role and nature of fluctuations in the system is not clear.

1.4 Scope of the thesis

The approach followed in this thesis is to investigate the collective dynamics of dislocations by deriving them through the GENERIC framework, in order to identify the collective effects. Attention is restricted to a simplified model of straight and parallel dislocations that are not created or annihilated. DDD simulations have shown that simulations of such a system yield reliable results. Moreover, it is expected that if emergent phenomena are important for the collective dynamics of straight and parallel dislocations, that they are also important for more realistic dislocation systems.

The fine scale description of the system considered coincides with the setup used in DDD simulations, i.e. where dislocations are treated as discrete objects embedded in a continuous linear elastic material. The coarse scale is characterized by a dislocation density profile in the same elastic material. As in the BBGKY approaches, a configurational temperature is used to describe the, usually disordered, dislocation distribution. Moreover, the temperature of the environment is used to describe the thermodynamic state of the elastic material.

Dislocation systems are in general far from equilibrium. More specifically, these systems can be under strong applied mechanical loads, and the dislocation distribution is usually not in thermal equilibrium with the environmental temperature. Namely, the energy associated with thermal fluctuations in the lattice is very small compared to the interaction energy of the dislocations, which implies that dislocations should occur in a rather ordered

state. However, dislocations are usually distributed quite randomly, which corresponds to a high temperature associated with the dislocation configuration. Hence, the dislocation distribution is “frozen in” at this high configurational temperature, which is different from the environmental temperature.

As the system is far from equilibrium, it is beneficial to use the GENERIC framework, as GENERIC is not restricted to close-to-equilibrium systems, and the coarse-graining can be done in a systematic manner without a priori assumptions on the role of fluctuations.

statics	Chapter 2	Grand-canonical partition function
	Chapter 3	Canonical free energy and the Local Density Approximation (LDA) for a single slip system
	Chapter 4	LDA for multiple slip systems
dynamics	Chapter 5	Macroscopic evolution equations
	Chapter 6	Stress-dependence of the effective, macroscopic mobility

Table 1.1: Outline of the thesis

The thesis starts with a discussion of the thermodynamic potentials of the system in Chap. 2 to 4, as their derivatives act as driving forces for the dynamics in the system. In Chap. 2, the focus is on the derivation of the grand-canonical partition function for a given local chemical potential of the dislocations, configurational temperature and deformation of the boundary. An approximation is made that only holds far away from the critical temperature. The new and innovative aspects of this work are that aspects that have shown to be important for the mechanical response, such as a finite domain and applied mechanical load, have been incorporated in the partition function.

Subsequently, the free energy is derived in Chap. 3 by performing a Legendre transform of the grand-canonical partition function obtained in Chap. 2. This yields an implicit expression for the free energy of the dislocation density profile at a given configurational temperature and boundary deformation. This expression is made explicit by means of a local density approximation for edge dislocations on a single slip system in this chapter, and for edge dislocations on multiple slip systems in Chap. 4.

In Chap. 5, the thesis continues with a derivation of the collective dynamics. The resulting evolution equation for the density is written as a driving force times an emergent transport coefficient. The driving force can be split in the derivative of the configurational free energy of the dislocation density profile at the configurational temperature, and a correction that accounts for the difference between configurational and environmental temperature. Note that for the former, the result of Chap. 2 to 4 can be used.

In Chap. 6, the emergent transport coefficient is studied by determining correlations of fluctuations in DDD simulations. In this chapter, focus is put on the dependence of the mobility on the applied mechanical load.

Finally, in Chap. 7 the results of the different chapters are summarized into a single set of evolution equations. Subsequently, the main conclusions are drawn and recommendations for further research are given.

Chapter 2

Collective behaviour of dislocations in a finite medium

Largely reproduced from: Kooiman, M., Hütter, M., and Geers, M.G.D.,
Collective behaviour of dislocations in a finite medium. *Journal of Sta-
tistical Mechanics Theory and Experiment*, P04028, 2014



Abstract

We derive the grand-canonical partition function of straight and parallel dislocation lines without making a priori assumptions on the temperature regime. Such a systematic derivation for dislocations has, to our knowledge, not been carried out before, and several conflicting assumptions on the free energy of dislocations have been made in the literature. Dislocations have gained interest as they are the carriers of plastic deformation in crystalline materials and solid polymers, and they constitute a prototype system for two-dimensional Coulomb particles. Our microscopic starting level is the description of dislocations as used in the Discrete Dislocation Dynamics (DDD) framework. The macroscopic level of interest is characterized by the temperature, the boundary deformation and the dislocation density profile. By integrating over state space, we obtain a field theoretic partition function, which is a functional integral of the Boltzmann weight over an auxiliary field. The Hamiltonian consists of a term quadratic in the field and an exponential of this field. The partition function is strongly non-local, and reduces in special cases to the sine-Gordon model. Moreover, we determine implicit expressions for the response functions and the dominant scaling regime for metals, namely the low temperature regime.

2.1 Introduction

Dislocations are lines along which there is a mismatch in crystal structure, see e.g. [55]. A dislocation can be represented by a discontinuity in the distortion field of the lattice. Dislocations have attracted a lot of research interest in the context of mechanical engineering and as a toy model in theoretical physics.

In mechanical engineering, dislocations are considered to be important for the underlying mechanism of plastic deformation of metals. Under sufficient applied stress, dislocations move, which causes plastic deformation. Often, focus is on straight and parallel dislocations. Several approaches have been used to study the emergent behaviour of many dislocations, as discussed in the following.

First, dislocations have been studied numerically within the framework of Discrete Dislocation Dynamics (DDD) [110]. In this framework, dislocations are considered as discontinuities in the displacement field. For a finite volume with given boundary conditions that contains discrete dislocations, the displacement field is calculated numerically by means of a superposition method. From the displacement, the stress and the resulting Peach-Koehler force on the dislocations are calculated. Together with constitutive rules for the motion, creation and annihilation of dislocations, this gives evolution equations for the dislocations. Within this framework, important engineering phenomena, such as fatigue loading and the effect of boundaries can be studied [17, 2, 67, 68]. Furthermore, these calculations serve as a reference for many enriched continuum models [74, 119].

Second, the BBGKY hierarchy of equations is applied to dislocations [32]. This hierarchy relates the n body density to the $n + 1$ body density. This hierarchy can be closed by an assumption for the $n + 1$ body density in terms of the n body density. In [32, 120, 73], the mean-field-, the Kirkwood and the Bogliubov closure were proposed for the two and three body correlations. In the long range, the resulting pair correlations seem to match the pair correlation that is obtained numerically by DDD calculations. However, the short range correlations are not checked in the numerical simulations. Besides that, the values of the fitting parameters indicate a low temperature regime, in which the approximations used are invalid. Furthermore, the two-body density has also been calculated numerically within DDD, see e.g. [113]. This study indicates the arrangement of dislocations in small, charge-neutral pairs, which indicates that short range correlations are important.

Third, strain gradient plasticity models were developed to describe dislocation mediated plasticity phenomenologically, [24, 25, 6, 7]. In these models, the dislocation density is directly related to gradients in the plastic strain. The evolution of dislocation density profiles, and hence of strain gradients, is determined by the force on the dislocations. The latter can either be calculated directly from the stress in the material [6], or from the derivative of the free energy of dislocation density profiles [42].

In theoretical physics, dislocations are used as a toy model, as straight and parallel dislocations are a prototype system of two dimensional (2D) particles with Coulomb interaction. It was shown by Kosterlitz and Thouless and later by Nelson and Halperin [63, 81, 82] that two dimensional crystals melt via the unbinding of dislocation pairs. At low temperature, dislocations occur in pairs, and do not respond individually to the applied load. At high temperature, the dislocations are free, and respond even to infinitesimally small loads. Most calculations on 2D Coulomb-type particles were done in infinite space. Moreover, only the isotropic, logarithmic part of the dislocation interaction was taken into account

and the anisotropic part was neglected.

Despite all these efforts, there is no crystal plasticity model available that is obtained by systematic coarse-graining from the rich microscopic description of discrete dislocations to a macroscopic level. In this chapter, we calculate the partition function of parallel and straight dislocations in a finite, three dimensional volume in the grand-canonical ensemble. External mechanical loads were applied at the boundary of the system, as typically done in DDD [110]. No a priori assumptions on the magnitude of the coupling parameters are made.

Multiple slip systems were considered here. The treatment of multiple slip geometries has proven to be problematic in the literature, while multiple slip is important in a realistic description of crystal structures, see e.g. [24]. However, in the work presented here, multiple slip systems could be incorporated in a systematic way.

In this contribution, the framework of equilibrium statistical mechanics is employed. Within equilibrium statistical mechanics, microstates are summed in an ensemble of fixed temperature, pressure and number of particles to obtain the partition function. However, this set of macroscopic control variables can be extended to describe inhomogeneous dislocation density profiles under applied boundary loading. A similar procedure is also applied in classical DFT [23]. In this procedure, while the set of control variables is extended, the subsequent counting of states that are commensurate with these control parameters leads in the usual way to a partition function, see e.g. [31][89].

The system is here considered at a finite temperature, although it was realized in the literature that the physical temperature of dislocations in metals at room temperature is generally very low. The rationale behind this is that the behaviour of the system at zero temperature is a special case of the behaviour at finite temperature, and could thus also be obtained from an analysis at finite temperature. This issue is further addressed in the discussion.

As straight and parallel dislocations are part of a wider class of problems of particles in two dimensions with vector charges and as we make no assumptions on the temperature regime, methods and results of this contribution can likely be extended to similar systems, such as defects in two dimensional crystals [93] and dislocations in colloidal crystals [100, 48].

The chapter is organized as follows. In Sec. 4.3, a general expression for the partition function is derived by systematic coarse-graining. The result is interpreted in Sec. 2.3. In Sec. 2.4, approximations are used to obtain explicit expressions for the response functions of the system in a special case. In Sec. 6.4, the results and limitations are discussed, and an outlook on future work is given.

2.2 Derivation of the free energy expression

In this section, the grand-canonical partition function is derived. The main steps of this derivation are listed in table 2.1. The coordinate system is introduced in Fig. ??.

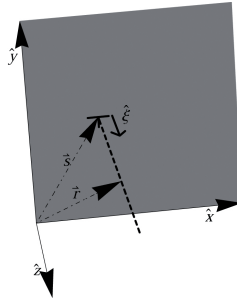


Figure 2.1: The coordinate system used in this chapter. The line direction $\hat{\xi}$ is parallel to the \hat{z} -direction. The vector \mathbf{r} is used to indicate positions in three dimensional space, the vector \mathbf{s} is used to indicate the position in the plane perpendicular to the line-direction $\hat{\xi} = \hat{z}$. The vector \mathbf{r} can thus be written as $\mathbf{r} = \mathbf{s} + z\hat{\xi}$.

Main steps in the calculation	Conceptual origin	Section
Use of the grand-canonical ensemble with local chemical potential	DFT	2.2.1
Loading via an imposed deformation, applied at the boundary	DDD	2.2.2
Discrete dislocations embedded in a continuous distortion field	DDD	2.2.2
Restriction to distortion fields that match the imposed incompatibility using a delta functional		2.2.2
Thermodynamic relation between stiffness and free energy derivative	Thermodynamics	2.3.2
Computational techniques		
Source term for the distortion field	Field Theory	2.2.4
Fourier representation of the delta functional	[60]	2.2.4
Gaussian path integral over the distortion field	Field Theory	2.2.4
Integration over dislocation positions	[83]	2.2.4
Definition of discrete glide plane density		2.2.4
Shift of the potential to separate external loading and interaction effects	DFT-inspired	2.2.4
Rescaling of variables to obtain coupling parameters		2.3

Table 2.1: Main steps of the derivation of the partition function

2.2.1 Microscopic description of the system

In this study, long, straight and parallel dislocations are considered, that are embedded in an elastic continuum with volume Ω . Dislocations are characterized by their line orientation vector $\hat{\xi}$ and Burgers vector \mathbf{b} , the latter describing the closure fault vector in the crystal lattice. As the dislocations are parallel, the line orientation vector $\hat{\xi}$ is equal

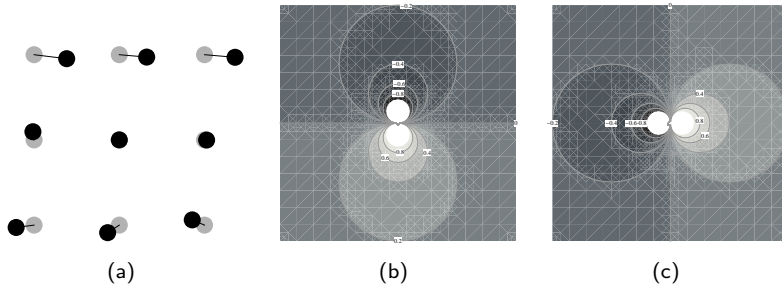


Figure 2.2: In Fig. 2.2(a) the local distortion of the lattice is depicted. The grey dots are the equilibrium positions of the atoms with respect to the central atom, and the black dots are the real positions. From such a detailed picture, the local value of the distortion field can be calculated. This picture is a representation of the distortion field at the particle level, whereas in the rest of the chapter, the distortion field is a function of space.

In Figs. 2.2(b) and 2.2(c), the (x, z) and (y, z) -components of the equilibrium distortion field around a screw dislocation are depicted, see Eq. (2.3). In the white circles, the values are very large (positive or negative), which indicates that the field is singular at the origin. In these pictures, only the equilibrium distortion field is depicted, whereas in the sequel of the chapter, all distortion fields are taken into account, as long as they have a singularity at the origin that matches the incompatibility imposed by the dislocation.

for all dislocations. On the contrary, the Burgers vector is not necessarily the same for all dislocations. Dislocations with equal Burgers vectors can be considered as dislocations of the same species, in close analogy to chemical species.

In this study, we only consider the motion of dislocations on their glide plane. The orientation of these planes is specific for the species of dislocations. As dislocations thus stay at the glide plane on which they nucleate, e.g. through Frank-Read sources on that plane, there is only a discrete set of glide planes $\{j_s\}$ associated with each species s on which dislocations of that species can occur.

For each species s and each glide plane j_s of that species, there are N_{sj_s} dislocations on this plane. In the derivation presented here, it is convenient to define the Nye tensor $\hat{\alpha}(s)$, as defined in [85], and the density profile $\hat{\omega}_s(s)$ of dislocations of species s as field variables that are defined for every position in space. Defining the dislocation density as a field variable was also done in for example [34]. The fields $\hat{\alpha}(s)$ and $\hat{\omega}_s(s)$ are defined as

$$\hat{\alpha}(s) = \sum_{s \in \text{species}} \sum_{j_s \in \text{glide planes}} \sum_{k=1}^{N_{sj_s}} \hat{\xi} \hat{\mathbf{b}}_s \delta^{(2)}(s - s_k) \equiv \sum_{s \in \text{species}} \hat{\xi} \hat{\mathbf{b}}_s \hat{\omega}_s(s), \quad (2.1)$$

where the position vector s is used for the position in the 2D plane perpendicular to the line direction $\hat{\xi}$. Note that the Nye tensor and the dislocation density can just have non-zero values on the glide planes. Hence, the macroscopic partition function will depend on the positions of the glide planes. However, the positions of the glide planes are considered as material constants here. Therefore, the dependency on the glide plane positions is not indicated explicitly.

Besides through dislocation positions, the microscopic state of the system is characterized by the elastic distortion $\mathbf{\Delta}$ in the continuum. This distortion results from the local deviation of the particle positions from the equilibrium lattice, and hence it can be seen as the derivative of the displacement from the equilibrium lattice in the immediate neighbourhood.

Only distortion fields that match the incompatibility imposed by the dislocations in the material in every point should be allowed. An example of such a field is shown in Figs. 2.2(b) and 2.2(c). Distortion fields that match the incompatibility imposed by the dislocations satisfy, see e.g. [64],

$$\nabla \wedge \mathbf{\Delta} = \hat{\boldsymbol{\alpha}}, \quad (2.2)$$

where $\mathbf{v} \wedge \mathbf{A}$ is the cross product of vector \mathbf{v} and second rank tensor \mathbf{A} on the first index, i.e. $(\mathbf{v} \wedge \mathbf{A})_{ij} = \epsilon_{ikl} v_k A_{lj}$. Note that as the field $\hat{\boldsymbol{\alpha}}$ is a collection of delta peaks, see Eq. (2.1), that $\nabla \wedge \mathbf{\Delta}$ is singular at points where there is a dislocation present, and has to vanish elsewhere.

As Eq. (2.2) is linear in both $\mathbf{\Delta}$ and $\hat{\boldsymbol{\alpha}}$, the distortion field due to many dislocations is simply the superposition of the distortion fields of the individual dislocations. The distortion field that satisfies mechanical equilibrium and that corresponds to a single screw dislocation in the origin with line direction vector $\hat{\boldsymbol{\xi}} = \hat{\mathbf{z}}$ and Burgers vector $\mathbf{b} = b\hat{\mathbf{z}}$ is (see e.g. [55])

$$\mathbf{\Delta}(\mathbf{r}) = \frac{b}{2\pi} \begin{pmatrix} 0 & 0 & \frac{-r_y}{r_x^2 + r_y^2} \\ 0 & 0 & \frac{r_x}{r_x^2 + r_y^2} \\ 0 & 0 & 0 \end{pmatrix}. \quad (2.3)$$

Mechanical loading of the system is also considered, as mechanical loads influence the distribution of dislocations. In this chapter, the focus is on boundary loads rather than volumetric loading, which is more relevant in practice. Only displacement controlled loading is considered here for convenience. To incorporate the loading, the space of allowed elastic distortion field is restricted to those fields that match the imposed elastic distortion along the boundary resulting from the loading. These are the fields that satisfy

$$\hat{\mathbf{n}} \wedge \mathbf{\Delta} = (\hat{\mathbf{n}} \times \nabla) \mathbf{u}_b \quad \text{on the boundary}, \quad (2.4)$$

where $\hat{\mathbf{n}}$ is the boundary normal and \times is the cross product between two vectors. Note that \mathbf{u}_b is the displacement of the boundary, and hence this is a variable that is only defined on the boundary and not in the bulk. Therefore, only the surface derivative is well-defined and can be used to impose the loading. As $(\hat{\mathbf{n}} \times \nabla)$ is used, the components of the derivative parallel to the surface normal do not appear in the above equation, and hence the RHS is well-defined.

Note that $(\hat{\mathbf{n}} \times \nabla) \mathbf{u}_b = \hat{\mathbf{n}} \wedge (\nabla \mathbf{u}_b)$, and hence that in Eq. (2.4) the transversal components of the distortion $\mathbf{\Delta}$ have to be equal to the transversal components of the imposed distortion $\nabla \mathbf{u}_b$. However, $\nabla \mathbf{u}_b$ is only well-defined for an \mathbf{u}_b that is also defined in the bulk, whereas Eq. (2.4) only involves surface derivatives, $\hat{\mathbf{n}} \times \nabla$. Therefore, Eq. (2.4) is not equivalent to $\mathbf{\Delta} = \nabla \mathbf{u}_b$.

The boundary conditions in Eq. (2.4) put a constraint on the overall net dislocation

content of the system. Thus, to describe systems with a net dislocation content, the boundary deformation \mathbf{u}_b should have jumps.

Elasticity problems are usually solved in terms of the displacement field, rather than the distortion field. For elasticity problems without dislocations, the displacement field is a natural variable, as the incompatibility Eq. (2.2) reduces to $\nabla \wedge \Delta = 0$, which is automatically satisfied for $\Delta = \nabla \mathbf{u}$. For elasticity with dislocations, a system description with distortion fields may be more convenient. Within DDD, even the elasticity problem with dislocations is written in terms of the displacement as well. However, since the RHS of the incompatibility Eq. (2.2) is non-zero, one should either use displacement fields with branch cuts (see [49] and Eq. (3.10) and (3.47) therein), or define a total, compatible distortion that can be split into an elastic and a plastic part. The choice for both the branch cuts and the plastic distortion are not unique, as these are not measurable quantities. This arbitrariness is circumvented here by using only the elastic distortion field itself as a variable, rather than the displacement.

To conclude, the microstate is characterized by the position of all dislocations and the distortion field in which they are embedded. The latter should match the incompatibility imposed by the discrete dislocations and the boundary deformation, see Eq. (2.2) and (2.4), respectively.

The energy of a microstate is the elastic strain energy

$$E_{\text{elas}} = \frac{1}{2} \int_{\Omega} d^3 \mathbf{r} \Delta^s(\mathbf{r}) : \mathbb{C} : \Delta^s(\mathbf{r}), \quad (2.5)$$

where \mathbb{C} is the stiffness tensor and the superscript “s” stands for the symmetric part of the tensor. Within the linear elastic regime, the stiffness tensor relates the stress to the distortion, and is therefore a measurable quantity. Here, we make the choice not to use a stiffness tensor that is symmetric in the last two indices. The advantage is that the tensor \mathbb{C} is invertible in this case. The disadvantage is that we should take into account the symmetrization of Δ into account explicitly.

As we will integrate over all elastic distortion fields that match the incompatibility due to the dislocations, lattice vibrations around the energy minimum are taken into account as well. Namely, the most likely distortion field Δ is the field that minimizes the energy under the incompatibility constraint. As shown in A.1, this corresponds to the mechanical equilibrium solution. However, distortion fields with thermal fluctuations around the minimum are considered as well, due to our focus on statistics at non-zero absolute temperatures. The incorporation of microstates that do not satisfy mechanical equilibrium implies that Eqs. (2.2) and (2.4) do not completely fix the distortion field Δ . Thus, although the transversal component of Δ is fixed on the boundary, all components of Δ in the bulk can fluctuate locally. Note that fluctuations related to the presence of discrete dislocations are already incorporated in the minimum energy contribution. Namely, the distortion field at minimum energy has to satisfy the incompatibility Eq. (2.2) as well, see also A.1.

In the energy expression (2.5), the interaction potential between dislocations is not incorporated explicitly, as opposed to what is done for example in reference [49, Eq. 5-16], and reference [73]. The standard interaction potential between dislocations is usually derived from the Peach-Koehler force on one dislocation due to the stress field generated by a second dislocation and the virtual work needed for a small displacement of the dislocation

segment. It turns out that in Eq. (2.5), the interaction energy is incorporated implicitly by the incompatibility constraint for the elastic distortion field. Namely, in Sec. 2.3, it will be shown that in the special case without loading and in infinite space, the partition function obtained here is equivalent to the partition function of particles in 2D that interact via the common dislocation interaction potential.

Besides that, the interaction potential used in literature is only valid in infinite space. As the analysis presented here is also valid in finite space, it is incorrect to use this interaction potential explicitly.

2.2.2 Macroscopic control variables

In this section, the macroscopic variables that control the state of the system are determined. First, the system is loaded mechanically. In this study, the microscopic deformation of the boundary is equal to the macroscopically imposed boundary deformation for every microstate. Hence the boundary deformation \mathbf{u}_b is a macroscopic control variable. This means that no coarse-graining for the boundary conditions is considered here.

Second, the system is in thermal contact with the environment, and hence the average energy is controlled by a Lagrange parameter β , which is related to the inverse temperature by $\beta \equiv 1/k_B T$. The meaning of temperature is further addressed in the discussion.

Third, the average dislocation density profile is controlled by the local chemical potential of each species, $\mu_s(\mathbf{s})$. Using the chemical potential as a variable, rather than the dislocation density profile itself, facilitates calculations. The use of the grand-canonical ensemble implies that the number of dislocations in the volume can fluctuate. In a dislocation system, this number can, for example, change due to creation and annihilation processes. However, the result of the analysis presented here is independent of the details of the dynamical processes that allow the number of dislocations to fluctuate. In the context of dislocations, the grand-canonical ensemble was used before by Limkumnerd and Van der Giessen [73].

The total ‘chemical energy’ of the dislocations is defined as

$$E_c = - \sum_{s \in \text{species}} \int d^2 \mathbf{s} \mu_s(\mathbf{s}) \hat{\omega}_s(\mathbf{s}). \quad (2.6)$$

The minus sign in this expression is a convention, which is also used in for example [14, Eq. 3.1.8]. Note that both the chemical potential $\mu_s(\mathbf{s})$ and $\hat{\omega}_s(\mathbf{s})$ are only a function of the position vector perpendicular to the line direction $\hat{\xi}$. This follows naturally from the fact that the dislocations are considered to be straight and infinitely long.

As both the boundary deformation \mathbf{u}_b and the average dislocation density profile are used as macroscopic control variables, the resulting partition function does not only give the free energy of the equilibrium dislocation density profile for a certain boundary loading, but for all other density profiles as well. Thus, also the free energy of evolving dislocation density profiles can in principle be determined from the partition function presented here. The equilibrium dislocation density profile can be obtained by taking the partial derivative of the free energy with respect to the local chemical potential.

2.2.3 Upscaling method

To calculate the partition function, the grand-canonical Boltzmann weight is summed over the space of microstates, see e.g. [14]. The Boltzmann weight of a state is the exponential of the sum of the elastic energy and the chemical energy of the dislocations, see Eqs. (2.5) and (2.6). The summation over microstates consists of a summation over all possible numbers of dislocations on each glide plane. Hence if we denote $\mathbf{N} \equiv \{N_{s,j_s}\}$ the matrix that contains for each species s and glide plane j_s the number of dislocations, we sum over all possible \mathbf{N} . Furthermore, the summation consists of an integration of the dislocation position in the glide plane and of a functional integration over all distortion fields that satisfy the incompatibility condition (2.2) and the macroscopically applied boundary condition (2.4). The functional integral is denoted by $\int \mathcal{D}[\Delta]$. This yields for the partition function \mathcal{Z}

$$\mathcal{Z}[\beta, \mu_s(\mathbf{s}), \mathbf{u}_b] = \sum_{\mathbf{N}=0}^{\infty} \left\{ \prod_{s \in \text{species}} \prod_{j_s \in \text{glide planes}} \left(\frac{1}{N_{sj_s}!} \frac{1}{\lambda_{th,s}^{N_{sj_s}}} \int dx_1 \dots dx_{N_{sj_s}} \right) \right. \quad (2.7)$$

$$\int \mathcal{D}[\Delta] \delta_{\Omega} [\nabla \wedge \Delta - \hat{\alpha}(\mathbf{r})] \delta_{\partial\Omega} [\hat{\mathbf{n}} \wedge \Delta - (\hat{\mathbf{n}} \times \nabla) \mathbf{u}_b]$$

$$\left. \exp \left[-\frac{\beta}{2} \int_{\Omega} d^3 \mathbf{r} \Delta^{\mathbf{s}} : \mathbb{C} : \Delta^{\mathbf{s}} + \beta \sum_{s \in \text{species}} \int_{\Omega} d^2 \mathbf{s} \mu_s(\mathbf{s}) \hat{\omega}_s(\mathbf{s}) \right] \right\},$$

where $\sum_{\mathbf{N}=0}^{\infty}$ denotes the summation of all numbers N_{sj_s} from 0 to ∞ and where $\lambda_{th,s}$ is the thermal wavelength of dislocation species s . It is necessary to introduce a thermal wavelength to be able to write a discrete summation over particle positions as a continuous integration over space. The thermal wavelength is introduced analogous to the standard procedure for the ideal gas, where the phase space is divided in bins with the same energy. The integration over particle momenta then suggests that the thermal wavelength is inversely proportional to the square-root of the temperature, see eg. [14].

The first line in Eq. (2.7) is the summation over dislocation positions and the second line the functional integration over distortion fields that match the incompatibility imposed by the dislocations. All spatial integrals and delta functionals are defined on the volume of the body Ω . The dependence on the glide plane density is hidden in the dislocation density $\hat{\omega}_s(\mathbf{s})$, as this density is only non-zero at the glide planes.

The delta functional to take into account the incompatibility is more conveniently used in its Fourier representation, see reference [60] and Eq. (2.6b) therein:

$$\delta_{\Omega} [\nabla \wedge \Delta - \hat{\alpha}(\mathbf{r})] \propto \int \mathcal{D}[\Psi] \exp \left[-i\beta \int_{\Omega} d^3 \mathbf{r} \Psi : (\nabla \wedge \Delta - \hat{\alpha}) \right], \quad (2.8)$$

where the integration over Ψ is over the space of real fields. The auxiliary field Ψ is loosely speaking the analogue of the wave vector in an ordinary Fourier transform.

A common technique to calculate the expectation value of microscopic variables is to add source terms [121, 104]. Hence, to calculate the expectation value of the microscopic strain field, the integrand in the partition function (2.7) is multiplied by the source-related

factor

$$f_{\text{src}} = \exp \left[\int_{\Omega} d^3 \mathbf{r} \mathbf{J}_{\Delta}(\mathbf{r}) : \Delta^s(\mathbf{r}) \right], \quad (2.9)$$

where \mathbf{J}_{Δ} is the source-term related to Δ . This yields a partition function $\mathcal{Z}[\beta, \mu_s(\mathbf{s}), \mathbf{u}_b, \mathbf{J}_{\Delta}(\mathbf{r})]$, where for $\mathbf{J}_{\Delta} = 0$ the original partition function is found back. The moments of the strain are then calculated as derivatives of the partition function with respect to \mathbf{J}_{Δ} :

$$\langle \Delta^s(\mathbf{r}_1) \dots \Delta^s(\mathbf{r}_n) \rangle = \frac{1}{\mathcal{Z}} \frac{\delta^n \mathcal{Z}}{\delta \mathbf{J}_{\Delta}(\mathbf{r}_1) \dots \delta \mathbf{J}_{\Delta}(\mathbf{r}_n)} \Big|_{\mathbf{J}_{\Delta}=0}. \quad (2.10)$$

Combining Eqs. (2.7), (2.8) and (2.9) yields

$$\begin{aligned} \mathcal{Z}[\beta, \mu_s(\mathbf{s}), \mathbf{u}_b, \mathbf{J}_{\Delta}] &= \sum_{N=0}^{\infty} \left\{ \prod_{s \in \text{species}} \prod_{j_s \in \text{glide planes}} \left(\frac{1}{N_s j_s!} \frac{1}{\lambda_{th,s}^{N_s j_s}} \int dx_1 \dots dx_{N_s j_s} \right) \right. \\ &\quad \int \mathcal{D}[\Delta] \int \mathcal{D}[\Psi] \delta_{\partial\Omega} [\hat{\mathbf{n}} \wedge \Delta - (\hat{\mathbf{n}} \times \nabla) \mathbf{u}_b] \exp \left[-\imath \beta \int_{\Omega} d^3 \mathbf{r} \Psi : (\nabla \wedge \Delta - \hat{\alpha}) \right] \\ &\quad \left. \exp \left[-\frac{\beta}{2} \int_{\Omega} d^3 \mathbf{r} \Delta^s : \mathbb{C} : \Delta^s + \beta \sum_{s \in \text{species}} \int_{\Omega} d^2 \mathbf{s} \mu_s(\mathbf{s}) \hat{\omega}_s(\mathbf{s}) + \int_{\Omega} d^3 \mathbf{r} \mathbf{J}_{\Delta} : \Delta^s \right] \right\}. \end{aligned} \quad (2.11)$$

2.2.4 Performing the integrations

The integrand in Eq. (2.11) is a product of terms that depend either on the elastic distortion Δ or on dislocation positions. This split implies that the integrations over Δ and over dislocation positions can be performed independently.

To split off the effect of loading, i.e. the term dependent on \mathbf{u}_b , it turns out to be convenient to perform the shift $\Delta = \tilde{\Delta} + \Delta_0$, where Δ_0 is defined by

$$\begin{aligned} \nabla \wedge \Delta_0 &= 0 \\ \nabla \cdot (\mathbb{C} : \Delta_0^s) &= 0 \\ \hat{\mathbf{n}} \wedge \Delta_0 &= \hat{\mathbf{n}} \wedge \nabla \mathbf{u}_b, \end{aligned} \quad (2.12)$$

in the bulk and on the boundary respectively. Note that Δ_0 is the mechanical equilibrium solution for a linear elasticity problem without dislocations and with imposed boundary deformation \mathbf{u}_b . As $\mathbb{C} : \Delta_0^s$ is symmetric and divergence free, the field Ψ_0 can be defined as

$$\nabla \wedge \Psi_0 = (\nabla \wedge \Psi_0)^s = \imath \mathbb{C} : \Delta_0^s. \quad (2.13)$$

Note that Ψ_0 is uniquely defined up to a divergence term. As $\mathbb{C} : \Delta_0^s$ is the stress field due to the distortion Δ_0 , Ψ_0 is related to the Beltrami stress potential Φ , as used in [12], namely by $\nabla \hat{\wedge} \Phi = -\imath \Psi_0(\mathbf{r})$, where $\mathbf{v} \hat{\wedge} \mathbf{A}$ is the cross product between the vector \mathbf{v}

and the second order tensor \mathbf{A} on the second index: $\epsilon_{jmn}v_m A_{in}$.

After the shift in $\mathbf{\Delta}$, $\hat{\mathbf{n}} \wedge \tilde{\mathbf{\Delta}}$ vanishes at the boundary. Then, partial integration can be applied at the second term in the exponent containing $\nabla \wedge \tilde{\mathbf{\Delta}}$. After this, the integral only depends on $\tilde{\mathbf{\Delta}}$ and not on its derivative. This implies that the functional integration over $\tilde{\mathbf{\Delta}}$ at the boundary and over $\tilde{\mathbf{\Delta}}^a$ and $\tilde{\mathbf{\Delta}}^s$ in the bulk can be performed independently. The superscript a stand for the anti-symmetric part of a tensor.

The functional integration over $\tilde{\mathbf{\Delta}}$ at the boundary gives an irrelevant multiplicative constant. The integration over $\tilde{\mathbf{\Delta}}^a$ in the bulk is proportional to $\delta_\Omega [(\nabla \wedge \Psi)^a]$. The integration over $\tilde{\mathbf{\Delta}}^s$ in the bulk can be performed by completing the squares. After this, the integration over $\tilde{\mathbf{\Delta}}^s$ is purely Gaussian, and can thus be performed straightforwardly. See A.2 for the details of the calculation. These steps finally yield

$$\begin{aligned} & \int \mathcal{D}[\mathbf{\Delta}] \delta_{\partial\Omega} [\hat{\mathbf{n}} \wedge \mathbf{\Delta} - (\hat{\mathbf{n}} \times \nabla) \mathbf{u}_b] \\ & \exp \left[-\frac{\beta}{2} \int_{\Omega} d^3\mathbf{r} \mathbf{\Delta}^s : \mathbb{C} : \mathbf{\Delta}^s - \imath\beta \int_{\Omega} d^3\mathbf{r} \Psi : \nabla \wedge \mathbf{\Delta} + \int_{\Omega} d^3\mathbf{r} \mathbf{J}_{\mathbf{\Delta}} : \mathbf{\Delta}^s \right]. \quad (2.14) \\ & = C \delta_\Omega [(\nabla \wedge \Psi)^a] \exp \left[-\frac{\beta}{2} \int_{\Omega} d^3\mathbf{r} \mathbf{\Delta}_0^s : \mathbb{C} : \mathbf{\Delta}_0^s + \int_{\Omega} d^3\mathbf{r} \mathbf{J}_{\mathbf{\Delta}}^s : \mathbf{\Delta}_0^s \right] \times \\ & \exp \left[-\frac{\beta}{2} \int_{\Omega} d^3\mathbf{r} (\nabla \wedge (\Psi - \Psi_0) + \imath\beta^{-1} \mathbf{J}_{\mathbf{\Delta}})^s : \mathbb{S} : (\nabla \wedge (\Psi - \Psi_0) + \imath\beta^{-1} \mathbf{J}_{\mathbf{\Delta}})^s \right], \end{aligned}$$

where C is a multiplicative constant that is independent of the loading and dislocation positions. It can thus be ignored in the rest of the calculations.

The integration over dislocation positions can be performed analogous to Netz [83], see Sec. 2 therein. When the dislocation density $\hat{\omega}_s(\mathbf{s})$ and the Nye tensor $\hat{\alpha}(\mathbf{r})$ are explicitly written as a sum of delta peaks, the spatial integrations in the exponent are easily performed. Then, the exponent can be written as a product of terms that depend on one dislocation coordinate only. After slight reorganization of the terms, the series expansion of the exponent, $\exp(x) = \sum_{n=0}^{\infty} \frac{1}{n!} x^n$, can be recognized.

It is convenient to express the result in terms of a field variable that indicates the positions of the glide planes. To this end, the density of glide planes of species s is a collection of delta peaks at the glide plane positions. This glide plane density $\rho_{gl,s}(\mathbf{s})$ of species s is defined by

$$\rho_{gl,s}(\mathbf{s}) = \sum_{j_s \in \text{glide planes}} \delta(y - y_{j_s}). \quad (2.15)$$

Using this, the integration over dislocation positions yields

$$\begin{aligned}
& \sum_{N=0}^{\infty} \left\{ \prod_{s \in \text{species}} \prod_{j_s \in \text{glide planes}} \left(\frac{1}{N_{sj_s}!} \frac{1}{\lambda_{th,s}^{N_{sj_s}}} \int dx_1 \dots dx_{N_{sj_s}} \right) \right. \\
& \quad \left. \exp \left[\beta \sum_{s \in \text{species}} \int_{\Omega} d^2 \mathbf{s} \mu_s(\mathbf{s}) \hat{\omega}_s(\mathbf{s}) + \iota \beta \int_{\Omega} d^3 \mathbf{r} \hat{\alpha}(\mathbf{r}) : \Psi(\mathbf{r}) \right] \right\} \\
& = \exp \left[\sum_{s \in \text{species}} \frac{1}{\lambda_{th,s}} \int_{\Omega} d^2 \mathbf{s} \rho_{gl,s}(\mathbf{s}) \exp \left[\beta \left(\mu_s(\mathbf{s}) + \iota (\hat{\xi} \mathbf{b}_s) : \int dz \Psi(\mathbf{s}, z) \right) \right] \right].
\end{aligned} \tag{2.16}$$

Details can be found in A.3.

Note that the functional integration over Ψ is invariant under constant shifts in Ψ . Therefore, the field Ψ can be replaced by $\Psi + \Psi_0$ in both Eq. (2.14) and (2.16). Combining Eqs. (2.11), (2.14) and (2.16) yields

$$\begin{aligned}
\mathcal{Z}[\beta, \mu_s(\mathbf{s}), \mathbf{u}_b, \mathbf{J}_{\Delta}] & = \exp \left[-\frac{\beta}{2} \int_{\Omega} d^3 \mathbf{r} \Delta_0^s : \mathbb{C} : \Delta_0^s + \int_{\Omega} d^3 \mathbf{r} \mathbf{J}_{\Delta}^s : \Delta_0^s \right] \\
& \int \mathcal{D}[\Psi] \delta_{\Omega} [(\nabla \wedge \Psi)^a] \exp \left[\frac{-\beta}{2} \int_{\Omega} d^3 \mathbf{r} (\nabla \wedge \Psi + \iota \beta^{-1} \mathbf{J}_{\Delta})^s : \mathbb{S} : (\nabla \wedge \Psi + \iota \beta^{-1} \mathbf{J}_{\Delta})^s \right] \\
& \times \exp \left[\sum_{s \in \text{species}} \frac{1}{\lambda_{th,s}} \int_{\Omega} d^2 \mathbf{s} \rho_{gl,s}(\mathbf{s}) \exp \left[\beta \left(\mu_s(\mathbf{s}) + \iota (\hat{\xi} \mathbf{b}_s) : \int dz (\Psi + \Psi_0)(\mathbf{s}, z) \right) \right] \right].
\end{aligned} \tag{2.17}$$

The path integral over Ψ cannot be performed analytically. Hence further simplifications of the partition function will involve approximations. An example of such an approximation is shown in Sec. 2.4. In the next section, properties of the full partition function are discussed.

2.3 Interpretation of the Partition Function (2.17)

2.3.1 The terms in the exponent

The free energy of the system can be determined from the partition function by $\mathcal{F} = -\beta \ln \mathcal{Z}$. Hence the exponents in the partition function (2.17) for $\mathbf{J}_{\Delta} = 0$ can be interpreted as different energy contributions.

The term quadratic in Δ_0 is the energy contribution from the elastic deformation of the material due to boundary loading. Namely, the field Δ_0 is the elastic strain field one would find without dislocations, and hence the term quadratic in Δ_0 is the linear elastic strain energy related to the background deformation.

The path integral is similar to the path integral of a system of charges [83], see Eq. (23) therein, where Ψ plays the role of the elastostatic potential analogous to the electrostatic potential ϕ . The term quadratic in $(\nabla \wedge \Psi)^s$ gives the 'kinetic contribution' to the path integral, which can be interpreted as phonon energy, i.e. the energy of lattice vibrations

or waves. The last line represents the contribution of the dislocations. Namely, when the fugacity $\exp[\beta\mu_s]$ would vanish for all species of dislocations, no dislocations would be present in the material and this contribution vanishes as well.

The term $\iota(\hat{\xi}\mathbf{b}_s) : \int dz \Psi_0(\mathbf{s}, z)$ can be interpreted as the potential energy of dislocations due to loading. Namely the Peach-Koehler force on a dislocation in the distortion field Δ_0 is, using Eq. (2.13):

$$\begin{aligned} \mathbf{F}_{PK} &= \int dz ((\mathbb{C} : \Delta_0) \cdot \mathbf{b}) \times \hat{\xi} = -\iota \int dz \nabla \times (\Psi_0 \cdot \mathbf{b}) \times \hat{\xi} \\ &= -\iota \int dz \hat{\xi} \cdot \nabla (\Psi_0 \cdot \mathbf{b}) - \nabla (\hat{\xi} \mathbf{b} : \Psi_0) = \nabla \int dz \iota \hat{\xi} \mathbf{b} : \Psi_0, \end{aligned} \quad (2.18)$$

where the term proportional to $\hat{\xi} \cdot \nabla$ vanishes in the integration over z . The Peach-Koehler force is thus minus the gradient of $-\iota \int dz \hat{\xi} \mathbf{b} : \Psi_0$, and hence the latter can be interpreted as the potential energy of a dislocation in the distortion field Δ_0 .

2.3.2 Thermodynamic relations in mechanical systems

The effective stiffness and compliance tensor of a mechanical system are related to fluctuations in the strain. The compliance is the inverse of the stiffness, defined by $\mathbb{C} : \mathbb{S} = \mathbb{C}_{ijkl} \mathbb{S}_{kl} \delta_{ij}$. It was shown by Parrinello and Rahman [91] that the variance of the strain in the stress-controlled ensemble is proportional to the compliance \mathbb{S} :

$$\langle \mathbf{r}, \mathbf{r}' \rangle = \beta (\langle (\Delta(\mathbf{r}) \Delta(\mathbf{r}'))_{\sigma} \rangle - \langle \Delta(\mathbf{r}) \rangle_{\sigma} \langle \Delta(\mathbf{r}') \rangle_{\sigma}). \quad (2.19)$$

However, this expression cannot be applied straightforwardly to our case presented in this chapter. In the work of Parrinello and Rahman, the strain can fluctuate in arbitrary directions in function space, whereas we only consider strain fields that satisfy the incompatibility condition (2.2). This results in a relation different from (2.19), as explained in the following.

For a linear elastic system without dislocations, the statistics of strain fluctuations is described in the book of Chaikin and Lubenski [14], see Eq. (6.4.23) therein. As no dislocations are present, the distortion field is curl-free according to Eq. (2.2), i.e. $\Delta = \nabla \mathbf{u}$, and therefore, the displacement field $\mathbf{u}(\mathbf{r})$ can be used as a variable. The elastic energy is then $\frac{1}{2} \int \frac{d\mathbf{q}}{(2\pi)^3} (\mathbf{q} \tilde{\mathbf{u}}(\mathbf{q})) : \mathbb{C} : (\mathbf{q} \tilde{\mathbf{u}}(-\mathbf{q}))$, and hence the distribution is Gaussian. Therefore, the variance of the displacement field in Fourier space is

$$\langle \tilde{u}_j(\mathbf{q}) \tilde{u}_{j'}(-\mathbf{q}) \rangle - \langle \tilde{u}_j(\mathbf{q}) \rangle \langle \tilde{u}_{j'}(-\mathbf{q}) \rangle = \beta^{-1} D_{jj'}^{-1}(\mathbf{q}), \quad (2.20)$$

with $D_{jj'}(\mathbf{q}) \equiv q_k q_{k'} \mathbb{C}_{kjk'j}$. The variance of the elastic distortion that follows from this expression is

$$\begin{aligned} \langle \Delta_{ij}^s(\mathbf{q}) \Delta_{i'j'}^s(-\mathbf{q}) \rangle - \langle \Delta_{ij}^s(\mathbf{q}) \rangle \langle \Delta_{i'j'}^s(-\mathbf{q}) \rangle &= \\ &= \frac{\beta^{-1}}{4} \left(q_i q_{i'} D_{jj'}^{-1}(\mathbf{q}) + q_j q_{j'} D_{ii'}^{-1}(\mathbf{q}) + q_i q_{j'} D_{j'i}^{-1}(\mathbf{q}) + q_j q_{i'} D_{i'j}^{-1}(\mathbf{q}) \right). \end{aligned} \quad (2.21)$$

In the case of an isotropic solid, this reduces to

$$\begin{aligned} \langle \Delta_{ij}^s(\mathbf{q}) \Delta_{i'j'}^s(-\mathbf{q}) \rangle - \langle \Delta_{ij}^s(\mathbf{q}) \rangle \langle \Delta_{i'j'}^s(-\mathbf{q}) \rangle &= \\ = \beta^{-1} (\delta_{il} \delta_{jn} - Q_{il} Q_{jn}) \frac{1}{2\mu} \left(\delta_{ll'} \delta_{nn'} - \frac{\nu}{1-\nu} \delta_{ln} \delta_{l'n'} \right)^{ls} & (\delta_{i'l'} \delta_{j'n'} - Q_{i'l'} Q_{j'n'}), \end{aligned} \quad (2.22)$$

with \mathbf{Q} the projection perpendicular to \mathbf{q} , i.e. $Q_{il} \equiv \delta_{il} - q_i q_l / q^2$, and where the superscript “ls” (left-symmetric) indicates the symmetric part with respect to the first two indices, i.e. $\mathbf{A}_{ij i' j'}^{ls} = (\mathbf{A}_{ij i' j'} + \mathbf{A}_{j i' j' i}) / 2$.

The compliance of an isotropic solid is $\mathbb{S}_{lnl'n'} = (\delta_{ll'} \delta_{nn'} - \frac{\nu}{1+\nu} \delta_{ln} \delta_{l'n'}) / 2\mu$. Hence the variance of the compatible distortion differs from the compliance by (i) multiplication with a tensor $(\delta_{il} \delta_{jn} - Q_{il} Q_{jn})$ from left and right, and (ii) a factor $\frac{\nu}{1-\nu}$ instead of $\frac{\nu}{1+\nu}$. This is different from what was stated in Eq. (2.19) for general distortion fields. However, it is possible to reconstruct parameters of the stiffness from the variance of compatible distortions, as shown by Walz and Fuchs [115], see Eq. (91) therein.

2.3.3 Observables

From the partition function, general expressions for observables in the system can be calculated. In this section, the expectation value of the strain field and the second moment of strain will be determined from Eqs. (2.10) and (2.17), and the dislocation density and pair correlation will be determined from derivatives of the free energy with respect to the local chemical potential.

For the strain field, we find from Eq. (2.10) that

$$\langle \Delta^s(\mathbf{r}) \rangle = \Delta_0^s(\mathbf{r}) - \imath \mathbb{S} : (\nabla \wedge \langle \Psi(\mathbf{r}) \rangle)^s. \quad (2.23)$$

Note that the LHS of Eq. (2.23) is real, as this is an observable. Therefore the RHS should also be real, which implies that $\langle \Psi(\mathbf{r}) \rangle$ is purely imaginary. This is shown explicitly in A.4. In this derivation, it is crucial to realize that the ‘probability density’ used to calculate $\langle \Psi(\mathbf{r}) \rangle$ is not real-valued, see Eq. (2.11). It is not problematic to find a purely imaginary expectation value for Ψ , as this field is an auxiliary field, and hence it is not a measurable quantity.

Note that $\mathbb{C} : \langle \Delta^s(\mathbf{r}) \rangle$, which can be interpreted as the stress field, is divergence free. Therefore, the expectation value of the distortion satisfies mechanical equilibrium, which was to be expected.

The variance of the distortion, which follows from Eq. (2.10), is

$$\begin{aligned} \langle \Delta^s(\mathbf{r}) \Delta^s(\mathbf{r}') \rangle - \langle \Delta^s(\mathbf{r}) \rangle \langle \Delta^s(\mathbf{r}') \rangle &= \frac{\delta}{\delta \mathbf{J}_\Delta(\mathbf{r})} \frac{1}{\mathcal{Z}} \frac{\delta \mathcal{Z}}{\delta \mathbf{J}_\Delta(\mathbf{r}')} \Big|_{\mathbf{J}_\Delta=0} \\ &= \beta^{-1} \mathbb{S}^{ls} \delta(\mathbf{r}, \mathbf{r}') - (\mathbb{S} : \nabla \wedge) \left(\mathbb{S} : \nabla \hat{\wedge} \right) (\langle \Psi(\mathbf{r}) \Psi(\mathbf{r}') \rangle - \langle \Psi(\mathbf{r}) \rangle \langle \Psi(\mathbf{r}') \rangle). \end{aligned} \quad (2.24)$$

For the dislocation density profile, it follows that

$$\begin{aligned} \langle \hat{\omega}_s(\mathbf{s}) \rangle &= -\frac{\delta \mathcal{F}}{\delta \mu_s(\mathbf{s})} = \beta \frac{1}{\mathcal{Z}} \frac{\delta \mathcal{Z}}{\delta \mu_s(\mathbf{s})} \\ &= \frac{e^{\beta \mu_s(\mathbf{s})}}{\lambda_{th,s}} \rho_{gl,s}(\mathbf{s}) e^{i\beta(\hat{\boldsymbol{\xi}}\mathbf{b}_s):\int dz \Psi_0(\mathbf{s},z)} \langle e^{i\beta(\hat{\boldsymbol{\xi}}\mathbf{b}_s):\int dz \Psi(\mathbf{s},z)} \rangle \equiv p_s(\mathbf{s}) \langle e^{i\beta(\hat{\boldsymbol{\xi}}\mathbf{b}_s):\int dz \Psi(\mathbf{s},z)} \rangle, \end{aligned} \quad (2.25)$$

where in the last expression, p_s is shorthand notation for

$p_s = \frac{e^{\beta \mu_s(\mathbf{s})}}{\lambda_{th,s}} \rho_{gl,s}(\mathbf{s}) e^{i\beta(\hat{\boldsymbol{\xi}}\mathbf{b}_s):\int dz \Psi_0(\mathbf{s},z)}$. From expression (2.25), it follows that dislocations indeed only occur on glide planes. The dependence on \mathbf{u}_b is both in Ψ_0 in the prefactor and in the averaging $\langle \dots \rangle$, as the partition function depends on Ψ_0 as well. For the two body dislocation density, we find that

$$\begin{aligned} \langle \omega_s(\mathbf{s}) \omega_{s'}(\mathbf{s}') \rangle &= \beta^{-2} \frac{1}{\mathcal{Z}} \frac{\delta^2 \mathcal{Z}}{\delta \mu_s(\mathbf{s}) \delta \mu_{s'}(\mathbf{s}')} \\ &= \delta_{s,s'} \delta(\mathbf{s} - \mathbf{s}') \langle \omega_s(\mathbf{s}) \rangle + p_s(\mathbf{s}) p_{s'}(\mathbf{s}') \langle e^{i\beta(\hat{\boldsymbol{\xi}}\mathbf{b}_s):\int dz \Psi(\mathbf{s},z)} e^{i\beta(\hat{\boldsymbol{\xi}}\mathbf{b}_{s'}):\int dz \Psi(\mathbf{s}',z)} \rangle. \end{aligned} \quad (2.26)$$

The first term is the autocorrelation of a dislocation with itself. The second term describes the influence of dislocation-dislocation interactions. This term is the density squared times the pair correlation function of dislocations.

2.3.4 Dislocations as interacting particles

In Sec. 2.2.1, it was stated that, in infinite space and without loading, the partition function obtained here could also have been constructed using an interaction potential. This implies that a microscopic description that uses the interaction potential between dislocations yields the same macroscopic behaviour as the microscopic description used here, i.e. a description with the distortion field and only the elastic energy, although the latter contains fluctuations of the lattice as well.

In this section, this is shown explicitly by rewriting Eq. (2.17) to the grand-canonical partition function for particles that interact with the dislocation interaction potential in [49].

The first step is to expand Eq. (2.17) for $\mathbf{J}_\Delta = 0$ in powers of $\lambda_{th,s}^{-1}$. This yields an infinite sum of Gaussian path integrals, see Eq. (A.11). The second step is to perform all path integrations over Ψ . Up to a multiplicative constant, this yields

$$\mathcal{Z}[\beta, \mu_s(\mathbf{s})] = \prod_{s \in \text{species}} \sum_{N_s=0}^{\infty} \frac{1}{N_s!} \prod_{j=1}^{N_s} \left(\int d^2 \mathbf{s}_j \frac{\rho_{gl,s}(\mathbf{s}_j)}{\lambda_{th,s}} e^{\beta(\mu_s(\mathbf{s}_j) + i(\hat{\boldsymbol{\xi}}\mathbf{b}_s):\int dz \Psi_0(\mathbf{s}_j,z))} \right) \quad (2.27)$$

$$\exp \left[\frac{-\beta}{2} \sum_{s,s' \in \text{species}} \sum_{j=1}^{N_s} \sum_{j'=1}^{N_{s'}} (\hat{\boldsymbol{\xi}}\mathbf{b}_s) : \left(\int dz dz' \mathbf{G}_0((\mathbf{s}_j, z) - (\mathbf{s}'_{j'}, z')) \right) : (\hat{\boldsymbol{\xi}}\mathbf{b}_{s'}) \right],$$

where the fourth order tensor \mathbf{G}_0 must satisfy the condition

$$\Psi(\mathbf{r}) = \int d^3 \mathbf{r}' (\nabla_{\mathbf{r}'} \wedge \Psi(\mathbf{r}'))^s : \mathbb{S} : (\nabla_{\mathbf{r}'} \wedge \mathbf{G}_0(\mathbf{r}', \mathbf{r}))^s, \quad (2.28)$$

where $\nabla_{\mathbf{r}'}$ denotes the derivative with respect to \mathbf{r}' . Details on $G_0(\mathbf{r}', \mathbf{r})$ can be found in A.5. It is shown in A.6 that $(\hat{\xi}\mathbf{b}_s) : (\int dzdz' G_0((\mathbf{s}_j, z) - (\mathbf{s}'_{j'}, z')) : (\hat{\xi}\mathbf{b}_{s'}))$ is the conventional interaction potential between dislocations of species s and s' , as in the work of Hirth and Lothe [49]. Hence Eq. (2.27) is the grand-canonical partition function of particles in 2D that interact via the dislocation interaction potential.

2.3.5 Effect of the finite medium

Within DDD calculations, the effect of the finite medium is twofold: corrections to the infinite-space solutions of the strain field should be added to account for the finite volume, and the loading is applied only at the boundary, but influences the behaviour of dislocations inside the material. The starting level of our calculations was similar to the DDD description, and therefore the two effects of the finite volume in these calculations can also be recognized in the partition function (2.17) obtained here.

First, all spatial integrals in Eq. (2.17) are over the finite volume Ω . This implies that the integration in the defining Eq. (2.28) for G_0 is over the volume Ω as well. Therefore, the resulting Green's function will depend on this volume Ω and will thus differ from the infinite space solution derived in A.6.

Second, the field Ψ_0 depends on the boundary deformation \mathbf{u}_b , see Eq. (2.13). This field shows up in a bulk integral in the exponential term in the partition function (2.17). This implies that the effect of applied loading spans over the whole volume and influences dislocations deep in the bulk as well.

2.3.6 Coupling parameters

The dominant behaviour of the system is identified by determining the typical values of the coupling parameters. First, the coupling parameters are determined in infinite space and without deformation of the boundary, i.e. for $\mathbf{u}_b = 0$ and hence $\Psi_0 = 0$. Now, the potential is written as $\Psi = \psi\check{\Psi}$ and all lengths are scaled as $\mathbf{r} = \zeta\check{\mathbf{r}}$. This also implies that $\mathcal{D}[\Psi] \propto \mathcal{D}[\check{\Psi}]$ and $\delta_\Omega [(\nabla \wedge \Psi)^a] \propto \delta_\Omega [(\check{\nabla} \wedge \check{\Psi})^a]$. The compliance is written as $\mathbb{S} = c^{-1}\check{\mathbb{S}}$, with $\check{\mathbb{S}}$ a dimensionless tensor. The Burgers vector is written as $\mathbf{b}_s = b\check{\mathbf{b}}_s$. The volume integration in dimensionless variables reads

$$\int d^3\mathbf{r} \rightarrow \zeta^3 \int d^3\check{\mathbf{r}} = \zeta^3 \int d\check{x}d\check{y} \int_0^{L/\zeta} d\check{z}. \quad (2.29)$$

The macroscopic control variables of the system, the local chemical potential $\mu_s(\mathbf{s})$ and also the temperature, do not depend on the z -coordinate. Therefore, it is expected that the \check{z} -integral is proportional to L/ζ , and hence that $\frac{\zeta}{L} \int d^3\check{\mathbf{r}}$ is independent of the system parameters.

Furthermore, the local dimensionless fugacity is defined by $\check{f}_s(\check{\mathbf{s}}) \equiv \frac{\zeta^2}{\lambda_{th,s}} \rho_{gl,s}(\zeta\check{\mathbf{s}}) e^{\beta\mu_s(\zeta\check{\mathbf{s}})}$.

This yields for the partition function (2.17):

$$\begin{aligned} \mathcal{Z}[\beta, \check{f}_s(\check{\mathbf{s}})] &\propto \int \mathcal{D}[\check{\Psi}] \delta_{\Omega} \left[\left(\check{\nabla} \wedge \check{\Psi} \right)^a \right] \exp \left[-\frac{\beta L \psi^2}{c} \frac{1}{2} \frac{\zeta}{L} \int d^3 \check{\mathbf{r}} (\check{\nabla} \wedge \check{\Psi})^s : \check{\mathcal{S}} : (\check{\nabla} \wedge \check{\Psi})^s \right] \\ &\times \exp \left[\sum_{s \in \text{species}} \int d^2 \check{\mathbf{s}} \check{f}_s(\check{\mathbf{s}}) \exp \left[\beta b L \psi \iota(\hat{\xi} \hat{\mathbf{b}}_s) : \frac{\zeta}{L} \int d\check{z} \check{\Psi}(\check{\mathbf{s}}, \check{z}) \right] \right]. \end{aligned} \quad (2.30)$$

It follows from this equation that there are three dimensionless groups in the system, namely $\beta L \psi^2 / c$, $\beta b L \psi$ and $\check{f}_s(\check{\mathbf{s}})$. The typical value of the stiffness c is 2μ . The potential scale ψ can now be chosen such that one of these groups is 1. To this end, we choose $\psi = (\beta b L)^{-1}$, and obtain the dimensionless coupling parameter Ξ defined by

$$\Xi \equiv \beta 2 \mu b^2 L. \quad (2.31)$$

The coupling parameter Ξ can be interpreted as the interaction energy over the thermal energy. Namely, $\mu b^2 L$ is the prefactor of the interaction potential, see Eq. (A.19) and $\beta \equiv 1/k_B T$ is one over the thermal energy. The partition function in terms of Ξ reads

$$\begin{aligned} \mathcal{Z}[\Xi, \check{f}_s(\check{\mathbf{s}})] &\propto \int \mathcal{D}[\check{\Psi}] \delta_{\Omega} \left[\left(\check{\nabla} \wedge \check{\Psi} \right)^a \right] \exp \left[-\frac{1}{\Xi} \frac{1}{2} \frac{\zeta}{L} \int d^3 \check{\mathbf{r}} (\check{\nabla} \wedge \check{\Psi})^s : \check{\mathcal{S}} : (\check{\nabla} \wedge \check{\Psi})^s \right] \\ &+ \sum_{s \in \text{species}} \int d^2 \check{\mathbf{s}} \check{f}_s(\check{\mathbf{s}}) \exp \left[\iota(\hat{\xi} \hat{\mathbf{b}}_s) : \frac{\zeta}{L} \int d\check{z} \check{\Psi}(\check{\mathbf{s}}, \check{z}) \right]. \end{aligned} \quad (2.32)$$

Both coupling parameters Ξ and $\check{f}_s(\check{\mathbf{s}})$ depend on the temperature. The temperature dependence of the former is easy, as $\Xi \propto \beta$. For the latter, it is used that the thermal wavelength behaves as $\lambda_{th,s} \propto \beta^{1/2}$ and that the glide plane density is independent of temperature. Furthermore, the combination $\beta \mu_s(\mathbf{s})$ is considered to be independent of the temperature, for the following reason. As can be seen in the partition function (2.17), while the parameter to control the average elastic energy E_{elas} is given by β , the parameter to control the average dislocation density profile is $-\beta \mu_s(\mathbf{s})$. Thus from the perspective of statistical mechanics, $-\beta \mu_s(\mathbf{s})$ is a more natural quantity than $\mu_s(\mathbf{s})$. This also surfaces in the context of thermodynamic potentials. While the microcanonical partition function is related to the entropy, (generalized) canonical ensembles are related to the Legendre-transforms of the entropy. From the differential of the thermodynamic potential entropy

$$dS = \beta dE - \int d^2 \mathbf{s} \beta \mu_s(\mathbf{s}) d\omega_s(\mathbf{s}) + \dots, \quad (2.33)$$

slightly adapted from the equilibrium form, it is eminent that the pairs of conjugate variables are given by (β, E) , and $(-\beta \mu_s(\mathbf{s}), \omega_s(\mathbf{s}))$. This again underlines that $-\beta \mu_s(\mathbf{s})$ should in our context be considered an independent variable. The symbol $\mu_s(\mathbf{s})$ is nevertheless used throughout this chapter as it is a well-established and physically intuitive quantity when discussing the control of populations of species. In summary, then, this implies that the fugacity is proportional to the square-root of temperature; $f_s \propto \beta^{-1/2}$,

and hence that $\sqrt{\Xi} \check{f}$ is independent of temperature.

The coupling parameter Ξ can be calculated from experimental data. For aluminium at room temperature one finds $\Xi = 10^2 \times L[\text{\AA}]$, where $\mu = 26$ GPa, $b = 2.9$ \AA (see [101]), $k_B T = 4 \times 10^{-21}$ J at room temperature (298 K) and $L[\text{\AA}]$ is the persistence length of a dislocation in \AAngstrom. Although this length is hard to obtain experimentally, it can be safely assumed that the dislocation length should be much larger than the Burgers vector, i.e. $L \gg b = 2.9$ \AA, as straight dislocations are modeled. It can thus be concluded that $\Xi \gg 1$. This indicates that dislocations in aluminium at room temperature are in the low temperature regime, where energy minimization determines the equilibrium behaviour, rather than entropy maximization. Furthermore, this implies that the path integral in Eq. (2.32) cannot be replaced by its maximum value, which is a saddle point approximation, but that all fields contribute to the integral.

Note that the length scale ζ does not appear in the coupling parameter Ξ . Hence ζ can be chosen such that the fugacity $\check{f}_s(\check{\mathbf{s}})$ is of order 1. This indicates that there is no intrinsic length scale in the system other than the density, which was to be expected. Namely, the bare interaction potential between dislocations is logarithmic, and has thus no intrinsic length scale either.

Now, a system under loading is considered, i.e. where $\mathbf{u}_b \neq 0$ and thus $\Psi_0 \neq 0$. A length scale can be associated with the potential Ψ_0 . Namely, from Eq. (2.13), it can be seen that, with χ the typical length scale over which Ψ_0 varies and $|(\hat{\mathbf{n}} \times \nabla) \mathbf{u}_b|$ the typical value of the surface derivative of the imposed boundary displacement, one finds

$$\frac{1}{2\mu} \chi^{-1} \psi = |(\hat{\mathbf{n}} \times \nabla) \mathbf{u}_b|; \quad \chi = \frac{1}{\beta 2\mu b L |(\hat{\mathbf{n}} \times \nabla) \mathbf{u}_b|} = \frac{b}{\Xi |(\hat{\mathbf{n}} \times \nabla) \mathbf{u}_b|}, \quad (2.34)$$

where $|(\hat{\mathbf{n}} \times \nabla) \mathbf{u}_b|$ is the typical elastic strain applied at the boundary.

The length χ can be interpreted as the length over which the energy of a dislocation varies with $k_B T$ due to the Peach Koehler force resulting from external loading. Namely, $2\mu |(\hat{\mathbf{n}} \times \nabla) \mathbf{u}_b|$ is the typical value for the stress, and the Peach-Koehler force is linear in b and L , so $2\mu |(\hat{\mathbf{n}} \times \nabla) \mathbf{u}_b| b L \chi$ is the work done by the Peach-Koehler force on a dislocation over distance χ . This is analogous to the Gouy-Chapman length for charges in water.

In thermodynamic equilibrium, the thermal extension of a pile-up of dislocations against a dislocation wall is expected to be of the order of χ , as further extensions cost more than a few $k_B T$ in energy. As the coupling constant Ξ is large for metals, it is to be expected for moderate loading (i.e. $|(\hat{\mathbf{n}} \times \nabla) \mathbf{u}_b| \approx 0.1\%$), that $\chi \lesssim b$. On this small length scale, strong coupling effects between dislocations will probably dominate the structure of the pile-up, rather than thermal effects. Moreover, linear elasticity, which was used to derive the governing equations, is not valid on such small length scales.

2.4 Case study

In this section it is demonstrated how one can make use of the partition function obtained in Eq. (2.17). It is shown that if the coupling parameter Ξ (and hence the temperature) is either very low or very high, that the partition function can be approximated by a single Gaussian.

For notational convenience the partition function in Eq. (2.17) is slightly rewritten. First, the local fugacity of each species s is defined by

$$f_s(\mathbf{s}) \equiv \frac{\rho_{gl,s}(\mathbf{s})}{\lambda_{th,s}} \exp \left[\beta(\mu_s(\mathbf{s}) + \iota \int dz \hat{\xi} \mathbf{b}_s : \Psi_0(\mathbf{s}, z)) \right]. \quad (2.35)$$

Second, with the definition of the bare Green's function G_0 in Eq. (2.28), the quadratic term in Ψ in the partition function (2.17) can be rewritten as $\int d^3 \mathbf{r} d^3 \mathbf{r}' \Psi(\mathbf{r}) : G_0^{-1}(\mathbf{r}, \mathbf{r}') : \Psi(\mathbf{r}')$.

Using the above notation in the partition function (2.17) reads

$$\begin{aligned} \mathcal{Z}[\beta, f_s(\mathbf{s})] &= \int \mathcal{D}[\Psi] \exp \left[\frac{-\beta}{2} \int d^3 \mathbf{r} d^3 \mathbf{r}' \Psi(\mathbf{r}) : G_0^{-1}(\mathbf{r} - \mathbf{r}') : \Psi(\mathbf{r}') + \right. \\ &\quad \left. + \sum_{s \in \text{species}} \int d^2 \mathbf{s} f_s(\mathbf{s}) \exp \left[\iota \beta(\hat{\xi} \mathbf{b}) : \int dz \Psi(\mathbf{s}, z) \right] \right] \equiv \int \mathcal{D}[\Psi] \mathcal{R}[\Psi], \end{aligned} \quad (2.36)$$

where the last equality defines the functional $\mathcal{R}[\Psi]$.

2.4.1 The effective Green's function

The above path-integral (2.36) can not be performed exactly. However, it was shown in A.7 that for the scalar analogue of this problem, a Gaussian approximation of the integrand is accurate for low and high coupling constants Ξ , but not for intermediate Ξ . Therefore, it is assumed that $\mathcal{R}[\Psi]$ can be approximated by a Gaussian functional $\mathcal{R}_G[\Psi]$. Then, the path integrations can be performed.

A single Gaussian is the simplest approximation that allows one to evaluate the functional integral in Eq. (2.17). In literature, more advanced approximations, such as the Villain approximation [61], are available. These are more accurate, but more computationally expensive as well. Therefore, only the simplest approximation with a single Gaussian is studied here to show the applicability of the obtained partition function.

The Gaussian probability density $\mathcal{R}_G[\Psi]$ used here is defined by

$$\begin{aligned} \mathcal{Z}_G[\beta, f] &\equiv \int \mathcal{D}[\Psi] \mathcal{R}_G[\Psi] = \int \mathcal{D}[\Psi] \exp \left[\frac{-\beta}{2} \int d^3 \mathbf{r} d^3 \mathbf{r}' (\Psi(\mathbf{r}) + \iota \mathbf{B}(\mathbf{r})) \right. \\ &\quad \left. : G^{-1}(\mathbf{r} - \mathbf{r}') : (\Psi(\mathbf{r}') + \iota \mathbf{B}(\mathbf{r}')) + \gamma \right] \\ &= \exp \left[\gamma - \frac{1}{2} \text{Tr} [\ln (\beta G^{-1})] \right], \end{aligned} \quad (2.37)$$

where γ is a scalar, $\mathbf{B}(\mathbf{r})$ is a second order tensor and the Green's function G is a fourth order tensor. For the last equality, the Gaussian path integral was performed as for example in [104]. The trace is over both discrete and continuous indices, and the logarithm is the logarithm of a tensor. This relation holds for all positive definite Hermitian matrices. The parameters G , \mathbf{B} and γ can now be chosen such that $\mathcal{R}_G[\Psi]$ approximates $\mathcal{R}[\Psi]$ best. As the Gaussian approximation is not necessarily accurate for all values of the coupling parameters, the accuracy of the Gaussian approximation should be assessed afterwards.

The Green's function \mathbf{G} , the tensor \mathbf{B} and the scalar γ are chosen such that both distributions have the same normalization and produce the same first and second moment:

$$\begin{aligned} \int \mathcal{D}[\Psi] \mathcal{R}[\Psi] &= \int \mathcal{D}[\Psi] \mathcal{R}_G[\Psi] \\ \langle \Psi(\mathbf{r}) \rangle_G &= \langle \Psi(\mathbf{r}) \rangle \\ \langle \Psi(\mathbf{r}) \Psi(\mathbf{r}') \rangle_G &= \langle \Psi(\mathbf{r}) \Psi(\mathbf{r}') \rangle. \end{aligned} \quad (2.38)$$

Physically, this means that $\mathcal{R}[\Psi]$ and $\mathcal{R}_G[\Psi]$ produce the same first and second moment of distortion, see Eqs. (2.23) and (2.24).

To evaluate the integrations in (2.38), it is assumed that when the Gaussian approximation is good, that either $\mathcal{R}_G[\Psi]$ is small or that the exponents of $\mathcal{R}_G[\Psi]$ and $\mathcal{R}[\Psi]$ are almost equal. Therefore, a first order Taylor approximation in the difference between the exponents of $\mathcal{R}[\Psi]$ and $\mathcal{R}_G[\Psi]$ can be made, which reads

$$\begin{aligned} \mathcal{R}_G[\Psi] - \mathcal{R}[\Psi] &\approx -\mathcal{R}_G[\Psi] \left(-\frac{\beta}{2} \int d^3\mathbf{r} d^3\mathbf{r}' \Psi(\mathbf{r}) : \mathbf{G}_0^{-1}(\mathbf{r}, \mathbf{r}') : \Psi(\mathbf{r}') \right. \\ &+ \frac{\beta}{2} \int d^3\mathbf{r} d^3\mathbf{r}' (\Psi(\mathbf{r}) + \iota \mathbf{B}(\mathbf{r})) : \mathbf{G}^{-1}(\mathbf{r} - \mathbf{r}') : (\Psi(\mathbf{r}') + \iota \mathbf{B}(\mathbf{r}')) - \gamma \\ &\left. + \sum_{s \in \text{Species}} \int d^2\mathbf{s} f_s(\mathbf{s}) \exp \left[\iota \beta (\hat{\boldsymbol{\xi}} \mathbf{b}) : \int dz \Psi(\mathbf{s}, z) \right] \right). \end{aligned} \quad (2.39)$$

The accuracy of this approximation will be checked afterwards. With this approximation, the functional integrals Eq. (2.38) can be performed. This yields three equations from which governing equations for the parameters γ , \mathbf{B} and \mathbf{G} can be determined (see A.8 for details):

$$\begin{aligned} \int d^3\mathbf{r}'' \mathbf{B}(\mathbf{r}'') : \mathbf{G}_0^{-1}(\mathbf{r}'', \mathbf{r}) &= - \sum_{s \in \text{Species}} f_s(\mathbf{r}_{2D}) \hat{\boldsymbol{\xi}} \mathbf{b}_s \cdot \\ &\cdot \exp \left[\beta \int dz \mathbf{B}(\mathbf{r}_{2D}, z) : \hat{\boldsymbol{\xi}} \mathbf{b}_s - \frac{\beta}{2} \int dz dz' \hat{\boldsymbol{\xi}} \mathbf{b}_s : \mathbf{G}(\mathbf{r}_{2D}, z; \mathbf{r}_{2D}, z') : \hat{\boldsymbol{\xi}} \mathbf{b}_s \right] \\ \mathbf{G}^{-1}(\mathbf{r} - \mathbf{r}') &= \mathbf{G}_0^{-1}(\mathbf{r} - \mathbf{r}') + \sum_{s \in \text{Species}} \beta f_s(\mathbf{r}_{2D}) \delta(\mathbf{r}_{2D} - \mathbf{r}'_{2D}) \hat{\boldsymbol{\xi}} \mathbf{b}_s \hat{\boldsymbol{\xi}} \mathbf{b}_s \cdot \\ &\cdot \exp \left[\beta \int dz \mathbf{B}(\mathbf{r}_{2D}, z) : \hat{\boldsymbol{\xi}} \mathbf{b}_s - \frac{\beta}{2} \int dz dz' \hat{\boldsymbol{\xi}} \mathbf{b}_s : \mathbf{G}(\mathbf{r}_{2D}, z; \mathbf{r}_{2D}, z') : \hat{\boldsymbol{\xi}} \mathbf{b}_s \right] \\ \gamma &= \frac{\beta}{2} \int d^3\mathbf{r} d^3\mathbf{r}' \mathbf{B}(\mathbf{r}) : \mathbf{G}_0^{-1}(\mathbf{r}, \mathbf{r}') : \mathbf{B}(\mathbf{r}') - \frac{1}{2} \text{Tr} [\mathbf{G} : (\mathbf{G}_0^{-1} - \mathbf{G}^{-1})] + \\ &+ \sum_{s \in \text{Species}} \int d^2\mathbf{s} f_s(\mathbf{s}) \exp \left[\beta \int dz \mathbf{B}(\mathbf{s}, z) : \hat{\boldsymbol{\xi}} \mathbf{b} - \frac{\beta}{2} \int dz dz' \hat{\boldsymbol{\xi}} \mathbf{b}_s : \mathbf{G}(\mathbf{s}, z; \mathbf{s}, z') : \hat{\boldsymbol{\xi}} \mathbf{b}_s \right]. \end{aligned} \quad (2.40)$$

In A.8, the quality of the approximations was evaluated for the special case of two species of dislocations with opposite Burgers vector and spatially constant fugacity f .

First, the accuracy of Eq. (2.39) is assessed by expanding up to the second order in the difference between the exponents in $\mathcal{R}[\Psi]$ and $\mathcal{R}_G[\Psi]$, and considering whether this affects

the Green's function G . It turns out that in the low temperature limit $\Xi \rightarrow \infty$, expanding up to second order hardly changes the Green's function G . Therefore, the approximation in Eq. (2.39) is considered to be accurate enough in this regime.

Second, the validity of the Gaussian approximation was assessed by estimating the difference in the charge correlator that follows from $\mathcal{R}[\Psi]$ and $\mathcal{R}_G[\Psi]$ using Eq. (2.39). This difference turned out to be negligible in the low temperature regime, and therefore, the Gaussian approximation is considered to be accurate as well.

2.4.2 Observables in a system of Statistically Stored Dislocations

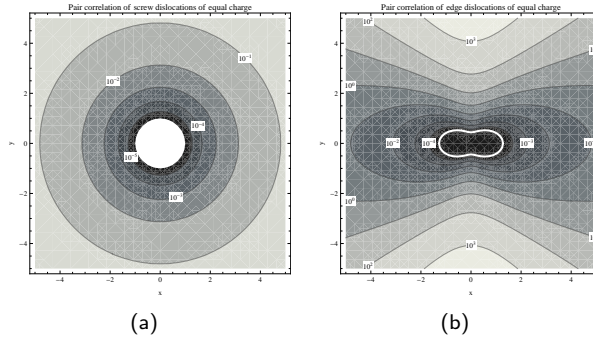


Figure 2.3: In these figures, $(\langle \omega_\alpha(\mathbf{s}) \omega_{\alpha'}(\mathbf{s}') \rangle_G - \omega \delta_{\alpha\alpha'} \delta(\mathbf{s}, \mathbf{s}')) / \omega^2$ is plotted for two dislocations with equal Burgers vector, see Eq. (2.43) for the explicit expression. In Fig. 2.3(a), a screw dislocation with parallel Burgers and line vector is considered; $\hat{\mathbf{b}} = \hat{\boldsymbol{\xi}} = \hat{\mathbf{z}}$. In Fig. 2.3(b), an edge dislocation with perpendicular Burgers and line vector is considered; $\hat{\boldsymbol{\xi}} = \hat{\mathbf{z}}$ and $\hat{\mathbf{b}} = \hat{\mathbf{x}}$. The parameters used are $\Xi = 10$ and $m = 0.3$.

Using the Gaussian approximation, the expectation values of the observables in this system can be determined. In this section, the observables will be determined for so-called Statistically Stored Dislocations in a system without mechanical loading. This is done by considering only two species of dislocations with opposite Burgers vector $\pm \mathbf{b}$ and a fugacity that is equal for both species and on each glide plane. Hence the fugacity can be written as $f_s(\mathbf{s}) = f_1 \rho_{gl}(\mathbf{s})$. By this means, it is expected that the dislocation density of both species is equal, and hence that the net dislocation content of the system is zero. In this special case, the sine-Gordon model is recovered.

The governing Eqs. (2.40) for \mathbf{B} and \mathbf{G} read for this special case

$$\begin{aligned}
 \int d^3 \mathbf{r}'' \mathbf{B}(\mathbf{r}'') : \mathbf{G}_0^{-1}(\mathbf{r}'', \mathbf{r}) &= -2f_1 \rho_{gl}(\mathbf{r}_{2D}) \hat{\boldsymbol{\xi}} \mathbf{b} \\
 \exp \left[-\frac{\beta}{2} \int dz dz' \hat{\boldsymbol{\xi}} \mathbf{b} : \mathbf{G}(\mathbf{r}_{2D}, z; \mathbf{r}_{2D}, z') : \hat{\boldsymbol{\xi}} \mathbf{b} \right] &\sin \left[\beta \int dz \mathbf{B}(\mathbf{r}_{2D}, z) : \hat{\boldsymbol{\xi}} \mathbf{b} \right] \\
 \mathbf{G}^{-1}(\mathbf{r} - \mathbf{r}') &= \mathbf{G}_0^{-1}(\mathbf{r} - \mathbf{r}') + 2\beta f_1 \rho_{gl}(\mathbf{r}_{2D}) \delta(\mathbf{r}_{2D} - \mathbf{r}'_{2D}) \hat{\boldsymbol{\xi}} \mathbf{b} \hat{\boldsymbol{\xi}} \mathbf{b} \\
 \cdot \exp \left[-\frac{\beta}{2} \int dz dz' \hat{\boldsymbol{\xi}} \mathbf{b} : \mathbf{G}(\mathbf{r}_{2D}, z; \mathbf{r}_{2D}, z') : \hat{\boldsymbol{\xi}} \mathbf{b} \right] &\cos \left[\beta \int dz \mathbf{B}(\mathbf{r}_{2D}, z) : \hat{\boldsymbol{\xi}} \mathbf{b} \right]
 \end{aligned} \tag{2.41}$$

The solution of Eq. (2.40) in the low temperature limit is $\mathbf{B} = 0$ and $\mathbf{G} = \mathbf{G}_0$, see A.8 for details.

The expectation values calculated from $\mathcal{R}_G[\Psi]$ instead of $\mathcal{R}[\Psi]$ are denoted by $\langle \dots \rangle_G$. First, the dislocation density is determined from Eq. (2.23)

$$\begin{aligned} \langle \omega_{\pm}(\mathbf{s}) \rangle_G &= f_1 \rho_{gl}(\mathbf{s}) \left\langle \exp \left[\pm i \beta (\hat{\boldsymbol{\xi}} \mathbf{b}) : \int dz \Psi(\mathbf{s}, z) \right] \right\rangle_G \\ &= f_1 \rho_{gl}(\mathbf{s}) \exp \left[-\frac{\beta}{2} \int dz dz' \hat{\boldsymbol{\xi}} \mathbf{b} : \mathbf{G}_0(\mathbf{0}, z - z') : \hat{\boldsymbol{\xi}} \mathbf{b} \right] \equiv \omega \rho_{gl}(\mathbf{s}) \end{aligned} \quad (2.42)$$

The average dislocation density of both species of dislocations is thus equal and spatially constant in the glide planes, which was to be expected. This implies that the net Burgers vector of the system vanishes. The above equation also implies that for low temperatures, and hence large β , the density of dislocations will be low.

Second, the two body dislocation density is calculated from the general expression in Eq. (2.26);

$$\begin{aligned} \langle \omega_{\alpha}(\mathbf{s}) \omega_{\alpha'}(\mathbf{s}') \rangle_G &= \omega \rho_{gl}(\mathbf{s}) \delta_{\alpha\alpha'} \delta(\mathbf{s}, \mathbf{s}') + \\ &+ \omega^2 \rho_{gl}(\mathbf{s}) \rho_{gl}(\mathbf{s}') \exp \left[-\beta \alpha \alpha' \hat{\boldsymbol{\xi}} \mathbf{b} : \int dz dz' \mathbf{G}_0(\mathbf{s} - \mathbf{s}', z - z') : \hat{\boldsymbol{\xi}} \mathbf{b} \right]. \end{aligned} \quad (2.43)$$

where $\alpha, \alpha' = \pm 1$ is the sign of the Burgers vector.

As explained in Sec. 2.3.3, the first term is the autocorrelation of a dislocation with itself. The second term is the pair correlation of dislocations. The exponential term is the Boltzmann weight of a dislocation pair that interacts with the effective interaction potential $\hat{\boldsymbol{\xi}} \mathbf{b} : \int dz dz' \mathbf{G}_0(\mathbf{s} - \mathbf{s}', z - z') : \hat{\boldsymbol{\xi}} \mathbf{b}$. Note that in \mathbf{G} , the effect of other dislocations via many body correlations is included as well.

We study the pair correlation of dislocations in details. The second contribution in the two body dislocation density (2.43) in terms of the fugacity reads

$$\begin{aligned} \langle \omega_{\alpha}(\mathbf{s}) \omega_{\alpha'}(\mathbf{s}') \rangle_G - \omega \rho_{gl}(\mathbf{s}) \delta_{\alpha\alpha'} \delta(\mathbf{s}, \mathbf{s}') &= \\ = f_1^2 \rho_{gl}(\mathbf{s}) \rho_{gl}(\mathbf{s}') \exp \left[-\beta \hat{\boldsymbol{\xi}} \mathbf{b} : \int dz dz' (\mathbf{G}_0(\mathbf{0}, z - z') + \alpha \alpha' \mathbf{G}_0(\mathbf{s} - \mathbf{s}', z - z')) : \hat{\boldsymbol{\xi}} \mathbf{b} \right]. \end{aligned} \quad (2.44)$$

As $\mathbf{G}_0(\mathbf{s}, z - z')$ is a positive, monotonically decaying function of \mathbf{s} (see A.6), this decays exponentially for large values of the coupling parameter Ξ . Hence it is only non-zero when the exponent vanishes, which is for $\alpha = -\alpha'$ and $\mathbf{s} = \mathbf{s}'$. This implies that it is thus likely to find a dislocation with opposite Burgers vector close to each dislocation. This pairing of dislocations was also found numerically by Vinogradov [113].

The exact position of two dislocations in a pair cannot be predicted using this theory. In this region, the core energy of dislocations plays an important role. But at such small length scales, linear elasticity is not valid. As linear elasticity was used to derive the partition function in this chapter, no results can be derived for these small length scales. In Fig. 2.3, the second term of Eq. (2.43) is plotted for two dislocations with equal Burgers vector. The parameters m and Ξ are chosen such that the plot is not completely dominated by the behaviour close to the origin. It can be seen that it is highly unlikely to find two equal screw dislocations with equal Burgers vector close to each other, and

that it is likely to find two equal edge dislocations above each other. This is in good agreement with what was found by Groma [37].

Third, the macroscopic variance of the distortion can be determined from Eq. (2.24). Note that from the Gaussian distribution in Eq. (2.37) it follows that $\langle \Psi(\mathbf{r}) \rangle = -\iota \mathbf{B}(\mathbf{r}) \approx 0$ and $\langle \Psi(\mathbf{r}) \Psi(\mathbf{r}') \rangle = \beta^{-1} \mathbf{G}(\mathbf{r} - \mathbf{r}') \approx \beta^{-1} \mathbf{G}_0(\mathbf{r} - \mathbf{r}')$ in the low temperature limit. This yields

$$\begin{aligned} \langle \Delta_{ij}^s(\mathbf{q}) \Delta_{i'j'}^s(\mathbf{q}) \rangle - \langle \Delta_{ij}^s(\mathbf{q}) \rangle \langle \Delta_{i'j'}^s(\mathbf{q}) \rangle &= \beta^{-1} \mathbb{S}^{ls} - (\mathbb{S} : \mathbf{q} \hat{\wedge}) \left(\mathbb{S} : \mathbf{q} \hat{\wedge} \right) \beta^{-1} \mathbf{G}_0(\mathbf{q}) \\ &= (\delta_{il} \delta_{jn} - Q_{il} Q_{jn}) \frac{1}{2\mu} \left(\delta_{ll'} \delta_{nn'} - \frac{\nu}{1-\nu} \delta_{ln} \delta_{l'n'} \right)^{ls} (\delta_{i'l'} \delta_{j'n'} - Q_{i'l'} Q_{j'n'}), \end{aligned} \quad (2.45)$$

see A.9 for details. This expression is the same as what would follow for an elasticity problem with the same microscopic stiffness tensor but without dislocations, see Eq. (2.22). Hence the stiffness does not change due to the presence of dislocations in the low temperature limit.

We can thus conclude that the Gaussian approximation of the full partition function is a useful tool to obtain explicit expressions for the observables of interest. In this section, it was shown that for metals at room temperature, dislocations will form strongly bound pairs that do not affect the compliance. It was also shown that the Gaussian approximation is a good approximation away from the phase transition between low and high temperature behaviour.

2.5 Summary and discussion

In this chapter, the partition function of a grand-canonical ensemble of dislocations in a finite medium was derived. The microscopic state space consisted of discrete dislocations embedded in an elastic continuum. The distortion field of the background matches the incompatibility imposed by the discrete dislocations. Mechanical boundary loading was applied by imposing the deformation of the boundary. The grand-canonical Boltzmann weight was integrated over the discrete dislocations and the elastic distortion fields to obtain the partition function as a functional of the temperature, the local chemical potential and the boundary deformation, see Eq. (2.17) for the result. This obtained partition function shows strong similarity with the widely studied sine-Gordon model.

The new aspects of the partition function, Eq. (2.17), derived in this chapter are:

- no a priori assumptions on temperature regime or specific dislocation arrangements;
- the incorporation of microscopic properties that have proven to be important for the mechanics of dislocations, namely the finite system size, the presence of glide planes, mechanical boundary loading and the tensorial character of the Nye tensor;
- the possibility to use a simple, Gaussian approximation to obtain explicitly the dominant behaviour of dislocations in the low temperature regime.

From the partition function, general expressions for the expectation value of the dislocation density and the elastic distortion field were derived. Likewise, the dislocation pair correlation and the compliance were calculated from derivatives of the partition function. Besides that, the relevant coupling parameter $\Xi \equiv \beta 2\mu Lb^2$ was identified from a scaling analysis on the partition function. Numerical values for aluminium at room temperature suggest that $\Xi > 100$, which indicates that dislocations in aluminium are in the low-temperature regime. The same is expected to hold for other metals.

As the system is considered at finite temperature, fluctuations in the energy are accounted for. In principle, the energy can be split in a contribution dependent on the dislocation configuration and a contribution of small fluctuations around this configuration. In this work, the distinction between these contributions is not made, and consequently, the temperature associated with both energy contributions is the same and equal to the physical temperature.

However, it is not always obvious that both energy contributions should be treated equally. Namely, the relaxation of the small fluctuations can be much faster than the relaxation of the configuration. In that case, the dislocations can be frozen in a glassy state. The small fluctuations can then be described by a Boltzmann distribution characterized by the physical temperature, while a second, phenomenological temperature is needed to describe the configuration. More literature on phenomenological temperatures can be found in e.g. [10][94].

Often, dislocation systems are studied at zero temperature, where the driving forces for dislocation dynamics do not have a random, fluctuating contribution. This is justified by the value of the coupling parameter Ξ obtained in this contribution.

Our choice to treat the system nevertheless at finite temperature is in our opinion merely a matter of taste. Namely, the limit $T \rightarrow 0$ could be taken afterwards, which should yield the same result. The advantage of an analysis at finite temperature is twofold: first, the effect of a small-but-finite temperature or a finite phenomenological temperature could be derived; and second, the calculation at finite temperature can be easier as the minimum energy state does not have to be known exactly.

The main obstacle to use the partition function in Eq. (2.17) is the non-Gaussian functional integral over the auxiliary field Ψ that can not be performed. As shown in Sec. 2.4, in the low temperature regime approximating the functional integral by a Gaussian is a suitable approximation that allows one to determine accurate, explicit expressions for the observables. From the Gaussian approximation, it was concluded that dislocations in the low temperature regime combine into strongly bound pairs of dislocations with opposite Burgers vector, as was also found by Vinogradov [113]. Moreover, the presence of dislocations does not influence the compliance.

Future research should therefore focus on finding approximation methods that are valid for a wider class of cases. Possible approximation techniques can be obtained from the similarity between the partition function found in this chapter and that of other systems with Coulombic interactions, for example ions in water, as obtained by Netz [83], charged plasmas, see [114] and the sine-Gordon model. This suggests that widely studied approximation techniques for electrostatics can be applicable to describe systems of dislocations as well. Examples of such techniques are density functional theory [54], renormalization group theory for the sine-Gordon model [116, 1], a saddle point approximation for the partition function which yields Poisson-Boltzmann theory, see [95], and the Villain ap-

proximation, see [61].

The difference between our partition function and electrostatics is that our field Ψ is a tensor field instead of a scalar electric potential field. This difference originates from the vector character of the ‘charge’ of a dislocation, namely the Burgers vector \mathbf{b} , as opposed to scalar values for the electric charge. Moreover, dislocations are coupled to the elastic distortion field with a rotation as in Eq. (2.2), instead of the divergence-type coupling between charges and the electric field in Gauss’ law. The anisotropy of the interaction potential between dislocations, as determined in Eq. A.19, is a direct consequence of the vectorial character of the dislocation ‘charge’. However, we expect that approximation techniques used for electrostatics can be modified to make them applicable for tensor fields as well.

The free energy expression of dislocations can be used as an ingredient to formulate the dynamics of the system. Examples of free energy-based dynamic frameworks are the strain gradient plasticity model of Gurtin [42], Ginzburg-Landau theory [108], the bracket formalism of Beris and Edwards [8] and the GENERIC framework [31], [89]. In these, derivatives of the free energy are used as driving forces for dislocation dynamics.

Besides that, explicit dislocation pair correlations can be determined from the partition function obtained here. These can be used as a closure for the BBGKY hierarchy of dynamical dislocation equations. The pair correlation obtained here for statistically stored dislocations can already be used as a reference case to check whether the proposed closure has the correct limiting behaviour.

Chapter 3

Microscopically derived free energy of dislocations

Largely reproduced from: Kooiman, M., Hütter, M., and Geers, M.G.D., Microscopically derived free energy of dislocations. *Journal of the Mechanics and Physics of Solids*, 78: 186-209 (2015)



Abstract

The dynamics of large amounts of dislocations is the governing mechanism in metal plasticity. The free energy of a continuous dislocation density profile plays a crucial role in the description of the dynamics of dislocations, as free energy derivatives act as the driving forces of dislocation dynamics.

In this contribution, an explicit expression for the free energy of straight and parallel dislocations with different Burgers vectors is derived. The free energy is determined using systematic coarse-graining techniques from statistical mechanics. The starting point of the derivation is the grand-canonical partition function derived in an earlier work, in which we accounted for the finite system size, discrete glide planes and multiple slip systems. In this chapter, the explicit free energy functional of the dislocation density is calculated and has, to the best of our knowledge, not been derived before in the present form.

The free energy consists of a mean-field elastic contribution and a local defect energy, that can be split into a statistical and a many-body contribution. These depend on the density of positive and negative dislocations on each slip system separately, instead of GND-based quantities only. Consequently, a crystal plasticity model based on the here obtained free energy, should account for both statistically stored and geometrically necessary dislocations.

3.1 Introduction

The governing mechanism of metal plasticity is the dynamics of dislocations, which are line-like defects in the crystal structure. Crystals can contain up to 10^9 dislocation lines intersecting a square millimeter. Therefore, the collective behavior of many dislocations together determines the mechanical properties associated with crystal plasticity.

A number of dynamical frameworks have been developed to describe the dynamics of dislocation densities, in which the free energy plays a key role, see e.g. [32, 39, 41, 42, 43, 44]. Moreover, stationary states have been derived from the free energy, see eg. [35, 99, 29]. To obtain the equilibrium behavior and driving forces for dislocations on a macroscopic scale, it is thus necessary to have a free energy expression that results from coarse-graining the microscopic description of dislocations. Furthermore, a derivation from the microscopic level could help in choosing proper macroscopic variables for a dynamical model.

In the literature, several attempts have been made to retrieve the free energy of dislocations. First, different phenomenological assumptions are made to match different macroscopic plasticity models, see eg. [21, 7, 105, 62, 4]. These free energy expressions are all local or weakly non-local in terms of the dislocation densities.

Second, straight dislocations were considered as an example of two-dimensional Coulomb particles that interact with a logarithmic interaction potential, see e.g. the work of Kostelitz and Thouless [63, 81, 82], Mizushima [78], Ninomiya [84] and Yamamoto [118]. In these papers, the free energy of systems with an homogeneous dislocation density was derived. This system exhibits a dislocation mediated melting transition. Below the critical temperature, dislocations occur in tightly bound pairs, but above this temperature, dislocation pairs tend to unbind, and thereby destroy the long-range order in a two-dimensional crystal. However, the anisotropic character of the dislocation interaction was not taken into account in these works, and the effect of mechanical loading was not considered.

Third, the free energy of dislocations was derived by Groma and coworkers using a mean-field assumption in the coarse-graining [33, 35, 36]. As the physical temperature of the system is almost zero relative to the other characteristic energy scales at hand, a second, phenomenological temperature is introduced to obtain a non-vanishing statistical contribution, which results in screening.

Fourth, the equilibrium dislocation profile of a single slip system of dislocations was determined by means of Γ -convergence of the energy expression, see [99, 29]. In this work, it was assumed that the dislocations are arranged in wall structures on equally spaced glide planes and that the system is at zero temperature.

Despite all these efforts, no explicit free energy expression has been proposed yet, that is derived from the microscopic properties of the system, and thus includes the anisotropy of the dislocation interaction, the finite system size and the presence of glide planes, and which is valid in different temperature regimes. The aim of this chapter is to obtain such a free energy expression. In this contribution, we limit ourselves to straight dislocations with parallel line orientation.

The free energy is derived by systematically coarse-graining the microscopic description of dislocations as used in Discrete Dislocation Dynamics (DDD) simulations. In Chap. 2, we derived the partition function of dislocations for a grand-canonical ensemble of straight and parallel dislocations. In this contribution, we derive the Helmholtz free energy of

dislocations from this by means of a Legendre transform. The obtained free energy contains elastic energy and statistical terms, as found earlier by Groma [35], but yields also a many-body contribution beyond these mean-field terms. It is, to our best knowledge, for the first time that the free energy was derived by coarse-graining only.

The resulting free energy depends on densities of positive and negative dislocations separately for each slip system. This implies that the defect forces in crystal plasticity models (see e.g. [43]) cannot be determined in terms of GND densities alone.

The chapter is organized as follows. In Sec. 4.3, we discuss the microscopic and macroscopic descriptions of the system. Then, we briefly outline the derivation of the grand-canonical partition function and perform a Legendre transform to obtain the canonical free energy in Eq. (3.22). In Sec. 3.3, we discuss the interpretation and limitations of the obtained free energy expression. In Sec. 3.4, three special cases are considered in which the free energy expression simplifies considerably, namely a local density approximation (LDA), the zero temperature limit, and equally spaced glide planes. In Sec. 3.5, the connection is made between this work and current dislocation-based crystal plasticity models.

3.2 Derivation

3.2.1 Mathematical Preliminaries

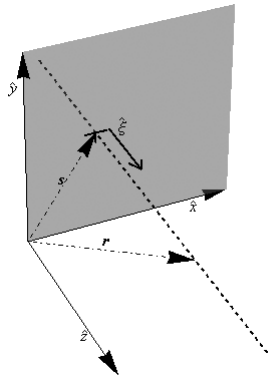


Figure 3.1: Sketch of the coordinate system used in this chapter.

In this chapter, both two-dimensional and three-dimensional position vectors are used. To avoid confusion, the two-dimensional position vector is denoted by s and consists of an x and a y -coordinate. Integration over this vector is denoted by $\int dA$. On the other hand, the three-dimensional position vector is denoted by r and consists of an x , y and z -coordinate. Integration over the 3D position vector is denoted by $\int dV$.

The line direction $\hat{\xi}$ of the straight and parallel dislocations is parallel to the \hat{z} -direction, and the position in this direction is denoted by z . Thus, the vector r can be expressed in s and z by $r = s + z\hat{\xi}$, and analogously, the integration over 3D position vectors can be expressed as $\int dV = \int dA \int dz$. See Fig. 3.1 for a sketch of the coordinate system.

In this work, the cross product on a tensor is interpreted as the cross product on the first index, so the cross product between vector \mathbf{v} and second rank tensor \mathbf{A} is $(\mathbf{v} \times \mathbf{A})_{ij} = \epsilon_{ikl} v_k A_{lj}$, where ϵ is the anti-symmetric Levi-Civita tensor. A contraction of a second rank tensor \mathbf{A} and a fourth rank tensor \mathbf{B} is defined by $(\mathbf{A} : \mathbf{B})_{kl} = A_{ij} B_{ijkl}$, and the trace of a fourth rank tensor \mathbf{B} is $\text{Tr}[\mathbf{B}] = B_{ijij}$. The symmetric and anti-symmetric parts of a second rank tensor are indicated with a superscript s and a; $(\mathbf{A}^{\text{s,a}})_{ij} = (A_{ij} \pm A_{ji})/2$. The \otimes -symbol is used to indicate a dyadic product.

In this work, round brackets indicate a function, and square brackets indicate a functional. Furthermore, Fourier transforms are used multiple times in this contribution. We use the non-unitarian convention here, and hence the 2D Fourier transform is defined by

$$\mathcal{F}_{2D}[f(\mathbf{s})](\mathbf{q}_{2D}) = \tilde{f}(\mathbf{q}_{2D}) = \int dA f(\mathbf{s}) e^{-i\mathbf{q}_{2D} \cdot \mathbf{s}}, \quad (3.1)$$

where \mathbf{q}_{2D} is the 2D wave-vector. Consequently, the inverse 2D Fourier transform is defined by

$$\mathcal{F}_{2D}^{-1}[\tilde{f}(\mathbf{q}_{2D})](\mathbf{s}) = \int \frac{d^2 \mathbf{q}_{2D}}{(2\pi)^2} \tilde{f}(\mathbf{q}_{2D}) e^{i\mathbf{q}_{2D} \cdot \mathbf{s}}. \quad (3.2)$$

The Fourier transform in 3D is defined analogously.

3.2.2 Multiscale description of the problem

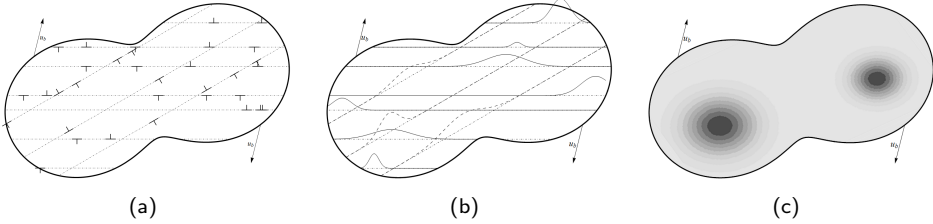


Figure 3.2: In Fig. 3.2(a), the microstate is depicted. The microstate is characterized by the positions of discrete dislocations in an elastic body Ω subjected to a boundary deformation \mathbf{u}_b . In Fig. 3.2(b), the macrostate is depicted. The macrostate is characterized by the density of dislocations in the same elastic body Ω , subjected to the same boundary deformation \mathbf{u}_b . The density of dislocations can be defined either on discrete glide planes only, see e.g. Fig. 3.2(b), or on the whole space, see e.g. Fig. 3.2(c). The body is held at a fixed temperature T .

Microscale The microscopic description of our system is closely related to the description of crystals with dislocations used in DDD simulations, see e.g. [110].

A linear elastic body is considered. The volume of the body is denoted by Ω , and the elastic properties of the matrix material are governed by the fourth order stiffness tensor \mathbb{C} that relates the stress to the strain. For convenience, the fourth order compliance tensor \mathbb{S} is also defined as the inverse of the stiffness tensor: $\mathbb{C}_{ijkl} \mathbb{S}_{klj' i'} = \delta_{ii'} \delta_{jj'}$, where the Einstein summation convention is used.

In this linear elastic body, straight and parallel dislocations are embedded. Each dislocation is characterized by its Burgers vector \mathbf{b} and the direction of its line vector $\hat{\xi}$. As straight and parallel dislocations are considered, the line vector is equal for all dislocations. In this study, climb of dislocations is not accounted for. For the static states of the system, this implies that dislocation can only be positioned on discrete glide planes.

The elastic body is furthermore subjected to a boundary deformation \mathbf{u}_b . The dependence of the free energy on the boundary deformation obtained in Chap. 2 is implicit. Therefore, two quantities related to \mathbf{u}_b are defined here. Since the positions of the dislocations are independent of the z -coordinate, it only makes sense to consider deformations of the boundary that are independent of z as well.

Hypothetical strain- and stress fields Δ_0 and σ_0 can be defined as the strain- and stress field one would find in the same elastic body Ω with the same boundary deformation \mathbf{u}_b , but without dislocations. These fields have to satisfy mechanical equilibrium in the bulk, and it has to match the imposed boundary deformation \mathbf{u}_b :

$$\Delta_0 \equiv (\nabla \mathbf{u})^s \quad (3.3a)$$

$$\sigma_0 \equiv \mathbb{C} : \Delta_0 \quad (3.3b)$$

$$\nabla \cdot (\sigma_0) = 0 \quad (3.3c)$$

$$\mathbf{u} = \mathbf{u}_b. \quad (3.3d)$$

Due to Eq. (3.3c), a second field Ψ_0 can be defined by

$$\nabla \times \Psi_0 \equiv \sigma_0. \quad (3.4)$$

The field Ψ_0 is thus uniquely defined up to a gradient. The Beltrami stress potential Φ_0 , as used in [12], is related to Ψ_0 by $\Psi_0 = (\nabla \times \Phi_0)^T$, where T indicates the transpose. Note that, as \mathbf{u}_b is independent of the z -coordinate, both Δ_0 and Ψ_0 are independent of the z -coordinate as well.

The field Ψ_0 turns out to be convenient to work with, as it is related to the Peach-Koehler force on a dislocation line. Namely, a dislocation with Burgers vector \mathbf{b} would experience the following Peach-Koehler force in the hypothetical strain field Δ_0 :

$$\begin{aligned} F_{PK,0} &= \int dz (\sigma_0(\mathbf{s}) \cdot \mathbf{b}) \times \hat{\xi} = \int dz (\nabla \times \Psi_0(\mathbf{s}) \cdot \mathbf{b}) \times \hat{\xi} \\ &= \int dz (\hat{\xi} \cdot \nabla) \Psi_0(\mathbf{s}) \cdot \mathbf{b} - \nabla \left(\hat{\xi} \otimes \mathbf{b} : \Psi_0(\mathbf{s}) \right), \end{aligned} \quad (3.5)$$

which is the integral of the Peach-Koehler force on a dislocation line element, see e.g. [71], integrated along the line. The first term vanishes as Ψ_0 is independent of the z -coordinate, and hence $(\hat{\xi} \cdot \nabla) \Psi_0(\mathbf{s}) = \partial_z \Psi_0(\mathbf{s}) = 0$. Then this expression implies that $\int dz \hat{\xi} \otimes \mathbf{b} : \Psi_0(\mathbf{s}, z)$ can be interpreted as the potential energy of a dislocation with Burgers vector \mathbf{b} in the strain field Δ_0 . Therefore, we define the Peach-Koehler potential for dislocations with Burgers vector \mathbf{b} by

$$V_{b,0}(\mathbf{s}) = \int dz \hat{\xi} \otimes \mathbf{b} : \Psi_0(\mathbf{s}). \quad (3.6)$$

This potential is uniquely defined up to a constant. The free energy will only depend on \mathbf{u}_b via Δ_0 and $V_{b,0}$.

Finally, microstates are characterized by the strain field Δ in the body. This strain field has to match the incompatibility imposed by the dislocations and the applied boundary deformation \mathbf{u}_b , but it does not have to be in mechanical equilibrium. This implies that we allow for elastic waves or phonons in the material, on top of a mechanical equilibrium state.

Macroscale On the macroscopic level, the same elastic body Ω with the same bare stiffness tensor \mathbb{C} is considered. This body is subjected to the same boundary deformation \mathbf{u}_b . Therefore, in view of Eqs. (3.3) and (3.6), Δ_0 and $V_{b,0}$ are also defined on the macroscopic scale. Hence no coarse-graining of the boundary conditions is considered. But rather than discrete dislocation positions, the coarse-grained density profile of dislocations with Burgers vector \mathbf{b} , $\rho_b(\mathbf{s})$, is used as a variable on the macroscopic level.

For the coarse-graining procedure it is more convenient to control the average of the dislocation density profile by controlling the local chemical potential $\mu_b(\mathbf{s})$ of dislocations with Burgers vector \mathbf{b} . This is called the grand-canonical ensemble. We refer the reader to [14] for more details. It can be proven that the relation between $\mu_b(\mathbf{s})$ and $\rho_b(\mathbf{s})$ is unique, see e.g. [23]. This means that for every density profile one can find the corresponding local chemical potential, and that every local chemical potential corresponds to just one dislocation density profile. Hence once the free energy is known as a functional of the local chemical potential, it can also be obtained in terms of the density profile.

The coarse-graining of dislocation positions can be performed in two ways. First, one can average the density in the glide plane, but keep the discrete character of the glide planes, as depicted in Fig. 3.2(b). The glide plane positions should then be considered as material parameters. An example of this is worked out in Sec. 3.4.2, where it is assumed that glide planes are equally spaced, and the spacing h is a material parameter.

Second, the averaging can be done both in the glide plane and in the direction perpendicular to it, as depicted in Fig. 3.2(c). Then, the glide plane distribution is no longer a material parameter. An example of this averaging is worked out in Sec. 3.4.1.

In both cases, the free energy can be determined by the expression obtained in this chapter. In the first case, the density should be zero in between the glide planes, and only take non-zero values at these glide planes. In the second case, there are no restrictions on the density profile.

One could also consider a hybrid version of the above two averaging techniques, where glide planes are smeared out, but not necessarily to a homogeneous profile. This would imply that some regions are almost empty (these are the regions in between the smeared out glide planes), whilst others are more likely to contain a lot of dislocations. Such a hybrid version is not considered here.

3.2.3 Coarse-graining method

In this contribution, the coupling between the microscale and the macroscale is made with averaging techniques from statistical physics. This means that the macroscopic free

energy F can be determined from the so-called partition function Z , see e.g. [14]:

$$F = -k_B T \ln Z. \quad (3.7)$$

The partition sum is a sum over all microstates weighted with their Boltzmann weight, and hence it can, in principle, be calculated from the microscopic system description. The Boltzmann weight depends on the macroscopic state variables and is defined as the exponent of minus the energy E_{micro} of the microstate divided by the thermal energy; $\exp(-E_{\text{micro}}/k_B T)$. Here, k_B is the Boltzmann constant, equal to $1.4 \times 10^{-23} \text{ J/K}$, and T is the absolute temperature. The Boltzmann weight is a measure for how likely a microstate is; microstates with lower energy are more likely, and this preference is stronger at lower temperature T . So to conclude, the partition function reads:

$$Z = \sum_{\text{microstates}} \exp(-E_{\text{micro}}/k_B T). \quad (3.8)$$

In Chap. 2, we already determined an expression for the partition function of a crystal with dislocations. In this chapter, this partition sum is used to obtain an explicit expression for the free energy as a function of the dislocation density.

When the free energy is calculated as in Eq. (3.7), local organization of dislocations is also accounted for. Namely, microstates in which dislocations locally organize themselves in low energy states are more likely, and hence contribute more to the partition function. This lowers the overall free energy in the system.

In this work, average quantities should be interpreted as the statistical average, as opposed to for example a spatial or time averages. Thus, if one would be able to consider multiple microscopic realizations of the same macroscopic system, this is the average one would find. For perfectly ergodic systems, the statistical average matches the time average by definition.

It has been suggested that the ergodicity assumption might not be valid on realistic timescales for dislocation systems. Namely, the behavior in discrete dislocation simulations is very sensitive to the initial dislocation distribution, as the system exhibits high energy barriers. However, it has been shown recently, see [59], that the statistical average of the behavior in discrete dislocation simulations over many randomly selected initial dislocation distributions gives realistic predictions for the response of large systems.

Therefore, it is assumed here that a statistical average is representative for the macroscopically observed behavior.

3.2.4 The partition sum

To evaluate the partition function in Eq. (3.8), one should sum the Boltzmann weight over all possible microstates. The summation over microstates involves an integration over the positions of the dislocations in the glide-plane, and a summation over all possible numbers of dislocations from zero to infinity in each glide plane.

Furthermore, the summation involves an integration over all possible strain fields Δ that match the incompatibility imposed by the dislocations and the applied deformation of the boundary. The integration over fields can be performed by means of a path integral.

The Boltzmann weight follows from the energy of a microstate, see Eq. (3.8). This energy

consists of the elastic strain energy and the so-called chemical energy of dislocations. The elastic energy reads

$$E_{\text{elas}} = \frac{1}{2} \int dV \mathbf{\Delta} : \mathbb{C} : \mathbf{\Delta}. \quad (3.9)$$

This automatically incorporates the energy due to the dislocations and due to boundary conditions, as the elastic strain field in the body matches the incompatibility of the dislocations and the imposed boundary conditions.

The chemical energy of a dislocation with Burgers vector \mathbf{b} at position \mathbf{s} is minus the chemical potential $\mu_{\mathbf{b}}(\mathbf{s})$ at that position. The total chemical energy of the dislocations together is thus

$$E_{\text{chem}} = - \sum_{\mathbf{b}} \left(\sum_{k=1}^{N_{\mathbf{b}}} \mu_{\mathbf{b}}(\mathbf{s}_k) \right), \quad (3.10)$$

where $N_{\mathbf{b}}$ is the number of dislocations with Burgers vector \mathbf{b} and \mathbf{s}_k is the position of the k^{th} dislocation.

The summation over microstates, as described in the previous paragraph, was performed analytically in our earlier work. The only approximation that was made in the derivation is that the system is far from its transition point. In Sec. 3.3.3, we will comment further on the implications of this approximation. In this section, the results for the partition function and dislocation density of Chap. 2 are summarized.

The partition function is most conveniently expressed in terms of the average dislocation

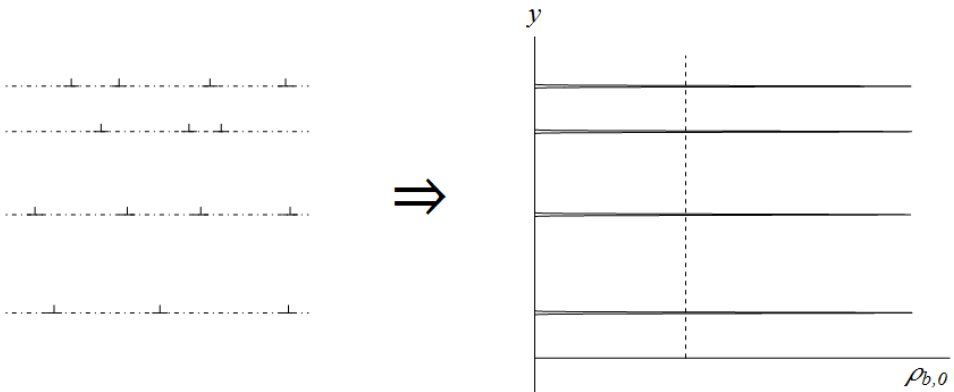


Figure 3.3: When glide planes are defined on the macroscopic scale (as in Fig. 3.2(b)), the parameter $\rho_{\mathbf{b},0}(\mathbf{s})$ indicates the presence of glide planes (solid line). When glide planes are not defined (as in Fig. 3.2(c)), $\rho_{\mathbf{b},0}(\mathbf{s})$ is a spatial constant (dashed line).

density, although it is a functional of the chemical potential, and not of the dislocation

density. The partition function and dislocation density obtained in Chap. 2 read

$$Z[\mu_{\mathbf{b}}(\mathbf{s}), \mathbf{u}_{\mathbf{b}}, T] = \exp \left[\frac{1}{2k_B T} \int dV \Delta_0 : \mathbb{C} : \Delta_0 + \sum_{\mathbf{b}} \int dA \rho_{\mathbf{b}}(\mathbf{s}) + \right. \quad (3.11a)$$

$$\begin{aligned} & + \frac{1}{2k_B T} \sum_{\mathbf{b}, \mathbf{b}'} \int dA dA' \rho_{\mathbf{b}}(\mathbf{s}) u_{\mathbf{b}, \mathbf{b}'}(\mathbf{s}, \mathbf{s}') \rho_{\mathbf{b}'}(\mathbf{s}') + \sum_{\mathbf{b}} \frac{1}{2k_B T} \int dA \rho_{\mathbf{b}}(\mathbf{s}) u_{\text{eff}, \mathbf{b}, \mathbf{b}}(\mathbf{0}) \\ & \left. - \frac{1}{2} \text{Tr} \left[\ln \left[l\delta(\mathbf{s} - \mathbf{s}') + \frac{1}{k_B T} \sum_{\mathbf{b}} \int dz dz' G_0(\mathbf{s}, z; \mathbf{s}', z') : \rho_{\mathbf{b}}(\mathbf{s}') \hat{\xi} \otimes \mathbf{b} \otimes \hat{\xi} \otimes \mathbf{b} \right] \right] \right] \\ \rho_{\mathbf{b}}(\mathbf{s}) = & \rho_{\mathbf{b}, 0}(\mathbf{s}) \exp \left[\frac{\mu_{\mathbf{b}}(\mathbf{s}) - V_{\mathbf{b}, 0}(\mathbf{s})}{k_B T} \right. \quad (3.11b) \\ & \left. - \frac{1}{k_B T} \sum_{\mathbf{b}'} \int dA u_{\mathbf{b}, \mathbf{b}'}(\mathbf{s}, \mathbf{s}') \rho_{\mathbf{b}'}(\mathbf{s}') - \frac{1}{2k_B T} u_{\text{eff}, \mathbf{b}, \mathbf{b}}(\mathbf{0}) \right] \end{aligned}$$

where $\rho_{\mathbf{b}, 0}(\mathbf{s})$ is a parameter indicating glide planes when these are defined on the macroscopic scale. In this case, $\rho_{\mathbf{b}, 0}(\mathbf{s})$ is zero in those points where there is no discrete glide plane for dislocations with Burgers vector \mathbf{b} and a Dirac delta function at the glide planes, see Fig. 3.3. When no discrete glide planes are considered, as in Fig. 3.2(c), the parameter $\rho_{\mathbf{b}, 0}(\mathbf{s})$ is a spatial constant. The trace runs over both discrete and continuous indices. The natural logarithm in the last term is the logarithm of an operator, and not just the logarithm of the components. This means that the last term in Eq. (3.11a) can be written as the sum of the logarithm of all eigenvalues of the operator $l\delta(\mathbf{s} - \mathbf{s}') + \frac{1}{k_B T} \sum_{\mathbf{b}} \int dz dz' G_0(\mathbf{s}, z; \mathbf{s}', z') : \rho_{\mathbf{b}}(\mathbf{s}') \hat{\xi} \otimes \mathbf{b} \otimes \hat{\xi} \otimes \mathbf{b}$.

The dependence on the boundary deformation $\mathbf{u}_{\mathbf{b}}$ is via $V_{\mathbf{b}, 0}$, and the functions $G_0(\mathbf{r}; \mathbf{r}')$, $u_{\mathbf{b}, \mathbf{b}'}(\mathbf{s}, \mathbf{s}')$ and $u_{\text{eff}, \mathbf{b}, \mathbf{b}'}(\mathbf{s}, \mathbf{s}')$ are the bare Greens function and the bare and effective interaction between dislocations, that will be defined next.

The function $u_{\mathbf{b}, \mathbf{b}'}(\mathbf{s}, \mathbf{s}')$ is the interaction energy of two dislocations with Burgers vector \mathbf{b} and \mathbf{b}' at positions \mathbf{s} and \mathbf{s}' in finite space. The interaction energy is the extra energy that is needed to create a dislocation in the material while another dislocation is already present. The interaction energy can be written in terms of the Green's function $G_{0, ijkl}(\mathbf{r}, \mathbf{r}')$ by

$$u_{\mathbf{b}, \mathbf{b}'}(\mathbf{s}, \mathbf{s}') = \int dz dz' \hat{\xi} \otimes \mathbf{b} : G_{0, ij'ij'}(\mathbf{s}, z; \mathbf{s}', z') : \hat{\xi} \otimes \mathbf{b}'. \quad (3.12)$$

In Chap. 2, it was found that the fourth order tensor $G_0(\mathbf{r}, \mathbf{r}')$ is such that, for all fields $\Psi(\mathbf{r})$ that are divergence free ($\nabla \cdot \Psi = 0$) and for which $\nabla \times \Psi(\mathbf{r})$ is symmetric, one finds

$$\int dV \nabla \times \Psi(\mathbf{r}) : \mathbb{S} : \nabla \times \Psi(\mathbf{r}) = \int dV dV' \Psi(\mathbf{r}) : G_0^{-1}(\mathbf{r}, \mathbf{r}') : \Psi(\mathbf{r}'). \quad (3.13)$$

Furthermore, $G_0^{-1}(\mathbf{r}, \mathbf{r}')$ is defined such that the RHS of this equation is infinite for all fields that are either not divergence free or for which $\nabla \times \Psi(\mathbf{r})$ is not symmetric. The defining equation (3.13) of $G_0^{-1}(\mathbf{r}, \mathbf{r}')$ is thus rather implicit and cannot be written in an easier form. Namely, the spatial integration acts over a finite volume, and hence the above

cannot be written in a partial differential equation for $G_0(\mathbf{r}, \mathbf{r}')$. However, in this form, Eq. (3.13) incorporates the effect of finite space and can be used to derive a differential equation for the dislocation density profile.

It was shown that in infinite space and for an isotropic material, Eqs. (3.12) and (3.13) yield the interaction energy per unit length between dislocations as known from literature, see e.g. [49, 97]:

$$\tilde{G}_{0,ijkl}(\mathbf{q}) = \frac{\mu}{q^2} \left(Q_{ik}Q_{jl} + R_{il}R_{jk} + \frac{2\nu}{1-\nu}R_{ij}R_{kl} \right), \quad (3.14a)$$

$$\begin{aligned} \Rightarrow \frac{u_{\mathbf{b},\mathbf{b}'}(\Delta\mathbf{s})}{L} &= \frac{\mu}{2\pi} \left(\left(\mathbf{b} \cdot \hat{\boldsymbol{\xi}}\mathbf{b}' \cdot \hat{\boldsymbol{\xi}} + \frac{(\mathbf{b} \times \hat{\boldsymbol{\xi}}) \cdot (\mathbf{b}' \times \hat{\boldsymbol{\xi}})}{1-\nu} \right) \ln \left(\frac{|\Delta\mathbf{s}|}{s_0} \right) \right. \\ &\quad \left. + \frac{(\mathbf{b} \times \hat{\boldsymbol{\xi}}) \cdot \Delta\mathbf{s}(\mathbf{b}' \times \hat{\boldsymbol{\xi}}) \cdot \Delta\mathbf{s}}{(1-\nu)|\Delta\mathbf{s}|^2} \right) \end{aligned} \quad (3.14b)$$

where $Q_{ij} = \delta_{ij} - q_i q_j / q^2$ and $R_{ij} = \epsilon_{ijk} q_k / q$, where ϵ_{ijk} is the anti-symmetric Levi-Civita tensor. Furthermore, μ is the shear modulus, and ν is the Poisson's ratio, such that the isotropic compliance tensor reads $S_{ijij'} = 2\mu(\delta_{ij'}\delta_{jj'} - \frac{\nu}{1+\nu}\delta_{ij}\delta_{ij'})$.

The function $u_{\text{eff},\mathbf{b},\mathbf{b}'}(\mathbf{s}, \mathbf{s}')$ in Eq. (3.11b) can be interpreted as the effective interaction energy between two dislocations, in which the effect of screening is incorporated as well. It can analogously be written as

$$u_{\text{eff},\mathbf{b},\mathbf{b}'}(\mathbf{s}, \mathbf{s}') = \int dzdz' \hat{\boldsymbol{\xi}} \otimes \mathbf{b} : \mathbf{G}_{ijij'}(\mathbf{s}, z; \mathbf{s}', z') : \hat{\boldsymbol{\xi}} \otimes \mathbf{b}', \quad (3.15)$$

where it was shown in Eq. (2.40) that the two tensors G_0 and G are related by the implicit relation

$$\begin{aligned} G(\mathbf{r}, \mathbf{r}') &= G_0(\mathbf{r}, \mathbf{r}') \\ &+ \sum_{\mathbf{b}} \int dzdz' \int dA'' G(\mathbf{r}; \mathbf{s}'', z) : \rho_{\mathbf{b}}(\mathbf{s}'') \hat{\boldsymbol{\xi}} \otimes \mathbf{b} \otimes \hat{\boldsymbol{\xi}} \otimes \mathbf{b} : G_0(\mathbf{s}'', z'; \mathbf{r}'). \end{aligned} \quad (3.16)$$

Then, $u_{\text{eff},\mathbf{b},\mathbf{b}}(\mathbf{0})/2$ can be interpreted as the effective self-energy of a dislocation with Burgers vector \mathbf{b} . Note that the relation between $\rho_{\mathbf{b}}(\mathbf{s})$ and $\mu_{\mathbf{b}}(\mathbf{s})$ in Eq. (3.11b) is an implicit expression as the terms in the exponent depend on the density. The dependence of Z on the local chemical potential $\mu_{\mathbf{b}}(\mathbf{s})$ in Eq. (3.11a) is therefore implicit as well.

The average density profile for a given chemical potential can be determined directly from Eq. (3.11b) without using a free energy expression in terms of the density profile. However, the free energy does not only yield the equilibrium dislocation configuration, but also other static properties of the system, and the driving forces for dislocation dynamics.

From Eq. (3.7) and (3.11a), the thermodynamic potential can be determined:

$$\begin{aligned} \Omega[\mu_{\mathbf{b}}(\mathbf{s}), \mathbf{u}_{\mathbf{b}}, T] &\equiv -k_B T \ln(Z[\mu_{\mathbf{b}}(\mathbf{s}), \mathbf{u}_{\mathbf{b}}, T]) = \frac{1}{2} \int dV \Delta_0 : \mathbb{C} : \Delta_0 - \\ &- \frac{1}{2} \sum_{\mathbf{b}, \mathbf{b}'} \int dA dA' \rho_{\mathbf{b}}(\mathbf{s}) u_{\mathbf{b}, \mathbf{b}'}(\mathbf{s}, \mathbf{s}') \rho_{\mathbf{b}'}(\mathbf{s}') \\ &- k_B T \sum_{\mathbf{b}} \int dA \rho_{\mathbf{b}}(\mathbf{s}) - \frac{1}{2} \sum_{\mathbf{b}} \int dA \rho_{\mathbf{b}}(\mathbf{s}) u_{\text{eff}, \mathbf{b}, \mathbf{b}}(\mathbf{0}) \\ &+ \frac{k_B T}{2} \text{Tr} \left[\ln \left(|\delta(\mathbf{s} - \mathbf{s}') + \frac{1}{k_B T} \sum_{\mathbf{b}} \int dz dz' G_0(\mathbf{s}, z; \mathbf{s}', z') : \rho_{\mathbf{b}}(\mathbf{s}') \hat{\xi} \otimes \mathbf{b} \otimes \hat{\xi} \otimes \mathbf{b} \right) \right]. \end{aligned} \quad (3.17)$$

3.2.5 Legendre transform

To obtain the free energy from the thermodynamic potential of the grand-canonical ensemble, the following Legendre transform is applied

$$F[\rho_{\mathbf{b}}(\mathbf{s}), \mathbf{u}_{\mathbf{b}}, T] = \Omega[\mu_{\mathbf{b}}[\rho_{\mathbf{b}}(\mathbf{s}), \mathbf{u}_{\mathbf{b}}, T; \mathbf{s}], \mathbf{u}_{\mathbf{b}}, T] + \sum_{\mathbf{b}} \int dA \rho_{\mathbf{b}}(\mathbf{s}) \mu_{\mathbf{b}}[\rho_{\mathbf{b}}(\mathbf{s}), \mathbf{u}_{\mathbf{b}}, T; \mathbf{s}], \quad (3.18)$$

where $\frac{\delta \Omega}{\delta \mu_{\mathbf{b}}(\mathbf{s})} = \rho_{\mathbf{b}}(\mathbf{s})$. It can be checked that this is indeed the case by taking the derivative with respect to $\mu_{\mathbf{b}}(\mathbf{s})$ in Eq. (3.17). To perform this transformation, it is thus necessary to find the chemical potential in terms of the dislocation density profile. This can be done by inverting Eq. (3.11b):

$$\mu_{\mathbf{b}}(\mathbf{s}) = k_B T \ln \left(\frac{\rho_{\mathbf{b}}(\mathbf{s})}{\rho_{0, \mathbf{b}}(\mathbf{s})} \right) + V_{\mathbf{b}, 0}(\mathbf{s}) + \sum_{\mathbf{b}'} \int dA' u_{\mathbf{b}, \mathbf{b}'}(\mathbf{s}, \mathbf{s}') \rho_{\mathbf{b}'}(\mathbf{s}') + \frac{1}{2} u_{\text{eff}, \mathbf{b}, \mathbf{b}}(\mathbf{0}). \quad (3.19)$$

Combining Eqs. (3.17), (3.18) and (3.19) yields:

$$\begin{aligned} F[\rho_{\mathbf{b}}(\mathbf{s}), \mathbf{u}_{\mathbf{b}}, T] &= \frac{1}{2} \int dV \Delta_0 : \mathbb{C} : \Delta_0 + \frac{1}{2} \sum_{\mathbf{b}, \mathbf{b}'} \int dA dA' \rho_{\mathbf{b}}(\mathbf{s}) u_{\mathbf{b}, \mathbf{b}'}(\mathbf{s}, \mathbf{s}') \rho_{\mathbf{b}'}(\mathbf{s}') \\ &+ \sum_{\mathbf{b}} \int dA \rho_{\mathbf{b}}(\mathbf{s}) V_{\mathbf{b}, 0}(\mathbf{s}) + k_B T \sum_{\mathbf{b}} \int dA \rho_{\mathbf{b}}(\mathbf{s}) \left(\log \left(\frac{\rho_{\mathbf{b}}(\mathbf{s})}{\rho_{0, \mathbf{b}}(\mathbf{s})} \right) - 1 \right) \\ &+ \frac{k_B T}{2} \text{Tr} \left[\ln \left(|\delta(\mathbf{s} - \mathbf{s}') + \frac{1}{k_B T} \sum_{\mathbf{b}} \int dz dz' G_0(\mathbf{s}, z; \mathbf{s}', z') : \rho_{\mathbf{b}}(\mathbf{s}') \hat{\xi} \otimes \mathbf{b} \otimes \hat{\xi} \otimes \mathbf{b} \right) \right]. \end{aligned} \quad (3.20)$$

The first three terms can be recombined in a single term that captures the mean-field contributions of the system. This term can be written in terms of the mean-field elastic

strain, Δ_{mf} , defined by

$$\left. \begin{aligned} \nabla \times \beta^p &= -\sum_b \hat{\xi} \mathbf{b} \rho_b(s) \\ \Delta_{\text{mf}} &= (\nabla \mathbf{u} - \beta^p)^s \\ \sigma_{\text{mf}} &= \mathbb{C} : \Delta_{\text{mf}} \\ \nabla \cdot \sigma_{\text{mf}} &= 0 \end{aligned} \right\} \text{in the bulk} \quad (3.21a)$$

$$\left. \begin{aligned} \mathbf{u} &= \mathbf{u}_b \\ \beta^p &= 0 \end{aligned} \right\} \text{on the boundary.} \quad (3.21b)$$

Note that $\Delta_{\text{mf}}(\mathbf{r})$ is a strongly non-local functional of the dislocation density profiles $\rho_b(s)$, as a dislocation at position s causes a strain field in the whole volume, and not only at s . The free energy in terms of Δ_{mf} reads (see B.1 for the derivation):

$$\begin{aligned} F[\rho_b(s), \mathbf{u}_b, T] &= \frac{1}{2} \int dV \Delta_{\text{mf}} : \mathbb{C} : \Delta_{\text{mf}} + k_B T \sum_b \int dA \rho_b(s) \left(\log \left(\frac{\rho_b(s)}{\rho_{b,0}} \right) - 1 \right) \\ &+ \frac{k_B T}{2} \text{Tr} \left[\ln \left(|\delta(s-s') + \frac{1}{k_B T} \sum_b \int dz dz' G_0(\mathbf{s}, z; \mathbf{s}', z') : \rho_b(s') \hat{\xi} \otimes \mathbf{b} \otimes \hat{\xi} \otimes \mathbf{b} \right) \right]. \end{aligned} \quad (3.22)$$

The dependence of the free energy on the boundary deformation \mathbf{u}_b in this expression enters via the boundary conditions on Δ_{mf} in Eqs. (3.21). The dependence on the finite volume is via Δ_{mf} and $G_0(\mathbf{r}; \mathbf{r}')$, as the finite volume appears explicitly in the definitions in Eqs. (3.21) and (3.13) respectively. Analogously, the free energy expression in Eq. (3.20) depends on the loading via $V_{b,0}(s)$, and on the finite volume via both $V_{b,0}(s)$ and $G_0(\mathbf{r}; \mathbf{r}')$.

The expressions in Eqs. (3.20) and (3.22) are equivalent. The advantage of the former is that it is an explicit functional of the dislocation density profiles $\rho_b(s)$. Namely, the interaction potential $u_{b,b'}(s, s')$ and the Green's function $G_0(\mathbf{r}, \mathbf{r})$, as implicitly defined in Eqs. (3.12) and (3.13), are independent of the dislocation density profile. The advantage of the latter is that the first contribution in terms of the mean-field elastic strain, is quite common in literature. For example, this term is equivalent to the contribution to the internal power in the work of Gurtin, see Eq. (3.1) in [43] that relates stress to the rate of elastic distortion. Therefore, the latter will be used primarily for comparison with literature. The rest of the chapter is devoted to the interpretation of the free energy expressions in Eqs. (3.20) and (3.22), and examples of how they can be used.

3.3 Interpretation of the free energy expression

3.3.1 Interpretation of different contributions

In this section, the different terms of the obtained expression for the free energy, Eq. (3.22), are interpreted.

The first term in Eq. (3.22) can be interpreted as the mean-field elastic energy:

$$F_{\text{elas}} \equiv \frac{1}{2} \int dV \Delta_{\text{mf}} : \mathbb{C} : \Delta_{\text{mf}}. \quad (3.23)$$

The strain field Δ_{mf} is the strain field in the body due to boundary loading and the average dislocation density. Consequently, F_{elas} contains three effects: first, the elastic energy, due to loading, which is there when no dislocations are present, second, the interaction between net amounts of dislocations due to the strain field that they produce, and third the influence of mechanical loading on dislocations. These three effects are separated in Eq. (3.20), and one can define the background elastic energy, the two-body interaction energy and the loading energy by

$$F_{\text{background}} \equiv \frac{1}{2} \int dV \Delta_0 : \mathbb{C} : \Delta_0 \quad (3.24a)$$

$$F_{2b} \equiv \frac{1}{2} \sum_{\mathbf{b}, \mathbf{b}'} \int dA dA' \rho_{\mathbf{b}}(\mathbf{s}) u_{\mathbf{b}, \mathbf{b}'}(\mathbf{s}, \mathbf{s}') \rho_{\mathbf{b}'}(\mathbf{s}') \quad (3.24b)$$

$$F_{\text{loading}} \equiv \sum_{\mathbf{b}} \int dA \rho_{\mathbf{b}}(\mathbf{s}) V_{\mathbf{b}, 0}(\mathbf{s}). \quad (3.24c)$$

The definition of the two-body contribution F_{2b} is motivated by $u_{\mathbf{b}, \mathbf{b}'}(\mathbf{s}, \mathbf{s}')$, which is the interaction energy of two discrete dislocations with Burgers vector \mathbf{b} and \mathbf{b}' at positions \mathbf{s} and \mathbf{s}' , respectively. This expression for the two-body interaction is a mean-field expression, as the two-body density is written as the product of one-body densities, see eg. [32]. The mean-field contribution is expected to be the leading order term for the interaction between dislocations.

Furthermore, the definition of the loading contribution F_{loading} is motivated by Eq. (3.6), which shows that $V_{\mathbf{b}, 0}(\mathbf{s})$ is the potential energy corresponding to the Peach-Koehler force that a dislocation would feel in an otherwise dislocation-free body where \mathbf{u}_b is the imposed boundary deformation. Hence $V_{\mathbf{b}, 0}(\mathbf{s})$ is the work that the external Peach-Koehler force has performed to move a dislocation with Burgers vector \mathbf{b} from infinity to position \mathbf{s} .

The second term in Eq. (3.22) is a statistical contribution of the dislocations. This is what the free energy of the dislocations would be if they would not interact (i.e. if it would be a sort of an ideal gas). Following the work of Evans for inhomogeneous systems [23], this contribution reads

$$F_{\text{stat}} \equiv k_B T \sum_{\mathbf{b}} \int dA \rho_{\mathbf{b}}(\mathbf{s}) \left(\log \left(\frac{\rho_{\mathbf{b}}(\mathbf{s})}{\rho_{\mathbf{b}, 0}} \right) - 1 \right). \quad (3.25)$$

A similar contribution is also accounted for by Groma [35], based on phenomenological arguments.

The third term in Eq. (3.22) is a truly many-body contribution that arises from the coarse description of the system:

$$F_{mb} \equiv \frac{k_B T}{2} \text{Tr} \left[\ln \left(\mathbb{1} \delta(\mathbf{s} - \mathbf{s}') + \frac{1}{k_B T} \sum_{\mathbf{b}} \int dz dz' \mathbf{G}_0(\mathbf{s}, z; \mathbf{s}', z') : \rho_{\mathbf{b}}(\mathbf{s}') \hat{\xi} \otimes \mathbf{b} \otimes \hat{\xi} \otimes \mathbf{b} \right) \right] \quad (3.26)$$

This term accounts for the effect of the local arrangement of dislocations. As we found in Chap. 2, Statistically Stored Dislocations are likely to arrange themselves in pairs, which are low energy structures. This was confirmed by DDD simulations in [37]. The

local arrangement of dislocations can reduce the energy of the system, and thus yields a correction to the two-body interaction term that accounts only for the leading order mean-field term. This correction is what is accounted for in the many-body contribution.

3.3.2 Influence of dislocation length

In the derivation in Chap. 2, and hence in the above derivation, it was used that the dislocations are straight and of infinite length. The question thus arises to what extent the results obtained in this chapter are also applicable to dislocations that are curved.

To this end, we consider a slab of the material with a thickness L in which dislocations can be considered approximately straight. To be more precise, we consider the case where the radius of curvature of the dislocation line is substantially larger than the slab thickness L .

The dependence on the slab thickness L of the free energy expression in Eq. (3.22) is non-trivial, as both volume and surface integrals are present. These differ by a factor L . The origin of this different dependency is that on the microscale, the elastic energy scales linearly with the dislocation length, see Eq. (3.9), while the chemical energy in Eq. (3.10) and the number of possible arrangements are independent of the dislocation length, as the arrangement of straight and parallel dislocations is described by points in a two-dimensional plane (independent of the z -coordinate).

There is no experimental value for the typical radius of curvature of dislocations, as measurements on individual dislocations are notoriously difficult. Even so, one can give a rough estimate on the absolute lower bound for this radius. Namely, this radius could not be shorter than the lattice spacing, and moreover, it would not make sense to model dislocations with a radius of curvature shorter than a few Burgers' vectors as straight and infinitely long. Therefore, one can safely assume that the slab thickness L is longer than one Burgers' vector: $|b| < L$.

To study the influence of L on the qualitative behavior of the system, it is most convenient to study the free energy expression in Eq. (3.22) in units of $k_B T$. When no external loading is applied, the elastic contribution F_{elas} reduces to the two-body contribution F_{2b} , see Eqs. (3.24), which is proportional to $\Xi \equiv \frac{\mu b^2 L}{k_B T}$, cf. Eq. (3.14b). It can be shown that also in the many body contribution, the term in the logarithm depends on the coupling parameter Ξ . The overall prefactor of both the statistical and many body contribution is 1. Physical results thus only depend on the value of the coupling parameter Ξ .

The parameter Ξ is a dimensionless coupling parameter that compares the typical interaction energy with the thermal energy. When Ξ is much larger than 1, the energetic effects are more important than thermal fluctuations. As for aluminium at room temperature, the shear modulus, the length of the Burgers vector and $k_B T$ are known¹. Therefore, the lower bound of Ξ is $\Xi > 1.6 \times 10^2$ (from the lower bound of L estimated above). This implies that, in aluminium at room temperature, the characteristic energy of the dislocation interaction ($\mu b^2 L$) dominates over the characteristic energy of the thermal lattice vibrations ($k_B T$), even at the lower bound for L . It is expected that this holds for other metals as well. Therefore, the exact value of the slab thickness L will not affect qualitatively the behavior of dislocations.

¹For aluminium at room temperature, $\mu = 26$ GPa, $\nu = .33$, $b = 2.9$ Å (see [101]) and $k_B T = 4 \times 10^{-21}$ J at 298 K.

In the limit of infinitely long dislocations, Ξ goes to infinity. As Ξ is already large for dislocations in a reasonably thick slab, it can be concluded that they will behave as if they are infinitely long.

3.3.3 Limitations

The grand-canonical partition function in Eq. (3.11a) was derived using a Gaussian approximation for the partition function. This approximation is accurate far away from transition points, around which the macroscopic behaviour of the material changes qualitatively. An example of a transition point in this model is dislocation-mediated melting, see for example the work of Kosterlitz and Thouless [63] and Mizushima [78]. Below a certain critical temperature, dislocations tend to arrange themselves in tightly bound pairs and the material is considered to be solid. Above this temperature, dislocations are able to move more or less freely through the crystal.

Another example is of a transition point is the change from elastic to plastic material response.

The proposed free energy expression is, because of this Gaussian approximation, inaccurate close to transition points of dislocation systems. To study the properties of the system close to the transition, it is better to use the more involved partition function without Gaussian approximation obtained in Chap. 2. For example, renormalization group theory can be used to study transition points, even for complicated partition functions. Another option is to use more sophisticated approximation techniques instead of a single Gaussian approximation. For example, the Villain approximation [61] is accurate in a much larger range of parameters, but this approximation is computationally more involved.

3.4 Application to specific cases

In this section, the free energy expression in Eq. (3.22) will be applied to three specific cases. First, a Local Density Approximation (LDA) will be considered, as this is often assumed in literature. The validity of the LDA is examined and the resulting energy expression is compared to literature. Then, the dislocation density profile and the total energy are determined for simple shear loading within the LDA. Second, the zero temperature limit of the free energy will be studied. And third, a completely regular, equally spaced arrangement of glide planes will be considered in the zero temperature limit.

3.4.1 Local Density Approximation (LDA)

In several dynamical models, a local form is assumed for the free energy. This means that the free energy is the spatial integral of a free energy density, where the latter is only a function of the dislocation density at that point, rather than a functional of the full dislocation density profile. Such an expression is easier to work with. Furthermore, the exact position of glide planes is not used as a material parameter in these models, and moreover, these are almost impossible to obtain experimentally.

In this section, local approximations and gradient corrections for the two body- and the many body contribution are determined from standard expressions from density functional theory, introduced in Eqs. (3.27) and (3.28). The glide planes are smeared out completely,

as depicted in Fig. 3.2(c). For simplicity, only a single slip system is considered. Furthermore, it is assumed that the infinite space solution can be used for the interaction potential $u_{\mathbf{b},\mathbf{b}'}(\mathbf{s} - \mathbf{s}')$ and for the Green's function $G_0(\mathbf{r} - \mathbf{r}')$. Namely, no explicit position dependence is expected within the LDA. Then, the explicit expressions in Eqs. (3.14) can be used.

First, it is shown that for the two body contribution, the gradient corrections dominate over the local term, and hence a local approximation for this term is not accurate. Second, the local approximation of the many body contribution is derived in Eq. (3.38) and it is shown that the gradient corrections do not dominate over the local term, provided that the density varies slowly enough.

In general, the local density approximation of a free energy functional \mathcal{F} and its gradient corrections can be written as, see e.g. [23],

$$\mathcal{F}[\rho(\mathbf{s})] = \int dA (f(\rho(\mathbf{s})) + \nabla\rho(\mathbf{s}) \cdot \mathbf{F}_2(\rho(\mathbf{s})) \cdot \nabla\rho(\mathbf{s}) + \mathcal{O}(\nabla^4)), \quad (3.27)$$

where $f(\rho)$ is a scalar-valued function, which gives the free energy density of a homogeneous system with density ρ . Furthermore, $\mathbf{F}_2(\rho)$ is a tensor-valued function given by

$$\mathbf{F}_2(\rho) = \frac{-1}{4} \int dA \mathbf{s} \otimes \mathbf{s} \left. \frac{\delta^2 \mathcal{F}[\rho(\mathbf{s})]}{\delta\rho(\mathbf{0})\delta\rho(\mathbf{s})} \right|_{\rho(\mathbf{s})=\rho}. \quad (3.28)$$

This expression could be obtained by a Taylor expansion of $\rho(\mathbf{s})$ around \mathbf{s} and an expansion of $\mathcal{F}[\rho(\mathbf{s})]$ in powers of ∇ .

It is assumed that it is sensible to make a local approximation, provided that both terms $f(\rho)$ and $\mathbf{F}_2(\rho)$ are finite, and the gradient correction does not dominate over the first term. The latter sets a lower limit for the typical length scale on which the density profile varies.

Single slip system

The system is simplified by only considering one slip system with only two possible Burgers vectors, namely edge dislocations with opposite Burgers vector. Hence without loss of generality, one can say that $\hat{\boldsymbol{\xi}} = \hat{\mathbf{z}}$ and $\mathbf{b} = \pm b\hat{\mathbf{x}}$. Using this simplification, the free energy expression in Eq. (3.20) reads

$$\begin{aligned} F[\rho_+(\mathbf{s}), \rho_-(\mathbf{s}), \mathbf{u}_b, T] &= \frac{1}{2} \int dV \boldsymbol{\Delta}_0 : \mathbb{C} : \boldsymbol{\Delta}_0 \\ &+ \frac{1}{2} \int dA dA' (\rho_+(\mathbf{s}) - \rho_-(\mathbf{s})) u_{\text{edge}}(\mathbf{s} - \mathbf{s}') (\rho_+(\mathbf{s}') - \rho_-(\mathbf{s}')) \\ &+ \int dA (\rho_+(\mathbf{s}) - \rho_-(\mathbf{s})) V_{0,\text{edge}}(\mathbf{s}) + k_B T \sum_{+,-} \int dA \rho_{\pm}(\mathbf{s}) \left(\ln \left(\frac{\rho_{\pm}(\mathbf{s})}{\rho_{\pm,0}} \right) - 1 \right) \\ &+ \frac{k_B T}{2} \text{Tr} \left[\ln(|\delta(\mathbf{s} - \mathbf{s}')| \right. \\ &\left. + \frac{1}{k_B T} \int dz dz' G_0(\mathbf{s} - \mathbf{s}', z - z') : \hat{\boldsymbol{\xi}} \otimes \mathbf{b} \otimes \hat{\boldsymbol{\xi}} \otimes \mathbf{b} (\rho_+(\mathbf{s}') + \rho_-(\mathbf{s}')) \right], \end{aligned} \quad (3.29)$$

where $V_{\text{edge},0}(\mathbf{s}) \equiv V_{b\hat{\mathbf{x}},0}(\mathbf{s})$ is the Peach Koehler potential that the edge dislocations feel, and where $u_{\text{edge}}(\mathbf{s} - \mathbf{s}') \equiv u_{b\hat{\mathbf{x}},b\hat{\mathbf{x}}}(\mathbf{s}, \mathbf{s}')$ is the interaction potential between two equal edge dislocations. It is convenient to use the interaction potential in Fourier space. Using Eqs. (3.14), this reads:

$$\begin{aligned} \tilde{u}_{\text{edge}}(\mathbf{q}) &= b^2 \int dA \int dz dz' \hat{\boldsymbol{\xi}} \otimes \hat{\mathbf{x}} : \mathbf{G}_{0,ijij'}(\mathbf{s} - \mathbf{s}', z - z') : \hat{\boldsymbol{\xi}} \otimes \hat{\mathbf{x}} e^{-i\mathbf{q}_{2D} \cdot (\mathbf{s} - \mathbf{s}')} \\ &= \frac{2\mu b^2 L q_y^2}{1 - \nu q^4}, \end{aligned} \quad (3.30)$$

where q_y is the y -component of \mathbf{q} : $q_y = \mathbf{q} \cdot \hat{\mathbf{y}}$, and where q is the length of \mathbf{q} : $q = |\mathbf{q}|$. The parameter L is the typical persistence length of a dislocation, as introduced in Sec. 3.3.2.

LDA and gradient corrections of the two body contribution

In this section, the first and second term in Eq. (3.27) are determined for the two-body contribution. First, the local term is determined from the two-body energy of a homogeneous system with a GND density ρ_{GND} :

$$\begin{aligned} \int dA f_{2b}(\rho_{GND}) &= F_{2b}[\rho_{GND}] = \frac{1}{2} \int dA dA' \rho_{GND}^2 u_{\text{edge}}(\mathbf{s} - \mathbf{s}') \\ &= \frac{1}{2} \int dA \rho_{GND}^2 \tilde{u}_{\text{edge}}(\mathbf{q}_{2D} = \mathbf{0}) = \frac{\rho_{GND}^2}{2} \left(\frac{2\mu b^2 L q_y^2}{1 - \nu q^4} \right) \Bigg|_{q=0} A, \end{aligned} \quad (3.31)$$

where A is the surface area. The term in parenthesis on the RHS diverges with q^{-2} for small q . The smallest wave number in the system is inversely proportional to the largest length scale, which is the system size R . The energy density thus diverges as R^2 .

Second, the gradient correction of the two-body contribution is determined using Eq. (3.28):

$$\begin{aligned} \mathbf{F}_{2,2b} &= \frac{-1}{4} \int dA \mathbf{s} \otimes \mathbf{s} u_{\text{edge}}(\mathbf{s}) = \frac{1}{4} \int dA \frac{d}{d\mathbf{q}} \otimes \frac{d}{d\mathbf{q}} (\exp[-i\mathbf{q} \cdot \mathbf{s}]) \Bigg|_{q=0} u_{\text{edge}}(\mathbf{s}) \\ &= \frac{1}{4} \frac{d}{d\mathbf{q}} \otimes \frac{d}{d\mathbf{q}} \tilde{u}_{\text{edge}}(\mathbf{q}_{2D}) \Bigg|_{q=0} = \frac{1}{4} \frac{d}{d\mathbf{q}} \otimes \frac{d}{d\mathbf{q}} \frac{2\mu b^2 L q_y^2}{1 - \nu q^4} \Bigg|_{q=0}, \end{aligned} \quad (3.32)$$

where the second equality is just a mathematical identity that is introduced for convenience. The RHS now diverges with q^{-4} , and hence it diverges as R^4 with the system size.

It can thus be concluded that (i) the local contribution is large for large systems and diverges with the system size, and (ii) that the gradient correction dominates over the local contribution when the typical length scale of density fluctuations is smaller than the system size. Therefore, the local density approximation is inaccurate for the two body contribution. This agrees with what was found by Mesarovic [76].

LDA and gradient corrections of the many body contribution

In this section, the local density approximation of the many body term will be determined by calculating the many-body contribution for a homogeneous system with total dislocation density $\rho_{tot} = \rho_+ + \rho_-$. To this end, first, the eigenvalues of the matrix in the logarithm will be determined, and second, the summation over the logarithm of all eigenvalues will be performed to obtain the trace. This yields the local expression in Eq. (3.38).

The first step is thus to determine the eigenvalues of $\frac{1}{k_B T} \int dz dz' G_0(\mathbf{s} - \mathbf{s}', z - z') : \hat{\xi} \otimes \mathbf{b} \otimes \hat{\xi} \otimes \mathbf{b} \rho_{tot}$. Note that this tensor is a convolution, and therefore, it can be read as a product in Fourier space. Therefore, it turns out to be more convenient to determine the eigenvalue in Fourier space. The eigenvalue in Fourier space reads

$$\tilde{\lambda}_U(\mathbf{q}_{2D}) \tilde{U}(\mathbf{q}_{2D}) = \left(\frac{\rho_{tot}}{k_B T} \mathcal{F} \left[\int dz dz' G_0(\mathbf{s} - \mathbf{s}', z - z') \right] (\mathbf{q}_{2D}) : \hat{\xi} \otimes \mathbf{b} \right) \cdot \left(\hat{\xi} \otimes \mathbf{b} : \tilde{U}(\mathbf{q}_{2D}) \right), \quad (3.33)$$

where \mathbf{q}_{2D} is the 2D wave-vector. Note that the term in the second bracket on the RHS is a scalar and that the term in the first bracket is a second order tensor independent of $U(\mathbf{q}_{2D})$. This implies that either the eigenvalue is 0, or that, up to a multiplicative constant, $\tilde{U}(\mathbf{q}_{2D}) = \tilde{G}_0(\mathbf{q}_{2D}) : \hat{\xi} \otimes \mathbf{b}$. Inserting this in Eq. (3.33) implies that the only non-zero eigenvalue is

$$\lambda(\mathbf{q}) = \frac{\rho_{tot}}{k_B T} \hat{\xi} \otimes \mathbf{b} : \tilde{G}_0(\mathbf{q}_{2D}) : \hat{\xi} \otimes \mathbf{b} = \rho_{tot} \frac{2\mu b^2 L}{k_B T (1 - \nu)} \frac{q_y^2}{q^4}. \quad (3.34)$$

The second step is to calculate the many body contribution from these eigenvalues. The logarithm in Eq. (3.29) is the sum of logarithm of the eigenvalues of $l\delta(\mathbf{s} - \mathbf{s}') + \frac{1}{k_B T} \int dz dz' G_0(\mathbf{s} - \mathbf{s}', z - z') : \hat{\xi} \otimes \mathbf{b} \otimes \hat{\xi} \otimes \mathbf{b} \rho_{tot}$, which is $1 + \lambda(\mathbf{q})$ in Fourier space. The trace over the continuous index can be taken by integrating over the wave vector \mathbf{q}_{2D} and by integrating over real space. This yields

$$F_{mb}(\rho_{tot}, T) = \frac{k_B T}{2} \int dA \int \frac{d^2 \mathbf{q}_{2D}}{(2\pi)^2} \ln \left(1 + \rho_{tot} \frac{2\mu b^2 L}{k_B T (1 - \nu)} \frac{q_y^2}{q^4} \right). \quad (3.35)$$

In this explicit form, the integral over \mathbf{q}_{2D} can be performed exactly. For readability, the shorthand notation $a \equiv \frac{\rho_{tot} 2\mu b^2 L}{k_B T (1 - \nu)}$ is introduced. Note that a has the dimension of density. Then, using polar coordinates for the integration over \mathbf{q} , the free energy density as introduced in Eq. (3.27) reads

$$\begin{aligned} f_{mb}(\rho_{tot}, T) &= \frac{1}{(2\pi)^2} \frac{k_B T}{2} \int_0^\infty dq \int_0^{2\pi} d\phi q \ln \left(1 + a \frac{\sin^2 \phi}{q^2} \right) \\ &= \frac{k_B T}{8\pi^2} \int_0^{2\pi} d\phi \left[\frac{q^2}{2} \ln \left(1 + \frac{a \sin^2 \phi}{q^2} \right) + \frac{a \sin^2 \phi}{2} \ln (q^2 + a \sin^2 \phi) \right]_{q=0}^\infty. \end{aligned} \quad (3.36)$$

At the lower boundary $q = 0$, the term in square brackets is equal to $\frac{a \sin^2 \phi}{2} \ln (a \sin^2 \phi)$, and hence it is finite. However, for large q it diverges. Large values of the wave vector

q correspond to small length scales. Integrating over q up to infinity thus corresponds to incorporating phenomena at very small length scales. However, at very small length scales, comparable to the atom spacing in the crystal, we already know that linear elasticity theory breaks down. Hence integrating q up to infinity is physically speaking not admissible, and one should introduce a large cutoff Λ_0 for the integration over q , such that $|\mathbf{q}_{2D}| \in [0, \Lambda_0]$. However, physical results should not depend on the exact value of the cutoff Λ_0 , since they do not depend on the exact length scale at which elasticity theory breaks down.

It is now assumed that Λ_0^2 is much larger than a . This yields for the many body contribution:

$$f_{mb}(\rho_{tot}, T) = \frac{k_B T}{8\pi^2} \int_0^{2\pi} d\phi \frac{a \sin^2 \phi}{2} \left(-\ln \left(\frac{a \sin^2 \phi}{\Lambda_0^2} \right) + 1 \right). \quad (3.37)$$

The integration over ϕ can now be performed straightforwardly using a symbolic toolbox. This finally yields for the free energy density

$$f_{mb}(\rho_{tot}, T) = -\frac{k_B T}{8\pi^2} a \ln \left(\frac{a}{4\Lambda_0^2} \right) = -\frac{\mu b^2 L}{8\pi(1-\nu)} \rho_{tot} \ln \left(\frac{\rho_{tot}}{\Lambda^2(T)} \right), \quad (3.38)$$

where Λ is introduced for convenience: $\Lambda^2 \equiv \frac{k_B T(1-\nu)}{2\mu b^2 L} 4\Lambda_0^2$. Note that Λ has the dimension of inverse length, and that $\Lambda^2 \gg \rho_{tot}$, which follows directly from $\Lambda_0^2 \gg a$. This implies that the cutoff length Λ^{-1} should be much smaller than the typical dislocation spacing. Hence the many-body contribution is non-zero if ρ_{tot} is non-zero.

As the free energy density $f_{mb}(\rho_{tot}, T)$ depends only on the logarithm of Λ , all physical quantities are independent of the exact value of the cutoff Λ_0 . Namely, if we would take the cutoff twice as large, the free energy would increase by an amount $\frac{\mu b^2 L}{8\pi(1-\nu)} \rho_{tot} \ln 4$, which is a constant times the density. The constant can thus be interpreted as an additive constant to the chemical potential, which has no physical meaning.

Now, the gradient correction, as introduced in Eq. (3.27), is determined for the many body contribution, see Eq. (3.40) for the result. From this expression, it is then determined under which conditions the gradient correction is small compared to the local contribution, see Eqs. (3.41) and (3.42).

To determine the gradient correction, the second derivative of the free energy with respect to the density profile is needed, see Eq. (3.27). For the many body correction, this derivative is

$$\begin{aligned} & \left. \frac{\delta^2 \mathcal{F}_{mb}[\rho_{tot}(\mathbf{s}'), T]}{\delta \rho_{tot}(\mathbf{0}) \delta \rho_{tot}(\mathbf{s})} \right|_{\rho_{tot}(\mathbf{s}) = \rho_{tot}} = & (3.39) \\ & = -\text{Tr} \left[\left(|\delta(\mathbf{s}_1 - \mathbf{s}_2) + \frac{1}{k_B T} \int dz dz' G_0(\mathbf{s}_1 - \mathbf{s}_2, z - z') : \right. \right. \\ & : \hat{\xi} \otimes \mathbf{b} \otimes \hat{\xi} \otimes \mathbf{b} \rho_{tot} \left. \left. \right) : \frac{1}{k_B T} \int dz dz' G_0(\mathbf{s}_2 - \mathbf{s}_3, z - z') : \hat{\xi} \otimes \mathbf{b} \otimes \hat{\xi} \otimes \mathbf{b} : \right. \\ & : \left(|\delta(\mathbf{s}_3 - \mathbf{s}_4) + \frac{1}{k_B T} \int dz dz' G_0(\mathbf{s}_3 - \mathbf{s}_4, z - z') : \hat{\xi} \otimes \mathbf{b} \otimes \hat{\xi} \otimes \mathbf{b} \rho_{tot} \right) : \\ & : \left. \frac{1}{k_B T} \int dz dz' G_0(\mathbf{s}_4 - \mathbf{s}_1, z - z') : \hat{\xi} \otimes \mathbf{b} \otimes \hat{\xi} \otimes \mathbf{b} \right] \delta(\mathbf{s}_1) \delta(\mathbf{s}_3 - \mathbf{s}). \end{aligned}$$

This is again a convolution, which results in a product in Fourier space. This can be expressed in the eigenvalues $\lambda(\mathbf{q})$ from the previous section. Again, the integration over the wave vector can be performed using a symbolic toolbox. Details of this derivation can be found in B.2. This yields for the gradient correction:

$$\mathbf{F}_{2,mB}(\rho_{tot}, T) = \frac{1}{24\pi} \frac{k_B T}{\rho_{tot}^2} \begin{pmatrix} 1 & 0 \\ 0 & -1 + \frac{3\sqrt{\rho_{tot}}R}{8} \sqrt{\frac{2\mu b^2 L}{k_B T(1-\nu)}} \end{pmatrix}, \quad (3.40)$$

where R is the system size. Derivatives in the x -direction do therefore not dominate over the local term provided that

$$\begin{aligned} \frac{1}{24\pi} \frac{k_B T}{\rho_{tot}^2} |\partial_x \rho_{tot}(\mathbf{s})|^2 &\ll \frac{\mu b^2 L}{8\pi(1-\nu)} \rho_{tot} \left| \ln \left(\frac{\rho_{tot}}{\Lambda^2(T)} \right) \right| \\ \Rightarrow \left(\frac{|\partial_x \rho_{tot}(\mathbf{s})|}{\rho_{tot}} \right)^2 &\ll 3 \frac{\Xi}{1-\nu} \rho_{tot} \left| \ln \left(\frac{\rho_{tot}}{\Lambda^2(T)} \right) \right|, \end{aligned} \quad (3.41)$$

where the parameter Ξ is defined in Sec. 3.3.2, and it is typically much larger than 1. Moreover, $\left| \ln \left(\frac{\rho_{tot}}{\Lambda^2(T)} \right) \right|$ is much larger than one, as $\Lambda^2 \gg \rho_{tot}$.

It can thus be concluded that the LDA is valid if the typical length scale of variations of the total dislocation density in x -direction, $\rho_{tot}/|\partial_x \rho_{tot}|$, is much longer than the average dislocation spacing $1/\sqrt{\rho_{tot}}$. As both Ξ and $\left| \ln \left(\frac{\rho_{tot}}{\Lambda^2(T)} \right) \right|$ are large, the condition in Eq. (3.41) is not very restrictive.

However, when the total dislocation density varies in the y -direction, the gradient does not dominate over the local term provided that

$$\begin{aligned} \frac{1}{64\pi} \frac{k_B T}{\rho_{tot}^{3/2}} R \sqrt{\frac{2\mu b^2 L}{k_B T(1-\nu)}} |\partial_y \rho_{tot}(\mathbf{s})|^2 &\ll \frac{\mu b^2 L}{8\pi(1-\nu)} \rho_{tot} \left| \ln \left(\frac{\rho_{tot}}{\Lambda^2(T)} \right) \right| \\ \Rightarrow \left(\frac{|\partial_y \rho_{tot}(\mathbf{s})|}{\rho_{tot}} \right)^2 &\ll 4 \sqrt{\frac{2\Xi}{1-\nu}} \frac{\sqrt{\rho_{tot}}}{R} \left| \ln \left(\frac{\rho_{tot}}{\Lambda^2(T)} \right) \right|. \end{aligned} \quad (3.42)$$

The LDA is thus valid if the typical length scale of variations in the y -direction, $\rho_{tot}/|\partial_y \rho_{tot}|$, is much larger than $\sqrt{R}/\sqrt{\rho_{tot}}$, which is much larger than the average dislocation spacing. If the system is infinitely large, Eq. (3.42) implies that no variations in the y -direction are allowed. Furthermore, the RHS of Eq. (3.42) is only inversely proportional to the square-root of Ξ . Therefore, the condition in Eq. (3.42) is much more restrictive than in Eq. (3.41).

The difference between variations in x - and y -direction originates from the difference in screening in both directions. As can be seen in Fig. 3.4, in the x -direction, dislocations with opposite Burgers vector are attracted. These dislocations screen the effect of the dislocation at the origin. However, in the y -direction, dislocations with equal Burgers vector are attracted. These dislocations enhance the effect of the dislocation at the origin. The restriction on the variations in density in the y -direction also restricts the possible choice for the glide-plane distribution. Namely, if a dislocation density profile is considered which is only nonzero at discrete glide-planes, this implies that the derivative of the density in y -direction is large, and hence that the condition in Eq. (3.42) is violated. Therefore, only profiles that are more or less homogeneous in the y -direction are allowed for. This means that the glide planes are smeared-out.

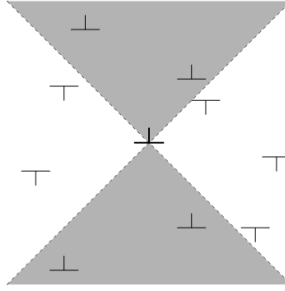


Figure 3.4: In the white regions, edge dislocations with opposite Burgers vector are attracted by the dislocation in the origin, and thereby they screen the effect of the central dislocation. In the shaded regions, edge dislocations with equal Burgers vector are attracted, which strengthens the effect of the central dislocation.

Conclusions about the LDA and comparison to literature

It was found in this section that the LDA is applicable for the many-body contribution, provided that the density profile varies slow enough, but that the LDA is not applicable for the two body contribution. As in Eq. (3.22), the background, two-body and loading contributions can be combined into the elastic contribution. This results in the following semi-local free energy expression:

$$\begin{aligned}
 F_{LDA}[\rho_+(\mathbf{s}), \rho_-(\mathbf{s}), \mathbf{u}_b, T] &= \frac{1}{2} \int dV \mathbf{\Delta}_{\text{mf}} : \mathbb{C} : \mathbf{\Delta}_{\text{mf}} \\
 &+ k_B T \sum_{+,-} \int dA \rho_{\pm}(\mathbf{s}) \left(\ln \left(\frac{\rho_{\pm}(\mathbf{s})}{\rho_{\pm,0}} \right) - 1 \right) \\
 &- \frac{\mu b^2 L}{8\pi(1-\nu)} \int dA (\rho_+(\mathbf{s}) + \rho_-(\mathbf{s})) \ln \left(\frac{\rho_+(\mathbf{s}) + \rho_-(\mathbf{s})}{\Lambda^2} \right).
 \end{aligned} \tag{3.43}$$

This expression might seem local at first glance, as it is written as a single spatial integral. However, one should realize that the free energy is not to be interpreted as a functional of the mean-field strain $\mathbf{\Delta}_{\text{mf}}$, but rather of the dislocation density profiles $\rho_+(\mathbf{s})$ and $\rho_-(\mathbf{s})$, and the displacement \mathbf{u}_b of the boundary. The mean-field strain itself is a strongly non-local functional of the dislocation density, see Eq. (3.21).

In the work of Mesarovic [76], it was also shown that the two-body interaction energy cannot be approximated by a local expression. Moreover, in later work [77], it was shown that the contribution due to coarsening can be approximated by a local form provided that the typical length over which the dislocation density profile varies is much longer than the average dislocation spacing. This agrees with the explicit expression obtained here.

In the work of Groma [38], it was argued that no new internal length scale should arise from coarse-graining, as the interaction between dislocations is scale-free. The free energy obtained here satisfies this constraint, as the many-body contribution depends only logarithmically on the cutoff Λ .

The free energy of a system with spatially constant dislocation density was determined

by Mizushima [78], Ninomiya [84], Yamamoto [118] and Burakovskiy [11]. The systems considered in their work do not have a net dislocation content, and the free energy expressions were used to explain the melting transition of crystals. The suggested expressions all entail a $-\rho \ln \rho$ -term with a prefactor proportional to the shear modulus and the Burgers vector squared, but independent of temperature, which is analogous to the expression for F_{mb} found here.

Additional terms proportional to ρ , $\rho^{3/2}$ and ρ^2 were suggested in [78, 84, 118, 11]. The terms linear in the density result from the energy of individual dislocation lines. In our study, self-energy contributions are neglected, and hence the linear contributions are absorbed in the chemical potential. The term proportional to $\rho^{3/2}$ results from the configurational entropy of dislocation networks. This term is not found in our work, as jogs and connections between dislocations do not occur in systems with only straight and parallel dislocations. The term quadratic in the density in [118] resulted from a non-overlapping condition for dislocations. This was not accounted for in our analysis, and hence such a term is not found.

In the work of Svendsen, [62, 4, 105], the free energy is separated in a linear elastic part, and another contribution that is written as a power series in the GND and SSD density separately. In later work [106], forms other than polynomials were also considered for this second term. Here it was shown that a local expression is indeed possible for the many body contribution, and a series expansion of the local expression obtained here could be valid in a certain regime.

In the work of Panyukov and Rabin [90], the free energy of a system of dislocation loops was determined. In that work, the density of dislocations was assumed to be independent of the Burgers vector, and hence no net dislocation was considered, both locally and globally. Despite the differences in problem setup with our analysis, the free energy expression found in [90, Eq. (65)] is remarkably similar to what we found in Eq. (3.35). As in our work, only straight and infinitely long dislocations are considered, it was possible to perform the integration over the wave vector in Eq. (3.35) explicitly, which was impossible in the work of Panyukov and Rabin [90].

3.4.2 Zero temperature

In this work, the coarse-graining was performed at non-zero temperature, and the temperature dependence in Eq. (3.22) is explicit. On the contrary, in literature, the temperature dependence is often not clear, as the system is considered at isothermal conditions. Sometimes, an explicit split is made between energetic and entropic contributions, for example in [35, 36]. In this section, we determined the zero temperature limit of our free energy expression, to see what the effect of working at non-zero temperature is. The result will be compared to literature.

To study the zero temperature limit of the free energy expression in Eq. (3.22), it is first noted that the mean-field elastic contribution F_{elas} as defined in Eq. (3.23), is independent of the temperature, and hence does not change in the limit.

Second, the statistical contribution defined in Eq. (3.25) is proportional to the temperature. Therefore, it vanishes in the zero temperature limit $\lim_{T \rightarrow 0} F_{\text{stat}} = 0$. And finally, the many body contribution as defined in Eq. (3.26) is considered. This term can be

written as

$$F_{mb} = \frac{k_B T}{2} \int dA \sum_{m=1}^9 \ln \left(1 + \frac{1}{k_B T} \lambda_m(\mathbf{s}) \right), \quad (3.44)$$

where $\lambda_m(\mathbf{s})$ is the m^{th} eigenvalue of the matrix $\sum_{\mathbf{b}} \int dz dz' \mathbf{G}_0(\mathbf{s}, z; \mathbf{s}', z') : \rho_{\mathbf{b}}(\mathbf{s}') \hat{\boldsymbol{\xi}} \otimes \mathbf{b} \otimes \hat{\boldsymbol{\xi}} \otimes \mathbf{b}$, and the sum runs over all eigenvalues. As $\mathbf{G}_0(\mathbf{s}, z; \mathbf{s}', z')$ is independent of the temperature T , the eigenvalues $\lambda_m(\mathbf{s})$ are independent of temperature as well. Thus, in the zero temperature limit, the many body contribution reads

$$\lim_{T \rightarrow 0} F_{mb} = \int dA \sum_{m=1}^9 \lim_{T \rightarrow 0} \frac{k_B T}{2} \ln \left(1 + \frac{1}{k_B T} \lambda_m(\mathbf{s}) \right) = \int dA \sum_{m=1}^9 0 = 0, \quad (3.45)$$

and hence vanishes.

At first glance, this result is contradictory with the explicit result that was obtained for a spatially homogeneous dislocation density in Eq. (3.38). Namely, that many body contribution is non-zero when the dislocation density is non-zero. However, in the derivation, it was used just before Eq. (3.38) that one can choose a cutoff wave number Λ_0 such that $\Lambda_0^2 \gg \frac{\rho_{\text{tot}} 2\mu b^2 L}{k_B T(1-\nu)}$, which is clearly impossible in the zero temperature limit.

Hence once the LDA is made at finite temperature, the zero temperature limit cannot be taken anymore. Other approximation techniques for the free energy might also involve additional assumptions on the temperature. Therefore, we think that in general one should be careful in taking the zero temperature limit when approximations are made.

So to conclude, the free energy at $T = 0$ can be expressed as

$$F[\rho_{\mathbf{b}}(\mathbf{s}), \mathbf{u}_{\mathbf{b}}, T = 0] = F_{\text{elas}}[\rho_{\mathbf{b}}(\mathbf{s}), \mathbf{u}_{\mathbf{b}}]. \quad (3.46)$$

It is tempting to interpret the free energy at zero temperature as the internal energy U of the system, as $F = U - TS$. However, the internal energy should formally be determined by first calculating the entropy from $S = -\frac{\partial F}{\partial T}$ and subsequently using the relation $U = F + TS$. When this is done using the free energy expression in Eq. (3.22), it turns out that the internal energy U differs from (3.46) by a contribution that vanishes only at zero temperature. Therefore, the internal energy U at $T > 0$ is not given by the free energy at zero temperature.

It was recognized in the work of Groma [35, 36] and Limkumnerd [73] that the physical temperature of the system is close to zero, which means that the statistical contribution F_{stat} is much smaller than the energetic contribution. Hence it was concluded that it plays no role. However, another ‘phenomenological temperature’ was introduced to cover many body effects. In our work here, it was indeed found that many body effects vanish at zero temperature. However, at small but finite temperature, many body effects appear naturally and in a scale-free form, as was anticipated in [38].

In the crystal plasticity model of Bammann [3], the temperature dependence is explicit. Three important differences with our model can be distinguished. First, the elastic constants depend on temperature. In our work, this dependence was not put in the model on the microscopic level, and therefore, it is not present in the result either. An extension to temperature dependence on the microscopic level could be made. Second, in the

work of Bammann, an energy contribution is found that depends only on temperature, and not on the strain of the material. This energy contribution is perhaps related to the phonon energy in the crystal. The mechanical response of the system was found to be independent of this energy contribution. In the work presented here, the focus was on deriving the free energy due to mechanical loading. Therefore, phonon energy was interpreted as an irrelevant constant contribution, and was therefore neglected. Third, the free energy expression obtained here comprises an statistical and a many body contribution that depends both on temperature and on dislocation density. Comparable terms were not proposed by Bammann. This is probably because these contributions are due to the effect of non-zero temperature on dislocation distributions, rather than only the effect of the temperature on the lattice.

Equally spaced glide planes

The free energy at zero temperature can be further simplified for dislocations on equally spaced glide planes. As shown in several papers [99, 29, 5], this geometry simplifies the mathematical analysis of the problem considerably and the coarse graining can be done using Γ -convergence, see [99, 29]. In this section, the free energy at zero temperature in Eq. (3.46) is evaluated in this special geometry, and the results are compared with those obtained using Γ -convergence. This case can be considered as an example in which the discrete glide planes are still resolved on the macroscopic level.

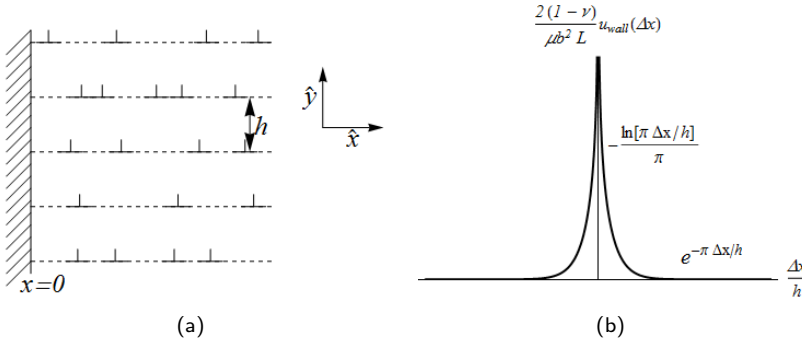


Figure 3.5: The geometry studied in this section: positive dislocations on equally spaced glide planes that pile-up against a wall at $x = 0$ (fig. (a)), and the interaction potential between two dislocation walls, as in Eq. (3.49) (fig. (b)).

The exact geometry that is used is depicted in Fig. 3.5(a). The glide planes are oriented in \hat{x} -direction and the dislocations pile up against an infinitely long, vertical wall at $x = 0$. The glide plane spacing is h , and, as in [99, 29], only positive dislocations are considered. Moreover, it is assumed that the loading is the same on each glide plane and hence Δ_0 and V_{edge} are both only functions of x .

Because of the symmetry of the system and loading under a translation over a distance h in \hat{y} -direction, the density of dislocations in the glide plane is independent of the y -

coordinate of the glide plane. Therefore, the density of dislocations can be written as

$$\rho_+(\mathbf{s}) = \rho(x) \sum_{n=-\infty}^{\infty} \delta(y - hn), \quad (3.47)$$

where the summation runs over all integers, and where the delta function indicates the positions of the glide planes as in Fig. 3.3. Hence, the density is zero if there is no glide plane, and $\rho(x)$ in the glide plane. Note that both $\delta(y - hn)$ and $\rho(x)$ have the dimension of inverse length. The background energy was not accounted for in [99, 29], and will thus be left out here as well. Using Eq. (3.47) in Eq. (3.46) for the free energy at zero temperature yields

$$\begin{aligned} F[\rho_b(\mathbf{s}), \mathbf{u}_b, T = 0] &= \int dA \rho(x) \sum_{n=-\infty}^{\infty} \delta(y - hn) V_{\text{edge}}(x) \\ &+ \frac{1}{2} \int dA dA' \rho(x) \sum_{n=-\infty}^{\infty} \delta(y - hn) u_{b,b'}(\mathbf{s}, \mathbf{s}') \rho(x') \sum_{n'=-\infty}^{\infty} \delta(y' - hn'). \end{aligned} \quad (3.48)$$

This expression can be rewritten by performing the summations over n and the integrations over y and y' . The energy can then be expressed in terms of the number of glide planes N_y and the interaction energy of a regular wall of dislocations with a single dislocations, $u_{\text{wall}}(\Delta x)$, which reads

$$u_{\text{wall}}(\Delta x) = \frac{\mu b^2 L}{2(1-\nu)} \left(\frac{\Delta x}{h} \coth \left(\pi \frac{\Delta x}{h} \right) - \pi^{-1} \ln \left(2 \sinh \left(\pi \frac{\Delta x}{h} \right) \right) \right), \quad (3.49)$$

as shown in B.3. The potential $u_{\text{wall}}(\Delta x)$ is plotted in Fig. 3.5(b). The free energy per glide plane thus reads

$$\frac{F[\rho_b(\mathbf{s}), \mathbf{u}_b, T = 0]}{N_y} = \int dx \rho(x) V_{\text{edge}}(x) + \frac{1}{2} \int dx dx' \rho(x) u_{\text{wall}}(x - x') \rho(x'). \quad (3.50)$$

As shown in Fig. 3.5(b), the interaction potential is not long-ranged anymore, as opposed to the original interaction potential u_{edge} . Therefore, the two body term can be approximated by a local expression as in Eq. (3.27), as long as the length scale associated with density fluctuations is small enough. This is clear by considering the LDA of Eq. (3.50) explicitly using the expressions in Eqs. (3.27) and (3.28). The free energy density of the homogeneous system reads

$$\frac{f_{2b}(\rho)}{N_y} = \rho^2 2 \int_0^{\infty} dx -x' u_{\text{wall}}(x - x') = \frac{\mu b^2 L}{2(1-\nu)} \rho^2 \frac{h}{3}, \quad (3.51)$$

and the gradient correction term reads

$$\frac{F_{2,2b}}{N_y} = \frac{-1}{4} 2 \int_0^{\infty} dx x^2 u_{\text{wall}}(x) = \frac{-1}{4} \frac{\mu b^2 L}{2\pi(1-\nu)} \frac{h^3 \pi}{45}, \quad (3.52)$$

where both integrals were evaluated straightforwardly using a symbolic toolbox. The gradient correction is thus much smaller than the local contribution as long as

$$\frac{\pi h}{3} \rho^2 \gg \frac{h^3 \pi}{180} |\rho'(x)|^2 \Rightarrow \frac{60}{h^2} \gg \left(\frac{|\rho'(x)|}{\rho} \right)^2, \quad (3.53)$$

so when the typical length scale of density changes $\rho/|\rho'(x)|$ is much larger than the glide plane spacing h . The energy in Eq. (3.48) can thus be rewritten as

$$\frac{F[\rho_{\mathbf{b}}(\mathbf{s}), \mathbf{u}_{\mathbf{b}}, T = 0]}{N_y} = \begin{cases} \int dx \rho(x) V_{\text{edge}}(x) + \frac{h}{12} \frac{\mu b^2 L}{(1-\nu)} \rho(x)^2 & \text{if } \left(\frac{|\rho'(x)|}{\rho} \right)^2 \ll \frac{60}{h^2} \\ \int dx \rho(x) V_{\text{edge}}(x) + \frac{1}{2} \int dx dx' \rho(x) \rho(x') u_{\text{wall}}(x - x') & \text{else.} \end{cases} \quad (3.54)$$

Now, the result in Eq. (3.54) is compared to what was found in [99, 29]. In these papers, three parameter regimes were distinguished in which different asymptotic forms of the energy expression were found. The exact separation of these regimes depend on the details of the coarse-graining method, and can thus not be compared with the result obtained here. However, in the three regimes good agreement with the expression in Eq. (3.54) is found.

In the so-called subcritical parameter regime, the glide plane spacing is large compared to the typical thickness of the pile-up. Therefore, the influence of different glide planes on each other is assumed to be negligible in [99, 29], and hence it is the "single glide plane regime". The scaling implies that the second case in Eq. (3.54) should be considered. The interaction energy $u_{\text{wall}}(x - x')$ is logarithmic at small distances, and hence the obtained expression is equivalent to Eq. (24) in [99].

In the intermediate parameter regime, the thickness of the pile-up is much longer than the glide plane spacing, but the typical distance between dislocations in x -direction is smaller than h . This implies that the first case in Eq. (3.54) should be considered. And indeed, this energy expression is equivalent to Eq. (40) in [99].

In the supercritical parameter regime, the typical distance between dislocations in x -direction is larger than h . This implies again that the second case in Eq. (3.54) should be considered. To study the extreme case, the limit $h \rightarrow 0$ should be taken. The result of this limit depends on the behavior of $\rho(x)$ in this limit. If $\rho(x)$ increases slower than $h^{-1/2}$ if h goes to 0, the second term in Eq. (3.54) vanishes. On the contrary, if $\rho(x)$ increases faster than $h^{-1/2}$, the second term blows up and dominates the integral. This extreme case is what was found in [99, 29]. However, the behavior under the limit $h \rightarrow 0$ is only a mathematical limit that cannot be achieved in an experimental setting.

An important difference between the coarse-graining using Γ -convergence, as performed in [99, 29], and the method employed in this work is that for the former, dislocations align in so-called tilt walls. This means that the discrete dislocation density is the same for all glide planes. In the latter procedure presented here, it is only assumed after coarse-graining that the average density of dislocations is independent of the glide plane. It is remarkable that despite this difference between the two coarse-graining methods, the resulting energy expressions are equivalent.

3.5 Implication for crystal plasticity

The free energy plays a crucial role in most crystal plasticity frameworks. In this section, the implications for crystal plasticity that follow from the free energy derivation presented in this chapter are presented. For clarity, our work is only compared with [43].

The free energy used in the work of Gurtin is “given by standard elastic strain energy, augmented by a defect energy $\Psi(\boldsymbol{\rho})$ ”, where

$\boldsymbol{\rho} = \{\rho_{\text{GND},e}^1, \dots, \rho_{\text{GND},e}^N, \rho_{\text{GND},s}^1, \dots, \rho_{\text{GND},s}^N\}$ with $\rho_{\text{GND},e}^i$ and $\rho_{\text{GND},s}^i$ the densities of geometrically necessary edge and screw dislocations on slip system i , respectively. The free energy density thus reads

$$\psi = \frac{1}{2} \mathbf{E}^e : \mathbb{C} \mathbf{E}^e + \Psi(\boldsymbol{\rho}). \quad (3.55)$$

The derivative of the defect energy with respect to the dislocation densities are used as a closure for the dynamic equations. These derivatives are referred to as the energetic defect forces.

The split between standard (mean-field) elastic energy and a local contribution that only depends on dislocation density, can also be recognized in our result in Eq. (3.38). The defect energy for a single slip system with only edge dislocations that follows from Eq. (3.38), reads

$$\begin{aligned} \Psi(\rho_+, \rho_-) &= k_B T \sum_{+,-} \rho_{\pm} \left(\ln \left(\frac{\rho_{\pm}}{\rho_{\pm,0}} \right) - 1 \right) - \frac{\mu b^2 L}{8\pi(1-\nu)} (\rho_+ + \rho_-) \ln \left(\frac{\rho_+ + \rho_-}{\Lambda^2} \right) \\ &= k_B T \sum_{+,-} \frac{\rho_{\text{tot}} \pm \rho_{\text{GND}}}{2} \left(\ln \left(\frac{\rho_{\text{tot}} \pm \rho_{\text{GND}}}{2\rho_{\pm,0}} \right) - 1 \right) - \frac{\mu b^2 L}{8\pi(1-\nu)} (\rho_{\text{tot}}) \ln \left(\frac{\rho_{\text{tot}}}{\Lambda^2} \right), \end{aligned} \quad (3.56)$$

where $\rho_{\text{tot}} = \rho_+ + \rho_-$ and $\rho_{\text{GND}} = \rho_+ - \rho_-$ are the total and GND density, respectively. The energetic defect forces are then different for positive and negative dislocations and read:

$$f_{\pm}(\rho_+, \rho_-) \equiv \frac{\partial \Psi(\rho_+, \rho_-)}{\partial \rho_{\pm}} = k_B T \ln \left(\frac{\rho_{\pm}}{\rho_{\pm,0}} \right) - \frac{\mu b^2 L}{8\pi(1-\nu)} \left(\ln \left(\frac{\rho_{\text{tot}}}{\Lambda^2} \right) + 1 \right). \quad (3.57)$$

The striking difference between Eqs. (3.55) and (3.56) is that in the former, the defect energy only depends on GND densities, while in the latter, the defect energy depends on both positive and negative density independently. To use the free energy expression obtained here, the modeling as performed in [43] should thus be extended to positive and negative densities separately.

At first sight, it is remarkable that the macroscopic free energy depends also on the total dislocation density, and not only on the GND density, whereas the driving force on microscopic level, i.e. the Peach-Koehler force, can be written in terms of GNDs only. However, the total density appears in the many body contribution, which is the screening correction to the leading order mean-field contribution, see the discussion in Sec. 3.3.1. Screening arises as a dislocation influences its environment, i.e. it is more likely to find positive dislocations in the immediate neighborhood of a negative dislocation, than to

find negative ones. Screening effects usually depend on the total dislocation density, and not on the GND density, see e.g. [73]. On the microscopic level there is no screening, as the positions of the dislocations are prescribed.

So to conclude, the research presented here implies that for a single slip system, a crystal plasticity model should incorporate the density and current of both positive and negative dislocations, and not just the net density. It is expected that the same holds for multiple slip systems. It is however beyond the scope of this research to decide whether it is more appropriate in a dynamical framework to use the total and GND density of dislocations for each slip system as a modeling variable, or to use densities of dislocations with different Burgers vectors.

Previously, it was indicated by Svendsen and Bargmann [106] that thermodynamically consistent crystal plasticity models based on the free energy are not restricted to the use of GND densities only. However, most models treated in that work use either only the GND density [69, 24, 25, 7, 21] or use a form of the free energy that can be split additively into a part depending on the GND or SSD density [19].

Another difference between this work and [43], is that here, it was shown that the full free energy expression in Eq. (3.38) is strongly non-local, and hence that local forms of thermodynamic laws do not apply. On the contrary, in the work of Gurtin [43], a local form of the second law, the local free energy imbalance, is used.

3.6 Summary and discussion

In this work, an explicit expression is derived for the free energy of a coarse-grained dislocation density profile in a finite medium, subjected to a prescribed boundary deformation. The free energy was determined by using statistical mechanics tools to average over many microscopic realizations of the system to retrieve the coarse-grained system properties.

The main result of this chapter is the free energy expression in Eq. (3.22). This has been obtained from the grand-canonical partition function, derived in Chap. 2. In the present chapter, a Legendre transform to the canonical ensemble is performed, which results in the free energy expression in terms of the dislocation density, Eq. (3.22). The obtained expression is an explicit functional of the dislocation density profile, the mechanical loading at the boundary and the temperature. The free energy depends on the finite volume as the elastic energy density is only integrated over a finite volume, and as the interaction between dislocations is determined in a finite medium.

The free energy in Eq. (3.22) comprises three terms: the mean-field elastic energy, the statistical contribution of the dislocations and the many-body contribution that results from the local arrangement of dislocations. Explicit expressions for these three terms arise naturally from the coarse-graining procedure.

For the statistical and many-body contribution, the local density approximation (LDA) can be used to obtain the semi-local expression in Eq. (3.38) in terms of the dislocation density, provided that the density profile does not vary too much on small length scales (see Sec. 3.4.1 for a detailed discussion). These two contributions together form the so-called defect energy, used in crystal plasticity models. From this, explicit expressions for the defect forces were derived, see Eq. (3.57).

The most prominent difference between the defect energy from most crystal plasticity

models and the defect energy derived here, is that the former depends usually only on GND densities, while the latter depends on the density of both positive and negative dislocations separately. This implies that a microscopically based crystal plasticity model should incorporate the density and current of both positive and negative dislocations for slip system, rather than the GND-related quantities only.

Furthermore, it was shown that the statistical and many-body contribution vanish at zero temperature. However, at low but finite temperature, the many-body contribution cannot be neglected.

The energy at zero temperature is simplified further for a system with equally spaced glide planes. In this specific case, the coarse-graining was also done using Γ -convergence in the literature. It is concluded here that coarse-graining using statistical physics yields the same result as Γ -convergence.

The free energy was derived by systematic coarse-graining of microstates, characterized by a finite volume subjected to given boundary deformations which contains discrete dislocations with different possible Burgers vectors \mathbf{b} on discrete glide planes. The averaging is then performed over all possible numbers and positions of dislocations, and over all strain fields that match the incompatibility imposed by the dislocations and the applied deformation at the boundary.

The main approximation in the derivation is that the system is far away from criticality. This implies that the obtained free energy expression is only accurate far away from transition points. Examples of such points are the unbinding transition of dislocations and the transition from elastic to plastic material response.

So to conclude, the new and innovative aspects of the free energy expression in Eq. (3.22) are the following:

- The free energy expression originates from statistically averaging straight and parallel, discrete dislocations in a finite volume. Apart from the straight and parallel nature of the dislocations, no assumptions on the dislocation arrangement were made.
- Properties that have proven to be important for the mechanical behavior have been included, namely the presence of glide planes and the finite volume.
- In several special cases the free energy expression reduces to a simple expression that can be implemented efficiently in a numerical scheme. The special cases considered here are a local density approximation for a single slip system, the zero temperature limit, and equally spaced glide planes.
- This free energy expression yields microscopically derived expressions for energetic defect forces in crystal plasticity models [43]. Moreover, the derivation implies that crystal plasticity models can better be formulated in terms of densities and currents of both positive and negative dislocations on each slip system, rather than in terms of GND-related quantities only.

For future research, it would be interesting to weaken the limitations as described in Sec. 3.3.3. This can be done by replacing the Gaussian approximation by a more accurate one, for example the Villain approximation [61]. Then, the free energy expression could also be used to study the melting transition, as was also studied by Mizushima [78], Ninomiya

[84], Yamamoto [118] and Burakovsky [11].

Besides that, it may be possible to derive along the same lines a free energy expression for dislocations that are not straight and not parallel. Such an extended phase space was also argued for by Hochrainer [51]. A comparable analysis for a homogeneous system of curved dislocations was performed before by Panyukov and Rabin [90].

Furthermore, new simple expressions can be obtained by considering other special cases. For example, the local density approximation can be determined for multiple slip systems. From such an expression and the resulting dislocation density profiles, the importance of the different slip systems and their mutual influence can be determined.

As we have shown that the zero temperature limit is very sensitive to approximations made in the derivation of the free energy, it would be worthwhile to extend the mathematical coarse-graining procedure of Γ -convergence to non-zero temperatures to obtain results that are more generally valid.

Based on this work, crystal plasticity models should be improved by extending the set of variables, such that the obtained free energy expression could be used. Particularly, the extension concerns including the densities for both positive and negative dislocations on each slip system, rather than only the GND-related quantities. The current derivation also suggests that, as the free energy is a strongly non-local functional, only the global version of the dissipation inequality should be used in the derivation of crystal plasticity models. It would be worthwhile to compare such a new crystal plasticity model with DDD simulations and, ultimately, experiments.

Chapter 4

Free energy of dislocations in a multi-slip geometry

Largely reproduced from: Kooiman, M., Hütter, M., and Geers, M.G.D., Free energy of dislocations in a multi-slip geometry. (submitted for publication)



Abstract

The collective dynamics of dislocations is the underlying mechanism of plastic deformation in metallic crystals. Dislocation motion in metals generally occurs on multiple slip systems. The simultaneous activation of different slip systems plays a crucial role in crystal plasticity models. In this contribution, we study the energetic interactions between dislocations on different slip systems by deriving the free energy in a multi-slip geometry. In this, we restrict ourselves to straight and parallel edge dislocations.

The obtained free energy has a long-range mean-field contribution, a statistical contribution and a many body contribution. The many body contribution is a local function of the total dislocation density on each slip system, and can therefore not be written in terms of the net dislocation density only. Moreover, this function is a strongly non-linear and non-convex function of the density on different slip systems, and hence the coupling between slip systems is of great importance.

4.1 Introduction

The plastic deformation of metallic crystals is governed by the dynamics of dislocations, i.e. line-like defects in the crystal structure. As dislocations can contain many dislocations, up to 10^6 meters of dislocation line per cubic millimeter, the collective dynamics of dislocations determines the plastic response of the crystal.

Dislocations can occur on different crystallographic slip systems. The activation of the different slip systems is an important factor in any crystal plasticity theory. Hence, the mutual influence of the different slip systems significantly affects the resulting elasto-plastic behavior of the material.

In this contribution, an explicit expression for the free energy of dislocations on different slip systems is derived, based on the implicit free energy expression derived in Chap. 2 and 3. Here, we restrict ourselves to straight and parallel edge dislocations. The resulting free energy is a functional of the dislocation density profile on each slip system, the applied deformation on the boundary and the temperature.

The chapter is organized as follows. In Sec. 4.2, the previous work is summarized and in Sec. 4.3, the local, explicit expression for the many body contribution is derived. Then, the properties of the resulting expression are discussed in Sec. 6.4.

4.2 Summary of previous results

In Chap. 2 and 3, the free energy of a dislocation density profile in a finite volume was considered. To this end, a finite body with a surface Ω and a thickness L in the \hat{z} -direction was considered. In the body, straight and parallel edge dislocations were embedded, of which the line direction corresponds to the \hat{z} -direction. The density profile of dislocations with Burgers' vector \mathbf{b} was considered for each possible Burgers' vector separately. Hence, we do not consider the net amount of dislocations only. With each possible Burgers' vector \mathbf{b} a slip system can be identified, of which the glide planes are spanned by the Burgers' vector and the line direction.

The body has a stiffness tensor \mathbb{C} at a temperature T , and mechanical loading was applied by imposing an arbitrary boundary deformation \mathbf{u}_b on $\partial\Omega$.

The resulting free energy consists of three contributions. First, there is a mean-field elastic contribution, which accounts for the long-range interactions between dislocations, which does not account for the local organization of the dislocations. Second, there is a statistical contribution that accounts for the entropy of dislocations. This term is present even if they do not interact. The same term was encountered by Groma [35], based on phenomenological arguments. Third, there is a many body contribution that corrects for the local organization of dislocations.

The free energy as a functional of the boundary deformation \mathbf{u}_b , temperature T and dislocation density profile $\rho_{\mathbf{b}}(\mathbf{S})$ for each Burgers' vector \mathbf{b} reads

$$\begin{aligned}
 F[\rho_{\mathbf{b}}(\mathbf{S}), \mathbf{u}_b, T] &= \frac{L}{2} \int_{\Omega} dA \Delta_{\text{mf}}(\mathbf{S}) : \mathbb{C} : \Delta_{\text{mf}}(\mathbf{S}) \\
 &+ k_B T \sum_{\mathbf{b}} \left\{ \int_{\Omega} dA \rho_{\mathbf{b}}(\mathbf{S}) \left(\log \left(\frac{\rho_{\mathbf{b}}(\mathbf{S})}{\rho_{\mathbf{b},0}} \right) - 1 \right) \right\} + \int_{\Omega} dA f_{\text{mb}}(\rho_{\mathbf{b}}(\mathbf{S}), T),
 \end{aligned} \tag{4.1}$$

where k_B is the Boltzmann constant, \mathbf{S} indicates the position vector in the (x, y) -plane and where $\rho_{b,0}$ is the constant background density of dislocations, of which the exact value is irrelevant as it only appears in the logarithm. The tensor Δ_{mf} is the mean-field strain due to the coarse-grained dislocation density and the imposed boundary deformation \mathbf{u}_b . This can be calculated by the incompatibility- and mechanical equilibrium equations:

$$\left. \begin{aligned} \nabla \times \boldsymbol{\beta}^p &= -\sum_{\mathbf{b}} \hat{\boldsymbol{\xi}}_{\mathbf{b}} \rho_{\mathbf{b}}(\mathbf{s}) \\ \Delta_{\text{mf}} &= (\nabla \mathbf{u} - \boldsymbol{\beta}^p)^s \\ \boldsymbol{\sigma}_{\text{mf}} &= \mathbb{C} : \Delta_{\text{mf}} \\ \nabla \cdot \boldsymbol{\sigma}_{\text{mf}} &= 0 \end{aligned} \right\} \text{in the bulk} \quad (4.2a)$$

$$\left. \begin{aligned} \mathbf{u} &= \mathbf{u}_b \\ \boldsymbol{\beta}^p &= 0 \end{aligned} \right\} \text{on the boundary.} \quad (4.2b)$$

Note that the mean-field strain is a strongly non-local functional of the dislocation positions because of the rotation in the first equation. This is because a dislocation causes strain in the whole volume.

The many body free energy density $f_{\text{mb}}(\rho_{\mathbf{b}}(\mathbf{S}), T)$ can be expressed as

$$f_{\text{mb}}(\rho_{\mathbf{b}}(\mathbf{S}), T) = \frac{k_B T}{2} \sum_{k=1}^9 \int \frac{d^2 \mathbf{q}}{(2\pi)^2} \ln(1 + \lambda_k(\mathbf{q})), \quad (4.3)$$

where $\lambda_k(\mathbf{q})$ (k ranging from 1 to 9) are the eigenvalues of the fourth order tensor $\frac{L}{k_B T} \tilde{\mathbb{G}}_0(\mathbf{q}) : (\sum_{\mathbf{b}} \rho_{\mathbf{b}}(\mathbf{S}) \hat{\mathbf{z}} \otimes \mathbf{b} \otimes \hat{\mathbf{z}} \otimes \mathbf{b})$ and where \mathbf{q} is the two-dimensional wave vector in the (x, y) -plane. Note that only non-zero eigenvalues contribute. For the fourth order tensor $\tilde{\mathbb{G}}_0(\mathbf{q})$ an explicit expression is available in infinite space, which reads

$$\tilde{\mathbb{G}}_{0,ijkl}(\mathbf{q}) = \frac{\mu}{q^2} \left(Q_{ik} Q_{jl} + R_{il} R_{kj} + \frac{2\nu}{1-\nu} R_{ij} R_{kl} \right). \quad (4.4)$$

Here, q is the length of \mathbf{q} , \mathbf{Q} and \mathbf{R} are three-dimensional second order tensors, which read $Q_{ij} = \delta_{ij} - q_i q_j / q^2$ and $R_{ij} \equiv \epsilon_{ijk} q_k / q$ with ϵ_{ijk} the anti-symmetric Levi-Civita tensor. In real space, the tensor $\mathbb{G}_0(\mathbf{R} - \mathbf{R}')$ should be interpreted as the interaction potential in infinite space between dislocations with different Burgers' vectors.

4.3 Derivation of the many body contribution for multiple slip systems

In this section, we will derive an explicit expression for the local many body contribution in Eq. (4.3) for multiple slip systems with straight and parallel edge dislocations. The angle between the Burgers' vector \mathbf{b} and the x -axis is denoted by $\theta_{\mathbf{b}}$, see Fig. 4.1. Note that $\theta_{-\mathbf{b}} = \pi + \theta_{\mathbf{b}}$.

To determine the many body contribution explicitly, we will first determine the non-zero eigenvalues $\lambda_k(\mathbf{q})$. Subsequently, we will perform the integration over \mathbf{q} in Eq. (4.3).

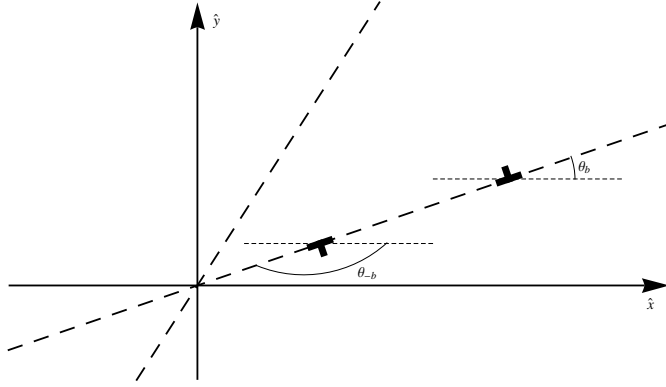


Figure 4.1: The multi-slip geometry for two slip systems.

4.3.1 Eigenvalues

To find the eigenvalues $\lambda_k(\mathbf{q})$, we will show that the fourth order tensor $\frac{L}{k_B T} \tilde{\mathbf{G}}_0(\mathbf{q}) : (\sum_b \rho_b(\mathbf{S}) \hat{\mathbf{z}} \otimes \mathbf{b} \otimes \hat{\mathbf{z}} \otimes \mathbf{b})$ can be rewritten as the diadic product of two second order tensors. Analogous to a matrix equal to the diadic product of two vectors, this form implies that there is only one non-zero eigenvalue, which is equal to the contraction of the two second order tensors.

For the simplification, we use that $Q_{ij}(\mathbf{q}) = \hat{z}_i \hat{z}_j + \frac{\epsilon_{ikl} q_k \hat{z}_l}{q} \frac{\epsilon_{jmn} q_m \hat{z}_n}{q}$ and that $R_{ij}(\mathbf{q}) = \hat{z}_i \frac{\epsilon_{jmn} q_m \hat{z}_n}{q} - \frac{\epsilon_{ikl} q_k \hat{z}_l}{q} \hat{z}_j$. In these expressions, it has been used that \mathbf{q} is perpendicular to $\hat{\mathbf{z}}$. This, and the fact that we consider only edge dislocations, i.e. for which $\mathbf{b} \perp \hat{\mathbf{z}}$, yields after some algebra

$$\begin{aligned} \frac{L}{k_B T} \delta(q_z) \tilde{\mathbf{G}}_{0,ijkl}(\mathbf{q}) \left(\sum_{\mathbf{b}} \rho_{\mathbf{b}} \hat{z}_k b_l \hat{z}_i b_j \right) &= \quad (4.5) \\ &= \frac{\mu L}{k_B T q^2} \left[2 \hat{z}_i \frac{\epsilon_{jmn} q_m \hat{z}_n}{q} + \frac{2\nu}{1-\nu} R_{ij} \right] \left[\hat{z}_i \frac{\epsilon_{lrs} q_r \hat{z}_s}{q} \left(\sum_{\mathbf{b}} \rho_{\mathbf{b}} b_l b_j \right) \right]. \end{aligned}$$

Hence the only non-zero eigenvalue is the contraction of the two second order tensors in the square brackets:

$$\begin{aligned} \lambda(\mathbf{q}) &= \frac{2\mu L}{(1-\nu)k_B T} \frac{1}{q^2} \sum_{\mathbf{b}} \rho_{\mathbf{b}} \left(\left(\frac{\mathbf{q} \times \hat{\boldsymbol{\xi}}}{q} \right) \cdot \mathbf{b} \right)^2 \quad (4.6) \\ &= \frac{2\mu L}{(1-\nu)k_B T} \frac{1}{q^2} \left[\sum_{\mathbf{b}} \rho_{\mathbf{b}} |\mathbf{b}|^2 \sin^2(\phi - \theta_{\mathbf{b}}) \right] \equiv \frac{2\mu L}{(1-\nu)k_B T} \frac{1}{2q^2} [\alpha - \beta \cos(2(\phi - \phi_0))] \end{aligned}$$

$$\text{with } \alpha = \sum_{\mathbf{b}} \rho_{\mathbf{b}} |\mathbf{b}|^2 \text{ and } \beta^2 = \sum_{\mathbf{b}, \mathbf{b}'} \rho_{\mathbf{b}} \rho_{\mathbf{b}'} |\mathbf{b}|^2 |\mathbf{b}'|^2 \cos(2(\theta_{\mathbf{b}} - \theta_{\mathbf{b}'})),$$

where ϕ is the angle between \mathbf{q} and the \hat{x} -axis. The second line was obtained by first using that $\sin^2 \phi = (1 - \cos(2\phi))/2$ for all ϕ , and second realizing that the sum

of cosine functions with a period π is again a cosine function with period π , and hence of the form $\beta \cos(2(\phi - \phi_0))$. The value of β^2 was obtained by integrating $(\sum_b \rho_b |\mathbf{b}|^2 \cos(2(\phi - \theta_b)))^2$ over $\phi \in [0, 2\pi]$ (note that $\alpha^2 \geq \beta^2$). The value of ϕ_0 was not determined explicitly, since it will turn out to be irrelevant.

4.3.2 Integration over wave vector

In this section, the integration in Eq. (4.3) over \mathbf{q} will be performed. Using the non-zero eigenvalue obtained in Eq. (4.6), the substitution $\mathbf{p} = \sqrt{\frac{(1-\nu)k_B T}{2\mu L}} \mathbf{q}$ and employing polar coordinates yields

$$f_{mb}(\rho_b, T) = \frac{\mu L}{(1-\nu)4\pi^2} \int_0^{2\pi} d\phi \int_0^\infty dp p \ln \left[\frac{\alpha + 2p^2}{2p^2} \left(1 - \frac{\beta \cos(2(\phi - \phi_0))}{\alpha + 2p^2} \right) \right]. \quad (4.7)$$

To perform the angular integral over ϕ , it is convenient to split the logarithm in the sum of two logarithms, and to expand the above expression in a power series in $\beta/(\alpha + 2p^2)$ around 0 up to infinite order. Note that this series converges as $|\alpha| > |\beta|$. In this way, the following identity can be used

$$\begin{aligned} \int d\phi \ln \left[1 - \frac{\beta \cos(2(\phi - \phi_0))}{\alpha + 2p^2} \right] &= - \sum_{n=1}^{\infty} \frac{1}{n} \int_0^{2\pi} d\phi \left(\frac{\beta \cos(2(\phi - \phi_0))}{\alpha + 2p^2} \right)^n \\ &= - \sum_{n=1}^{\infty} \frac{1}{2n} \left(\frac{\beta}{\alpha + 2p^2} \right)^{2n} \frac{2\sqrt{\pi}\Gamma(n+1/2)}{n!} = 2\pi \ln \left[\frac{1}{2} \left(1 + \sqrt{1 - \left(\frac{\beta}{\alpha + 2p^2} \right)^2} \right) \right], \end{aligned} \quad (4.8)$$

where it was used for the second line that $\int_0^{2\pi} d\phi \cos^n(2\phi) = \int_0^{2\pi} d\phi \sin^n(2\phi)$ vanishes for odd values of n , while for even values, it is equal to $2\sqrt{\pi}\Gamma(n+1/2)/n!$. Combining Eqs. (4.7) and (4.8) yields for the many body contribution

$$\begin{aligned} f_{mb}(\rho_b, T) &= \frac{\mu L}{(1-\nu)2\pi} \int_0^\infty dp p \ln \left(\frac{\alpha + 2p^2 + \sqrt{(\alpha + 2p^2)^2 - \beta^2}}{4p^2} \right) \\ &= \frac{\mu b^2 L}{(1-\nu)8\pi} \left[2p^2 - \sqrt{(\alpha + 2p^2)^2 - \beta^2} + 2p^2 \ln \left[\frac{\alpha + 2p^2 + \sqrt{(\alpha + 2p^2)^2 - \beta^2}}{4p^2} \right] + \right. \\ &\quad \left. + \alpha \ln \left[\alpha + 2p^2 + \sqrt{(\alpha + 2p^2)^2 - \beta^2} \right] \right]_0^\infty, \end{aligned} \quad (4.9)$$

Note that the last term in the square brackets diverges for large p . Therefore a large cutoff wavelength Λ_0 is introduced and the p -integration carries over the interval $[0, \Lambda_0]$. Note that a cutoff for large wavevectors corresponds to a cutoff for small length scales. This means that phenomena smaller than a certain length scale are neglected. This cutoff can be justified by noting that linear elasticity, which was used to derive Eq. (4.1), is not valid at length scales smaller than the lattice spacing. However, physical results should not depend on the exact value of the cutoff.

Finally, this yields for the many body contribution

$$\begin{aligned}
 f_{mb}(\rho_{\mathbf{b}}, T) &= \frac{\mu L}{(1-\nu)8\pi} \left[\sqrt{\alpha^2 - \beta^2} - \alpha \ln \left(\frac{\alpha + \sqrt{\alpha^2 - \beta^2}}{4\Lambda_0^2} \right) \right] \\
 &= \frac{\mu L}{(1-\nu)8\pi} \left(\sqrt{2 \sum_{\mathbf{b}, \mathbf{b}'} \rho_{\mathbf{b}} \rho_{\mathbf{b}'} |\mathbf{b} \times \mathbf{b}'|^2} \right. \\
 &\quad \left. - \left(\sum_{\mathbf{b}} \rho_{\mathbf{b}} |\mathbf{b}|^2 \right) \ln \left[\frac{(\sum_{\mathbf{b}} \rho_{\mathbf{b}} |\mathbf{b}|^2) + \sqrt{2 \sum_{\mathbf{b}, \mathbf{b}'} \rho_{\mathbf{b}} \rho_{\mathbf{b}'} |\mathbf{b} \times \mathbf{b}'|^2}}{4\Lambda_0^2} \right] \right).
 \end{aligned} \tag{4.10}$$

where we used that $1 - \cos(2\phi) = 2 \sin^2(\phi)$ to rewrite $\alpha^2 - \beta^2$. Note that this expression only depends on the logarithm of Λ_0 . Consequently, changes in the cutoff wavelength result in an additional term in the free energy, which is only linear in the density. This correspond to a constant shift of the chemical potential, which is not a physical quantity. Hence physical quantities do not depend on the value of this cutoff.

4.4 Conclusion and discussion

By combining Eqs. (4.1) and (4.10), the following free energy is obtained for edge dislocations on multiple slip systems

$$\begin{aligned}
 F[\rho_{\mathbf{b}}(\mathbf{S}), \mathbf{u}_b, T] &= \frac{1}{2} \int dV \Delta_{\text{mf}} : \mathbb{C} : \Delta_{\text{mf}} + k_B T \sum_{\mathbf{b}} \int dA \rho_{\mathbf{b}}(\mathbf{S}) \left(\log \left(\frac{\rho_{\mathbf{b}}(\mathbf{S})}{\rho_{\mathbf{b},0}} \right) - 1 \right) \\
 &+ \frac{\mu L}{(1-\nu)8\pi} \int dA \left(\sqrt{2 \sum_{\mathbf{b}, \mathbf{b}'} \rho_{\mathbf{b}} \rho_{\mathbf{b}'} |\mathbf{b} \times \mathbf{b}'|^2} \right. \\
 &\quad \left. - \left(\sum_{\mathbf{b}} \rho_{\mathbf{b}} |\mathbf{b}|^2 \right) \ln \left[\frac{(\sum_{\mathbf{b}} \rho_{\mathbf{b}} |\mathbf{b}|^2) + \sqrt{2 \sum_{\mathbf{b}, \mathbf{b}'} \rho_{\mathbf{b}} \rho_{\mathbf{b}'} |\mathbf{b} \times \mathbf{b}'|^2}}{4\Lambda_0^2} \right] \right).
 \end{aligned} \tag{4.11}$$

The many body contribution is written in terms of the total density of all dislocations $\sum_{\mathbf{b}} \rho_{\mathbf{b}}$ and the square of the perpendicular components of each two slip systems $\sum_{\mathbf{b}, \mathbf{b}'} \rho_{\mathbf{b}} \rho_{\mathbf{b}'} |\mathbf{b} \times \mathbf{b}'|^2$. Both can be written in terms of the total density on each slip system. For the latter, it should be used that $|(-\mathbf{b}) \times \mathbf{b}'|^2 = |\mathbf{b} \times \mathbf{b}'|^2$. Therefore, this term can be rewritten as

$$\begin{aligned}
 \sum_{\mathbf{b}, \mathbf{b}'} \rho_{\mathbf{b}} \rho_{\mathbf{b}'} |\mathbf{b} \times \mathbf{b}'|^2 &= \sum_{\mathbf{b}, \mathbf{b}'} \frac{\rho_{\mathbf{b}} \rho_{\mathbf{b}'} + \rho_{\mathbf{b}} \rho_{-\mathbf{b}'} + \rho_{-\mathbf{b}} \rho_{\mathbf{b}'} + \rho_{-\mathbf{b}} \rho_{-\mathbf{b}'}}{4} |\mathbf{b} \times \mathbf{b}'|^2 \\
 &= \sum_{s, s' \in \text{slip systems}} \rho_{\text{tot}, s} \rho_{\text{tot}, s'} |\mathbf{b}_s \times \mathbf{b}_{s'}|^2,
 \end{aligned}$$

Hence the free energy is also a functional of the total density on each slip system. Moreover, note that the many body contribution is a non-convex function of the dislocation density. For example, when the above expression is worked out for two slip systems

under an angle of 60° with Burgers' vectors of equal length, and the total density on the first slip system is kept fixed, the many body free energy density as a function of ρ_2/ρ_1 reads

$$f_{mb}(\rho_2/\rho_1, T) = \frac{\mu b^2 L}{(1-\nu)8\pi} \rho_1 \left(\sqrt{2 \left(1 + \left(\frac{\rho_2}{\rho_1} \right)^2 + \frac{3}{2} \frac{\rho_2}{\rho_1} \right)} - \left(1 + \frac{\rho_2}{\rho_1} \right) \ln \left[1 + \frac{\rho_2}{\rho_1} + \sqrt{2 \left(1 + \left(\frac{\rho_2}{\rho_1} \right)^2 + \frac{3}{2} \frac{\rho_2}{\rho_1} \right)} \right] - \left(1 + \frac{\rho_2}{\rho_1} \right) \ln \left[\frac{\rho_1}{\Lambda_0} \right] \right). \quad (4.12)$$

Note that the last term depends on ρ_1 and Λ_0 . However, it is linear in ρ_2/ρ_1 , and hence does not change the convex/concave form of the equation. The first two contributions are plotted in fig. 4.2. As one can see, this graph is not convex.

Non-convex free energy functions were used in the literature [62, 117] to explain inho-

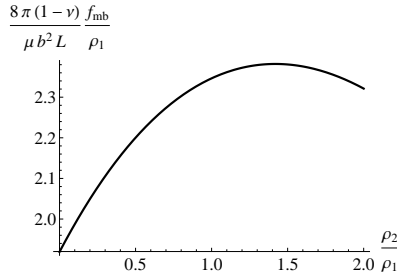


Figure 4.2: Many body free energy density as a function of the dislocation density. As one can see, this function is non-convex.

mogeneities in the strain distribution. The non-convex many body term will also yield inhomogeneous dislocation densities, and hence inhomogeneities in the strain distribution. A term depending on the gradient of the dislocation density was not derived here. This could in principle be derived from Eq. (4.1) as in Sec. 3.4.1, by means of an expansion in terms of the gradient. This would yield a weakly non-local expression in terms of the dislocation density.

Finally, one could wonder whether the the interaction between slip systems derived here could be approximated by a simple quadratic coupling as proposed by Gurtin [43]. To this end, one would have to expand the above expression around a reference density up to quadratic order. This is not feasible for two reasons. First, the many body contribution is non-convex, which implies that such a coupling would be negative, and hence that one expands around a maximum, rather than a minimum. Second, the obtained many body contribution is strongly non-linear in the dislocation density, and hence a series expansion would be an oversimplification.

Chapter 5

Effective mobility of dislocations from systematic coarse-graining

Largely reproduced from: Kooiman, M., Hütter, M., and Geers, M.G.D., Effective mobility of dislocations from systematic coarse-graining. *Journal of Statistical Mechanics Theory and Experiment*, P06005, 2015



Abstract

The dynamics of large amounts of dislocations governs the plastic response of crystalline materials. In this contribution we discuss the relation between the mobility of discrete dislocations and the resulting flow rule for coarse-grained dislocation densities. The mobilities used in literature on these levels are quite different, for example in terms of their intrinsic stress dependence. To establish the relation across the scales, we have derived the macroscopic evolution equations of dislocation densities from the equations of motion of individual dislocations by means of systematic coarse-graining. From this, we can identify a memory kernel relating the driving force and the flux of dislocations. This kernel can be considered as an effective macroscopic mobility with two contributions; a direct contribution related to the overdamped motion of individual dislocations, and an emergent contribution that arises from time correlations of fluctuations in the Peach-Koehler force. Scaling analysis shows that the latter contribution is dominant for dislocations in metals at room temperature. We also discuss several concerns related to the separation of timescales.

5.1 Introduction

The main carriers of plastic flow in metallic materials are dislocations, i.e. line-like defects in the crystal structure. Metals can contain up to 10^6 meters of dislocation lines per cubic millimeter. Therefore, the understanding of the collective dynamical behavior of dislocation densities is critical in developing a crystal plasticity model that is based on the underlying mechanism of dislocation transport. This chapter focusses on collective effects in the dynamical response. For simplicity, we will restrict ourselves to straight and parallel dislocations.

The transport relations used for individual dislocations are quite different from those generally used for dislocation densities. On the one hand, in discrete dislocation dynamics (DDD) simulations [110], the motion of dislocations is overdamped, and hence the velocity of dislocations is taken linearly proportional to the Peach-Koehler force on them. This assumption is supported by molecular dynamics simulations [65, 86, 96], where dislocation velocity is linearly proportional to the applied load in a quite large regime. On the other hand, a viscoplastic flow rule is commonly used in phenomenological modeling to relate the stress to the plastic flow of the material. This flow rule is often of power-law form [40, 43] to mimic rate-independent plasticity with a dynamic activation of different slip systems. The exponent is mostly not equal to one, and consequently, the flow is not linearly proportional to the stress. The exponent of this power-law is often chosen such that the material is almost rate independent: the material will only flow when a certain threshold value of the stress is reached.

The question thus arises how the microscopic and macroscopic evolution equations are related. Recent coarse-graining attempts focus on closures of the BBGKY-hierarchy of equations that relate the evolution of the n -body density to an integral of the $n + 1$ -body density, see e.g. [32, 120, 34]. Yet, these calculations do not result in a different mobility on macroscopic level. The reason for this is that the BBGKY-hierarchy is obtained by integrating out microscopic degrees of freedom, and hence there is only averaging over phase space, but a transition in observation-timescale is not involved. In other words, the BBGKY-hierarchy concentrates on the spatial correlation effects, while time-correlations are not examined.

An alternative approach to obtain macroscopic dynamics and transport coefficients are the Green-Kubo relations, where the macroscopic transport coefficient is the time-integral of correlations of fluctuations in the microscopic flux, see e.g. [66, 52, 53, 103]. This procedure thus includes both averaging over phase space and over correlations in the fluctuating dynamical processes, which results in a qualitatively different transport coefficient on macroscopic level. Green-Kubo relations thus demonstrate how (additional) irreversibility emerges when going to coarser levels of description.

It would be worthwhile to apply Green-Kubo relations to dislocation systems. However, these relations have originally been derived near equilibrium while dislocation distributions are far from equilibrium. Namely, they are not necessarily in thermal equilibrium with the environment and are mostly subjected to a mechanical load. As a result, the role and magnitude of the different kinds of fluctuations in the system are not clear. Therefore, we use in this contribution a systematic coarse graining method within the framework of the General Equations for the Non-Equilibrium Reversible-Irreversible Coupling (GENERIC-framework), see [89, 31, 87, 88], to derive macroscopic evolution equations for the dislo-

cation density based on the microscopic evolution equations, as shown in detail below.

The new and innovative aspect of the study presented here is that, for the first time, the macroscopic mobility of dislocations is derived by systematic coarse-graining, where also time-correlations are taken into account. By this means, an emergent contribution in the response functions of the dislocation density profile has been identified, which turns out to be dominant for dislocations in metals at room temperature. This could explain the apparent difference between the microscopic and macroscopic mobilities currently used in literature, but additional numerical investigations are needed to properly elucidate this. Furthermore, it was shown that the Markovian approximation is not appropriate to describe the dynamics of dislocation densities.

The chapter is organized as follows: in Sec. 5.2 we introduce the GENERIC framework that will be employed in this work. In Sec. 5.3.1, we discuss the evolution equations on the microscopic level of individual dislocations. In Sec. 5.3.2, we describe the macroscopic variables of interest, and their connection to the microscopic variables. Next, we derive the macroscopic evolution equation for the dislocation density profile in Eq. (5.22). In Sec. 5.4, we interpret our result and compare it to other approaches in literature. In Sec. 5.5, we discuss the effective, macroscopic mobility. In Sec. 5.6, we present a summary and an outlook for future work.

5.2 Introduction to GENERIC

In this section, the GENERIC framework is described, since it is used to derive the evolution equations for the macroscopic variables from the microscopic evolution equations. For more detailed information, we refer to e.g. [31, 89, 88].

A necessary condition for the applicability of the GENERIC framework is that the microstates are in quasi-equilibrium with the macroscopic control parameters, which is the analog of the ergodicity requirement in equilibrium thermodynamics. This however does not imply that the ensemble should be considered “as an exact representation of the true state of the atomistic system” [88], but rather as the best choice when only some average macroscopic variables are experimentally accessible.

It has been questioned previously whether the ergodicity assumption applies to dislocation systems. However, it has been shown recently [59] that statistical averages over many small dislocation systems yield a realistic macroscopic behavior. It is therefore assumed that the GENERIC framework can be applied to dislocation systems.

Microscopic variables are denoted with a subscript 1, and macroscopic variables with a subscript 2. The explicit connection between the two sets of independent variables, $\{\mathbf{x}_1\}$ and $\{\mathbf{x}_2\}$, is given by a map $\mathbf{\Pi} : \{\mathbf{x}_1\} \mapsto \{\mathbf{x}_2\}$ that maps the set of microstates $\{\mathbf{x}_1\}$ onto the set of macrostates $\{\mathbf{x}_2\}$. In other words, it associates a macrostate \mathbf{x}_2 with each microstate \mathbf{x}_1 . Furthermore, a probability density $\rho_{\mathbf{x}_2}(\mathbf{x}_1)$ is defined on the space of microstates. This gives the probability to find a certain microstate \mathbf{x}_1 , given that the macroscopic system is in the state \mathbf{x}_2 . The probability density should be normalized to 1. Both the microscopic and macroscopic variables are assumed to describe a closed system. It is assumed that on the microscopic level, the Markovian approximation holds. Then,

the time-evolution equations at the microscopic level can be written in the following form

$$\dot{\mathbf{x}}_1 = \mathbf{L}_1[\mathbf{x}_1] \cdot \frac{\delta E_1[\mathbf{x}_1]}{\delta \mathbf{x}_1} + \mathbf{M}_1[\mathbf{x}_1] \cdot \frac{\delta S_1[\mathbf{x}_1]}{\delta \mathbf{x}_1}, \quad (5.1)$$

where the inner product denotes a contraction over all components of microscopic variables \mathbf{x}_1 . If \mathbf{x}_1 entails field variables, this product also entails a spatial integral. Furthermore, E_1 and S_1 are the total energy and entropy function(al)s at the microscopic level, $\mathbf{L}_1[\mathbf{x}_1]$ is the Poisson matrix that represents the geometric structure, and $\mathbf{M}_1[\mathbf{x}_1]$ is the friction matrix describing dissipative material properties. The first term on the RHS represents the reversible evolution, and the second term the irreversible evolution.

In general, the dynamic matrices \mathbf{L}_1 and \mathbf{M}_1 should have certain properties to describe a thermodynamically consistent model. First, the Poisson matrix should satisfy the so-called Jacobi's Identity, and it should be anti-symmetric in a generalized operator sense. Second, the friction matrix should be positive semi-definite and symmetric. Third, the following degeneracy conditions have to be fulfilled

$$\mathbf{L}_1 \cdot \frac{\delta S_1}{\delta \mathbf{x}_1} = 0 \quad ; \quad \mathbf{M}_1 \cdot \frac{\delta E_1}{\delta \mathbf{x}_1} = 0. \quad (5.2)$$

The first degeneracy condition expresses the fact that reversible processes (governed by \mathbf{L}_1) do not produce entropy, and the second ensures, together with the anti-symmetry of \mathbf{L}_1 , the conservation of total energy in the system. Combined with the degeneracy condition, the symmetric and positive-definite nature of \mathbf{M}_1 reflects the fact that the entropy production is always positive.

In the following, it will be assumed that the microscopic dynamics of the system of interest is completely irreversible, as this simplifies the notation. It will be shown that this assumption is true for the dislocation system studied here. The evolution equations of the macroscopic system can then be expressed as follows, see [88, 22]

$$\dot{\mathbf{x}}_2 = \mathbf{M}'_2[\mathbf{x}_2] \cdot \frac{\delta S_2[\mathbf{x}_2(t)]}{\delta \mathbf{x}_2} + \frac{1}{k_B} \int_0^\tau d\Delta t \mathbf{K}_2[\mathbf{x}_2; \Delta t] \cdot \frac{\delta S_2[\mathbf{x}_2(t - \Delta t)]}{\delta \mathbf{x}_2}, \quad (5.3)$$

where S_2 is the macroscopic entropy functional, and \mathbf{M}'_2 and \mathbf{K}_2 contain the dynamical response functions of the macroscopic system. The matrix \mathbf{M}'_2 arises from the direct upscaling of the microscopic dynamics, while \mathbf{K}_2 captures the emerging irreversibility upon changing model-level from fast variables \mathbf{x}_1 to slow averaged variables \mathbf{x}_2 .

The timescale τ is the timescale on which \mathbf{K}_2 decays to zero. Note that the Markovian approximation is not used at the macroscopic level, as it is not a priori sure whether there is separation of timescales. When separation of timescales does apply, the entropy derivative at time $t - \Delta t$ can be replaced by the derivative at time t . In that case, Eq. (5.3) has the same GENERIC form as Eq. (5.1) with $\mathbf{M}_2 = \mathbf{M}'_2 + \frac{1}{k_B} \int_0^\tau d\Delta t \mathbf{K}_2$.

The building blocks on the RHS of Eq. (5.3) can be derived from the microscopic building blocks by (this is a straightforward modification of [88, Sec. 6.4.3])

$$S_2[\mathbf{x}_2] = \langle S_1(\mathbf{x}_1) - k_B \ln [\rho_{\mathbf{x}_2}(\mathbf{x}_1)] \rangle_{\mathbf{x}_2} \quad (5.4a)$$

$$\mathbf{M}'_2(\mathbf{x}_2) = \left\langle \frac{\delta \mathbf{\Pi}}{\delta \mathbf{x}_1} \cdot \mathbf{M}_1(\mathbf{x}_1) \cdot \frac{\delta \mathbf{\Pi}}{\delta \mathbf{x}_1} \right\rangle_{\mathbf{x}_2} \quad (5.4b)$$

$$\mathbf{K}_2(\mathbf{x}_2; \Delta t) = \langle\langle D\mathbf{\Pi}(\mathbf{x}_1, 0), D\mathbf{\Pi}(\mathbf{x}_1, \Delta t) \rangle\rangle \quad (5.4c)$$

with

$$D\Pi(\mathbf{x}_1) = \frac{\delta\Pi}{\delta\mathbf{x}_1} \cdot \left(\mathbf{M}_1(\mathbf{x}_1) \cdot \frac{\delta S_1}{\delta\mathbf{x}_1} + k_B \frac{\delta}{\delta\mathbf{x}_1} \cdot \mathbf{M}_1(\mathbf{x}_1) \right) + k_B \mathbf{M}_1(\mathbf{x}_1) : \frac{\delta^2\Pi}{\delta\mathbf{x}_1\delta\mathbf{x}_1}$$

where k_B is Boltzmann constant, and where the double dot denotes a double contraction over all components of \mathbf{x}_1 , so for an arbitrary matrix \mathbf{A} it is $\mathbf{M}_1 : \mathbf{A} = M_{1,\alpha\beta\gamma\delta} A_{\gamma\delta}$. The single and double angular brackets are defined by

$$\langle \hat{A}(\mathbf{x}_1) \rangle_{\mathbf{x}_2} = \int d\mathbf{x}_1 \rho_{\mathbf{x}_2}(\mathbf{x}_1) \hat{A}(\mathbf{x}_1) \quad (5.5a)$$

$$\begin{aligned} \langle\langle \hat{A}(\mathbf{x}_1, 0), \hat{B}(\mathbf{x}_1, \Delta t) \rangle\rangle &= \langle\langle \left(\hat{A}(\mathbf{x}_1(0)) - \langle \hat{A}(\mathbf{x}_1(0)) \rangle_{\mathbf{x}_2} \right) \\ &\quad \left(\hat{B}(\mathbf{x}_1(\Delta t)) - \langle \hat{B}(\mathbf{x}_1(\Delta t)) \rangle_{\mathbf{x}_2} \right) \rangle_{\text{Wiener}} \rangle_{\mathbf{x}_2}, \end{aligned} \quad (5.5b)$$

for two observables $\hat{A}(\mathbf{x}_1)$ and $\hat{B}(\mathbf{x}_1)$, that are function(al)s of the microscopic variables \mathbf{x}_1 . The single bracket thus denotes an ensemble average, and the double brackets denote the average over the time-correlations of fluctuations. Note that the double bracket entails two averages: an average over the stochastic Wiener process that governs the microscopic dynamics and an ensemble average over the ensemble of initial states.

5.3 Evolution equations

5.3.1 Microscale evolution equations

The objective of this contribution is to derive the evolution equations of dislocation density profiles under mechanical loading directly from the evolution equations of individual dislocations. From this, the dynamical response at the macroscopic level can be determined. As explained, we will restrict ourselves to straight and parallel dislocations for simplicity. As most of the dislocation transport is through the bulk, the focus of this work is on the dynamical response in the bulk. It is assumed that these are equal to the transport coefficients in an infinite, macroscopically homogeneous single crystal slab of material with the same properties and with a thickness L in the direction of the dislocation lines. The microscale system of interest thus consists of an infinite medium with a given, spatially constant elastic compliance tensor \mathbb{S} . In this medium, an arbitrarily large number N of straight and parallel dislocations is embedded. The dislocations could have all possible Burgers vectors allowed by the crystallographic planes. Moreover, we do not only consider net dislocations. As we restrict ourselves to straight and parallel dislocations, the system can be described as an effective two-dimensional system where the position of the dislocation lines are given by their intersection points with a plane perpendicular to the dislocation line direction. The position of the i^{th} dislocation is therefore denoted by the two-dimensional vector $\mathbf{R}(i)$ and its Burgers' vector by $\mathbf{b}(i)$. In this chapter, a Lagrangian frame of reference is used. Furthermore, the infinite medium is subjected to a macroscopic stress, which is the volume average of the total stress field:

$$\Sigma \equiv \frac{1}{V} \int dV \boldsymbol{\sigma}, \quad (5.6)$$

where V is the total volume. Note that the volume average of the stress due to a single dislocation is zero in the infinite, macroscopically homogeneous single crystal slab of material considered here. The total stress field σ could then be written as a sum of the macroscopic stress field Σ and the stress fields of the individual dislocations. The stress field due to a single dislocation in infinite space is given by e.g. Hirth and Lothe [49], and is denoted by $\tilde{\sigma}(i)$ for the i^{th} dislocation. The total stress field thus reads

$$\sigma = \Sigma + \sum_i \tilde{\sigma}(i). \quad (5.7)$$

The dislocations in this medium are assumed to move according to a linear drag relation, and the stochastic force on dislocations is neglected. Dislocations only move in their glide plane, i.e. the plane spanned by the Burgers vector and the line direction. This slip direction is indicated by \hat{s}_b . Note that climb of dislocations is thus excluded. The velocity of the dislocations is linearly proportional to the component of the Peach-Koehler force in the slip direction, and hence

$$\frac{d\mathbf{R}(i)}{dt} = \frac{\hat{s}_{b(i)}}{B_{b(i)}(T)} \frac{\hat{s}_{b(i)} \cdot \mathbf{F}_{pk}(i)}{L}, \quad (5.8)$$

where $B_b(T)$ is the temperature-dependent mobility. It follows from MD simulations that, to a good approximation, $B_b(T) \propto T$, see e.g. [86]. Note that the mobility could be different for dislocations with different Burgers vectors. Namely, it has been reported in literature [96], that the mobility of edge and screw dislocations can be quite different. Furthermore, $\mathbf{F}_{pk}(i)/L$ is the Peach-Koehler force per unit length of dislocation line on the i^{th} dislocation. This is given by $(\sigma(\mathbf{R}(i)) \cdot \mathbf{b}(i)) \times \hat{\xi}$, where $\hat{\xi}$ is the line direction, and where $\sigma(\mathbf{R}(i))$ is the stress field at the position of the i^{th} dislocation. It is thus not equal to $\tilde{\sigma}(i)$, which is the stress field due to the i^{th} dislocation.

We will now rewrite the evolution equation (5.8) in the GENERIC framework. As the GENERIC-framework is only applicable for closed systems, see [31], the heat bath should be modeled as well. For this system, the lattice will act as a thermal reservoir, as the energy that is dissipated by the overdamped motion of dislocations will heat up the lattice. To characterize the state of the lattice, one could model either temperature, lattice energy or lattice entropy. For convenience, we choose the lattice entropy S_{lat} as a variable. The microscopic GENERIC variables are thus the positions of the N dislocations and the lattice entropy; $\mathbf{x}_1 = \{\mathbf{R}(1), \dots, \mathbf{R}(N), S_{\text{lat}}\}$, where $\mathbf{R}(1), \dots, \mathbf{R}(N)$ denotes the set of position vectors.

Now, the GENERIC building blocks (i.e. the energy, entropy and friction matrix) that are consistent with the evolution equation (5.8) can be determined. The microscopic entropy $S_1(\mathbf{x}_1)$ is just the entropy of the lattice, and the microscopic energy $E_1(\mathbf{x}_1)$ is the sum of the thermal energy of the lattice and the elastic energy that follows from the total stress field σ . It is assumed that the elasticity of the material is of energetic nature (i.e. that the stiffness is independent of the temperature), which is the case for metals. This implies that the derivative of the energy with respect to strain or stress is independent of temperature (and hence of S_{lat}). Consequently, the energy has two decoupled contributions, namely, the elastic energy, which is independent of S_{lat} and the thermal energy of the lattice, which is independent of dislocation positions or mechanical

loading.

So to conclude, the microscopic entropy and energy, and their respective derivatives read

$$\begin{aligned} S_1(\mathbf{x}_1) &= S_{\text{lat}} & ; & \quad \frac{\delta S_1}{\delta \mathbf{x}_1} = (0, 1) \\ E_1(\mathbf{x}_1) &= E_{\text{lat}}(S_{\text{lat}}) + \frac{1}{2} \int dV \boldsymbol{\sigma} : \mathbb{S} : \boldsymbol{\sigma} & ; & \quad \frac{\delta E_1}{\delta \mathbf{x}_1} = (-\mathbf{F}_{pk}(1), \dots, -\mathbf{F}_{pk}(N), T_{\text{lat}}), \end{aligned} \quad (5.9)$$

where the lattice temperature T_{lat} is defined by $T_{\text{lat}} \equiv \frac{dE_{\text{lat}}}{dS_{\text{lat}}}$, and where

$\mathbf{F}_{pk}(1), \dots, \mathbf{F}_{pk}(N)$ denotes the set of Peach-Koehler forces on each dislocation. The derivation of $\frac{dE_1}{d\mathbf{R}(i)} = -\mathbf{F}_{pk}(i)$ was worked out previously in the literature, see e.g. [75, 110].

The microscopic friction matrix $\mathbf{M}_1(\mathbf{x}_1)$ should model the drag of dislocations through the lattice, as given in Eq. (5.8), and the resulting change in lattice entropy. Using the symmetry and degeneracy of the friction matrix, Eqs. (5.2), yields for the friction matrix

$$\mathbf{M}_1(\mathbf{x}_1) = \left(\frac{\hat{\mathbf{s}}_{\mathbf{b}(i)}}{\frac{\hat{\mathbf{s}}_{\mathbf{b}(i)} \cdot \mathbf{F}_{pk}(i)}{T_{\text{lat}}}} \right) \frac{T_{\text{lat}}}{LB_{\mathbf{b}(i)}(T_{\text{lat}})} \delta_{ii'} \left(\hat{\mathbf{s}}_{\mathbf{b}(i')}, \frac{\hat{\mathbf{s}}_{\mathbf{b}(i')} \cdot \mathbf{F}_{pk}(i')}{T_{\text{lat}}} \right). \quad (5.10)$$

It can be verified that $\frac{d\mathbf{x}_1}{dt} = \mathbf{M}_1(\mathbf{x}_1) \cdot \frac{\delta S_1}{\delta \mathbf{x}_1}$ yields Eq. (5.8) for the evolution of dislocation positions. The resulting evolution of the lattice entropy is given by

$$\frac{dS_{\text{lat}}}{dt} = \frac{1}{T_{\text{lat}}} \sum_i \mathbf{F}_{pk}(i) \cdot \frac{d\mathbf{R}(i)}{dt}. \quad (5.11)$$

This equation can be interpreted as follows: $\mathbf{F}_{pk}(i) \cdot \frac{d\mathbf{R}(i)}{dt}$ is the force on the i^{th} dislocation times its velocity, and hence the power dissipated by this dislocation. The sum over all dislocations is thus the total dissipated power. As the system is closed, this is equal to the increase of the lattice energy per unit of time. The temperature $T_{\text{lat}} \equiv \frac{dE_{\text{lat}}}{dS_{\text{lat}}}$ indicates how the lattice energy changes as the lattice entropy changes.

5.3.2 Macroscopic evolution equations

The microscopic GENERIC building blocks can be coarse-grained to obtain macroscopic evolution equations. To do the upscaling, the macroscopic variables, the projection operators between the microscopic and macroscopic level, and the probability density on phase space need to be defined first, see Sec. 5.2.

The first macroscopic state variable is the average dislocation density profile $\rho_{\mathbf{b}}(\mathbf{R})$, which is defined for family of dislocations with the same Burgers vector $\mathbf{b}(i) = \mathbf{b}$ separately. Note that we do thus not only consider net densities of dislocations. As dislocations on the microscopic level are assumed to move only in their glide plane and will thus not climb, the dislocation density will be zero in between these glide planes. The positions of the glide planes are considered to be fixed in the material, and do thus not change during the evolution.

The other two macroscopic state variables are related to the temperature of the material. As mentioned in the introduction, the spatial distribution of dislocations is in general

far from thermal equilibrium with the environment as their dynamics is slow. A similar problem arises in glassy systems, where configurational degrees of freedom are not in equilibrium with the environmental temperature. To overcome this problem, systems out of thermal equilibrium could be described by two temperatures, see e.g. [15, 72, 10]. To this end, the energy landscape is virtually split in different basins of attraction associated with local minima in the energy. The first temperature is then equal to the environmental temperature, and controls the vibrational energy of the system around local energy minima. The second temperature controls the distribution over the different local minima. These temperatures are only different if the energy barriers between the local minima are high, such that the transitions between different minima take place on a timescale much longer than the timescale of interest. A similar distinction between the ‘physical’ heat bath temperature and the configurational was made in the context of dislocations by Limkumnerd and Van der Giessen [73], and by Groma [35].

The first temperature used here is the temperature of the heat bath, T_B , that governs the *average* energy associated with thermal fluctuations, which is the average of the lattice energy $E_{\text{lat}}(S_{\text{lat}})$ in Eq. (5.9). The second temperature is the effective temperature of the configuration, T_C , that governs the average energy associated with the interaction energy of dislocations. This is the elastic contribution in Eq. (5.9).

As macroscopic state variables we thus use the average dislocation density profiles, the average energy of the lattice, \bar{E}_B , and the average configurational energy of the dislocations, \bar{E}_C , so $\mathbf{x}_2 = \{\{\rho_{\mathbf{b}}(\mathbf{R})\}, \bar{E}_B, \bar{E}_C\}$. The latter two are controlled by the temperature of the heat bath and the configurational temperature respectively.

The next step is to define the mapping $\mathbf{\Pi} : \{\mathbf{x}_1\} \mapsto \{\mathbf{x}_2\}$ between microscopic and macroscopic variables. Analogous to [56, Ch. 5], the projection and its derivative are defined by

$$\mathbf{\Pi} = \begin{pmatrix} \Pi_{\rho_{\mathbf{b}}}(\mathbf{R}) \\ \Pi_{\bar{E}_B} \\ \Pi_{\bar{E}_C} \end{pmatrix} = \begin{pmatrix} \sum_{i, \mathbf{b}(i)=\mathbf{b}} \delta(\mathbf{R}(i) - \mathbf{R}) \\ E_{\text{lat}}(S_{\text{lat}}) \\ \frac{1}{2} \int dV \boldsymbol{\sigma} : \mathbb{S} : \boldsymbol{\sigma} \end{pmatrix} \quad (5.12)$$

$$\frac{\delta \mathbf{\Pi}}{\delta \mathbf{x}_1} = \begin{pmatrix} -\delta_{\mathbf{b}(1), \mathbf{b}} \nabla_{\mathbf{R}} \delta(\mathbf{R}(1) - \mathbf{R}) \dots - \delta_{\mathbf{b}(N), \mathbf{b}} \nabla_{\mathbf{R}} \delta(\mathbf{R}(N) - \mathbf{R}) & 0 \\ 0 & T_{\text{lat}} \\ -\mathbf{F}_{pk}(i) \dots - \mathbf{F}_{pk}(N) & 0 \end{pmatrix},$$

where the summation denotes a sum over all dislocations i for which $\mathbf{b}(i) = \mathbf{b}$.

The last step is to define the probability density on phase space. As only average quantities are used as macroscopic variables, it is most convenient to work in a generalized canonical ensemble. To this end, three Lagrange parameters are defined, namely the local chemical potential $\mu_{\mathbf{b}}(\mathbf{R})$ (defined for each Burgers vector separately), the temperature of the heat bath T_B and the configurational temperature T_C . The probability density then reads (see e.g. [88])

$$\rho_{\mathbf{x}_2}(\mathbf{x}_1) = \frac{\exp\left[\frac{S_{\text{lat}}}{k_B} - \frac{\Pi_{\bar{E}_B}(S_{\text{lat}})}{k_B T_B}\right] \exp\left[-\frac{\Pi_{\bar{E}_C}(\mathbf{R}(i))}{k_B T_C} + \frac{1}{k_B T_C} \sum_{\mathbf{b}} \int d\mathbf{R} \mu_{\mathbf{b}}(\mathbf{R}) \Pi_{\rho_{\mathbf{b}}}(\mathbf{R})\right]}{Z_B[T_B] Z_C[\mu_{\mathbf{b}}(\mathbf{R}), T_C]}, \quad (5.13)$$

where $Z_B[T_B]$ and $Z_C[\mu_{\mathbf{b}}(\mathbf{R}), T_C]$ are the partition functions of the lattice and dislocations, respectively. The latter depends on the macroscopic mechanical loading $\boldsymbol{\Sigma}$, as the

configurational energy depends on the loading. The partition functions are determined by the normalization of the first and second term on the RHS separately. For the first, one should integrate over the lattice entropy, and for the second, one should sum over all possible numbers of dislocations and integrate over dislocation positions.

The multiplicative split in the probability density results from the additive split of the microscopic energy in Eq. (5.9) into two parts that depend either on S_{lat} or on $\{\mathbf{R}(i)\}$. This split also implies that ensemble averages can be split multiplicatively. Hence, for two arbitrary functions $g_1(S_{\text{lat}})$ and $g_2(\mathbf{R}(i))$, one finds

$$\langle g_1(S_{\text{lat}})g_2(\mathbf{R}(i)) \rangle_{\mathbf{x}_2} = \langle g_1(S_{\text{lat}}) \rangle_{T_B} \langle g_2(\mathbf{R}(i)) \rangle_{\mu_b(\mathbf{R}), T_C}. \quad (5.14)$$

The Lagrange parameters are implicitly defined in terms of the macroscopic variables by

$$\bar{E}_B = \langle \Pi_{\bar{E}_B} \rangle_{T_B} \quad ; \quad \bar{E}_C = \langle \Pi_{\bar{E}_C} \rangle_{\mu_b(\mathbf{R}), T_C} \quad ; \quad \rho_b(\mathbf{R}) = \langle \Pi_{\rho_b(\mathbf{R})} \rangle_{\mu_b(\mathbf{R}), T_C}. \quad (5.15)$$

Together with the multiplicative split in Eq. (5.14), these definitions imply that the temperature of the heat bath T_B only depends on \bar{E}_B , and moreover that the configurational temperature T_C and the local chemical potential $\mu_b(\mathbf{R})$ are independent of \bar{E}_B , and hence of the temperature of the heat bath. This once more illustrates the split of the system into two different subsystems.

Now, the macroscopic GENERIC building blocks S_2 , M_2 and K_2 can be derived systematically. The macroscopic entropy is by definition a Legendre transform of the thermodynamic potential that follows from the partition functions in Eq. (5.13), see [88, Eq. (6.57)]. Hence the macroscopic entropy reads, see C.1 for details

$$S_2(\mathbf{x}_2) = \frac{-F_B(T_B) + \bar{E}_B}{T_B} + \frac{-F_C[\rho_b(\mathbf{R}), T_C] + \bar{E}_C}{T_C}, \quad (5.16)$$

where F_B and F_C follow from Z_B and Z_C . $F_B(T_B)$ should be interpreted as the free energy of the lattice at temperature T_B and $F_C[\rho_b(\mathbf{R}), T_C]$ as the free energy of the dislocation density profile $\rho_b(\mathbf{R})$ at a configurational temperature T_C . Note that the latter also depends on the volume-average stress Σ , as $\Pi_{\bar{E}_C}$ depends on Σ . To work with this entropy in practice, a free energy functional is thus needed for both the lattice and the dislocation density. For more details on the determination of the free energy of dislocations, we refer to Chap. 2-4.

To determine the entropy derivative with respect to the macroscopic variables, one should note that both temperatures are implicit functionals of the macroscopic variables by Eq. (5.15). Hence the chain rule should be used to obtain these derivatives. However, the explicit relation in Eq. (5.15) turns out not to be necessary in the derivation. Instead, the thermodynamic relations $\frac{dF_B}{dT_B} = -S_B(T_B)$ and $\frac{dF_C}{dT_C} = -S_C(T_C)$ only, are sufficient to obtain the following entropy derivatives:

$$\frac{\delta S_2}{\delta \mathbf{x}_2} = \left(-T_C^{-1} \left. \frac{\delta F_C}{\delta \rho_b(\mathbf{R})} \right|_{T_C}, T_B^{-1}, T_C^{-1} \right), \quad (5.17)$$

where the free energy derivative in the first component is at constant configurational temperature, rather than at constant configurational energy. By combining Eqs. (5.4b), (5.10) and (5.12), one finds that the matrix M'_2 can be written as

$$M'_2(\mathbf{x}_2) = C_2 \cdot D'_2(\mathbf{x}_2) \cdot C_2^T \quad (5.18)$$

with

$$\mathbf{C}_2^\top = \begin{pmatrix} -\hat{\mathbf{s}}_b \cdot \nabla_{\mathbf{R}}(\delta(\mathbf{R}'' - \mathbf{R})) & 0 & 0 \\ 0 & 1 & -1 \end{pmatrix}$$

$$\mathbf{D}'_2(\mathbf{x}_2) = T_B \begin{pmatrix} \frac{\delta(\mathbf{R}'' - \mathbf{R}''')\delta_{b,b'}\rho_b(\mathbf{R}'')}{LB_b(T_B)} & \frac{\langle \sum_{i,b(i)=b'} \delta(\mathbf{R}(i) - \mathbf{R}'') \hat{\mathbf{s}}_{b'} \cdot \mathbf{F}_{pk}(i) \rangle_{\mathbf{x}_2}}{LB_{b'}(T_B)} \\ \frac{\langle \sum_{i,b(i)=b} \delta(\mathbf{R}(i) - \mathbf{R}'') \hat{\mathbf{s}}_b \cdot \mathbf{F}_{pk}(i) \rangle_{\mathbf{x}_2}}{LB_b(T_B)} & \sum_i \frac{\langle (\hat{\mathbf{s}}_{b(i)} \cdot \mathbf{F}_{pk}(i))^2 \rangle_{\mathbf{x}_2}}{LB_{b(i)}(T_B)} \end{pmatrix},$$

where the multiplicative split of Eq. (5.14) was used, and the fact that $T_{\text{lat}}/B_b(T_{\text{lat}})$ is almost independent of temperature. Therefore, $\langle T_{\text{lat}}/B_b(T_{\text{lat}}) \rangle_{T_B}$ was replaced by its value at the most likely value of S_{lat} , namely where $T_{\text{lat}} = T_B$. The off-diagonal terms in this matrix can be rewritten using that $\mathbf{F}_{pk}(i) = -\frac{d\Pi_{\overline{E}C}}{d\mathbf{R}(i)}$, see Eq. (5.9), and by using the definitions in Eqs. (5.13) and (5.15), see C.2 for details. This yields

$$\left\langle \sum_{i,b(i)=b} \delta(\mathbf{R}(i) - \mathbf{R}) \mathbf{F}_{pk}(i) \right\rangle_{\mathbf{x}_2} = -\rho_b(\mathbf{R}) \nabla_{\mathbf{R}} \frac{\delta F_C}{\delta \rho_b(\mathbf{R})} + k_B T_C \nabla_{\mathbf{R}} \rho_b(\mathbf{R}) \quad (5.19)$$

To determine \mathbf{K}_2 , the forward time derivative $D\Pi$ is needed, which follows from Eqs. (5.4c), (5.9) and (5.10). The vector $D\Pi$ contains the derivative $k_B \frac{dB_b(T_{\text{lat}})}{dS_{\text{lat}}}$. Since $B_b(T_{\text{lat}})$ is almost linearly proportional to T_{lat} , this can be rewritten in terms of the heat capacity of the lattice. Typical values for the heat capacity of metallic lattices then suggest that $k_B \frac{dB_b(T_{\text{lat}})}{dS_{\text{lat}}} \ll B_b(T_{\text{lat}})$, and hence this contribution can be neglected. Details of the derivation can be found in C.3. It is thus found that

$$D\Pi = \mathbf{C}_2 \cdot \begin{pmatrix} \mathcal{J}_b(\mathbf{R}'') \\ \mathcal{Q} - \sum_b \int \mathbf{R} \mathcal{J}_b(\mathbf{R}) \hat{\mathbf{s}}_b \cdot \nabla_{\mathbf{R}} \left(\frac{\delta F_C}{\delta \rho_b(\mathbf{R})} - k_B T_C \log \left[\frac{\rho_b(\mathbf{R})}{\Lambda_b^2} \right] \right) \end{pmatrix} \quad (5.20)$$

$$\equiv \mathbf{C}_2 \cdot \begin{pmatrix} \mathcal{J}_b(\mathbf{R}'') \\ \mathcal{P} \end{pmatrix}$$

with

$$\mathcal{J}_b(\mathbf{R}) \equiv \frac{\sum_{i,b(i)=b} (\delta(\mathbf{R}(i,t) - \mathbf{R}) \hat{\mathbf{s}}_b \cdot \mathbf{F}_{pk}(i,t)) - k_B T_{\text{lat}} (\hat{\mathbf{s}}_b \cdot \nabla_{\mathbf{R}}) \Pi_{\rho_b}(\mathbf{R},t)}{LB_b(T_{\text{lat}})}$$

$$\delta \mathbf{F}_{pk}(i) \equiv \mathbf{F}_{pk}(i) + \nabla_{\mathbf{R}} \left(\frac{\delta F_C}{\delta \rho_b(\mathbf{R})} - k_B T_C \log \left[\frac{\rho_b(\mathbf{R})}{\Lambda_b^2} \right] \right) \Big|_{\mathbf{R}=\mathbf{R}(i)}$$

$$\mathcal{Q} \equiv \sum_i \frac{k_B T_{\text{lat}} \left(\hat{\mathbf{s}}_{b(i)} \cdot \frac{d}{d\mathbf{R}_1(i)} \right) (\hat{\mathbf{s}}_{b(i)} \cdot \delta \mathbf{F}_{pk}(i)) + (\hat{\mathbf{s}}_{b(i)} \cdot \mathbf{F}_{pk}(i)) (\hat{\mathbf{s}}_{b(i)} \cdot \delta \mathbf{F}_{pk}(i))}{LB_{b(i)}(T_{\text{lat}})}.$$

The interpretation of these terms is as follows; it will follow from the evolution equation of the dislocation density that $\langle \mathcal{J}_b(\mathbf{R}) \rangle_{\mathbf{x}_2}$ is the direct average of the dislocation flux, and hence $\mathcal{J}_b(\mathbf{R})$ should be interpreted as the instantaneous dislocation flux of a microstate; $-\nabla_{\mathbf{R}} \left(\frac{\delta F_C}{\delta \rho_b(\mathbf{R})} - k_B T_C \log \left[\frac{\rho_b(\mathbf{R})}{\Lambda_b^2} \right] \right)$ is the expectation value of the Peach-Koehler force at \mathbf{R} , and hence $\delta \mathbf{F}_{pk}(i)$ is the fluctuation in the Peach-Koehler force on the i^{th} dislocation;

$\langle \mathcal{P} \rangle_{\mathbf{x}_2}$ will turn out to be the direct average of the energy flux from the configurational subsystem to the lattice. The power \mathcal{P} was split into \mathcal{Q} and a term proportional to \mathcal{J}_b as this facilitates rewriting the final result. The term proportional to \mathcal{J}_b should be interpreted as the flux times the expectation value of the force. Then \mathcal{Q} contains only the correlation effects between the force and flux on dislocations.

The expression for $D\Pi$ yields for the matrix \mathbf{K}_2

$$\mathbf{K}_2(\mathbf{x}_2) = \mathbf{C}_2 \cdot \mathbf{D}_2''(\mathbf{x}_2) \cdot \mathbf{C}_2^T \quad (5.21)$$

$$\text{with } \mathbf{D}_2''(\mathbf{x}_2) = \begin{pmatrix} \langle\langle \mathcal{J}_b(\mathbf{R}, 0), \mathcal{J}_{b'}(\mathbf{R}', \Delta t) \rangle\rangle & \langle\langle \mathcal{J}_b(\mathbf{R}, 0), \mathcal{P}(\Delta t) \rangle\rangle \\ \langle\langle \mathcal{P}(0), \mathcal{J}_{b'}(\mathbf{R}', \Delta t) \rangle\rangle & \langle\langle \mathcal{P}(0), \mathcal{P}(\Delta t) \rangle\rangle \end{pmatrix}.$$

Finally, inserting Eqs. (5.17-5.21) into the GENERIC framework in Eq. (5.3) yields the macroscopic evolution equations for the density:

$$\begin{aligned} \frac{\partial \rho_b(\mathbf{R})}{\partial t} = & -\hat{\mathbf{s}}_b \cdot \nabla_{\mathbf{R}} \left(\frac{\rho_b(\mathbf{R})}{LB_b(T_B)} \left(-\hat{\mathbf{s}}_b \cdot \nabla_{\mathbf{R}} \frac{\delta \tilde{F}}{\delta \rho_b(\mathbf{R})} \right) \right) \quad (5.22) \\ & + \sum_{b'} \int d\mathbf{R}' \int_0^{\tau_2} d\Delta t \frac{\langle\langle \mathcal{J}_b(\mathbf{R}, 0), \mathcal{J}_{b'}(\mathbf{R}', \Delta t) \rangle\rangle}{k_B T_B} \left(-\hat{\mathbf{s}}_{b'} \cdot \nabla_{\mathbf{R}'} \frac{\delta \tilde{F}(t - \Delta t)}{\delta \rho_{b'}(\mathbf{R}')} \right) \\ & + \int_0^{\tau_2'} d\Delta t \langle\langle \mathcal{J}_b(\mathbf{R}, 0), \mathcal{Q}(\Delta t) \rangle\rangle \left(\frac{1}{k_B T_B} - \frac{1}{k_B T_C} \right) (t - \Delta t) \end{aligned}$$

with

$$\tilde{F}[\rho_b(\mathbf{R}), T_C, T_B] \equiv F_C[\rho_b(\mathbf{R}), T_C] - k_B(T_C - T_B) \int d\mathbf{R} \rho_b(\mathbf{R}) \left(\log \left[\frac{\rho_b(\mathbf{R})}{\Lambda_b^2} \right] - 1 \right),$$

where τ_2 and τ_2' are the decay times of the corresponding correlation functions, and where Λ_b^2 is in principle arbitrary, but it is needed for dimensional reasons. The evolution equation of the density is given in C.4.

5.4 Interpretation and comparison to literature

In this section, Eq. (5.22) will be interpreted. The first line results from direct averaging of the microscopic evolution, which does not yield a new mobility.

The second and third line in Eq. (5.22) represent the emergent contribution to the macroscopic mobility, that results from time-correlations in the fluctuating microscopic dynamical processes. As in the Green-Kubo relations, this contribution is equal to correlations of fluctuations in fluxes. This can be seen in Eq. (5.21), where the emergent, macroscopic transport coefficients are written as correlations of fluctuations in dislocation- and heat fluxes, \mathcal{J}_b and \mathcal{P} .

Note that the emergent contribution is in principle non-local in both space and time. This means that the driving force in position \mathbf{R}' influences the flow in position \mathbf{R} directly, and that the relations are in principle non-Markovian. We will discuss the importance of the non-local character in the next section.

The driving force for dislocation dynamics is the derivative of a modified free energy $\tilde{F}[\rho_b(\mathbf{R}), T_C, T_B]$, which differs from the configurational free energy $F_C[\rho_b(\mathbf{R}), T_C]$ by $-k_B(T_C - T_B) \int d\mathbf{R} \rho_b(\mathbf{R}) \left(\log \left[\frac{\rho_b(\mathbf{R})}{\Lambda_b^2} \right] - 1 \right)$. The configurational free energy F_C obtained in the work of Groma [35, 36] and in Chap. 2-4 contains a similar “statistical” or “ideal gas” contribution $k_B T_C \int d\mathbf{R} \rho_b(\mathbf{R}) \left(\log \left[\frac{\rho_b(\mathbf{R})}{\Lambda_b^2} \right] - 1 \right)$. Consequently, the modified free energy $\tilde{F}[\rho_b(\mathbf{R}), T_C, T_B]$ has a modified statistical contribution $k_B T_B \int d\mathbf{R} \rho_b(\mathbf{R}) \left(\log \left[\frac{\rho_b(\mathbf{R})}{\Lambda_b^2} \right] - 1 \right)$. When this contribution is inserted in the first line of Eq. (5.22), a diffusive term in the density evolution is obtained: $\left. \frac{\partial \rho_b(\mathbf{R})}{\partial t} \right|_{\text{diff}} = \frac{k_B T_B}{L B_b(T_B)} \nabla^2 \rho_b(\mathbf{R})$. Therefore, the correction to the free energy should be interpreted as that the driving force for diffusion is representative for the state of the system held at T_B , while the rest of the driving force is representative for the state of the system held at T_C . We will now discuss in which limit the obtained evolution equations reduce to results from literature. To this end, we will compare our work with the variational approach proposed in [36], and to the BBGKY-like hierarchies of equations proposed in [32, 120, 34]. We will show that our result reduces to these works in the limit in which the interaction forces between dislocations are relatively weak compared to the other forces on dislocations, such as mechanical loading of the sample.

First, note that in this limit correlations of fluctuations are small, and hence the last two lines of the density evolution equation are not important. The only difference with for example [36] is then the notion of a second, configurational temperature in the driving force. To elucidate this better, the evolution equation of the configurational temperature is considered:

$$\frac{dT_C}{dt} = \left. \frac{\partial T_C}{\partial \bar{E}_C} \right|_{\rho_b(\mathbf{R})} \frac{d\bar{E}_C}{dt} + \sum_b \int d\mathbf{R} \left. \frac{\partial T_C}{\partial \rho_b(\mathbf{R})} \right|_{\bar{E}_C} \frac{d\rho_b(\mathbf{R})}{dt}. \quad (5.23)$$

Note that $\left. \frac{\partial T_C}{\partial \bar{E}_C} \right|_{\rho_b(\mathbf{R})}$ is the inverse of the heat capacity of the configurational subsystem. Yet, the heat capacity is small when the interaction strength is small, and hence $\left. \frac{\partial T_C}{\partial \bar{E}_C} \right|_{\rho_b(\mathbf{R})}$ is large. For similar reasons, one could argue that $\left. \frac{\partial T_C}{\partial \rho_b(\mathbf{R})} \right|_{\bar{E}_C}$ is large, see C.5.

However, in the limit of weak interactions, $\frac{d\bar{E}_C}{dt}$ and $\frac{d\rho_b(\mathbf{R})}{dt}$ do not decrease to zero, which implies that $\left| \frac{dT_C}{dt} \right|$ is large. The configurational temperature will thus cool down quickly to the environmental temperature, and hence temperature differences are prohibited when the interaction forces are relatively weak.

So to conclude: in the absence of significant correlation effects, the macroscopic evolution of the dislocation density reduces to the equations proposed in [36, Eq. (37-43)], where the free energy derivative plays the role of the driving force, and where the macroscopic mobility is simply equal to the microscopic mobility.

In this limit, our result also matches the results obtained by Groma [32, 34] and Zaiser [120], where the dislocation flux is proportional to the expectation value of the Peach-Koehler force. To see the equivalence, one should realize that the free energy derivative in Eq. (5.22) is approximately equal to the expectation value of the Peach-Koehler force when T_C is equal to T_B , see Eq. (5.19).

$\rho_b(\mathbf{R}) = R^{-2} \check{\rho}_b(\check{\mathbf{R}})$ $\mathbf{R} = \xi \check{\mathbf{R}}$	$\xi = \sqrt{2/\Xi_C} R$	typical dislocation density typical length on which correlations still exist, see [73] for the relation
$T_{\text{lat}} = T_B \check{T}_{\text{lat}}$ $\delta F_{pk,b}(\mathbf{R}) = F \delta \check{F}_{pk,b}(\check{\mathbf{R}})$ $F_{pk,b}(\mathbf{R}) = S \check{F}_{pk,b}(\check{\mathbf{R}})$	$F = \frac{\mu b^2 L}{(1-\nu)\zeta}$ $S = \max(F, b\Sigma L)$	typical lattice temperature typical value of force fluctuations typical value of force
$\mathbf{B}_b(T) = B \check{B}_b(\check{T})$ $\Delta t = \tau \check{\Delta t}$		typical microscopic mobility typical decay time of fluctuations

Table 5.1: Rescaling of the parameters. Quantities indicated with a $\check{}$ are of order unity.

However, we would like to stress that the limit of weak interactions is most likely not applicable to most dislocation systems, as dislocations tend to strongly organize themselves in low-energy structures.

5.5 Macroscopic mobility

5.5.1 Dominant contribution to the scaling analysis

To determine which contributions in \mathcal{J}_b and \mathcal{Q} in Eq. (5.22) are dominant, a scaling analysis is performed. All variables are rescaled to dimensionless quantities of order unity, as summarized in table 5.1. The typical length scale over which correlations could exist is expected to be equal to the typical length scale associated with the pair correlation of dislocations, see e.g. [73].

For the scaling, it is necessary to get a feeling for the relation between T_B and T_C . It is most likely that during the slow relaxation of the configurational degrees of freedom, the configurational energy will decrease, and that this energy flows towards the heat bath. As energy flows from high to low temperature, we thus conclude that $T_C > T_B$. This assumption is supported by literature on dislocation systems, see e.g. [73, 35].

To determine the typical magnitude of the terms in \mathcal{J}_b , the typical magnitude of force fluctuations, rather than the total force is needed. We expect that fluctuations in the Peach-Koehler force are due to density fluctuations, and hence due to interactions between dislocations, and not due to the macroscopically imposed stress Σ . Therefore, the typical value of fluctuations in the Peach-Koehler force is expected to scale with the typical interaction energy between dislocations, $\mu b^2 L / (1 - \nu)$, divided by a yet unknown length ζ . The typical magnitude of the Peach-Koehler force S is the maximum of the typical force due to loading, $b\Sigma L$, and the typical strength of interaction forces F .

It will turn out to be convenient to define two dimensionless coupling constants $\Xi_B \equiv \frac{\mu b^2 L}{(1-\nu)k_B T_B}$ and $\Xi_C \equiv \Xi_B T_B / T_C$. These coupling constants compare the typical energy associated with dislocation interactions via the Peach-Koehler force ($\mu b^2 L / (1 - \nu)$) with the thermal energies ($k_B T_B$ and $k_B T_C$, respectively). It was shown in Sec. 3.3.2 that

$\Xi_B \gg 1$ for metals at room temperature, at least when the slab thickness L is larger than a single Burgers vector.

It can now be determined which contribution in \mathcal{J}_b and \mathcal{Q} are dominant:

$$\mathcal{J}_b(\mathbf{R}) = \frac{F}{LB} \frac{1}{R^2} \frac{\sum_{i, \mathbf{b}(i)=\mathbf{b}} \left(\delta(\check{\mathbf{R}}(i) - \check{\mathbf{R}}) \hat{\mathbf{s}}_{\mathbf{b}} \cdot \check{\mathbf{F}}_{pk}(i) \right) - \Xi_B^{-1} \zeta T_{\text{lat}}^{\check{\vee}} (\hat{\mathbf{s}}_{\mathbf{b}} \cdot \check{\nabla}_{\mathbf{R}}) \check{\Pi}_{\rho_b}(\check{\mathbf{R}})}{\check{B}_b(T_{\text{lat}})} \quad (5.24a)$$

$$\mathcal{Q} = \frac{FS}{LB} \frac{\xi^2}{R^2} \sum_i \frac{\frac{k_B T_B}{\xi S} \left(\hat{\mathbf{s}}_{\mathbf{b}(i)} \cdot \frac{d}{d\mathbf{R}_1(i)} \right) \left(\hat{\mathbf{s}}_{\mathbf{b}(i)} \cdot \delta \mathbf{F}_{pk}(i) \right) + \left(\hat{\mathbf{s}}_{\mathbf{b}(i)} \cdot \check{\mathbf{F}}_{pk}(i) \right) \left(\hat{\mathbf{s}}_{\mathbf{b}(i)} \cdot \delta \check{\mathbf{F}}_{pk}(i) \right)}{\check{B}_{b(i)}(T_{\text{lat}})} \quad (5.24b)$$

where the delta function and Π_{ρ_b} in Eq. (5.24a) scale with R^{-2} . Moreover, it was assumed for the second contribution that $\nabla_{\mathbf{R}} = \xi^{-1} \check{\nabla}_{\check{\mathbf{R}}}$. Namely, the spatial derivative can be taken out of the ensemble average. Then this derivative acts on correlations of density fluctuations, for which the typical length scale is ξ . The factor ξ^2/R^2 in Eq. 5.24b should be interpreted as the number of dislocations in a (2D-)volume of size ξ , which is the volume in which correlations are expected to be non-zero.

The typical size of the two contributions in \mathcal{J}_b thus differ by a factor $\Xi_B^{-1} \zeta$. The typical length scale ζ associated the Peach-Koehler force is not known, but it is not expected to be orders of magnitude larger than either the dislocation spacing R or the correlation length ξ . In the first case, the factor reads $\Xi_B^{-1} \sqrt{\Xi_C/2} = \Xi_B^{-1/2} \sqrt{T_B/T_C}$, whereas in the second case, the factor is simply Ξ_B^{-1} . As $T_B/T_C < 1$ and $\Xi_B \gg 1$ for metals at room temperature, the factor is small in both cases and hence the first term is dominant. This implies that $\langle\langle \mathcal{J}_b, \mathcal{J}_{b'} \rangle\rangle$ can be determined from fluctuations in the Peach-Koehler force only, and fluctuations in the gradient of the density can safely be ignored.

The typical size of the contributions in \mathcal{Q} differ by a factor equal to the minimum of $\frac{k_B T_B}{\xi F} = \Xi_B^{-1} \zeta$ and $\frac{k_B T_B}{\xi \Sigma b L}$. The former is already small, and hence the second contribution to \mathcal{Q} is dominant.

Furthermore, note that $(\hat{\mathbf{s}}_{\mathbf{b}(i)} \cdot \mathbf{F}_{pk}(i)) (\hat{\mathbf{s}}_{\mathbf{b}(i)} \cdot \delta \mathbf{F}_{pk}(i))$ could be split in a linear and a quadratic term in $\delta \check{\mathbf{F}}_{pk}(i)$, while \mathcal{J}_b is linear in $\delta \mathbf{F}_{pk}(i)$. Therefore, the leading order term in $\langle\langle \mathcal{J}_b, \mathcal{Q} \rangle\rangle$ has a quadratic and a cubic term in $\delta \mathbf{F}_{pk}(i)$. As the latter is odd in the fluctuation, this will probably be small after averaging, and hence the leading order term in $\langle\langle \mathcal{J}_b, \mathcal{Q} \rangle\rangle$ could in principle be expressed in terms of $\langle\langle \mathcal{J}_b, \mathcal{J}_{b'} \rangle\rangle$.

Now, the flux in the RHS of Eq. (5.22) could be rescaled, to determine which term is dominant:

$$\begin{aligned} & \frac{S}{LBR^2} \frac{\check{\rho}_b(\mathbf{R})}{\check{B}_b(T_B)} \left(-\hat{\mathbf{s}}_{\mathbf{b}} \cdot \check{\nabla}_{\check{\mathbf{R}}} \frac{\delta \check{\mathbf{F}}}{\delta \check{\rho}_b(\check{\mathbf{R}})} \right) \quad (5.25) \\ & + \frac{\xi^2 S \tau}{k_B T_B} \left(\frac{F}{LBR^2} \right)^2 \sum_{b'} \int d\check{\mathbf{R}}' \int_0^{\tau_2/\tau} d\check{\Delta} t \langle\langle \check{\mathcal{J}}_b(\check{\mathbf{R}}, 0), \check{\mathcal{J}}_{b'}(\check{\mathbf{R}}', \check{\Delta} t) \rangle\rangle \left(-\hat{\mathbf{s}}_{\mathbf{b}'} \cdot \check{\nabla}_{\check{\mathbf{R}}'} \frac{\delta \check{\mathbf{F}}}{\delta \check{\rho}_{b'}(\check{\mathbf{R}}')} \right) \\ & + \frac{\xi^2 S \tau}{k_B T_B} \left(\frac{F}{LBR^2} \right)^2 \int_0^{\tau_2/\tau} d\check{\Delta} t \langle\langle \check{\mathcal{J}}_b(\mathbf{R}, 0), \check{\mathcal{Q}}(\check{\Delta} t) \rangle\rangle \left(1 - \frac{T_B}{T_C} \right) (t - \check{\Delta} t), \end{aligned}$$

where it was used that the typical size of the driving force $-\hat{s}_b \cdot \check{\nabla}_{\mathbf{R}} \frac{\delta \tilde{F}}{\delta \rho_b(\mathbf{R})}$ is S , see Eq. (5.19). The second and third term are thus equally important. Moreover, the ratio between the first and second contribution equals $\frac{\tau}{k_B T_B} \frac{2}{\Xi_C} \frac{F^2}{LB} = \frac{T_C}{T_B} \frac{\tau F}{LB \zeta}$. The term $\frac{F}{LB}$ can be interpreted as the typical dislocation velocity due to fluctuation in the Peach-Koehler force. Hence, $\frac{\tau F}{LB}$ is the “free-glide distance” that a dislocation typically travels due to fluctuations. This implies that the emergent contributions are dominant when the free-glide distance is not much shorter than ζ , especially when $T_C \gg T_B$. This can be verified numerically, but it is to be expected that the emergent contributions are indeed dominant.

Note that from the microscopic evolution equations, Eq. (5.8), it follows that the typical timescale τ is linearly proportional with B , and hence the free-glide distance is independent of the microscopic mobility. This implies that the macroscopic mobility scales linearly with the microscopic mobility, which was to be expected.

5.5.2 The non-local character of the memory kernel

Now, the non-local character of $\langle\langle \mathcal{J}_b, \mathcal{J}_{b'} \rangle\rangle$ will be discussed. It is expected that this nonlocality is only important when the typical length scale over which the driving force varies is much shorter than the typical length scale over which $\langle\langle \mathcal{J}_b(\mathbf{R}, 0), \mathcal{J}_{b'}(\mathbf{R}', \Delta t) \rangle\rangle$ is non-zero. Therefore, the driving force $\hat{s}_{b'} \cdot \nabla_{\mathbf{R}'} \left(\frac{\delta \tilde{F}}{\delta \rho_{b'}(\mathbf{R}')} \right)$ in Eq. (5.22) is considered as a function of \mathbf{R}' and will be expanded around \mathbf{R} . This yields for the second contribution to the dislocation flux

$$\sum_{n=0}^{\infty} \frac{1}{n!} \int_0^{\tau_2} d\Delta t \sum_{b'} H_{bb'}^{(n)}(\Delta t) \stackrel{n}{:} (\nabla_{\mathbf{R}})^{\otimes n} \hat{s}_{b'} \cdot \nabla_{\mathbf{R}} \left(\frac{\delta \tilde{F}(t - \Delta t)}{\delta \rho_{b'}(\mathbf{R})} \right)$$

with $H_{bb'}^{(n)}(\Delta t) \equiv \int d\mathbf{R}' \frac{\langle\langle \mathcal{J}_b(\mathbf{R}, 0), \mathcal{J}_{b'}(\mathbf{R}', \Delta t) \rangle\rangle}{k_B T_B} (\mathbf{R}' - \mathbf{R})^{\otimes n},$ (5.26)

where \otimes^n denotes a diadic product of n copies, and $\stackrel{n}{:}$ denotes a contraction of n indices. It is expected that $\langle\langle \mathcal{J}_b(\mathbf{R}, 0), \mathcal{J}_{b'}(\mathbf{R}', \Delta t) \rangle\rangle$ only depends on $\mathbf{R} - \mathbf{R}'$ and that it is symmetric in $\mathbf{R} - \mathbf{R}'$, and hence that the odd coefficients $H_{bb'}^{(n)}(\Delta t)$ vanish.

This local expression only makes sense when the coefficients $H_{bb'}^{(n)}(\Delta t)$ exist, and is only useful if it can be truncated after the zeroth order term. For this, the higher order terms should be sufficiently smaller than the zeroth order term, which in turn depends on the typical length scale over which the driving force changes. Numerical comparison of $H_{bb'}^{(0)}(\Delta t)$ and $H_{bb'}^{(2)}(\Delta t)$ provides a minimum for this length scale.

5.5.3 Separation of timescales

The last question that arises from the evolution in Eq. (5.22) is whether the memory kernels $\langle\langle \mathcal{J}_b, \mathcal{J}_{b'} \rangle\rangle$ and $\langle\langle \mathcal{J}_b, \mathcal{Q} \rangle\rangle$ could be replaced by a single coefficient, or equivalently, whether there is separation of timescales on the macroscopic level. Separation of timescales applies when the driving forces corresponding to these memory kernels hardly changes during the typical timescales τ_2 and τ_2' on which the memory kernel is non-zero. By expanding the driving force at $t - \Delta t$ up to first order in Δt around zero, conditions

could be derived under which separation of timescales applies. For $\langle\langle \mathcal{J}_b, \mathcal{J}_{b'} \rangle\rangle$, separation of timescales applies if for each order n the following inequality holds:

$$\begin{aligned} & - \left[\int_0^{\tau_2} d\Delta t H_{bb'}^{(n)}(\Delta t) \Delta t \right]^n \frac{d}{dt} (\nabla_{\mathbf{R}})^{\otimes n} \hat{s}_{b'} \cdot \nabla_{\mathbf{R}} \left(\frac{\delta \tilde{F}(t)}{\delta \rho_{b'}(\mathbf{R})} \right) \\ & \ll \left[\int_0^{\tau_2} d(\Delta t) H_{bb'}^{(n)}(\Delta t) \right]^n (\nabla_{\mathbf{R}})^{\otimes n} \hat{s}_{b'} \cdot \nabla_{\mathbf{R}} \left(\frac{\delta \tilde{F}(t)}{\delta \rho_{b'}(\mathbf{R})} \right). \end{aligned} \quad (5.27)$$

Comparing the terms in angular brackets on the LHS and RHS of this equation yields a typical timescale. If the driving force $\hat{s}_{b'} \cdot \nabla_{\mathbf{R}} \left(\frac{\delta \tilde{F}(t)}{\delta \rho_{b'}(\mathbf{R})} \right)$ does not change significantly within this time, separation of timescales applies.

Analogously, one finds for $\langle\langle \mathcal{J}_b, \mathcal{Q} \rangle\rangle$ that separation of timescales applies if the following inequality holds

$$\begin{aligned} & - \left[\int_0^{\tau'} d\Delta t \langle\langle \mathcal{J}_b(\mathbf{R}, 0), \mathcal{Q}(\Delta t) \rangle\rangle \Delta t \right] \frac{d}{dt} \left(\frac{1}{k_B T_B} - \frac{1}{k_B T_C} \right) \\ & \ll \left[\int_0^{\tau'} d\Delta t \langle\langle \mathcal{J}_b(\mathbf{R}, 0), \mathcal{Q}(\Delta t) \rangle\rangle \right] \left(\frac{1}{k_B T_B} - \frac{1}{k_B T_C} \right). \end{aligned} \quad (5.28)$$

Again, comparing the terms in angular brackets yields a typical timescale. If the temperature difference does not change significantly within this time, separation of timescales applies for $\langle\langle \mathcal{J}_b, \mathcal{Q} \rangle\rangle$.

Thus, to check whether separation of timescales applies, one should determine a typical timescale by comparing the terms in angular brackets on the LHS and RHS of Eqs. (5.27) and (5.28), and check whether changes in the corresponding driving force are slow compared to this timescale.

5.6 Summary and outlook

In this contribution, the dynamical response functions of the dislocation density were derived from the evolution equations of individual dislocations, see Eq. (5.22) for the result. This research was motivated by the difference between the microscopic mobility of dislocations observed in MD simulations [65, 86, 96], and the macroscopic mobility of dislocations used in phenomenological crystal plasticity models [40, 43]. For example, the stress-dependence of the two mobilities is qualitatively different, for which a good justification seems to be lacking.

Current approaches to link microscopic and macroscopic dynamics focus only on the averaging over phase space using BBGKY-hierarchies of equations, see e.g. [32, 120, 34], in which a transition in timescale is not involved. Therefore, such an approach does not yield an emergent, macroscopic mobility. To overcome this, we have used the GENERIC-framework of non-equilibrium thermodynamics to derive macroscopic evolution equations based on the microscopic dynamics.

The main characteristics of the obtained dynamical response function of the dislocation density are:

- Apart from a direct contribution arising from the microscopic irreversible dynamics, it was found that the dynamical response function of the dislocation density entails an emergent contribution in the form of a memory kernel.
- The emergent memory kernel is probably dominant over the contribution from microscopic irreversible dynamics. The emergent contribution may therefore be used to explain the apparent qualitative difference between microscopic and macroscopic mobilities in literature.
- As in the Green-Kubo relations, the emergent contribution in the transport coefficient follows from time-correlations of fluctuations in the dislocations flux.
- Separation of timescales on macroscopic level only arises when the typical timescale on which the driving force changes is much smaller than the timescale on which fluctuations in the driving forces decay, see the conditions in Eqs. (5.27) and (5.28). Whether and when this is satisfied is not trivial and should be investigated in a numerical study.

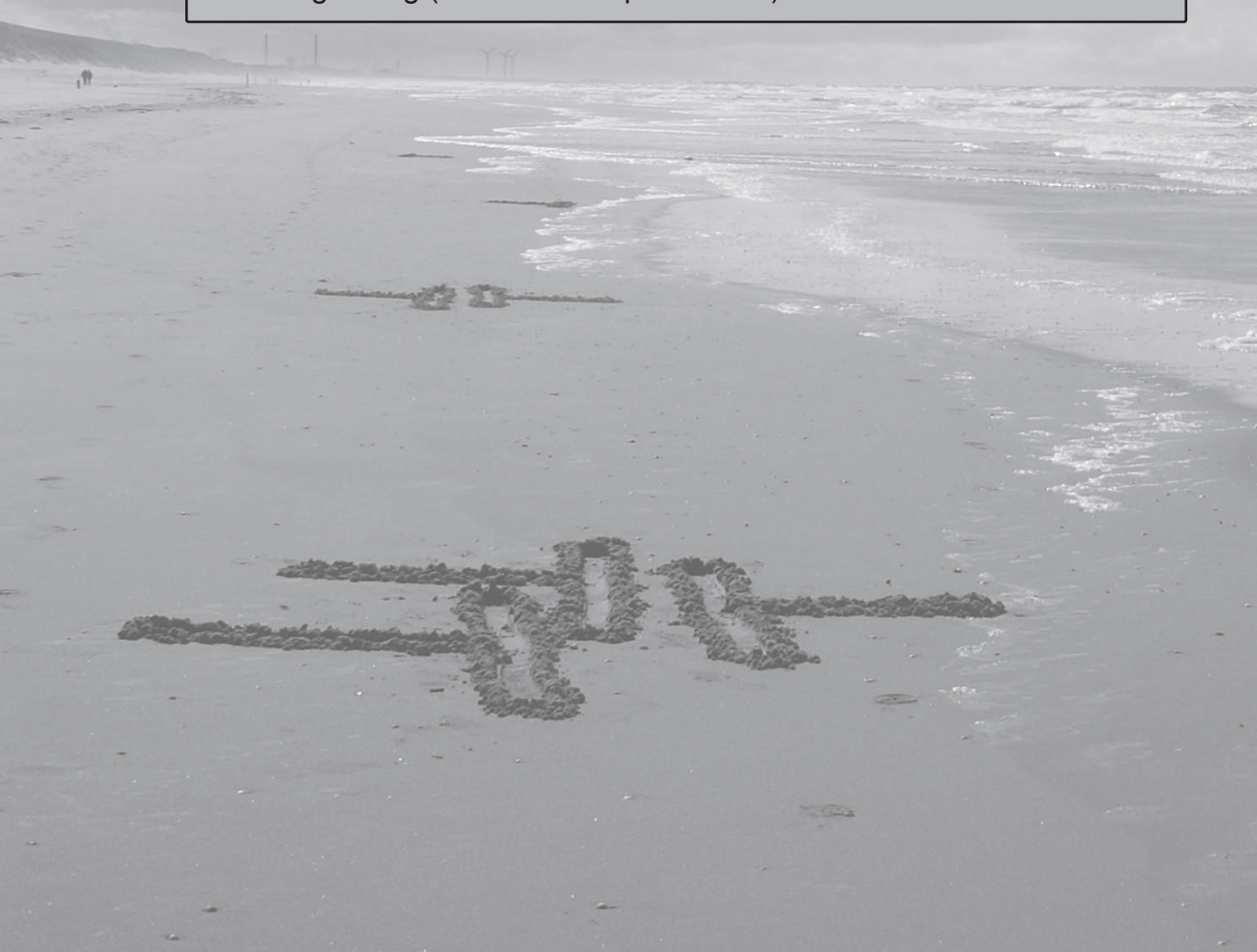
The emergent memory kernel can, most likely, not be evaluated further analytically. However, computer simulations may be used to determine the dependence of the effective macroscopic mobility on the heat bath- and configurational temperature, the dislocation density and the macroscopically imposed average stress Σ . These dependencies could be far from trivial, and it would be worthwhile to compare these to macroscopic plasticity models.

Moreover, the current upscaling procedure can also be applied to more advanced dynamical equations at the microlevel. For example, for screw dislocations in α -Fe below a certain transition stress, the relation between stress and strain is not linear, but rather exponential, see e.g. [30, 107]. Moreover, climb of dislocations could also be included. Finally, we expect that the procedure applied to dislocations presented here could be extended to other systems quite easily. Indeed, the derivation presented here did not make use of special properties of the Peach-Koehler force, and hence the generalization to particle systems governed by other forces should be straightforward. The fact that the emergent contribution determines the mechanical response of dislocation systems suggests that such an emergent contribution might also be non-negligible for other systems.

Chapter 6

Viscoplastic flow rule for dislocation-mediated plasticity from systematic coarse-graining

Largely reproduced from: Kooiman, M., Hütter, M., and Geers, M.G.D.,
Viscoplastic flow rule for dislocation-mediated plasticity from systematic
coarse-graining (submitted for publication)



Abstract

The plastic response of metals is determined by the collective, coarse-grained dynamics of dislocations, rather than by the dynamics of individual dislocations. The evolution equations at both levels are quite different, for example considering their dependence on the applied mechanical load. On the one hand, the relation between load and dislocation velocity for individual dislocations is linear. On the other hand, in phenomenological crystal plasticity models, the relation between load and plastic slip is highly non-linear and often taken of power-law form. In this work, it is shown that this difference is justified and a consequence of emergent effects. In Chap. 5, an expression for the macroscopic dislocation flux was derived by systematic coarse graining. This expression has been evaluated numerically in this chapter. The resulting relation between dislocation flux and applied mechanical load is found to be of power-law form with an exponent 3.7, while the underlying Discrete Dislocation Dynamics has a linear flux-load relation.

6.1 Introduction

The transport of dislocations, i.e. line-like defects in a crystal structure, is the underlying mechanism of plastic deformation of metals. As metals can contain many dislocations (up to 1000 km of dislocation line per cubic millimeter), capturing the collective behavior of dislocations is key in modeling plastic deformation of metals. For simplicity, attention in this work is restricted to straight and parallel dislocations.

For single dislocations, a linear response, i.e. the dislocation velocity is linearly proportional to the applied load, has shown to be appropriate in a large range of load conditions and temperatures, see e.g. [65, 86, 96]. In contrast, in crystal plasticity models based on the dynamics of dislocation densities [40, 43], the relation between plastic flow and applied mechanical load is generally assumed to be strongly non-linear. The dependence of these transport relations on the imposed mechanical load is thus quite different between the two levels of description.

Previously, the connection between evolution equations of individual dislocations and that of the dislocation density has been made by means of the BBGKY-hierarchy of equations [32, 120, 34], where one averages over phase space. However, these do not yield an emergent mobility, as no transition in observation-timescale is made.

Recently, we have derived evolution equations for the dislocation density, see Chap. 5. This was done by means of systematic coarse-graining using the General Equation for the Non-Equilibrium Reversible-Irreversible Coupling (GENERIC), in which a transition in observation timescale is one of the key features. The evolution equation could be written as a driving force times a transport coefficient. The latter is dominated by an emergent contribution of Green-Kubo type, i.e. which results from correlations in fluctuations of the dislocation velocity. Our hypothesis is that the non-linear stress dependence of the transport relations of large amounts of dislocations is an emergent phenomenon.

In this contribution, this hypothesis is assessed by considering the stress dependence of the emergent transport coefficient by means of numerical simulations. To this end, Discrete Dislocation Dynamics (DDD) simulations of an ensemble of dislocation configurations are considered, and both the average driving force and the correlations in fluctuations of the dislocation velocity are quantified.

The new and innovative aspect of this work is that, for the first time, we are able to explain the apparent difference in stress dependence of the transport relations at the level of discrete dislocations compared to that of dislocation densities.

The chapter is organized as follows: in Sec. 6.2.1 previous work is summarized and the details of the ensemble are explained. In Sec. 6.2.2, the numerical scheme is elaborated. Subsequently, the results of the simulations are presented in Sec. 6.3, and discussed in Sec. 6.4.

6.2 Methods

6.2.1 Theoretical Background

Summary of previous results

In this section, we summarize the results obtained in Chap. 5, in which we have derived the evolution equation of the dislocation density by systematic coarse-graining of the evolution equations of individual, discrete dislocations. From now on, we will refer to the scale of individual dislocations as the microscale, and to the scale of dislocation densities as the macroscale.

The microscale system consists of an arbitrary large number N of straight and parallel edge dislocations of length L . The position of each dislocation is indicated by $\mathbf{R}(i)$ and its Burgers vector by $\mathbf{b}(i)$. These dislocations are embedded in a body with an infinite surface, a thickness L and a stiffness \mathbb{C} , held at a temperature T_B , on which a volume-average stress Σ is imposed. It is assumed that the mechanical response in this infinite volume is representative for the bulk.

Only dislocation glide is considered. Hence dislocations only move in the slip direction corresponding to their Burgers vector, $\hat{\mathbf{s}}_b$. Discrete dislocations move when a Peach-Koehler force is exerted on them. This force results from stresses due to externally imposed mechanical loading and due to the presence of other dislocations, as described in [110]. The evolution equation for the positions of the dislocations then reads

$$\frac{d\mathbf{R}(i)}{dt} = \hat{\mathbf{s}}_{\mathbf{b}(i)} v(i) \quad ; \quad v(i) = \frac{\hat{\mathbf{s}}_{\mathbf{b}(i)} \cdot \mathbf{F}_{pk}(i)}{LB_{\mathbf{b}(i)}(T_B)}, \quad (6.1)$$

where $v(i)$ is the velocity of the i^{th} dislocation and where $B_{\mathbf{b}(i)}(T_B)$ is the mobility of a discrete dislocation segment, which depends on the temperature but not on the applied mechanical load. The linear drag law is motivated by Molecular Dynamics simulations of single dislocations [65, 86, 96].

The macroscale system consists of the same body with the same stiffness, temperature and volume-average stress. However, instead of discrete dislocations, we now consider dislocation density profiles $\rho_{\mathbf{b}}(\mathbf{R})$ for each possible Burgers vector \mathbf{b} . In addition to the dislocation density profiles, an additional configurational temperature is needed to describe the state of the dislocations. Particularly, it turns out that the dislocation distributions emerging from solutions of Eq. (6.1) are not in thermal equilibrium with the environment. A similar problem arises in glasses, where configurational degrees of freedom are frozen in at a higher, configurational temperature because of high energy barriers in the system. In this context, the idea of a second, configurational temperature was developed, see e.g. [15, 72, 10]. It is thereby assumed that the system stays for a long time in a basin of attraction around a local minimum. Vibrations of the system in this basin are assumed to be in equilibrium with the environmental temperature T_B , while the distribution of microstates over the different basins of attraction is described by a higher, configurational temperature T_C . For dislocations, the concept of a configurational temperature was also used in other work, see e.g. [73, 35].

As derived in Chap. 5, the leading order terms in the obtained evolution equation for the

dislocation dislocation density read (see appendix D.1)

$$\frac{\partial \rho_{\mathbf{b}}(\mathbf{R})}{\partial t} = -\hat{\mathbf{s}}_{\mathbf{b}} \cdot \nabla_{\mathbf{R}} \left(\int_0^\infty d\Delta t \sum_{\mathbf{b}'} \frac{H_{\mathbf{b}\mathbf{b}'}^{(0)}(\Delta t)}{k_B T_B} \left(-\hat{\mathbf{s}}_{\mathbf{b}'} \cdot \nabla_{\mathbf{R}} \left(\frac{\delta \tilde{F}(t - \Delta t)}{\delta \rho_{\mathbf{b}'}(\mathbf{R})} \right) \right) \right) \quad (6.2)$$

with

$$H_{\mathbf{b}\mathbf{b}'}^{(0)}(\Delta t) \equiv \frac{2}{\Omega} \left\langle \sum_{i, \mathbf{b}(i)=\mathbf{b}} \delta v(i, 0) \sum_{i', \mathbf{b}(i')=\mathbf{b}'} \delta v(i', \Delta t) \right\rangle, \quad (6.3)$$

where the angular brackets $\langle \dots \rangle$ indicate an ensemble average at constant configurational temperature and density, where $\delta v(i) \equiv v(i, 0) - \langle v(i) \rangle$ is the fluctuation in the velocity of the i^{th} dislocation and where Ω is the cross sectional area.

In Eq. (6.2), $\tilde{F}[\rho_{\mathbf{b}}(\mathbf{R}), T_C, T_B]$ is the free energy, whose derivative acts as a driving force for the dynamics. This driving force also includes the influence of the applied mechanical load. It was shown in Chap. 5 that the driving force can also be calculated numerically from the average force per dislocation, see also Eq. (D.4):

$$-\hat{\mathbf{s}}_{\mathbf{b}} \cdot \nabla_{\mathbf{R}} \left(\frac{\delta \tilde{F}}{\delta \rho_{\mathbf{b}}(\mathbf{R})} \right) = \langle \hat{\mathbf{s}}_{\mathbf{b}} \cdot \mathbf{F}_{pk}(i) \rangle - \hat{\mathbf{s}}_{\mathbf{b}} \cdot \nabla_{\mathbf{R}} \left(k_B T_B \log \left[\frac{\rho_{\mathbf{b}}(\mathbf{R})}{\Lambda_{\mathbf{b}}^2} \right] \right), \quad (6.4)$$

where $\langle \hat{\mathbf{s}}_{\mathbf{b}} \cdot \mathbf{F}_{pk}(i) \rangle$ is the average Peach-Koehler force per dislocations, equal to $N_{\mathbf{b}}^{-1} \left\langle \sum_{i, \mathbf{b}(i)=\mathbf{b}} \hat{\mathbf{s}}_{\mathbf{b}} \cdot \mathbf{F}_{pk}(i) \right\rangle$. The second term on the RHS of Eq. (6.4) should be interpreted as a diffusive force. As the energy associated with the heat bath temperature, $k_B T_B$, is small compared to the other energy scales in the system, this term will be neglected in the rest of this chapter.

The memory kernel $H_{\mathbf{b}\mathbf{b}'}^{(0)}(\Delta t)$ is expressed as a correlation of fluctuations in the velocity of dislocations. This expression could therefore be interpreted as a Green-Kubo relation that relates correlations of fluctuations to transport coefficients. Note that $H_{\mathbf{b}\mathbf{b}'}^{(0)}(\Delta t)$ has the dimension of inverse time squared.

In this work, both the driving force and the memory kernel will be determined numerically. The flux of dislocations follows from these two quantities.

To derive Eq. (6.2) two assumptions were made, which will be verified numerically, see Sec. 6.3.1 and 6.4.1. First, separation of length scales is assumed. The velocity of a dislocation is only correlated with that of dislocations in its close neighborhood. For the separation of length scales, the typical dimensions of this neighborhood should be smaller than the length scale over which the driving force on the macroscale typically varies. An estimate for the size of this neighborhood follows from the field $H_{\mathbf{b}\mathbf{b}'}(\Delta R, \Delta t)$, defined by

$$H_{\mathbf{b}\mathbf{b}'}(\Delta R, \Delta t) \equiv \frac{2}{\Omega} \left\langle \sum_{i, \mathbf{b}(i)=\mathbf{b}} \sum_{i', \mathbf{b}(i')=\mathbf{b}'} \delta(\mathbf{R}(i) - \mathbf{R}(i')) \delta v(i, 0) \delta v(i', \Delta t) \right\rangle. \quad (6.5)$$

Note that the spatial integral of this field over ΔR is equal to $H_{\mathbf{b}\mathbf{b}'}^{(0)}(\Delta t = 0)$. The field $H_{\mathbf{b}\mathbf{b}'}(\Delta R, \Delta t)$ should thus be interpreted as the contribution to the memory kernel from

pairs at a certain distance ΔR .

Second, it was assumed that expectation values of odd powers of the fluctuations can be neglected. To verify this, the following condition should hold:

$$\left\langle \sum_{i, \mathbf{b}(i)=\mathbf{b}} \delta v(i, 0) \sum_{i', \mathbf{b}(i')=\mathbf{b}'} (\delta v(i', \Delta t)^2 - \langle \delta v(i', \Delta t)^2 \rangle) \right\rangle \ll \left\langle \sum_{i, \mathbf{b}(i)=\mathbf{b}} \delta v(i, 0) \sum_{i', \mathbf{b}(i')=\mathbf{b}'} \delta v(i', \Delta t) \right\rangle \langle v(i) \rangle, \quad (6.6)$$

where the LHS is cubic in the fluctuation, while the RHS is quadratic. Note that the RHS can be rewritten in terms of $H^{(0)}(\Delta t)$.

One may question whether the memory kernel in Eq. (6.2) is really needed. In steady state, where the driving force is independent of time, the evolution equation reads

$$\frac{\partial \rho_{\mathbf{b}}(\mathbf{R})}{\partial t} = -\hat{\mathbf{s}}_{\mathbf{b}} \cdot \nabla_{\mathbf{R}} (J_{\mathbf{b}}) \quad (6.7a)$$

$$\text{with } J_{\mathbf{b}} \equiv \sum_{\mathbf{b}'} \frac{\Gamma_{\text{eff}, \mathbf{b}\mathbf{b}'}}{k_B T_B} \left(-\hat{\mathbf{s}}_{\mathbf{b}'} \cdot \nabla_{\mathbf{R}} \left(\frac{\delta \tilde{F}(t)}{\delta \rho_{\mathbf{b}'}(\mathbf{R})} \right) \right) \quad (6.7b)$$

$$\Gamma_{\text{eff}, \mathbf{b}\mathbf{b}'} \equiv \int_0^{\tau_{\text{decay}}} d\Delta t H_{\mathbf{b}\mathbf{b}'}^{(0)}(\Delta t). \quad (6.7c)$$

The advantage of this equation is that it allows to interpret $\Gamma_{\text{eff}, \mathbf{b}\mathbf{b}'}$ as the effective, macroscopic mobility and $J_{\mathbf{b}}$ as the steady state current, and that no convolution is needed.

Eq. (6.7) could also be used when the driving force changes sufficiently slow. To this end, one should compare the typical timescale τ_{corr} on which $H_{\mathbf{b}\mathbf{b}'}^{(0)}(\Delta t)$ decays with the typical timescale τ_{relax} on which small perturbations in the density profile decay. The correlation time τ_{corr} can be determined numerically, and is defined as:

$$\tau_{\text{corr}} \equiv \left(\int_0^{\tau_2} d\Delta t H_{\mathbf{b}\mathbf{b}'}^{(0)}(\Delta t) \right) / H_{\mathbf{b}\mathbf{b}'}^{(0)}(\Delta t = 0). \quad (6.8)$$

The typical time on which fluctuations decay can be determined by considering fluctuations in the density on top of a steady-state solution of Eq. (6.7a) and by expanding the driving force around the steady-state. To this end, we considered as a steady-state solution a spatially constant density profile ρ_0 that is equal for all possible Burgers vectors, such that the system has no net dislocation content. As a fluctuation, we considered for one Burgers vector \mathbf{b} a density fluctuation, such that $\rho_{\mathbf{b}}(\mathbf{R}) = \rho_0 + \delta\rho(\mathbf{R})$. The free energy expression from Chap. 3 was used in the scaling analysis, where the dominant contribution in the force results from the Peach-Koehler force. Then, the typical timescale for the dynamics of this fluctuation is, see Appendix D.2

$$\tau_{\text{relax}} = \frac{1}{\Gamma_{\text{eff}, \mathbf{b}\mathbf{b}'} \mu b^2 L / k_B T_B}, \quad (6.9)$$

where $\Gamma_{\text{eff}, \mathbf{b}\mathbf{b}'}$ should be determined at the appropriate mechanical load.

Some important remarks on ensemble averages

For dislocations in metals, it is a legitimate question whether the system is ergodic, and hence whether statistical, average measures are relevant. Energy barriers are high compared to the thermal energy of the environment, $k_B T_B$, and hence the system will not evolve by passing barriers in phase space, but rather stay in its own basin of attraction. It has been shown [59] that statistical averages of many small dislocation systems yield a realistic macroscopic behavior. We therefore assume that the ensemble average over the whole phase space of $H_{bb',\text{basin}}^{(0)}(\Delta t)$ in each basin of attraction yields $H_{bb'}^{(0)}(\Delta t)$ for the entire ensemble, and hence the macroscopic transport coefficient $\Gamma_{bb',\text{eff}}$.

However, to obtain $H_{bb',\text{basin}}^{(0)}(\Delta t)$, one cannot use the ensemble average over the whole phase space to obtain $\langle v(i) \rangle$, but one should rather use the ensemble average in the basin of attraction only. Unfortunately, as the phase space is high-dimensional, averages for each basin of attraction separately cannot be obtained. To overcome this, long-time averages of each trajectory will be used, which are close to, but not equal to the basin-ensemble average. In fig. 6.1(a), the different averages are sketched for a two-dimensional phase space.

To write $H_{bb'}^{(0)}(\Delta t)$ in terms of long-time averages, we write

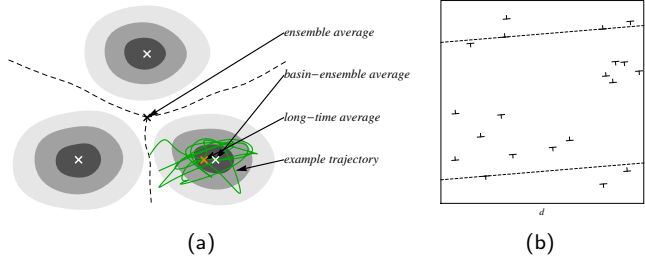


Figure 6.1: (a) Sketch of a two-dimensional phase space with different basins of attraction, the ensemble average, the ensemble average in each basin of attraction and the long-time average for an example trajectory. (b) A sketch of a microstate with positive and negative dislocations on different slip systems. Periodic boundary conditions are imposed.

$$\begin{aligned}
 \frac{H_{bb'}^{(0)}(\Delta t)}{2\Omega^{-1}} &= \left\langle \left\langle \sum_{i, \mathbf{b}(i)=\mathbf{b}} (v(i, 0) - \langle v(i) \rangle_{\text{time}} + \langle v(i) \rangle_{\text{time}} - \langle v(i) \rangle_{\text{basin-ens.}}) \right. \right. \\
 &\quad \cdot \left. \left. \sum_{i', \mathbf{b}(i')=\mathbf{b}'} (v(i', \Delta t) - \langle v(i') \rangle_{\text{time}} + \langle v(i') \rangle_{\text{time}} - \langle v(i') \rangle_{\text{basin-ens.}}) \right\rangle_{\text{basin-ens.}} \right\rangle_{\text{ensemble}} \\
 &= \left\langle \left\langle \sum_{i, \mathbf{b}(i)=\mathbf{b}} (v(i, 0) - \langle v(i) \rangle_{\text{time}}) \sum_{i', \mathbf{b}(i')=\mathbf{b}'} (v(i', \Delta t) - \langle v(i') \rangle_{\text{time}}) \right\rangle_{\text{ensemble}} \right. \\
 &\quad \left. + \left\langle \left(\sum_{i, \mathbf{b}(i)=\mathbf{b}} (\langle v(i) \rangle_{\text{time}} - \langle v(i) \rangle_{\text{basin-ens.}}) \right)^2 \right\rangle_{\text{ensemble}} \right\rangle, \quad (6.10)
 \end{aligned}$$

where for the second equality, it was used that the subsequent ensemble average within a basin and over the whole ensemble is simply equal to the ensemble average.

The first term in Eq. (6.10) is independent of the basin-average, and hence can be determined in a straightforward manner. To obtain a value for the second term, first note that this is the expectation value of the square of the difference between long-time and (basin-)ensemble average. This is inversely proportional to the number of independent measurements, see e.g. [26], and hence to the measurement time. This implies that the second term is positive and that its time-integral is non-negligible.

Second, note that the correlation of fluctuations in the velocity around the basin-ensemble average after a long time is zero. As the second term is square and thus positive, the first term will attain a constant, negative value after a long time. This value is therefore equal to minus the second term in Eq. (6.10).

In the above, it is assumed that the deviation of the first contribution from zero is only due to the difference in long-time and basin-ensemble averages. It is thus silently assumed that there are no other systematic errors that cause a constant shift. To verify this, we can make use of the fact that the second contribution is inversely proportional to the measurement time. Namely, the first contribution can be determined for several measurement times τ_2 and the second contribution for one of these times. The second contribution for the other measurement times then follows immediately, as it is inversely proportional to the measurement time. The resulting curves for $H^{(0)}(\Delta t)$ for the different measurement times should then collapse, if no other systematic errors are made.

Moreover, it is assumed that the average force per dislocation and the transport coefficient in each basin are not correlated. Namely, the ensemble average of the transport coefficient and the driving force are taken separately, while one could also have taken the ensemble-average of the flux in each basin. This assumption is verified in Sec. 6.3.1.

6.2.2 Numerical implementation

In this study, the influence of applied stresses on the effective, macroscopic mobility is studied, but the influence of the overall dislocation density and the two temperatures T_C and T_B is not further examined. For this reason, the overall dislocation density is fixed at a representative value of $1\mu m^{-2} = 10^{12}m^{-2}$. In the numerical simulations, the thermal noise has been neglected, as it has been shown in Chap. 2 that the typical energy associated with thermal fluctuations in the heat bath, $k_B T_B$, is negligible compared to the typical interaction energy between dislocations. In the simulations, we therefore set $T_B = 0$. The configurational temperature T_C is fixed at ∞ , as it has been shown that the ensemble-average of the dynamics of random dislocation configurations yields physical results that are representative for the dynamics of many dislocations[59]. An infinite configurational temperature results in a random dislocation distribution.

The effective, macroscopic transport coefficient is obtained from the evolution of 336 random dislocation configurations under applied mechanical load. See Fig. 6.1(b) for an example sketch of a microstate. For simplicity, only one slip system is considered. Each microstate contains 144 dislocations in a square periodic unit cell, of which 72 have a positive Burgers vector and 72 a negative one. Note that, as there is only one slip system and no net dislocation content, the total force on all dislocations with positive Burgers vector is equal to minus the force on all dislocations with negative Burgers vector. As a

consequence, the sum of all $v(i)$ is equal for dislocations with either positive or negative Burgers vector, which implies that $H_{++}^{(0)} = H_{+-}^{(0)} = H_{-+}^{(0)} = H_{--}^{(0)} \equiv H^{(0)}$. Therefore, only $H^{(0)}$ will be considered.

Periodic boundary conditions are applied to mimic the bulk behavior of dislocations. The glide planes are slightly tilted with respect to the direction of periodicity. If the glide planes would be horizontal, dislocations would end up in their initial position only after short time. This would cause spurious autocorrelations, which are largely avoided using tilted glide planes. The tilt angle is chosen to be $\phi = \arctan(1/12) \approx 4.8^\circ$.

Two dimensionless parameters arise in the expression for the force on a dislocation. For convenience, all forces are measured in units of $F_{\text{int}} \equiv \mu b^2 L / (1 - \nu) R$, which is the interaction force between two dislocations at a distance R . R is the typical dislocation spacing, which for the density considered ($10^{12} m^{-2}$) equals $R = 1 \mu m$. The first dimensionless parameter is $S \equiv \Sigma_{\text{res}} b L / F_{\text{int}}$, which is the Peach-Koehler force due to the applied mechanical load in units of F_{int} . The second dimensionless parameter is $\tau \equiv \frac{R^2 B_b (T_B) (1 - \nu)}{\mu b^2}$, which is the typical timescale during which a dislocation travels the typical dislocation spacing R due to loading at $S = 1$. Due to the periodic boundary conditions, the force on each dislocation is the sum of the Peach-Koehler component due to applied mechanical load and the components due to the other dislocations and their periodic copies. The former is equal to $b L \Sigma_{\text{res}}$, where Σ_{res} is the resolved shear stress. For the latter, we use the stress field for a periodic array of dislocations, as determined by Kuykendall and Cai [70], to derive the Peach-Koehler force due to a dislocation and all its periodic copies, see Appendix D.3. This yields

$$\begin{aligned} \frac{\tau}{R} v(i) = S + \frac{R}{2d} \sum_{i'} \sum_{k=-\infty}^{\infty} \frac{b(i')}{|b(i')|} & \left(\frac{\sin(\Delta \check{x}_{ii'})}{\cosh(\Delta \check{y}_{ii'}^k) - \cos(\Delta \check{x}_{ii'})} \cos(\phi) \cos(2\phi) + \right. \quad (6.11) \\ & - \frac{\Delta \check{y}_{ii'}^k \sinh(\Delta \check{y}_{ii'}^k) \sin(\Delta \check{x}_{ii'})}{(\cosh(\Delta \check{y}_{ii'}^k) - \cos(\Delta \check{x}_{ii'}))^2} \cos(3\phi) + \Delta \check{y}_{ii'}^k \frac{1 - \cosh(\Delta \check{y}_{ii'}^k) \cos(\Delta \check{x}_{ii'})}{(\cosh(\Delta \check{y}_{ii'}^k) - \cos(\Delta \check{x}_{ii'}))^2} \sin(\phi) + \\ & \left. + \frac{\sinh(\Delta \check{y}_{ii'}^k)}{\cosh(\Delta \check{y}_{ii'}^k) - \cos(\Delta \check{x}_{ii'})} \cos(\phi) \sin(2\phi) \right), \end{aligned}$$

where $\Delta \check{x}_{ii'} = \frac{2\pi(x_i - x_{i'})}{d}$ and $\Delta \check{y}_{ii'}^k = \frac{2\pi(x_i - x_{i'} + kd)}{d}$ are the position differences. In practice for the summation over k , it is sufficient to use three rows of dislocations below and on top, see fig. D.1 in Appendix D.1.

When two dislocations with opposite Burgers vector are on a very short distance, the force between them is large and attractive. This force is unphysical, as these dislocations tend to annihilate in a real metal. To avoid such forces, only predefined glide planes are considered, on which only dislocations with either positive or negative Burgers vector occur. The spacing between these glide planes used here is 50 nm, or $0.05R$, which is the typical annihilation distance for dislocations in several different metals at room temperature [92]. Moreover, there is an initial relaxation towards the steady state solution. Namely, the initial random configuration of dislocations is in thermal equilibrium with the infinite configurational temperature. However, one would expect that within each basin of attraction, the dislocation configuration would be in thermal equilibrium with the environmental temperature, which is set to zero here. Therefore, we are only interested in the steady state,

and hence an initial relaxation time is needed. The length of this will be determined from the results.

6.3 Simulation results

6.3.1 Illustration of the procedure

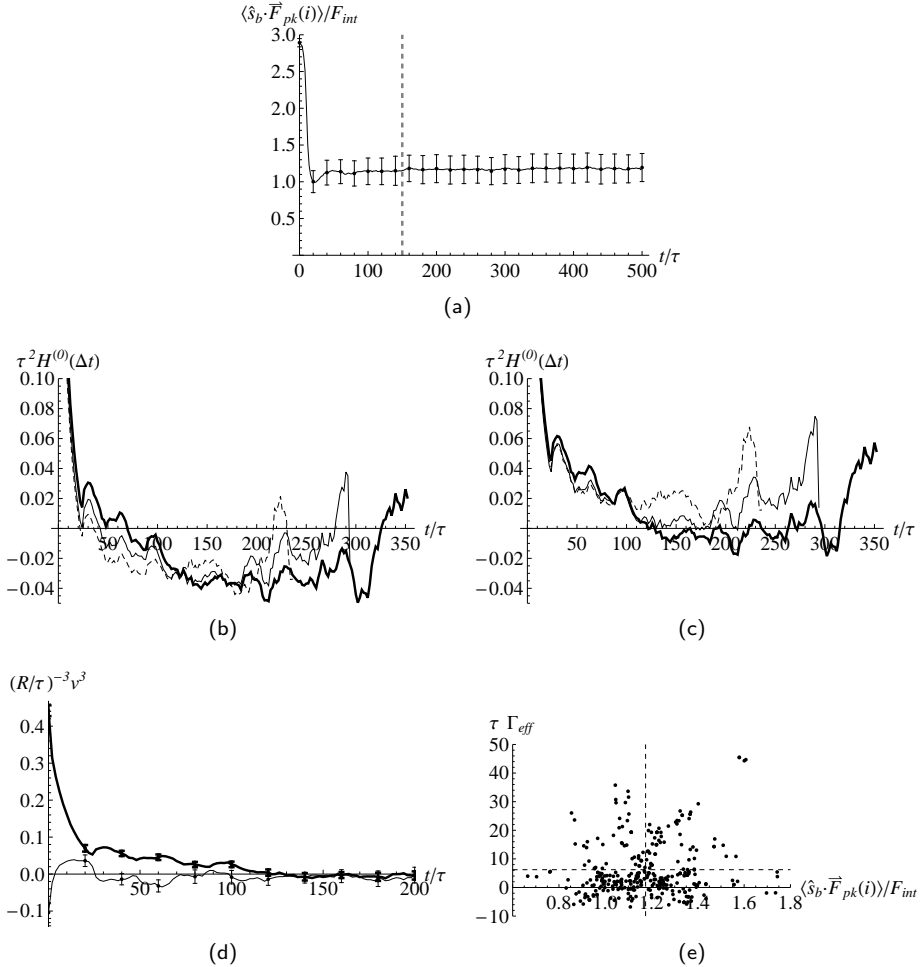


Figure 6.2: (a) The average force per dislocation. (b) A detailed picture of the tail of the first contribution to $H^{(0)}(\Delta t)$ in Eq. (6.10) and (c) $H^{(0)}(\Delta t)$ with the correction as described in Sec. 6.2.1, both for interval lengths of 350τ (thick), 262τ (solid) and 218τ (dashed). (d) The LHS (solid) and RHS (thick) of Eq. (6.6). (e) The average force per dislocation and the transport coefficient for each microstate. The dashed lines indicate the averages. The errorbars in (a) and (d) indicate the standard deviation.

In this subsection, the numerical results at a loading of $S = 3.0$ will be discussed as a representative example. In Fig. 6.2(a), the average force per dislocation as a function of time is plotted. The initial relaxation is less than 150τ until a constant, steady force is reached. The average force experienced by a dislocation is far below $\langle \hat{\mathbf{s}}_{\mathbf{b}} \cdot \mathbf{F}_{pk}(i) \rangle / F_{\text{int}} = S$, which would be the force in the absence of interactions. The influence of interactions at this load is thus quite strong.

In fig. 6.2(b), the tail of the first contribution to $H^{(0)}(\Delta t)$ in Eq. (6.10) is plotted for several measurement times. After long time, all three graphs saturate at a slightly negative value, as expected. In fig. 6.2(c), $H^{(0)}(\Delta t)$ is plotted, where the second contribution in Eq. (6.10) was determined from the longest curve only, as described in Sec. 6.2.1. The first halves of the three curves collapse, which suggests that it is possible to determine $H^{(0)}(\Delta t)$ using the long-time average of each trajectory, as described in Sec. 6.2.1.

In fig. 6.2(d), the left- and right hand side of Eq. (6.6) are plotted. Clearly, the odd power of the fluctuations (solid line) is much smaller than the even power (thick line), and moreover, the odd power does not differ significantly from zero. It is therefore justified to neglect odd powers of the fluctuations.

In fig. 6.2(e), the average force per dislocation and the transport coefficient Γ_{eff} are plotted. No clear trend is visible in these data, and the correlation between both quantities is 17%, which is weak. This implies that one can take averages of the average force per dislocation and the transport coefficient separately, as was assumed in Sec. 6.2.1.

We have checked that our results are insensitive to a refinement of the time step. However, the our quantitative results are sensitive to a change in glide plane spacing. This is probably because the maximum strength of the interaction changes when the minimum distance between dislocations changes, which implies that the influence of interactions that lowers the mean velocity is different. However, the qualitative trends described in the next section are not affected.

6.3.2 Effective mobility

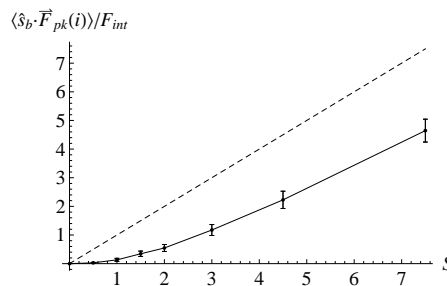


Figure 6.3: The mean force per dislocations in units of the interaction force at a distance R for several values of the load S . The dashed line corresponds to the case where interactions between dislocations are neglected. The errorbars indicate the standard deviation in the ensemble and the connecting solid lines are a guide to the eye.

In Fig. 6.3, the average force per dislocation is plotted against the applied load. The dashed line is the line $\langle \hat{\mathbf{s}}_{\mathbf{b}} \cdot \mathbf{F}_{pk}(i) \rangle / F_{\text{int}} = S$, which would be the average force per

dislocation in the absence of interactions. Hence, the difference between the measured values and the dashed line is the reduction of the average force due to interactions between dislocations.

In Fig. 6.4(a), the memory kernel is plotted as a function of the time interval Δt for

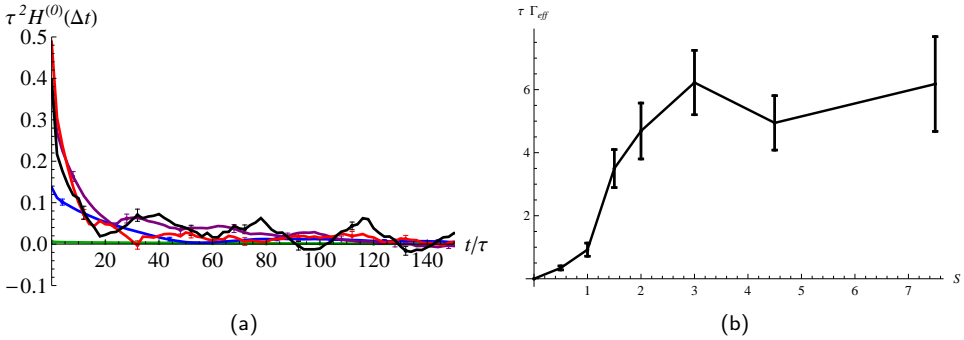


Figure 6.4: (a) The memory kernel $H^{(0)}(\Delta t)$ for different values of the load (0.5 (green), 1.5 (blue), 3.0 (purple), 4.5 (red), 7.5 (black)). (b) The effective mobility Γ_{eff} defined in Eq. (6.7c). The errorbars indicate the 95% confidence interval.

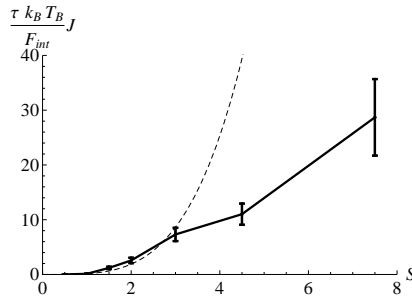


Figure 6.5: The dislocation current J as defined in Eq. (6.7b). The dashed line is a power-law fit with exponent 3.7. The errorbars indicate the 95% confidence interval and the connecting lines are for visualization purposes only.

several values of the applied load. The value at $\Delta t = 0$ seems to increase with increasing applied load up to $S = 4.5$, but the value for $S = 7.5$ is again lower.

In Fig. 6.4(b), the integral of the memory kernel is plotted, which can be interpreted as the effective, macroscopic mobility. The resulting steady state current is the product of the effective, macroscopic mobility Γ_{eff} and the driving force. This quantity is plotted in fig. 6.5. The current is thus stress-dependent. For small loads ($S \leq 3$), the current increases in a strongly non-linear manner with the applied load. For larger loads ($S \geq 3$), the relation between applied load and current is more or less linear.

For further use, we have determined the typical correlation time- and length. In Fig. 6.6, the correlation times as defined in Eq. (6.8) are plotted. The correlation time decreases with increasing applied load, but seems to saturate at a value of 10τ . In Fig. 6.7, the

distance-dependence of the field H at $\Delta t = 0$ is plotted. Inspection of the field shows that correlations are strongest in the x -direction, and therefore only these are depicted. The H_{++} -field is dominated by autocorrelations of the dislocations with themselves. At $\Delta x \approx \pm 2R$, small secondary peaks are visible, but correlations are not apparent beyond $\Delta x = 3R$. The H_{+-} -field is mainly determined by correlations within pairs of dislocations. Correlations beyond $4R$ are not present, but they are by far the largest at $S = 1.5$. It might be that this intermediate value of the load is strong enough to stretch dislocation pairs significantly, but not strong enough to separate them. As a result, correlations span relatively long distances.

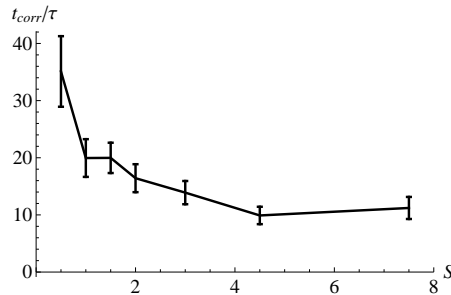


Figure 6.6: The correlation times. The lines are a for visualization purposes only. The errorbars indicate the 95% confidence interval.

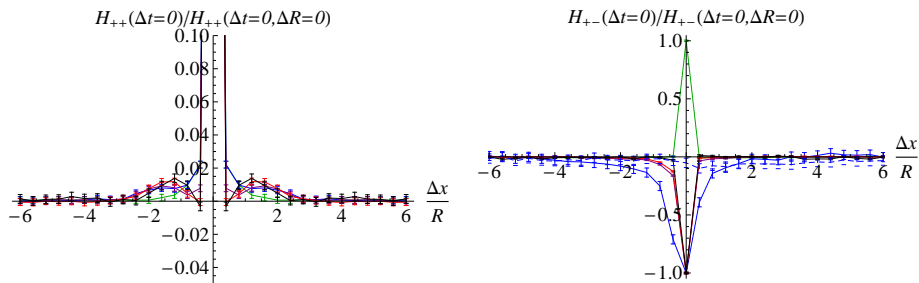


Figure 6.7: The field H in the x -direction, normalized by its value at $\Delta R = 0$. Solid line is at $\Delta y = 0$ and dashed line at $\Delta y = 0.96R$. Colors indicate different values of the load (0.5 (green), 1.5 (blue), 3.0 (purple), 4.5 (red), 7.5 (black)). The lines are for visualization purposes only and the errorbars indicate the noise level in the far field.

6.4 Interpretation and comparison to literature

6.4.1 Examination of the separation of length- and timescales

In this subsection, we discuss the separation of length- and timescales. Considering the separation of length scales, we have obtained correlations that do not span over a distance

larger than $4R$. This implies that when the driving force does not vary significantly over distances smaller than four dislocation spacings, there is separation of length scales. The driving force only changes when $\rho_b(\mathbf{R})$ changes. On length scales as small as four dislocation spacings, it is not likely that the ensemble average of the dislocation density changes in the bulk, and hence the local expression in Eq. (6.2) is a good approximation. To compare the timescales τ_{corr} and τ_{relax} in Eqs. (6.8) and (6.9), we exploit the fact that τ_{corr} is at least 10τ , see fig. (6.6), and that Γ_{eff} is larger than $0.2\tau^{-1}$, which is the value at $S = 0.5$, see fig. 6.4(b). Moreover, the dimensionless quantity $\mu b^2 L/k_B T_B$, which is needed to determine τ_{relax} (see Eq. (6.9)), can be estimated using typical values for aluminium. This indicates that $\mu b^2 L/k_B T_B > 2.4 \times 10^2$. Hence, $\tau_{\text{corr}}/\tau_{\text{relax}} \geq 470$, which indicates that the decay time of the correlation function is much longer than the typical time a density fluctuation exists. Therefore, the temporal convolution in Eq. (6.2) can in general not be approximated by a product as in Eq. (6.7a). Therefore, Eq. (6.7a) can only be used to determine the steady state currents.

6.4.2 Hypothesis

The central hypothesis behind this work is that the observed non-linear load-dependence at the macroscopic level is an emergent phenomenon. It is shown in this work that both the expectation value of the average force per dislocation and the effective, macroscopic mobility depend non-linearly on the applied mechanical load, see figs. 6.3 and 6.4. At the level of discrete dislocations, the force on an individual dislocation is linearly proportional to the applied load, whereby the microscopic mobility of dislocations $B_b(T_B)$ is independent of the applied load. The obtained non-linear dependency on the applied load at the macroscopic level therefore constitutes an emergent phenomenon, which confirms our hypothesis.

The non-linear dependence of the driving force on the applied load obtained from the numerical simulations in Fig. 6.3 would not result from the expression in Eq. (6.4) when free energy expressions from Chap. 2 and 3 are used, as these predict a linear dependence on the applied mechanical load.

A first possible cause of this is that the modeling of the configurational temperature in Chap. 5 does not agree with the numerical simulations performed here. Namely in the simulations, the organization of dislocations is locally in a minimum energy state, but globally homogeneous. On the contrary, a dislocation distribution at a high configurational temperature T_C , as modeled in 5, is both locally and globally homogeneous. To solve this problem, another split should be made between the configurational energy and the energy of the heat bath. A different split was also suggested in literature [10] in the context of the thermodynamics of the system. However, this split was not worked out further in literature.

A second possible cause of the discrepancy between the driving force obtained here numerically, and the free energy expressions in Chap. 2-4, is that the free energy expression in those works is asymptotically correct far away from criticality. A load-induced transition may be regarded as a critical phenomenon, which limits the applicability of the obtained expression. To solve this problem, the free energy expression may be systematically improved by using the Villain approximation [61], as also discussed Chap. 2.

6.4.3 Relation to literature

The difference between the applied load and the average force experienced by dislocations has also been discussed in literature [43, 119]. In this work, no gradients in the GND- or total density of dislocations were considered. Yet, we have obtained a non-linear relation between the applied load and the average force, in fig. 6.3. We therefore think that current phenomenological models can be improved by accounting for an internal stress that depends explicitly on the applied mechanical load, and not only implicitly via gradients in the dislocation density.

This contribution to the average force could be explained by the stretching of dislocation pairs due to load. Namely, pairs of dislocations with opposite Burgers vectors will stretch in the direction of the load, which induces a force between the dislocations in the opposite direction. This was also hinted upon by Zaiser and coworkers [120].

The obtained force-flux relation in fig. 6.5 can also be related to current strain gradient crystal plasticity models [43]. Namely, in these models the following relationship is assumed between the driving force τ and the slip rate $\dot{\gamma}$:

$$\dot{\gamma} \propto R \left(\frac{|\Sigma_{\text{res}}|}{\Sigma_0} \right) \text{sign}(\Sigma_{\text{res}}) \quad (6.12)$$

where $R(0) = 0$ and $R(|\Sigma_{\text{res}}|/\Sigma_0) > 0$ for $\Sigma_{\text{res}} \neq 0$. Often, the function R is assumed to be of power-law form. The slip rate can also be expressed as $\dot{\gamma} = b(j_{\mathbf{b}} - j_{-\mathbf{b}})$, where $j_{\mathbf{b}}$ is the flux of dislocations with Burgers vector \mathbf{b} . Hence the function R can be obtained from fig. 6.5.

In fig. 6.5, two regimes can be identified. In the high load regime ($S \geq 3$), force and flux are approximately linearly related. In the low load regime ($S \leq 3$), the relation is strongly non-linear. The dashed line is a power-law fit with exponent 3.7.

For aluminium¹ with a dislocation density of $1\mu\text{m}^{-2}$, $S = 1$ corresponds to a resolved shear stress of $\Sigma_{\text{res}} = 11 \text{ MPa}$, which is of the same order as the yield stress for pure aluminium (7 – 11 MPa). This suggests that the low load regime, in which the relation between force and flux is strongly non-linear, is most relevant in practical cases. It should however be emphasized that the current model is highly idealized, and hence that one should therefore focus on qualitative aspects only.

The exponent typically used in crystal plasticity models ranges from 10 to 100. The powerlaw relation in these models is often only used to mimic an elasto-plastic flow relation with a threshold stress above which the material deforms entirely plastic. The viscous response is then only introduced to circumvent numerical problems.

In this work, a much lower value for exponent (namely 3.7) is obtained. On the one hand, the microscopic evolution treated here is undoubtedly oversimplified. When more interaction mechanisms and creation and annihilation of dislocations is accounted for, the effect of interactions is stronger. As interactions are the cause of the non-linearity, it is expected that the exponent increases upon including these effects. On the other hand, the result obtained here might also suggest that there is a physical basis for the viscous contribution in the dynamics, and that viscous terms should thus be accounted for.

¹For aluminium, $\mu = 26 \text{ GPa}$, $\nu = .33$, $b = 2.9 \text{ \AA}$ (see [101]).

6.5 Summary and outlook

In this work, the dependence of the macroscopic transport relations for dislocation systems on the applied mechanical load is studied. It has been shown in Chap. 5 that the macroscopic transport coefficient has, on top of the simply “translated” microscopic transport coefficient, an additional contribution that results from the transition in timescale from the microscopic to the macroscopic level. The latter results from correlations in the rapid fluctuations. Moreover, it was shown that the driving force for dislocation dynamics equals the average force experienced by the dislocations. Both quantities have been evaluated numerically in this work using steady-state Discrete Dislocation Dynamics simulations. The main conclusions of this work are the following:

- The driving force for dislocation dynamics depends on the applied load in a non-linear manner, which implies that there is a load-dependent internal stress.
- The effective, macroscopic transport coefficient is load-dependent, while the microscopic mobility is independent of the load.
- The resulting dislocation flux depends non-linearly on the applied load in the relevant regime, which is in agreement with current crystal plasticity models.
- The obtained non-linearity is an emergent phenomenon and does thus not result from non-linearities at the microscopic level.
- In this system, there is no separation of timescales. This implies that the dynamics at the macroscopic level is non-Markovian, and hence that a memory kernel is needed to describe the dynamics of dislocation density profiles accurately.

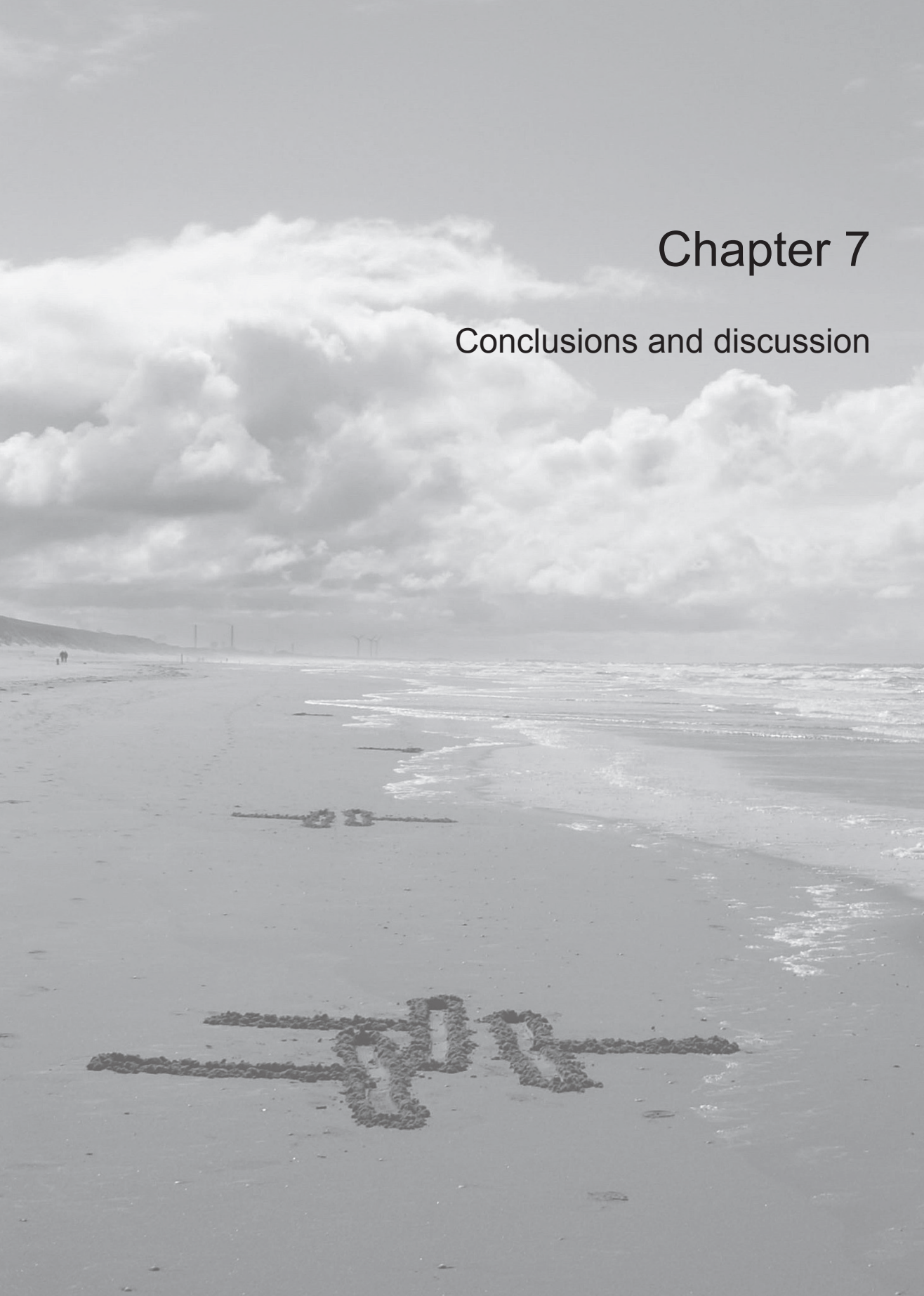
This study indicates that the dominant term in the macroscopic mobility of dislocation systems is the additional irreversibility that arises from going to a coarser level of description and making a transition in timescale. The latter implies that we have accounted for correlations of fluctuations in the fast dynamics, which gives rise to a transport coefficient of Green-Kubo type. Therefore, the transition in timescale should as well be part of other coarse-graining schemes for dislocation systems.

The same coarse-graining procedure as employed in Chap. 5 and this chapter could be extended to more realistic microscopic descriptions of dislocation motion, which include for example production and annihilation of dislocations or curved dislocations that are not necessarily parallel.

The results of this study could also be used in phenomenological Crystal Plasticity modeling. To improve these models, we would suggest to account for a direct load-dependence of the internal stress, and not only for an indirect dependence via the gradient of total and GND densities. Moreover, we have given a microscopically based argument for the non-linear relation between driving force and plastic slip. The relation obtained here might suggest that there is a physical basis for including viscous effects in the evolution equation.

Chapter 7

Conclusions and discussion



7.1 Conclusions

The work presented in this thesis confirms the central hypothesis:

“The collective, coarse-grained dynamics of dislocations reveals emergent phenomena that dominate the macroscopic system response. ”

The implications of the obtained results will now be discussed in more detail. The work of this thesis can be split into a part on the statics of the system, and a part on the dynamics.

The part on statics, Chap. 2-4, starts with systematic coarse-graining, specifically the calculation of the derivation of the grand-canonical partition function using systematic coarse-graining. The work was limited to straight and parallel dislocations, such that the problem is effectively two-dimensional. In the derivation, microscopic properties that have proven to be important in dislocation systems are accounted for, namely the finite system-size, the presence of glide planes, an applied deformation of the boundary (denoted by \mathbf{u}_b), the configurational temperature of the dislocations that is a measure for the energy associated with density fluctuations (denoted by T_C), the anisotropy of the stress field of edge dislocations and an inhomogeneous dislocation density profile $\rho_b(\mathbf{R})$. The key step in calculating the grand-canonical partition function was to extend the phase space, such that the integration over phase space also entails a path integral over the elastic field. In the absence of mechanical loading, the obtained partition function reduces to the well-studied Sine-Gordon model, that describes the Kosterlitz-Thouless phase transition. The obtained partition function has been simplified using a Gaussian approximation, which is valid far away from criticality.

Subsequently, the canonical free energy functional F_C was obtained by means of a Legendre transform of the grand potential:

$$\begin{aligned}
 F_C[\rho_b(\mathbf{R}), \mathbf{u}_b, T_C] = & L \underbrace{\int d\mathbf{R} \Delta_{\text{mf}} : \mathbb{C} : \Delta_{\text{mf}}}_{\text{mean-field contribution } F_{\text{mf}}} \quad (7.1) \\
 & - \underbrace{k_B T_C \sum_b \int d\mathbf{R} \rho_b(\mathbf{R}) \left(\log \left[\frac{\rho_b(\mathbf{R})}{\rho_{b,0}} \right] - 1 \right)}_{\text{statistical contribution}} + \underbrace{\int d\mathbf{R} f_{\text{mb}}(\rho_b(\mathbf{R}), T_C)}_{\text{many-body contribution } F_{\text{mb}}},
 \end{aligned}$$

where L is the typical length of a straight dislocation, where the spatial integral is over the cross-sectional area, and where $\rho_{b,0}$ is a reference density.

The first contribution on the RHS is the strain energy due to the mean-field strain Δ_{mf} , which is the strain field due to the applied boundary deformation and the other dislocations when correlations between dislocation positions are neglected. The second contribution on the RHS is the statistical contribution that results from the counting of states. The third contribution on the RHS is the many-body contribution, which results from the screening of dislocation interactions. Explicit expressions were found for the many-body free energy density $f_{\text{mb}}(\rho_b(\mathbf{R}), T_C)$ for two special cases, see Eqs. (3.43) and (4.11). The main conclusion about the statics of the system are:

- The many-body contribution is an emergent contribution to the free energy that can not be neglected, see Sec. 3.4
- For the many-body contribution, explicit expressions can be obtained by using a Local Density Approximation (LDA), see Sec. 3.4.1. It was shown that such a local approximation is applicable to dislocation systems, provided that the dislocation density varies over distances much larger than the average dislocation spacing.
- The many-body contribution vanishes at zero temperature, but quickly approaches a plateau value for finite temperatures. It was therefore concluded that the free energy at a finite temperature is qualitatively different from the energy at zero temperature, even for very low temperatures, see Sec. 3.4.2
- The many-body contribution depends on the total density per slip plane, see Sec. 3.5. Such a dependence has no counterpart at the microscopic level, where a complete anti-symmetry in the dislocation interaction potential exists between dislocations with opposite Burgers vectors. Based on this, it has been assumed in literature that the free energy only depends on the density of Geometrically Necessary Dislocations (GND's). The dependence of the macroscopic free energy on both the GND and the *total* density recovered here is therefore an emergent property of the system. This dependence should also be used in strain-gradient Crystal Plasticity models. In that case, and assuming that the Local Density Approximation holds, the current free energy expression could be used to determine energetic defect forces.

The dynamics part of this thesis, Chap. 5 and 6, starts with the derivation of the evolution equations for the dislocation density profile $\rho_b(\mathbf{R})$ and the configurational and heat bath temperatures, T_C and T_B . The evolution equation for the density is given by:

$$\underbrace{\frac{\partial \rho_b(\mathbf{R})}{\partial t}}_{\text{divergence}} = - \hat{\mathbf{s}}_b \cdot \nabla_{\mathbf{R}} \underbrace{\left(\sum_{b'} \int d\Delta t \overbrace{\frac{H_{bb'}^{(0)}(\Delta t)}{k_B T_B}}^{\text{memory kernel}} \left(\overbrace{-\hat{\mathbf{s}}_{b'} \cdot \nabla_{\mathbf{R}} \left(\frac{\delta \tilde{F}(t - \Delta t)}{\delta \rho_{b'}(\mathbf{R})} \right)}^{\text{driving force}} \right) \right)}_{\text{dislocation flux}} \quad (7.2)$$

with

$$\begin{aligned} \tilde{F}[\rho_b(\mathbf{R}), \mathbf{u}_b, T_C, T_B] &= F_C[\rho_b(\mathbf{R}), \mathbf{u}_b, T_C] \\ &+ k_B(T_C - T_B) \sum_b \int d\mathbf{R} \rho_b(\mathbf{R}) \left(\log \left[\frac{\rho_b(\mathbf{R})}{\rho_{b,0}} \right] - 1 \right). \end{aligned} \quad (7.3)$$

The time derivative of the dislocation density is the divergence of the dislocation flux. The total number of dislocations is thus conserved, which reflects the fact that no production or annihilation of dislocations is considered at the microscopic level. The dislocation flux is the convolution of a driving force with a memory kernel. The former can be determined from the previously obtained free energy. For the memory kernel, the dominant contribution can be written as time-correlations of fluctuations of the dislocation velocity,

which depends in principle on the applied deformation, the dislocation density and both temperatures.

The evolution equation for the configurational temperature reads

$$\frac{dT_C}{dt} = \frac{1}{\underbrace{k_B \sum_{\mathbf{b}} N_{\mathbf{b}}}_{\text{Configurational heat capacity}}} \quad (7.4)$$

$$\left\{ \int d\mathbf{R} \left[\underbrace{\left(\sum_{\mathbf{b}'} \int d\Delta t \frac{H_{\mathbf{b}\mathbf{b}'}^{(0)}(\Delta t)}{k_B T_B} \left(-\hat{\mathbf{s}}_{\mathbf{b}'} \cdot \nabla_{\mathbf{R}} \left(\frac{\delta \tilde{F}(t - \Delta t)}{\delta \rho_{\mathbf{b}'}(\mathbf{R})} \right) \right) \right)}_{\text{dislocation flux}} \right. \right.$$

$$\left. \cdot \underbrace{\left(-\hat{\mathbf{s}}_{\mathbf{b}} \cdot \nabla_{\mathbf{R}} \left(\frac{\delta F_{\text{mf}} + F_{\text{mb}}}{\delta \rho_{\mathbf{b}}(\mathbf{R})} \right) \right)}_{\text{average force}} \right]$$

$$+ \int d\Delta t \underbrace{\mathbf{K}(\Delta t)}_{\text{Transport coefficient for the heat flow}} \left. \underbrace{\left(\frac{1}{k_B T_C(t - \Delta t)} - \frac{1}{k_B T_B(t - \Delta t)} \right)}_{\text{Driving force for the heat flow}} \right\}.$$

The inverse of the configurational heat capacity indicates how much the configurational temperature T_C changes upon changing the configurational energy of the system. The terms in the curly brackets should therefore be interpreted as the change in configurational energy. The first contribution is the expected dislocation flux times the average force on a dislocation, i.e. the expected dissipated power. The second contribution relates to the heat flow from the configurational subsystem to the heat bath. This term results from the energy that is dissipated due to fluctuations in the velocity.

The main conclusions from this derivation are the following:

- On top of the a direct contribution arising from the microscopic irreversible dynamics, the dynamical response function for the dislocation density entails an emergent contribution in the form of a memory kernel. Scaling analysis indicates that the latter is dominant.
- The transport coefficient for the heat flow is an emergent term.
- The use of two temperatures influences the driving force as follows: using Eqs. (7.2) and (7.3), it can be shown that the diffusion of dislocations (due to the statistical contribution to the free energy) acts as if the system is at the heat bath temperature T_B , while the rest of the driving force (due to the mean-field and the many-body contributions in the free energy) acts as if the system is at the configurational temperature T_C .

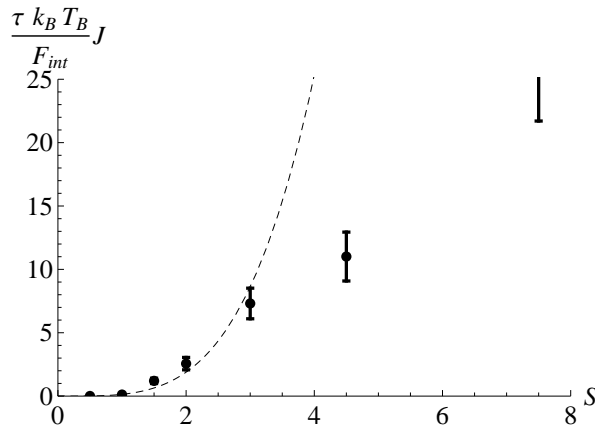


Figure 7.1: The macroscopic dislocation current J as a function of the applied mechanical load S . The dashed line is a power-law fit with exponent 3.7. The errorbars indicate the 95% confidence interval.

The macroscopic response function $H^{(0)}(\Delta t)$ and the driving force were examined numerically. The key step in performing the numerical simulations was to realize that the phase space can be separated in different basins of attraction, separated by energy barriers that cannot be overcome by diffusion on the timescales considered here. Therefore, fluctuations should be calculated with respect to the ensemble average in the corresponding basin of attraction. This average can be approximated by the long-time average. The obtained relation between the dislocation flux J and the applied mechanical load S is shown in Fig. 7.1. The main conclusions from this numerical study are the following:

- Both the driving force and the macroscopic response function $H^{(0)}(\Delta t)$ depend on the applied mechanical load in a non-linear manner.
- As a result, a nonlinear dependence of the dislocation flux on the applied mechanical load emerges in the regime of engineering relevance, which is in agreement with viscoplastic flow rules used in many Crystal Plasticity models.
- The dynamics of the dislocation density is non-Markovian, i.e. there is no separation of timescales.

7.2 Outlook

The research presented in this thesis has revealed new insights in the collective dynamics of dislocations, but also triggers new, unresolved questions. Considering the statics of the system, the following open questions and suggestions for future research are identified:

- In the derivation of the free energy, a Gaussian approximation was used, which is only valid far away from criticality. Using an analog of the Villain approximation [61]

instead of a Gaussian one will extend the temperature- and loading regime in which the free energy functional is valid. It would be particularly interesting to consider the load-dependence of the many-body contribution, as the numerical simulations suggest a non-linear dependence of the driving force on the mean-field stress, while the current expression predicts a linear dependence, see Chap. 3.

- The Sine-Gordon model is used to study dislocation-mediated melting. As a modification of the Sine-Gordon model due to loading was derived here, see Eq. (2.17), it might be possible to study the phase diagram of dislocations under applied mechanical load. If there would be a load-induced phase transition, this might be interpreted as the transition from elastic to plastic material behavior.
- In the dynamics part of the research presented here, two relevant temperatures have been identified in the dislocation system, namely the configurational temperature of the dislocations and the heat bath temperature. It could be worthwhile to investigate whether the phase behavior of dislocations is affected by using two temperatures instead of one.
- In this thesis, the attention was restricted to straight and parallel dislocations. It would be challenging to extend the current research to curved dislocations. To derive a free energy expression, a good starting point would be to combine the current approach with the work of [90]. However, one could also follow a more phenomenological approach by anticipating a free energy with a similar structure as obtained here, namely: a split in three contributions as in Eq. (7.1) and a local many-body free energy density that is scale-free and depends on the total dislocation density per slip system.
- The free energy at low but finite temperature is qualitatively different from the energy at zero temperature. Therefore, it might be interesting to introduce the concept of temperature and the corresponding randomness in other coarse-graining methods applied to dislocation systems, such as Γ -convergence [99, 29, 112].

Considering the dynamics part of the research presented here, the following recommendations for future work are made:

- Numerical simulations can be used to study the temperature- and density dependence of the macroscopic response function $H^{(0)}(\Delta t)$. Moreover, the response function for the energy flow, $K(\Delta t)$, can be determined.
- Current strain-gradient Crystal Plasticity models can be improved by using the lessons learned in this research. More specifically, the dislocation density should be modeled for each possible Burgers vector separately, rather than using only GND-based quantities. The free energy, which yields the driving force for dynamics, should have the same properties as obtained here, namely it should depend on both the total and the GND density of dislocations, and it should be scale-free.
- A further suggestion for improving Crystal Plasticity models is to use a powerlaw to relate the applied deformation to the dislocation flux. Viscoplastic powerlaw relations are already applied in current Crystal Plasticity models, but the exponent

is assumed to be much higher than the value 3.7 obtained in this work, as their main purpose is to mimic elasto-plastic behavior. As noted earlier, no quantitative predictions could be made from the idealized model treated here, and hence the value 3.7 could very well be larger for less idealized models. Nevertheless, the viscous nature of the obtained relation might also be relevant to incorporate in Crystal Plasticity models.

- The current microscopic dynamics that is used in this thesis is undoubtedly oversimplified. In more realistic two-dimensional DDD-simulations of straight and parallel dislocations, constitutive rules are used to describe pinning and depinning of dislocations by obstacles, and to account for multiplication and annihilation of dislocations. It would be worthwhile to incorporate these rules in the GENERIC upscaling procedure to make the system more realistic. An expected difficulty for this might be that some constitutive rules have some form of memory. For example, dislocation multiplication only occurs when the stress has been above a certain threshold for a certain time. This complicates the use of the GENERIC framework. Alternatively, one could incorporate these effects in a phenomenological manner in the macroscopic evolution equations for the dislocation density, for example by introducing a stress-dependent dislocation production term to mimic dislocation multiplication, see e.g. [20, 16].
- Moreover, the dynamics may be extended to curved dislocations as well. As a starting point, a three-dimensional DDD-simulation can be used as a microscopic description, see e.g. [79]. To define the macroscopic variables, one could use the variables used by Hochrainer [50, 51], and the corresponding kinematic relations.
- To account for two different temperatures, T_B and T_C , the energy of the system has to be split in two independent parts that are controlled by the different temperatures. Here, the Hamiltonian was split in the thermal energy of the lattice, which is controlled by the heat bath temperature T_B , and the strain energy, which is controlled by the configurational temperature T_C . However, another split can also be considered, where small deviations of the dislocation positions are also controlled by the heat bath temperature T_B . Conceptually, this was anticipated in the work of Bouchbinder on the thermodynamics of systems with two temperatures [72, 9, 10], but such a split was not defined in practice before, and is probably complicated.
- With the current set of macroscopic variables, there is no separation of timescales and hence the evolution is written in terms of a memory kernel. This is inconvenient in a numerical implementation. However, the memory in the system might only be apparent if there is some hidden microstructural evolution. Namely, when the microstructure slowly responds to changes in the driving force, this appears as memory of the system when too much microstructural information is integrated out. To solve this, an extra variable should be introduced that accurately describes the microstructure. Then, the slow response of the microstructure is modeled as well, and no memory is needed to describe the dynamics. Structural variables have been used before to explain apparent memory in complex fluid systems, see e.g. [88, 8]. In this work, the local organization of the dislocations is determined by the dislocation density and the configurational temperature. More

accurate modeling of the configurational temperature (as described in the previous bullet) may thus solve the problem. However, it might also be that extra tensorial- or field variables are needed to describe the microstructure accurately.

- The dislocation system studied here is quite simple, in the sense that it is a system of interacting point particles in two dimensions. Still, non-trivial collective effects were obtained for both the static and dynamic behavior of dislocations. It could therefore be worthwhile to apply the GENERIC upscaling procedure to other systems in order to get a thermodynamics view on emergent phenomena.

Appendix A

Details about calculations in Chap. 2

A.1 Energy minimum

In this section, it is shown that the distortion field that minimizes the elastic energy, Eq. (2.5), under the incompatibility constraint, Eq. (2.2), satisfies mechanical equilibrium. From an ensemble-perspective, this means that the mechanical equilibrium distortion field is also the most probable one.

To demonstrate this, the incompatibility constraint is incorporated using a Lagrange multiplier. Therefore, the following expression is minimized with respect to Δ and the Lagrange multiplier κ :

$$E' = \frac{1}{2} \int_{\Omega} d^3\mathbf{r} \Delta^s : \mathbb{C} : \Delta^s - \int_{\Omega} d^3\mathbf{r} (\nabla \wedge \Delta - \hat{\alpha}) : \kappa. \quad (\text{A.1})$$

Minimizing yields

$$\begin{aligned} 0 &= \mathbb{C}^{ls} : \Delta^s - \nabla \wedge \kappa, \\ 0 &= \nabla \wedge \Delta - \hat{\alpha}, \end{aligned} \quad (\text{A.2})$$

where \mathbb{C}^{ls} is \mathbb{C} symmetrized in the first two indices; $\mathbb{C}_{ij'j'j'}^{ls} = (\mathbb{C}_{ij'j'j'} + \mathbb{C}_{j'ij'j'})/2$. The divergence of the first equation is mechanical equilibrium, and the second equation is incompatibility. Therefore, the most probable field Δ is the standard mechanical equilibrium solution.

A.2 Integration over strain fields

In this section, Eq. (2.14) is derived by evaluating

$$\begin{aligned} I_{\Delta} \equiv \int \mathcal{D}[\Delta] \delta_{\partial\Omega} [\hat{\mathbf{n}} \wedge \Delta - (\hat{\mathbf{n}} \times \nabla) \mathbf{u}_b] \exp \left[-\frac{\beta}{2} \int_{\Omega} d^3\mathbf{r} \Delta^s : \mathbb{C} : \Delta^s \right. \\ \left. - i\beta \int_{\Omega} d^3\mathbf{r} \Psi : \nabla \wedge \Delta + \int_{\Omega} d^3\mathbf{r} \mathbf{J}_{\Delta} : \Delta^s \right]. \end{aligned} \quad (\text{A.3})$$

First, the shift $\Delta \rightarrow \tilde{\Delta} + \Delta_0$ is performed, where Δ_0 is defined in Eq. (2.12). Then partial integration is applied on the second term in the exponent. The boundary contribution vanishes because of the delta functional at the boundary. This yields

$$\begin{aligned} I_{\Delta} = \int \mathcal{D}[\tilde{\Delta}] \delta_{\partial\Omega} [\hat{\mathbf{n}} \wedge \tilde{\Delta}] \exp \left[-\frac{\beta}{2} \int_{\Omega} d^3\mathbf{r} (\tilde{\Delta}^s + \Delta_0^s) : \mathbb{C} : (\tilde{\Delta}^s + \Delta_0^s) \right. \\ \left. - i\beta \int_{\Omega} d^3\mathbf{r} \nabla \wedge \Psi : (\tilde{\Delta}^s + \Delta_0^s) + \int_{\Omega} d^3\mathbf{r} \mathbf{J}_{\Delta} : (\tilde{\Delta}^s + \Delta_0^s) \right], \end{aligned} \quad (\text{A.4})$$

where the superscript a indicates the anti-symmetric part of a second rank tensor.

As the integrand only depends on $\tilde{\Delta}$ and *not* on its spatial derivatives, the functional integration over $\tilde{\Delta}$ at the boundary and over $\tilde{\Delta}$ in the bulk can be performed independently. The first is independent of the boundary deformation \mathbf{u}_b and the auxiliary field Ψ . Therefore it can be considered as an irrelevant multiplicative constant.

The functional integration over $\tilde{\Delta}$ in the bulk can be split further in an integration over $\tilde{\Delta}^a$ and $\tilde{\Delta}^s$. From Eq. (2.8), it can be seen that the former is proportional to $\delta_\Omega [(\nabla \wedge \Psi)^a]$. For the latter, we proceed by completing the squares in the above expression for I_Δ :

$$\begin{aligned} I_\Delta &\propto \delta_\Omega [(\nabla \wedge \Psi)^a] \int_{\text{bulk}} \mathcal{D}[\tilde{\Delta}^s] \exp \left[-\frac{\beta}{2} \int_\Omega d^3\mathbf{r} \left(\tilde{\Delta} + \Delta_0 + \iota(\nabla \wedge \Psi) : \mathbb{S} - \beta^{-1} \mathbf{J}_\Delta : \mathbb{S} \right)^s : \right. \\ &\quad \left. : \mathbb{C} : \left(\tilde{\Delta} + \Delta_0 + \iota\mathbb{S} : (\nabla \wedge \Psi) - \beta^{-1} \mathbb{S} : \mathbf{J}_\Delta \right)^s \right] \times \quad (\text{A.5}) \\ &\quad \exp \left[-\frac{\beta}{2} \int_\Omega d^3\mathbf{r} \left(\nabla \wedge (\Psi - \Psi_0) + \iota\beta^{-1} \mathbf{J}_\Delta \right)^s : \mathbb{S} : \left(\nabla \wedge (\Psi - \Psi_0) + \iota\beta^{-1} \mathbf{J}_\Delta \right)^s \right] \times \\ &\quad \exp \left[-\frac{\beta}{2} \int_\Omega d^3\mathbf{r} \Delta_0^s : \mathbb{C} : \Delta_0^s + \int_\Omega d^3\mathbf{r} \mathbf{J}_\Delta^s : \Delta_0^s \right], \end{aligned}$$

where $\int_{\text{bulk}} \mathcal{D}[\tilde{\Delta}^s]$ denotes the functional integration over fields that only live in the bulk. Now, the following variable substitution can be made: $\tilde{\Delta}^s = \bar{\Delta}^s - \Delta_0^s - \iota\mathbb{S} : (\nabla \wedge \Psi)^s + \mathbb{S} : \mathbf{J}_\Delta^s$. Then, the integration over $\tilde{\Delta}^s$ in the bulk is independent of the boundary deformation \mathbf{u}_b and the auxiliary field Ψ , and hence it is a multiplicative constant. This finally yields

$$\begin{aligned} I_\Delta &\propto \delta_\Omega [(\nabla \wedge \Psi)^a] \exp \left[-\frac{\beta}{2} \int_\Omega d^3\mathbf{r} \Delta_0^s : \mathbb{C} : \Delta_0^s + \int_\Omega d^3\mathbf{r} \mathbf{J}_\Delta^s : \Delta_0^s \right] \times \quad (\text{A.6}) \\ &\quad \exp \left[-\frac{\beta}{2} \int_\Omega d^3\mathbf{r} \left(\nabla \wedge (\Psi - \Psi_0) + \iota\beta^{-1} \mathbf{J}_\Delta \right)^s : \mathbb{S} : \left(\nabla \wedge (\Psi - \Psi_0) + \iota\beta^{-1} \mathbf{J}_\Delta \right)^s \right]. \end{aligned}$$

This is Eq. (2.14).

A.3 Integration over dislocation positions

In this section, Eq. (2.16) is derived by evaluating

$$\begin{aligned} I_{\hat{\omega}} &\equiv \sum_{N=0}^{\infty} \left\{ \prod_{s \in \text{species}} \prod_{j_s \in \text{glide planes}} \prod \left(\frac{1}{N_{sj_s}!} \frac{1}{\lambda_{th,s}^{N_{sj_s}}} \int dx_1 \dots dx_{N_{sj_s}} \right) \right. \\ &\quad \left. \exp \left[\beta \int_\Omega d^2\mathbf{s} \mu_s(\mathbf{s}) \hat{\omega}_s(\mathbf{s}) + \iota\beta \int_\Omega d^3\mathbf{r} \boldsymbol{\alpha}(\mathbf{r}) : \Psi(\mathbf{r}) \right] \right\}. \quad (\text{A.7}) \end{aligned}$$

The spatial integrations in the exponent can be performed easily, as the densities $\hat{\omega}_s(\mathbf{s})$ are sums of delta peaks: $\hat{\omega}_s(\mathbf{r}) = \sum_{j_s \in \text{glide planes}} \sum_{k=1}^{N_{sj_s}} \delta(x - x_k) \delta(y - y_{j_s})$, and that

the dislocation density tensor is related to these densities, see Eq. (2.1). This yields

$$\begin{aligned}
 I_{\hat{\omega}} &\equiv \sum_{N=0}^{\infty} \left\{ \prod_{s \in \text{species}} \prod_{j_s \in \text{glide planes}} \left(\frac{1}{N_{sj_s}!} \frac{1}{\lambda_{th,s}^{N_{sj_s}}} \int dx_1 \dots dx_{N_{sj_s}} \right. \right. \\
 &\quad \left. \left. \exp \left[\beta \sum_{k=1}^{N_{sj_s}} \mu_s(x_k, y_{j_s}) + \iota \beta \int dz (\hat{\xi} \mathbf{b}_s) : \Psi(x_k, y_{j_s}, z) \right] \right) \right\} \\
 &\equiv \sum_{N=0}^{\infty} \left\{ \prod_{s \in \text{species}} \prod_{j_s \in \text{glide planes}} \frac{1}{N_{sj_s}!} \right. \\
 &\quad \left. \left(\frac{1}{\lambda_{th,s}} \int dx \exp \left[\beta \mu_s(x, y_{j_s}) + \iota \beta \int dz (\hat{\xi} \mathbf{b}_s) : \Psi(x, y_{j_s}, z) \right] \right)^{N_{sj_s}} \right\}
 \end{aligned} \tag{A.8}$$

Further simplification is possible using the series expansion of the exponent, $\exp(x) = \sum_{n=0}^{\infty} \frac{1}{n!} x^n$:

$$\begin{aligned}
 I_{\hat{\omega}} &= \prod_{s \in \text{species}} \prod_{j \in \text{glide planes}} \exp \left(\frac{1}{\lambda_{th,s}} \int dx \exp \left[\beta \left(\mu_s(x, y_j) + \iota (\hat{\xi} \mathbf{b}_s) : \int dz \Psi(x, y_j, z) \right) \right] \right) \\
 &= \exp \left(\sum_{s \in \text{species}} \frac{1}{\lambda_{th,s}} \sum_{j \in \text{glide planes}} \int dx \exp \left[\beta \left(\mu_s(x, y_j) + \iota (\hat{\xi} \mathbf{b}_s) : \int dz \Psi(x, y_j, z) \right) \right] \right).
 \end{aligned}$$

Finally, using the definition of the glide plane distribution, Eq. (2.15), yields

$$I_{\hat{\omega}} = \exp \left(\sum_{s \in \text{species}} \frac{1}{\lambda_{th,s}} \int d^2 \mathbf{s} \rho_{gl,s}(\mathbf{s}) \exp \left[\beta \left(\mu_s(\mathbf{s}) + \iota (\hat{\xi} \mathbf{b}_s) : \int dz \Psi(\mathbf{s}, z) \right) \right] \right). \tag{A.9}$$

A.4 Imaginary expectation value of Ψ

In this section it is shown that $\langle \Psi(\mathbf{r}) \rangle$ is purely imaginary. Starting from Eq. (2.11), it is found that

$$\begin{aligned}
 \langle \Psi \rangle &= \frac{1}{\mathcal{Z}} \sum_{N=0}^{\infty} \left\{ \prod_{s \in \text{species}} \prod_{j_s \in \text{glide planes}} \left(\frac{1}{N_s j_s!} \frac{1}{\lambda_{th,s}^{N_s j_s}} \int dx_1 \dots dx_{N_s j_s} \right) \right. \\
 &\quad \int \mathcal{D}[\Delta] \int \mathcal{D}[\Psi] \Psi \delta_{\partial\Omega} [\hat{\mathbf{n}} \wedge \Delta - (\hat{\mathbf{n}} \times \nabla) \mathbf{u}_b] \exp \left[-\iota \beta \int_{\Omega} d^3 \mathbf{r} \Psi : (\nabla \wedge \Delta - \hat{\alpha}) \right] \\
 &\quad \left. \exp \left[-\frac{\beta}{2} \int_{\Omega} d^3 \mathbf{r} \Delta^s : \mathbb{C} : \Delta^s + \beta \sum_{s \in \text{species}} \int_{\Omega} d^2 \mathbf{s} \mu_s(\mathbf{s}) \hat{\omega}_s(\mathbf{s}) \right] \right\}. \\
 &\propto \frac{\iota}{\beta} \frac{\delta}{\delta(\nabla \wedge \Delta - \hat{\alpha})} \int \mathcal{D}[\Psi] \exp \left[-\iota \beta \int d^3 \mathbf{r} \Psi : (\nabla \wedge \Delta - \hat{\alpha}) \right] \\
 &\propto \frac{\iota}{\beta} \delta'_{\Omega} [\nabla \wedge \Delta - \hat{\alpha}],
 \end{aligned} \tag{A.10}$$

where δ' is the functional derivative of the delta functional. Note that all quantities, except ι are real, and hence the expectation value of Ψ is purely imaginary.

A.5 Equivalence to the grand-canonical partition function

In this section, Eq. (2.17) is rewritten to the grand canonical partition function corresponding to particles in 2D with the dislocation interaction potential [49]. To this end, Eq. (2.17) is expanded in powers of $\lambda_{th,s}^{-1}$. This yields

$$\begin{aligned}
 \mathcal{Z}[\beta, \mu_s(\mathbf{s})] &= \int \mathcal{D}[\Psi] \delta[(\nabla \wedge \Psi)^a] \exp \left[\frac{-\beta}{2} \int d^3 \mathbf{r} (\nabla \wedge \Psi)^s : \mathbb{S} : (\nabla \wedge \Psi)^s \right] \\
 &\times \prod_{s \in \text{species}} \sum_{N_s=0}^{\infty} \frac{1}{N_s!} \prod_{j=1}^{N_s} \left(\int d^2 \mathbf{s}_j \frac{\rho_{gl,s}(\mathbf{s}_j)}{\lambda_{th,s}} e^{\beta(\mu_s(\mathbf{s}_j) + \iota(\hat{\xi} \mathbf{b}_s) : \int dz \Psi_0(\mathbf{s}_j, z))} \right) \\
 &\exp \left[\iota \beta \sum_{s \in \text{species}} \sum_{j=1}^{N_s} (\hat{\xi} \mathbf{b}_s) : \int dz \Psi(\mathbf{s}_j, z) \right]
 \end{aligned} \tag{A.11}$$

As will be shown in A.6, the quadratic term in Ψ can be written as

$$\int d^3 \mathbf{r} d^3 \mathbf{r}' \Psi(\mathbf{r}) : \mathbb{G}_0^{-1}(\mathbf{r} - \mathbf{r}') : \Psi(\mathbf{r}'). \tag{A.12}$$

Completing the squares yields

$$\begin{aligned}
 \mathcal{Z}[\beta, \mu_s(\mathbf{s})] &= \prod_{s \in \text{species}} \sum_{N_s=0}^{\infty} \frac{1}{N_s!} \prod_{j=1}^{N_s} \left(\int d^2 \mathbf{s}_j \frac{\rho_{gl,s}(\mathbf{s}_j)}{\lambda_{th,s}} e^{\beta(\mu_s(\mathbf{s}_j) + \iota(\hat{\boldsymbol{\xi}} \mathbf{b}_s) : \int dz \Psi_0(\mathbf{s}_j, z))} \right) \\
 &\int \mathcal{D}[\Psi] \exp \left[\frac{-\beta}{2} \int d^3 \mathbf{r} d^3 \mathbf{r}' \left(\Psi(\mathbf{r}) - \iota \sum_{s \in \text{species}} \sum_{j=1}^{N_s} (\hat{\boldsymbol{\xi}} \mathbf{b}_s) : \int dz G_0((\mathbf{s}_j, z) - \mathbf{r}) \right) : \right. \\
 &\quad \left. : G_0^{-1}(\mathbf{r} - \mathbf{r}') : \left(\Psi(\mathbf{r}') - \iota \sum_{s' \in \text{species}} \sum_{j'=1}^{N_{s'}} (\hat{\boldsymbol{\xi}} \mathbf{b}_{s'}) : \int dz' G_0(\mathbf{r}' - (\mathbf{s}'_{j'}, z')) \right) \right] \\
 &\exp \left[\frac{-\beta}{2} \sum_{s, s' \in \text{species}} \sum_{j=1}^{N_s} \sum_{j'=1}^{N_{s'}} (\hat{\boldsymbol{\xi}} \mathbf{b}_s) : \left(\int dz dz' G_0((\mathbf{s}_j, z) - (\mathbf{s}'_{j'}, z')) \right) : (\hat{\boldsymbol{\xi}} \mathbf{b}_{s'}) \right]. \tag{A.13}
 \end{aligned}$$

The middle two lines are independent of the dislocation positions and constitute therefore an irrelevant multiplicative prefactor. All together, this proves Eq. (2.27).

A.6 The dislocation interaction potential

The goal of this paragraph is to find an expression for the 'bare' Green's function G_0 , as defined in Eq. (2.28), but in infinite space. This Green's function can be used in the term quadratic in Ψ in the partition function, which is the second line of Eq. (2.17).

The exponent in Eq. (2.17) is invariant under certain gauge transformations, which should thus be fixed. This is also done in the Green's function.

First, the action is invariant under the transformation $\Psi \rightarrow \Psi + \nabla \gamma$. This gauge is fixed by restricting the integration to fields that satisfy $\nabla \cdot \Psi = 0$. Second, the action is invariant under a constant shift in Ψ . Therefore, a small 'mass term' m is needed to make the Green's function invertible. In the end, m can be sent to 0.

For convenience, the tensors \mathbf{Q} and \mathbf{R} are defined in terms of the wave vector \mathbf{q}

$$\mathbf{Q}_{ij}(\mathbf{q}) \equiv \delta_{ij} - q_i q_j / q^2 \quad \mathbf{R}_{ik}(\mathbf{q}) \equiv \epsilon_{ikl} q_l / q. \tag{A.14}$$

Note that these have the following group properties: $\mathbf{Q} \cdot \mathbf{Q} = \mathbf{Q}$, $\mathbf{Q} \cdot \mathbf{R} = \mathbf{R} \cdot \mathbf{Q} = \mathbf{R}$ and $\mathbf{R} \cdot \mathbf{R} = -\mathbf{Q}$. The quadratic part of the partition function thus reads

$$\begin{aligned}
 \int_{\text{constr.}} \mathcal{D}[\Psi] \exp[-\beta F_0[\Psi]] &= \int \mathcal{D}[\Psi] \delta[(\nabla \wedge \Psi)^a] \delta[\nabla \cdot \Psi] \\
 &\exp \left[-\frac{\beta}{2} \int d^3 \mathbf{r} (\nabla \wedge \Psi)^s : \mathbb{S} : (\nabla \wedge \Psi)^s + \frac{m^2}{2\mu} \Psi^2 \right] \tag{A.15}
 \end{aligned}$$

$$\begin{aligned}
&= \lim_{\zeta \rightarrow 0} \lim_{\eta \rightarrow 0} \int \mathcal{D}[\Psi] \exp \left[-\frac{\beta}{2 \cdot 2\mu} \zeta^{-1} \int d^3 \mathbf{r} (\nabla \wedge \Psi) : \mathbb{I}^{\text{la}} : (\nabla \wedge \Psi) \right] \\
&\quad \exp \left[-\frac{\beta}{4 \cdot 2\mu} \eta^{-1} \int d^3 \mathbf{r} (\nabla \cdot \Psi) \cdot (\nabla \cdot \Psi) \right] \\
&\quad \exp \left[-\frac{\beta}{2} \int d^3 \mathbf{r} (\nabla \wedge \Psi) : \mathbb{S}^{\text{ls}} : (\nabla \wedge \Psi) + \frac{m^2}{2 \cdot 2\mu} \Psi^2 \right] \\
&= \lim_{\zeta \rightarrow 0} \lim_{\eta \rightarrow 0} \int \mathcal{D}[\Psi] \exp \left[-\frac{\beta}{2} \int \frac{d^3 \mathbf{q}}{(2\pi)^3} \Psi_{kj}(\mathbf{q}) : \left[q^2 R_{ik} \mathbb{S}_{ij'j'}^{\text{ls}} R_{i'k'} \right. \right. \\
&\quad \left. \left. + \zeta^{-1} \frac{q^2}{2\mu} R_{ik} \mathbb{I}_{ij'j'}^{\text{la}} R_{i'k'} + \eta^{-1} \frac{q^2}{2 \cdot 2\mu} \frac{q_k q_{k'}}{q^2} \delta_{jj'} + \frac{m^2}{2\mu} \delta_{kk'} \delta_{jj'} \right] : \Psi_{k'j'}(-\mathbf{q}) \right] \\
&\equiv \lim_{\zeta \rightarrow 0} \lim_{\eta \rightarrow 0} \int \mathcal{D}[\Psi] \exp \left[-\frac{\beta}{2} \int \frac{d^3 \mathbf{q}}{(2\pi)^3} \Psi_{kj}(\mathbf{q}) : \mathbb{G}_{0,kjk'j'}^{-1}(\mathbf{q}) : \Psi_{k'j'}(-\mathbf{q}) \right],
\end{aligned}$$

where the superscript “ls” and “la” stand for symmetry and antisymmetry with respect to the first two indices of a fourth order tensor: $\mathbf{A}_{ij'j'}^{\text{ls}} = (\mathbf{A}_{ij'j'} \pm \mathbf{A}_{j'ij'})/2$.

The nascent delta functional representation $\delta(x) \propto \lim_{\epsilon \rightarrow 0} e^{-x^2/2\epsilon}/\sqrt{\epsilon}$ was used to impose the symmetry and divergence free conditions in the second equality. Using the isotropic compliance tensor $\mathbb{S}_{ij'j'} = \frac{1}{2\mu} (\delta_{ii'} \delta_{jj'} - \frac{\nu}{1+\nu} \delta_{ij} \delta_{i'j'})$, the inverse of the Green's function reads

$$\begin{aligned}
\mathbb{G}_{0,kjk'j'}^{-1}(\mathbf{q}) \equiv & \frac{1}{2\mu} \left[\frac{q^2}{2} ((1 + \zeta^{-1}) Q_{kk'} \delta_{jj'} + (1 - \zeta^{-1}) R_{jk'} R_{j'k}) \right. \\
& \left. - \frac{2\nu}{1 + \nu} R_{jk} R_{j'k'} + \eta^{-1} \frac{q_k q_{k'}}{q^2} \delta_{jj'} \right] + m^2 \delta_{kk'} \delta_{jj'}.
\end{aligned} \tag{A.16}$$

It is tedious but straightforward to check that

$$\begin{aligned}
\mathbb{G}_{0,k'j'k''j''}(\mathbf{q}) = & 2\mu \left(\frac{2\zeta}{q^2 + 2m^2\zeta + q^2\zeta} Q_{k'k''} \delta_{j'j''} + \frac{2\eta}{q^2 + 2m^2\eta} \frac{q_{k'} q_{k''}}{q^2} \delta_{j'j''} + \right. \\
& + \frac{q^4 (\zeta - 1)^2}{2(q^2 + m^2)(q^2 + m^2\zeta)(q^2 + 2m^2\zeta + q^2\zeta)} Q_{j'j''} Q_{k'k''} + \\
& \left. + \frac{q^2 \nu}{(m^2 + q^2)(m^2(1 + \nu) + q^2(1 - \nu))} R_{j'k'} R_{j''k''} + \frac{q^2(1 - \zeta)}{2(m^2 + q^2)(m^2\zeta + q^2)} R_{j'k'} R_{j''k''} \right).
\end{aligned} \tag{A.17}$$

The limits $\zeta \rightarrow 0$ and $\eta \rightarrow 0$ can be taken straightforwardly. However, the limit $m \rightarrow 0$ is more subtle, as this causes divergencies for $q = 0$. Therefore, this limit is postponed. The resulting expression for \mathbb{G}_0 is then

$$\begin{aligned}
\mathbb{G}_{0,k'j'k''j''}(\mathbf{q}) = & \frac{2\mu}{2(q^2 + m^2)} \\
& \left(Q_{j'j''} Q_{k'k''} + R_{j''k'} R_{j'k''} + \frac{2q^2 \nu}{q^2(1 - \nu) + m^2(1 + \nu)} R_{j'k'} R_{j''k''} \right).
\end{aligned} \tag{A.18}$$

From the ‘bare’ Green’s function, the interaction potential between dislocations can be derived. The form of the interaction potential is suggested by Eq. (2.27). Combined with

Eq. (A.18) for $m = 0$ this yields the well-known interaction potential between parallel dislocations [49, equation 5-16]:

$$\begin{aligned}
 V_{s,s'}(\mathbf{s}, \mathbf{s}') &= (\hat{\boldsymbol{\xi}}\mathbf{b}_s) : \left(\int dzdz' \mathbf{G}_0((\mathbf{s}, z) - (\mathbf{s}', z')) \right) : (\hat{\boldsymbol{\xi}}\mathbf{b}_{s'}) \quad (\text{A.19}) \\
 &= \int dzdz' \int \frac{d^3\mathbf{q}}{(2\pi)^3} (\hat{\boldsymbol{\xi}}\mathbf{b}_s) : \mathbf{G}_0(\mathbf{q}) : (\hat{\boldsymbol{\xi}}\mathbf{b}_{s'}) e^{i\mathbf{q}\cdot((\mathbf{s}, z) - (\mathbf{s}', z'))} \\
 &= \int \frac{d^3\mathbf{q}}{(2\pi)^2} \delta(q_z) \frac{2\mu L}{2q^2} \left((\hat{\boldsymbol{\xi}}\hat{\boldsymbol{\xi}}) : \mathbf{Q}(\mathbf{b}_s\mathbf{b}_{s'}) : \mathbf{Q} + \frac{1+\nu}{1-\nu} (\hat{\boldsymbol{\xi}}\mathbf{b}_s : \mathbf{R}) (\hat{\boldsymbol{\xi}}\mathbf{b}_{s'} : \mathbf{R}) \right) e^{i\mathbf{q}_{2D}\cdot(\mathbf{s}-\mathbf{s}')} \\
 &= \int \frac{d^2\mathbf{q}_{2D}}{(2\pi)^2} \frac{\mu L}{q^2} \left((\hat{\boldsymbol{\xi}} \cdot \mathbf{b}_s) (\hat{\boldsymbol{\xi}} \cdot \mathbf{b}_{s'}) + \frac{2 \left((\hat{\boldsymbol{\xi}} \times \mathbf{b}_{s'}) \cdot \mathbf{q} \right) \left((\hat{\boldsymbol{\xi}} \times \mathbf{b}_s) \cdot \mathbf{q} \right)}{(1-\nu)q^2} \right) e^{i\mathbf{q}_{2D}\cdot(\mathbf{s}-\mathbf{s}')} \\
 &= -\frac{\mu L}{2\pi} \left((\hat{\boldsymbol{\xi}} \cdot \mathbf{b}_s) (\hat{\boldsymbol{\xi}} \cdot \mathbf{b}_{s'}) \ln \left(\frac{|\mathbf{s} - \mathbf{s}'|}{s_0} \right) + \frac{1}{1-\nu} \left((\hat{\boldsymbol{\xi}} \times \mathbf{b}_{s'}) \cdot (\hat{\boldsymbol{\xi}} \times \mathbf{b}_s) \ln \left(\frac{|\mathbf{s} - \mathbf{s}'|}{s_0} \right) \right. \right. \\
 &\quad \left. \left. + \frac{\left((\hat{\boldsymbol{\xi}} \times \mathbf{b}_{s'}) \cdot (\mathbf{s} - \mathbf{s}') \right) \left((\hat{\boldsymbol{\xi}} \times \mathbf{b}_s) \cdot (\mathbf{s} - \mathbf{s}') \right)}{|\mathbf{s} - \mathbf{s}'|^2} \right) \right).
 \end{aligned}$$

This interaction potential diverges for $|\mathbf{s} - \mathbf{s}'| \rightarrow 0$, which is at short distances close to the dislocation core. However, linear elasticity as used here is not valid at such small distances. Therefore, to avoid these divergencies, the core energy should be treated separately as in [13]. When the interaction potential close to the origin is used, a regularization procedure is needed, see eg. [80].

The interaction potential diverges for $|\mathbf{s} - \mathbf{s}'| \rightarrow \infty$. This is due to the divergence as $q \rightarrow 0$ in Fourier space, which arises from setting $m = 0$ at an intermediate step.

A.7 Motivation of the Gaussian approximation

In this section, the Gaussian approximation in Eq. (2.37) is motivated by studying the analogous probability density for scalars. The scalar analog of Eqs. (2.36) and (2.37) is respectively

$$\begin{aligned}
 p(x; \Xi, f_s, \alpha_s) &= \exp \left[\frac{-\Xi}{2} x^2 / g_0 + \sum_{s \in \text{species}} f_s / \sqrt{\Xi} \exp [i\alpha_s x] \right] \quad (\text{A.20}) \\
 p_g(x; g, b) &= \exp \left[\frac{-\Xi}{2} (x + ib)^2 / g + \gamma \right],
 \end{aligned}$$

where the scaling of Sec. 2.3.6 was used, and where it was already realized that the thermal wavelength scales with $\beta^{1/2} \propto \Xi^{1/2}$.

First, the special, 'symmetric' case $f_{\pm} = 1$ and $\alpha_{\pm} = \pm 1$ is considered. In this case $p(x; \Xi, f_s, \alpha_s)$ is real-valued, and therefore $b = 0$ in $p_g(g, b)$ for all Ξ .

In Fig. A.3(a), $p(x; \Xi)$ is plotted for different values of Ξ . For low and high values of Ξ ,

the curves are bell-shaped. However, for an intermediate value $\Xi = 14$, the bell-shape is not found. As can be seen in Fig. A.3(b), the bell-shape is a Gaussian, as $\sqrt{-\ln(p(x; \Xi))}$ is a straight line.

In Fig. A.2(a), the least mean square residual of the Gaussian fit is plotted against Ξ . This curve has a peak around $\Xi \approx 14$, which indeed indicates that the fit is not accurate around this value, but is fairly good away from it.

In Fig. A.2(b), the fitting parameter g is plotted against Ξ . Note that g changes suddenly around $\Xi \approx 14$. This is a sign of a phase transition.

Second, the special case with only one dislocation species is considered: $f_s = 1$ and $\alpha_s = 1$. In this case $p(x; \Xi, f_s, \alpha_s)$ is complex-valued.

In Fig. A.3, the absolute value and the argument of $p(x; \Xi)$ are plotted for different values of Ξ . Again, for low and for high values of Ξ , the absolute value is a bell-shaped curve, but this is not true for intermediate values. The argument is linear in x for high values of Ξ , and vanishes for low values of Ξ . This agrees with the form of $p_g(g, b)$. However, for intermediate values of Ξ , the argument is not at all linear in x , and therefore, the approximation $p_g(g, b)$ is inaccurate in this regime.

From these two examples, it is expected that, also for the full partition function, the Gaussian approximation is accurate away from criticality, but fails close to the transition. It should be mentioned that, as the Gaussian approximation is invalid around the transition, no quantitative conclusions about the transition point can be drawn from the analysis presented here.

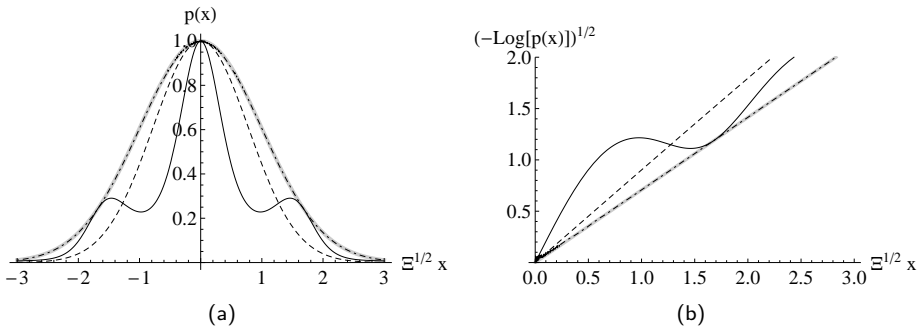


Figure A.1: The black lines are plots of $p(x)$. The parameters used are $g_0 = 1$, $f_s = 1$ and $\alpha_s = \pm 1$ for all curves, and $\Xi = 0.1, 14, 10^6$ for the dashed, solid and dot-dashed line respectively. The thick grey line is $p_g(x)$ for $g = 1$. As one can see, a Gaussian approximation is accurate for $\Xi = 0.1$ and $\Xi = 10^6$, but not for $\Xi = 14$.

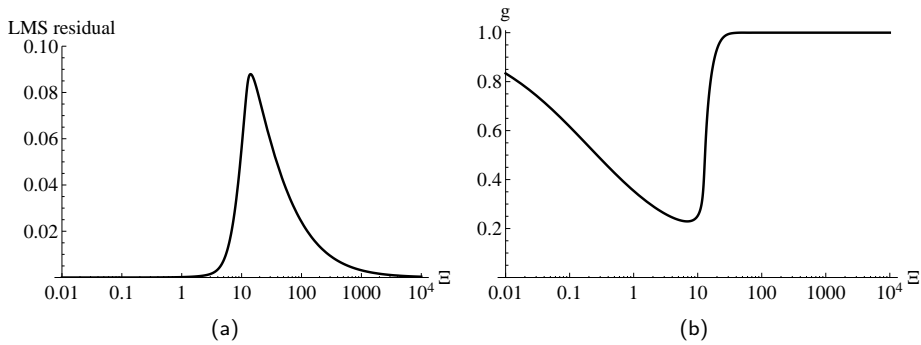


Figure A.2: In Fig. A.2(a), the least mean square (LMS) residual of the Gaussian fit $p_g(g)$ is plotted against Ξ for $g_0 = 1$, $f_s = 1$ and $\alpha_s = \pm 1$. The residual is maximal around $\Xi \approx 14$, and negligible far away from $\Xi = 14$. This confirms the hypothesis that a Gaussian fit is good for low and high values of Ξ , and bad for intermediate values. In Fig. A.2(b), the fitted value of g is plotted against Ξ . The step around $\Xi = 14$ indicates a phase transition around this point.

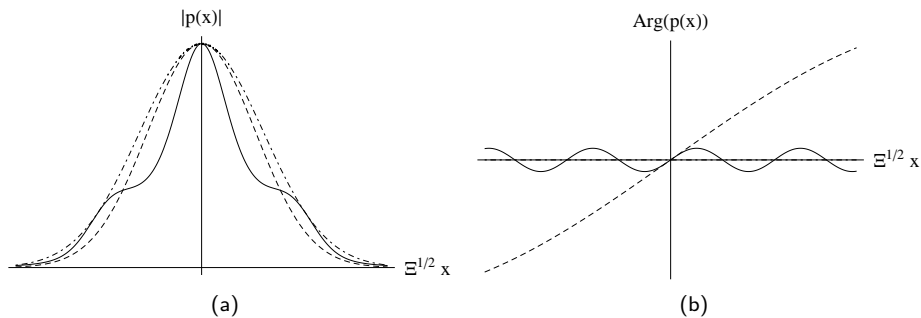


Figure A.3: These are plots of the absolute value and argument of $p(x)$. The parameters used are $g_0 = 1$, $f = 1$ and $\alpha_s = 1$ for all curves, and $\Xi = 0.1, 14, 10^6$ for the dashed, solid and dot-dashed line respectively. As one can see, the Gaussian approximation $p_g(g, b)$ is accurate for $\Xi = 0.1$ and $\Xi = 10^6$, but not for $\Xi = 14$.

A.8 The effective Green's function

In this section, Eqs. (2.38) and (2.39) are combined to find the governing equation for the Green's function, Eq. (2.40). Equating the normalizations of \mathcal{R} and \mathcal{R}_G yields

$$\begin{aligned}
0 &= \int \mathcal{D}[\Psi] \mathcal{R}_G[\Psi] - \mathcal{R}[\Psi] \tag{A.21} \\
&\approx -Z_G \left\langle -\frac{\beta}{2} \int d^3\mathbf{r} d^3\mathbf{r}' \Psi(\mathbf{r}) : G_0^{-1}(\mathbf{r}, \mathbf{r}') : \Psi(\mathbf{r}') + \right. \\
&\quad + \sum_{s \in \text{species}} \int d^2\mathbf{s} f_s(\mathbf{s}) \exp \left[i\beta(\hat{\xi}\mathbf{b}) : \int dz \Psi(\mathbf{s}, z) \right] + \\
&\quad \left. + \frac{\beta}{2} \int d^3\mathbf{r} d^3\mathbf{r}' (\Psi(\mathbf{r}) + i\mathbf{B}(\mathbf{r})) : G^{-1}(\mathbf{r} - \mathbf{r}') : (\Psi(\mathbf{r}') + i\mathbf{B}(\mathbf{r}')) - \gamma \right\rangle_G \\
&= -Z_G \left(\frac{\beta}{2} \int d^3\mathbf{r} d^3\mathbf{r}' \mathbf{B}(\mathbf{r}) : G_0^{-1}(\mathbf{r}, \mathbf{r}') : \mathbf{B}(\mathbf{r}') - \frac{1}{2} \text{Tr} [G : (G_0^{-1} - G^{-1})] - \gamma \right. \\
&\quad \left. + \sum_{s \in \text{species}} \int d^2\mathbf{s} f_s(\mathbf{s}) \exp \left[\beta \int dz \mathbf{B}(\mathbf{s}, z) : \hat{\xi}\mathbf{b} - \frac{\beta}{2} \int dz dz' \hat{\xi}\mathbf{b}_s : G(\mathbf{s}, z; \mathbf{s}, z') : \hat{\xi}\mathbf{b}_s \right] \right),
\end{aligned}$$

where the Gaussian integrations are performed in the last step and where the trace is a summation over the discrete indices and an integration over coordinates. In a similar way, equating the first moments of Ψ yields

$$\begin{aligned}
0 &= \int \mathcal{D}[\Psi] \Psi(\mathbf{r}) (\mathcal{R}_G[\Psi] - \mathcal{R}[\Psi]) \tag{A.22} \\
&\approx -Z_G \left\langle \Psi(\mathbf{r}) \left(-\frac{\beta}{2} \int d^3\mathbf{r} d^3\mathbf{r}' \Psi(\mathbf{r}) : G_0^{-1}(\mathbf{r}, \mathbf{r}') : \Psi(\mathbf{r}') \right. \right. \\
&\quad + \sum_{s \in \text{species}} \int d^2\mathbf{s} f_s(\mathbf{s}) \exp \left[i\beta(\hat{\xi}\mathbf{b}) : \int dz \Psi(\mathbf{s}, z) \right] \\
&\quad \left. \left. + \frac{\beta}{2} \int d^3\mathbf{r} d^3\mathbf{r}' (\Psi(\mathbf{r}) + i\mathbf{B}(\mathbf{r})) : G^{-1}(\mathbf{r} - \mathbf{r}') : (\Psi(\mathbf{r}') + i\mathbf{B}(\mathbf{r}')) - \gamma \right) \right\rangle_G \\
&= -Z_G \left(-i\mathbf{B}(\mathbf{r}) \left(\frac{\beta}{2} \int d^3\mathbf{r}' d^3\mathbf{r}'' \mathbf{B}(\mathbf{r}') : G_0^{-1}(\mathbf{r}', \mathbf{r}'') : \mathbf{B}(\mathbf{r}'') - \frac{1}{2} \text{Tr} [G : (G_0^{-1} - G^{-1})] - \gamma \right. \right. \\
&\quad \left. \left. + \sum_{s \in \text{species}} \int d^2\mathbf{s} f_s(\mathbf{s}) \exp \left[\beta \int dz \mathbf{B}(\mathbf{s}, z) : \hat{\xi}\mathbf{b} - \frac{\beta}{2} \int dz dz' \hat{\xi}\mathbf{b}_s : G(\mathbf{s}, z; \mathbf{s}, z') : \hat{\xi}\mathbf{b}_s \right] \right) \right. \\
&\quad \left. + i \int d^3\mathbf{r}' G(\mathbf{r}, \mathbf{r}') : \left(\int d^3\mathbf{r}'' G_0^{-1}(\mathbf{r}', \mathbf{r}'') : \mathbf{B}(\mathbf{r}'') + \sum_{s \in \text{species}} f_s(\mathbf{r}'_{2D}) \hat{\xi}\mathbf{b}_s \cdot \right. \right. \\
&\quad \left. \left. \exp \left[\beta \int dz \mathbf{B}(\mathbf{r}'_{2D}, z) : \hat{\xi}\mathbf{b}_s - \frac{\beta}{2} \int dz dz' \hat{\xi}\mathbf{b}_s : G(\mathbf{r}'_{2D}, z; \mathbf{r}'_{2D}, z') : \hat{\xi}\mathbf{b}_s \right] \right) \right)
\end{aligned}$$

and equating the second moments yields

$$\begin{aligned}
0 = & -Z_G \left((\beta^{-1} \mathbf{G}(\mathbf{r}, \mathbf{r}') - \mathbf{B}(\mathbf{r}) \mathbf{B}(\mathbf{r}')) \right. & \text{(A.23)} \\
& \left. \left(\frac{\beta}{2} \int d^3 \mathbf{r}'' d^3 \mathbf{r}''' \mathbf{B}(\mathbf{r}'') : \mathbf{G}_0^{-1}(\mathbf{r}'', \mathbf{r}''') : \mathbf{B}(\mathbf{r}''') - \frac{1}{2} \text{Tr} [\mathbf{G} : (\mathbf{G}_0^{-1} - \mathbf{G}^{-1})] - \gamma \right. \right. \\
& \left. \left. + \sum_{s \in \text{Species}} \int d^2 \mathbf{s} f_s(\mathbf{s}) \exp \left[\beta \int dz \mathbf{B}(\mathbf{s}, z) : \hat{\xi} \mathbf{b} - \frac{\beta}{2} \int dz dz' \hat{\xi} \mathbf{b}_s : \mathbf{G}(\mathbf{s}, z; \mathbf{s}, z') : \hat{\xi} \mathbf{b}_s \right] \right) \right) \\
& - \mathbf{B}(\mathbf{r}') \int d^3 \mathbf{r}'' \left(\int d^3 \mathbf{r}''' \mathbf{B}(\mathbf{r}''') : \mathbf{G}_0^{-1}(\mathbf{r}''', \mathbf{r}'') + \sum_{s \in \text{Species}} f_s(\mathbf{r}''_{2D}) \hat{\xi} \mathbf{b}_s \cdot \right. \\
& \left. \exp \left[\beta \int dz \mathbf{B}(\mathbf{r}''_{2D}, z) : \hat{\xi} \mathbf{b}_s - \frac{\beta}{2} \int dz dz' \hat{\xi} \mathbf{b}_s : \mathbf{G}(\mathbf{r}''_{2D}, z; \mathbf{r}''_{2D}, z') : \hat{\xi} \mathbf{b}_s \right] \right) : \mathbf{G}(\mathbf{r}'', \mathbf{r}') \\
& - \mathbf{B}(\mathbf{r}) \int d^3 \mathbf{r}'' \left(\int d^3 \mathbf{r}''' \mathbf{B}(\mathbf{r}''') : \mathbf{G}_0^{-1}(\mathbf{r}''', \mathbf{r}'') + \sum_{s \in \text{Species}} f_s(\mathbf{r}''_{2D}) \hat{\xi} \mathbf{b}_s \cdot \right. \\
& \left. \exp \left[\beta \int dz \mathbf{B}(\mathbf{r}''_{2D}, z) : \hat{\xi} \mathbf{b}_s - \frac{\beta}{2} \int dz dz' \hat{\xi} \mathbf{b}_s : \mathbf{G}(\mathbf{r}''_{2D}, z; \mathbf{r}''_{2D}, z') : \hat{\xi} \mathbf{b}_s \right] \right) : \mathbf{G}(\mathbf{r}'', \mathbf{r}') \\
& + \beta^{-1} \int d^3 \mathbf{r}'' d^3 \mathbf{r}''' \mathbf{G}(\mathbf{r}, \mathbf{r}'') : (\mathbf{G}^{-1}(\mathbf{r}'', \mathbf{r}''') - \mathbf{G}_0^{-1}(\mathbf{r}'', \mathbf{r}''')) \\
& - \beta \sum_{s \in \text{Species}} f_s(\mathbf{r}''_{2D}) \delta(\mathbf{r}''_{2D} - \mathbf{r}'''_{2D}) \hat{\xi} \mathbf{b}_s \hat{\xi} \mathbf{b}_s \cdot \\
& \left. \exp \left[\beta \int dz \mathbf{B}(\mathbf{r}''_{2D}, z) : \hat{\xi} \mathbf{b}_s - \frac{\beta}{2} \int dz dz' \hat{\xi} \mathbf{b}_s : \mathbf{G}(\mathbf{r}''_{2D}, z; \mathbf{r}''_{2D}, z') : \hat{\xi} \mathbf{b}_s \right] \right) : \mathbf{G}(\mathbf{r}''', \mathbf{r}').
\end{aligned}$$

Recombining the above equations results in Eqs. (2.40).

A.8.1 Validity of the assumptions

In this section it is first checked whether Eq. (2.39) is a good approximation. For simplicity, only two species of dislocations with opposite Burgers vector $\pm \mathbf{b}$ and spatially constant fugacity f are considered. To this end, Eqs. (A.22) and (A.23) are evaluated again, but with a second order series expansion in the exponent, instead of a first order expansion. It is then tested whether the solution of the second order equations is approximately equal to the solution of the first order equations, Eqs. (A.22) and (A.23).

The second order series expansion in the exponent reads

$$\begin{aligned}
\mathcal{R}_G[\Psi] - \mathcal{R}[\Psi] \approx & -\mathcal{R}_G[\Psi] \left(\left(\frac{\beta}{2} \int d^3 \mathbf{r} d^3 \mathbf{r}' \Psi(\mathbf{r}) : (\mathbf{G}^{-1}(\mathbf{r}, \mathbf{r}') - \mathbf{G}_0^{-1}(\mathbf{r}, \mathbf{r}')) : \Psi(\mathbf{r}') \right. \right. \\
& \left. \left. + 2f \int d^2 \mathbf{s} \cos \left[\beta(\xi \mathbf{b}) : \int dz \Psi(\mathbf{s}, z) \right] - \gamma \right) + \frac{1}{2} \left(2f \int d^2 \mathbf{s} \cos \left[\beta(\xi \mathbf{b}) : \int dz \Psi(\mathbf{s}, z) \right] \right. \right. \\
& \left. \left. - \gamma + \frac{\beta}{2} \int d^3 \mathbf{r} d^3 \mathbf{r}' \Psi(\mathbf{r}) : (\mathbf{G}^{-1}(\mathbf{r}, \mathbf{r}') - \mathbf{G}_0^{-1}(\mathbf{r}, \mathbf{r}')) : \Psi(\mathbf{r}') \right)^2 \right). & \text{(A.24)}
\end{aligned}$$

In an analogous way as for the first order expansion, a governing equation for G can be derived. The steps are equal to those taken in the beginning of this appendix, except for using Eq. (A.24) instead of Eq. (2.39). With the tensor $\Sigma(\mathbf{r}, \mathbf{r}') \equiv 2\beta f \hat{\xi} \mathbf{b} \hat{\xi} \mathbf{b} \delta(\mathbf{r}_{2D} - \mathbf{r}'_{2D}) \exp\left[\frac{-\beta}{2} \int dz dz' (\hat{\xi} \mathbf{b}) : G(\mathbf{0}, z - z') : (\hat{\xi} \mathbf{b})\right]$ this yields

$$\begin{aligned}
0 = & \mathbf{G}^{-1} - \mathbf{G}_0^{-1} - \Sigma + (\mathbf{G}^{-1} - \mathbf{G}_0^{-1} - \Sigma) \left(\frac{1}{2} \text{Tr} [(\mathbf{G}^{-1} - \mathbf{G}_0^{-1}) : \mathbf{G}] \right. & \text{(A.25)} \\
& + 2f \int d^2 \mathbf{s} \exp \left[\frac{-\beta}{2} \int dz dz' (\hat{\xi} \mathbf{b}) : G(\mathbf{0}, z - z') : (\hat{\xi} \mathbf{b}) \right] - \gamma \Big) \\
& + (\mathbf{G}^{-1} - \mathbf{G}_0^{-1} - \Sigma) : \mathbf{G} : (\mathbf{G}^{-1} - \mathbf{G}_0^{-1} - \Sigma) - \Sigma : \mathbf{G} : \Sigma \\
& - 2f \Sigma \int d^2 \mathbf{s} \left(\exp \left[\frac{-\beta}{2} \int dz dz' (\hat{\xi} \mathbf{b}) : G(\mathbf{0}, z - z') : (\hat{\xi} \mathbf{b}) \right] \right) \times \\
& \quad \left(\cosh \left[\beta \int dz dz' (\hat{\xi} \mathbf{b}) : G(\mathbf{s}, z - z') : (\hat{\xi} \mathbf{b}) \right] - 1 \right) \\
& - 2f(2\beta f) \left(\exp \left[\frac{-\beta}{2} \int dz dz' (\hat{\xi} \mathbf{b}) : G(\mathbf{0}, z - z') : (\hat{\xi} \mathbf{b}) \right] \right)^2 \times \\
& \quad \cosh \left[\beta \int dz dz' (\hat{\xi} \mathbf{b}) : G(\mathbf{r}_{2D} - \mathbf{r}'_{2D}, z - z') : (\hat{\xi} \mathbf{b}) \right] \hat{\xi} \mathbf{b} \hat{\xi} \mathbf{b}
\end{aligned}$$

To see whether using Eq. (A.24) changes the Green's function, G is written as $G = G_{(1)} + \delta G$, where $G_{(1)}$ satisfies Eqs. (A.22) and (A.23), and expanded up to first order in

$\delta\check{G}$. In rescaled form, this reads

$$\begin{aligned}
0 = & - \left(\check{G}_{(1)}^{-1} - \check{G}_0^{-1} \right) : \check{G}_{(1)} : \left(\check{G}_{(1)}^{-1} - \check{G}_0^{-1} \right) \tag{A.26} \\
& - (2\check{f})^2 \Xi \delta(\check{r}_{2D} - \check{r}'_{2D}) \hat{\xi} \hat{b} \hat{\xi} \hat{b} \int d^2 \check{s} \left(\exp \left[\frac{-\Xi}{2} \int d\check{z} d\check{z}' (\hat{\xi} \hat{b}) : \check{G}_{(1)}(\mathbf{0}, \check{z} - \check{z}') : (\hat{\xi} \hat{b}) \right] \right)^2 \times \\
& \quad \left(\cosh \left[\Xi \int d\check{z} d\check{z}' (\hat{\xi} \hat{b}) : \check{G}_{(1)}(\check{s}, \check{z} - \check{z}') : (\hat{\xi} \hat{b}) \right] - 1 \right) \\
& - (2\check{f})^2 \Xi \hat{\xi} \hat{b} \hat{\xi} \hat{b} \left(\exp \left[\frac{-\Xi}{2} \int d\check{z} d\check{z}' (\hat{\xi} \hat{b}) : \check{G}_{(1)}(\mathbf{0}, \check{z} - \check{z}') : (\hat{\xi} \hat{b}) \right] \right)^2 \times \\
& \quad \cosh \left[\Xi \int d\check{z} d\check{z}' (\hat{\xi} \hat{b}) : \check{G}_{(1)}(\check{r}_{2D} - \check{r}'_{2D}, \check{z} - \check{z}') : (\hat{\xi} \hat{b}) \right] \\
& + \check{G}_{(1)}^{-1} : \delta\check{G} : \check{G}_{(1)}^{-1} + \left(\check{G}_{(1)}^{-1} - \check{G}_0^{-1} \right) \frac{\Xi}{2} \int d\check{z} d\check{z}' (\hat{\xi} \hat{b}) : \delta\check{G}(\mathbf{0}, \check{z} - \check{z}') : (\hat{\xi} \hat{b}) \\
& + \Xi \int d\check{z} d\check{z}' (\hat{\xi} \hat{b}) : \delta\check{G}(\mathbf{0}, \check{z} - \check{z}') : (\hat{\xi} \hat{b}) \left(\check{G}_{(1)}^{-1} - \check{G}_0^{-1} \right) : \check{G}_{(1)} : \left(\check{G}_{(1)}^{-1} - \check{G}_0^{-1} \right) \\
& - \left(\check{G}_{(1)}^{-1} - \check{G}_0^{-1} \right) : \delta\check{G} : \left(\check{G}_{(1)}^{-1} - \check{G}_0^{-1} \right) \\
& + (2\check{f})^2 \Xi^2 \delta(\check{r}_{2D} - \check{r}'_{2D}) \hat{\xi} \hat{b} \hat{\xi} \hat{b} \int d^2 \check{s} \left(\exp \left[\frac{-\Xi}{2} \int d\check{z} d\check{z}' (\hat{\xi} \hat{b}) : \check{G}_{(1)}(\mathbf{0}, \check{z} - \check{z}') : (\hat{\xi} \hat{b}) \right] \right)^2 \times \\
& \quad \left(\cosh \left[\Xi \int d\check{z} d\check{z}' (\hat{\xi} \hat{b}) : \check{G}_{(1)}(\check{s}, \check{z} - \check{z}') : (\hat{\xi} \hat{b}) \right] - 1 \right) \int d\check{z} d\check{z}' (\hat{\xi} \hat{b}) : \delta\check{G}(\mathbf{0}, \check{z} - \check{z}') : (\hat{\xi} \hat{b}) \\
& - (2\check{f})^2 \Xi^2 \delta(\check{r}_{2D} - \check{r}'_{2D}) \hat{\xi} \hat{b} \hat{\xi} \hat{b} \int d^2 \check{s} \left(\exp \left[\frac{-\Xi}{2} \int d\check{z} d\check{z}' (\hat{\xi} \hat{b}) : \check{G}_{(1)}(\mathbf{0}, \check{z} - \check{z}') : (\hat{\xi} \hat{b}) \right] \right)^2 \times \\
& \quad \left(\sinh \left[\Xi \int d\check{z} d\check{z}' (\hat{\xi} \hat{b}) : \check{G}_{(1)}(\check{s}, \check{z} - \check{z}') : (\hat{\xi} \hat{b}) \right] \right) \int d\check{z} d\check{z}' (\hat{\xi} \hat{b}) : \delta\check{G}(\check{s}, \check{z} - \check{z}') : (\hat{\xi} \hat{b}) \\
& + (2\check{f})^2 \Xi^2 \hat{\xi} \hat{b} \hat{\xi} \hat{b} \left(\exp \left[\frac{-\Xi}{2} \int d\check{z} d\check{z}' (\hat{\xi} \hat{b}) : \check{G}_{(1)}(\mathbf{0}, \check{z} - \check{z}') : (\hat{\xi} \hat{b}) \right] \right)^2 \times \\
& \quad \cosh \left[\Xi \int d\check{z} d\check{z}' (\hat{\xi} \hat{b}) : \check{G}_{(1)}(\check{r}_{2D} - \check{r}'_{2D}, \check{z} - \check{z}') : (\hat{\xi} \hat{b}) \right] \int d\check{z} d\check{z}' (\hat{\xi} \hat{b}) : \delta\check{G}(\mathbf{0}, \check{z} - \check{z}') : (\hat{\xi} \hat{b}) \\
& - (2\check{f})^2 \Xi^2 \hat{\xi} \hat{b} \hat{\xi} \hat{b} \left(\exp \left[\frac{-\Xi}{2} \int d\check{z} d\check{z}' (\hat{\xi} \hat{b}) : \check{G}_{(1)}(\mathbf{0}, \check{z} - \check{z}') : (\hat{\xi} \hat{b}) \right] \right)^2 \times \\
& \quad \sinh \left[\Xi \int d\check{z} d\check{z}' (\hat{\xi} \hat{b}) : \check{G}_{(1)}(\check{r}_{2D} - \check{r}'_{2D}, \check{z} - \check{z}') : (\hat{\xi} \hat{b}) \right] \times \\
& \quad \int d\check{z} d\check{z}' (\hat{\xi} \hat{b}) : \delta\check{G}(\check{r}_{2D} - \check{r}'_{2D}, \check{z} - \check{z}') : (\hat{\xi} \hat{b}).
\end{aligned}$$

To determine the dominant terms in the low temperature limit $\Xi \rightarrow \infty$, it can be used that for large Ξ

$$\begin{aligned}
& \left(\exp \left[\frac{-\Xi}{2} \int d\check{z}d\check{z}'(\hat{\xi}\hat{\mathbf{b}}) : \check{\mathcal{G}}_{(1)}(\mathbf{0}, \check{z} - \check{z}') : (\hat{\xi}\hat{\mathbf{b}}) \right] \right)^2 \times \\
& \quad \left(\cosh \left[\Xi \int d\check{z}d\check{z}'(\hat{\xi}\hat{\mathbf{b}}) : \check{\mathcal{G}}_{(1)}(\check{\mathbf{s}}, \check{z} - \check{z}') : (\hat{\xi}\hat{\mathbf{b}}) \right] - 1 \right) \\
& \approx \left(\exp \left[\frac{-\Xi}{2} \int d\check{z}d\check{z}'(\hat{\xi}\hat{\mathbf{b}}) : \check{\mathcal{G}}_{(1)}(\mathbf{0}, \check{z} - \check{z}') : (\hat{\xi}\hat{\mathbf{b}}) \right] \right)^2 \times \\
& \quad \sinh \left[\Xi \int d\check{z}d\check{z}'(\hat{\xi}\hat{\mathbf{b}}) : \check{\mathcal{G}}_{(1)}(\check{\mathbf{s}}, \check{z} - \check{z}') : (\hat{\xi}\hat{\mathbf{b}}) \right] \\
& \approx \exp \left[-\Xi \int d\check{z}d\check{z}'(\hat{\xi}\hat{\mathbf{b}}) : \left(\check{\mathcal{G}}_{(1)}(\mathbf{0}, \check{z} - \check{z}') - \check{\mathcal{G}}_{(1)}(\check{\mathbf{s}}, \check{z} - \check{z}') \right) : (\hat{\xi}\hat{\mathbf{b}}) \right]. \quad (\text{A.27})
\end{aligned}$$

Furthermore, it can be used that $\check{\mathcal{G}}_{(1)}^{-1} - \check{\mathcal{G}}_0^{-1}$ has no algebraic corrections in Ξ^{-1} . This yields for the dominant terms in Eq. (A.28)

$$\begin{aligned}
0 = & -(2\check{f})^2 \Xi \delta(\check{\mathbf{r}}_{2D} - \check{\mathbf{r}}'_{2D}) \hat{\xi}\hat{\mathbf{b}}\hat{\xi}\hat{\mathbf{b}} \times \quad (\text{A.28}) \\
& \int d^2\check{\mathbf{s}} \exp \left[-\Xi \int d\check{z}d\check{z}'(\hat{\xi}\hat{\mathbf{b}}) : \left(\check{\mathcal{G}}_{(1)}(\mathbf{0}, \check{z} - \check{z}') - \check{\mathcal{G}}_{(1)}(\check{\mathbf{s}}, \check{z} - \check{z}') \right) : (\hat{\xi}\hat{\mathbf{b}}) \right] \\
& - (2\check{f})^2 \Xi \hat{\xi}\hat{\mathbf{b}}\hat{\xi}\hat{\mathbf{b}} \exp \left[-\Xi \int d\check{z}d\check{z}'(\hat{\xi}\hat{\mathbf{b}}) : \left(\check{\mathcal{G}}_{(1)}(\mathbf{0}, \check{z} - \check{z}') - \check{\mathcal{G}}_{(1)}(\check{\mathbf{r}}_{2D} - \check{\mathbf{r}}'_{2D}, \check{z} - \check{z}') \right) : (\hat{\xi}\hat{\mathbf{b}}) \right] \\
& + \check{\mathcal{G}}_{(1)}^{-1} : \delta\check{\mathcal{G}} : \check{\mathcal{G}}_{(1)}^{-1} \\
& + (2\check{f})^2 \Xi^2 \delta(\check{\mathbf{r}}_{2D} - \check{\mathbf{r}}'_{2D}) \hat{\xi}\hat{\mathbf{b}}\hat{\xi}\hat{\mathbf{b}} \int d^2\check{\mathbf{s}} \int d\check{z}d\check{z}'(\hat{\xi}\hat{\mathbf{b}}) : \left(\delta\check{\mathcal{G}}(\mathbf{0}, \check{z} - \check{z}') - \delta\check{\mathcal{G}}(\check{\mathbf{s}}, \check{z} - \check{z}') \right) : (\hat{\xi}\hat{\mathbf{b}}) \times \\
& \quad \exp \left[-\Xi \int d\check{z}d\check{z}'(\hat{\xi}\hat{\mathbf{b}}) : \left(\check{\mathcal{G}}_{(1)}(\mathbf{0}, \check{z} - \check{z}') - \check{\mathcal{G}}_{(1)}(\check{\mathbf{s}}, \check{z} - \check{z}') \right) : (\hat{\xi}\hat{\mathbf{b}}) \right] \\
& + (2\check{f})^2 \Xi^2 \hat{\xi}\hat{\mathbf{b}}\hat{\xi}\hat{\mathbf{b}} \int d\check{z}d\check{z}'(\hat{\xi}\hat{\mathbf{b}}) : \left(\delta\check{\mathcal{G}}(\mathbf{0}, \check{z} - \check{z}') - \delta\check{\mathcal{G}}(\check{\mathbf{r}}_{2D} - \check{\mathbf{r}}'_{2D}, \check{z} - \check{z}') \right) : (\hat{\xi}\hat{\mathbf{b}}) \times \\
& \quad \exp \left[-\Xi \int d\check{z}d\check{z}'(\hat{\xi}\hat{\mathbf{b}}) : \left(\check{\mathcal{G}}_{(1)}(\mathbf{0}, \check{z} - \check{z}') - \check{\mathcal{G}}_{(1)}(\check{\mathbf{r}}_{2D} - \check{\mathbf{r}}'_{2D}, \check{z} - \check{z}') \right) : (\hat{\xi}\hat{\mathbf{b}}) \right]
\end{aligned}$$

Now, the nascent delta function representation $\delta(x) \propto \lim_{\epsilon \rightarrow \infty} e^{x^2/2\epsilon} \epsilon^{-1/2}$ and the product rule for limits can be used to rewrite the exponents. This implies that in the limit $\Xi \rightarrow \infty$ the last term has contributions just when $\check{\mathcal{G}}_{(1)}(\mathbf{0}, \check{z} - \check{z}') = \check{\mathcal{G}}_{(1)}(\check{\mathbf{r}}_{2D} - \check{\mathbf{r}}'_{2D}, \check{z} - \check{z}')$, which implies that $\mathbf{0} = \check{\mathbf{r}}_{2D} - \check{\mathbf{r}}'_{2D}$. Therefore this term vanishes. The same holds for the second last term.

This furthermore implies that the first two lines are proportional to $-(2\check{f})^2 \Xi^{1/2} \delta(\check{\mathbf{r}}_{2D} - \check{\mathbf{r}}'_{2D}) \hat{\xi}\hat{\mathbf{b}}\hat{\xi}\hat{\mathbf{b}}$, which finally yields

$$\delta\check{\mathcal{G}} : \check{\mathcal{G}}_{(1)}^{-1} \propto (2\check{f})^2 \Xi^{1/2} \check{\mathcal{G}}_{(1)} : \hat{\xi}\hat{\mathbf{b}}\hat{\xi}\hat{\mathbf{b}} \delta(\check{\mathbf{r}}_{2D} - \check{\mathbf{r}}'_{2D}). \quad (\text{A.29})$$

The RHS of this equation vanishes with $\Xi^{-1/2}$ in the limit $\Xi \rightarrow \infty$ with $\sqrt{\Xi}\check{f}$ constant. The LHS can be interpreted as the relative change of the Green's function, which thus

vanishes in this limit. From this, it is concluded that the approximation in Eq. (2.39) is good in the low temperature limit.

The second approximation that has to be tested is the assumption that the Green's function is Gaussian. This is tested by comparing the difference $\langle \alpha(\mathbf{s})\alpha(\mathbf{s}') \rangle_G - \langle \alpha(\mathbf{s})\alpha(\mathbf{s}') \rangle$ with $\langle \alpha(\mathbf{s})\alpha(\mathbf{s}') \rangle_G$ using the approximation in Eq. (2.39). The difference in rescaled form is:

$$\begin{aligned}
 & \langle \check{\alpha}(\check{\mathbf{s}})\check{\alpha}(\check{\mathbf{s}}') \rangle_G - \langle \check{\alpha}(\check{\mathbf{s}})\check{\alpha}(\check{\mathbf{s}}') \rangle \approx \tag{A.30} \\
 & \approx - \left\langle \check{\alpha}(\check{\mathbf{s}})\check{\alpha}(\check{\mathbf{s}}') \left(\frac{1}{2\Xi} \int d\check{u}d\check{u}' \check{\Psi}(\check{\mathbf{u}}) : (\mathbb{G}^{-1}(\check{\mathbf{u}}, \check{\mathbf{u}}') - \mathbb{G}_0^{-1}(\check{\mathbf{u}}, \check{\mathbf{u}}')) : \check{\Psi}(\check{\mathbf{u}}') \right. \right. \\
 & \quad \left. \left. + 2\check{f} \int d^2\check{s}'' \cos \left[(\hat{\xi}\hat{\mathbf{b}}) : \int d\check{z}\check{\Psi}(\check{\mathbf{s}}'', \check{z}) \right] - \gamma \right) \right\rangle_G \\
 & = - \langle \check{\alpha}(\check{\mathbf{s}})\check{\alpha}(\check{\mathbf{s}}') \rangle_{\check{\mathbb{G}}} \left(\frac{\Xi}{2} \int d\check{z}d\check{z}' \hat{\xi}\hat{\mathbf{b}} : \check{\mathbb{G}} : (\check{\mathbb{G}}^{-1} - \check{\mathbb{G}}_0^{-1}) : \check{\mathbb{G}} : \hat{\xi}\hat{\mathbf{b}}(\check{\mathbf{s}}, \check{z}; \check{\mathbf{s}}, \check{z}) \right. \\
 & \quad + \frac{\Xi}{2} \int d\check{z}d\check{z}' \hat{\xi}\hat{\mathbf{b}} : \check{\mathbb{G}} : (\check{\mathbb{G}}^{-1} - \check{\mathbb{G}}_0^{-1}) : \check{\mathbb{G}} : \hat{\xi}\hat{\mathbf{b}}(\check{\mathbf{s}}', \check{z}; \check{\mathbf{s}}', \check{z}) \\
 & \quad \left. \frac{\Xi \int d\check{z}d\check{z}' \hat{\xi}\hat{\mathbf{b}} : \check{\mathbb{G}} : (\check{\mathbb{G}}^{-1} - \check{\mathbb{G}}_0^{-1}) : \check{\mathbb{G}} : \hat{\xi}\hat{\mathbf{b}}(\check{\mathbf{s}}, \check{z}; \check{\mathbf{s}}', \check{z})}{\tanh \left[\Xi \int d\check{z} \int d\check{z}' \hat{\xi}\hat{\mathbf{b}} : \check{\mathbb{G}}(\check{\mathbf{s}} - \check{\mathbf{s}}', \check{z} - \check{z}') : \hat{\xi}\hat{\mathbf{b}} \right]} \right. \\
 & \quad \left. + 2\check{f} \int d^2\check{s}'' \exp \left[-\frac{\Xi}{2} \int d\check{z} \int d\check{z}' \hat{\xi}\hat{\mathbf{b}} : \check{\mathbb{G}}(\mathbf{0}, \check{z} - \check{z}') : \hat{\xi}\hat{\mathbf{b}} \right] \right. \\
 & \quad \left(-1 + \cosh \left[\Xi \int d\check{z} \int d\check{z}' \hat{\xi}\hat{\mathbf{b}} : \check{\mathbb{G}}(\check{\mathbf{s}} - \check{\mathbf{s}}'', \check{z} - \check{z}') : \hat{\xi}\hat{\mathbf{b}} \right] \times \right. \\
 & \quad \cosh \left[\Xi \int d\check{z} \int d\check{z}' \hat{\xi}\hat{\mathbf{b}} : \check{\mathbb{G}}(\check{\mathbf{s}}' - \check{\mathbf{s}}'', \check{z} - \check{z}') : \hat{\xi}\hat{\mathbf{b}} \right] \\
 & \quad \left. - \sinh \left[\Xi \int d\check{z} \int d\check{z}' \hat{\xi}\hat{\mathbf{b}} : \check{\mathbb{G}}(\check{\mathbf{s}} - \check{\mathbf{s}}'', \check{z} - \check{z}') : \hat{\xi}\hat{\mathbf{b}} \right] \times \right. \\
 & \quad \left. \left. \frac{\sinh \left[\Xi \int d\check{z} \int d\check{z}' \hat{\xi}\hat{\mathbf{b}} : \check{\mathbb{G}}(\check{\mathbf{s}}' - \check{\mathbf{s}}'', \check{z} - \check{z}') : \hat{\xi}\hat{\mathbf{b}} \right]}{\tanh \left[\Xi \int d\check{z} \int d\check{z}' \hat{\xi}\hat{\mathbf{b}} : \check{\mathbb{G}}(\check{\mathbf{s}} - \check{\mathbf{s}}', \check{z} - \check{z}') : \hat{\xi}\hat{\mathbf{b}} \right]} \right) \right).
 \end{aligned}$$

The term between brackets is minus one in the limit $\Xi \rightarrow \infty$. Namely, the tanh term goes to one, and hence the sinh and cosh terms in the last four lines cancel. Furthermore, $\check{\mathbb{G}}_{(1)}^{-1} - \check{\mathbb{G}}_0^{-1}$ has no algebraic corrections in Ξ^{-1} , so the first three terms vanish as well. This implies that the prediction of the charge correlator using the Gaussian approximation is equal to the 'real' charge correlator from the full partition function. This justifies the Gaussian approximation.

A.8.2 Approximated solution

To find an approximate solution to Eq. (2.41) in the dominant scaling regime, the equation is rescaled using the scales introduced in Sec. 2.3. To find the scaling of G_0^{-1} , note that

$$\int d^3\mathbf{r}' G_0^{-1}(\mathbf{r} - \mathbf{r}') : \Psi(\mathbf{r}') = \nabla \wedge \mathbb{S} : \nabla \wedge \Psi(\mathbf{r})$$

$$(\zeta^2 L) |G_0^{-1}| = \zeta^{-2} (2\mu)^{-1}, \quad (\text{A.31})$$

where $|G_0^{-1}|$ is the typical size of G_0^{-1} . Hence the inverse Green's function scales with $(2\mu\zeta^4 L)^{-1}$, and hence the Green's function scales with $2\mu/L$. It is assumed that G scales in the same way. This yields for the rescaling of Eq. (2.41)

$$\beta \int dz \mathbf{B}(\mathbf{s}, z) : \hat{\xi} \hat{\mathbf{b}} = -2\Xi f \frac{\zeta}{L} \int d\check{\mathbf{r}} \frac{\zeta}{L} \int d\check{z} \hat{\xi} \hat{\mathbf{b}} : G(\check{\mathbf{r}}; \check{\mathbf{s}}, \check{z}) : \hat{\xi} \hat{\mathbf{b}}.$$

$$\cdot \exp \left[-\frac{\Xi}{2} \frac{\zeta}{L} \int d(\check{z} - \check{z}') \hat{\xi} \hat{\mathbf{b}} : \check{G}(\mathbf{0}, \check{z} - \check{z}') : \hat{\xi} \hat{\mathbf{b}} \right] \sin \left[\beta \int dz \mathbf{B}(\mathbf{r}_{2D}, z) : \hat{\xi} \hat{\mathbf{b}} \right]$$

$$\check{G}^{-1}(\check{\mathbf{r}} - \check{\mathbf{r}}') = \check{G}_0^{-1}(\check{\mathbf{r}} - \check{\mathbf{r}}') + 2\Xi \check{f} \delta(\check{\mathbf{r}}_{2D} - \check{\mathbf{r}}'_{2D}) \hat{\xi} \hat{\mathbf{b}} \hat{\xi} \hat{\mathbf{b}}.$$

$$\cdot \exp \left[\frac{-\Xi}{2} \frac{\zeta}{L} \int d(\check{z} - \check{z}') (\hat{\xi} \hat{\mathbf{b}}) : \check{G}(\mathbf{0}, \check{z} - \check{z}') : (\hat{\xi} \hat{\mathbf{b}}) \right] \cos \left[\beta \int dz \mathbf{B}(\mathbf{r}_{2D}, z) : \hat{\xi} \hat{\mathbf{b}} \right].$$

The solution of this equation in the low temperature limit $\Xi \rightarrow \infty$ where $\sqrt{\Xi} \check{f}$ is kept constant is $\beta \int dz \mathbf{B}(\mathbf{s}, z) : \hat{\xi} \hat{\mathbf{b}} = 0$ and $\check{G}^{-1} = \check{G}_0^{-1}$, and hence $\mathbf{B} = 0$ and $G = G_0$. There are no algebraic corrections in Ξ^{-1} .

A.9 Compliance

The variance of the distortion in the low temperature limit, Eq. (2.45), was derived as follows:

$$\langle \Delta_{ij}^s(\mathbf{q}) \Delta_{i'j'}^s(\mathbf{q}) \rangle - \langle \Delta_{ij}^s(\mathbf{q}) \rangle \langle \Delta_{i'j'}^s(\mathbf{q}) \rangle = \mathbb{S}_{ij i'j'}^{ls} - (q \mathbb{S}_{ijkl} \mathbf{C}_{kn}) (q \mathbb{S}_{i'j'k'l'} \mathbf{C}_{k'n'})$$

$$\frac{2\mu}{2q^2} \left(Q_{ll'} Q_{nn'} + \mathbf{C}_{l'n} \mathbf{C}_{ln'} + \frac{2\nu}{1-\nu} \mathbf{C}_{ln} \mathbf{C}_{l'n'} \right) \quad (\text{A.33})$$

$$= \mathbb{S}_{ij i'j'}^{ls} - \frac{2\mu}{2} \mathbb{S}_{ijkl} \mathbb{S}_{i'j'k'l'} \left(Q_{ll'} Q_{kk'} + Q_{l'k} Q_{lk'} + \frac{2\nu}{1-\nu} Q_{lk} Q_{l'k'} \right)$$

$$= \mathbb{S}_{ij i'j'}^{ls} - \frac{1}{2\mu} \left(\frac{1}{2} Q_{ii'} Q_{jj'} + \frac{1}{2} Q_{ij'} Q_{i'j} - \frac{\nu}{1-\nu} \delta_{ij} Q_{i'j'} - \frac{\nu}{1-\nu} Q_{ij} \delta_{i'j'} \right.$$

$$\left. + 2 \frac{\nu}{1-\nu} \frac{\nu}{1+\nu} \delta_{ij} \delta_{i'j'} + \frac{\nu}{1-\nu} Q_{ij} Q_{i'j'} \right)$$

$$= \frac{1}{2\mu} \frac{1}{2} (\delta_{ii'} \delta_{jj'} - Q_{ii'} Q_{jj'} + \delta_{ij'} \delta_{ji'} - Q_{ij'} Q_{ji'})$$

$$- \frac{2\nu}{1-\nu} (\delta_{ij} \delta_{i'j'} + Q_{ij} Q_{i'j'} - \delta_{ij} Q_{i'j'} - Q_{ij} \delta_{i'j'})$$

$$= (\delta_{il} \delta_{jn} - Q_{il} Q_{jn}) \frac{1}{2} \frac{1}{2\mu} \left(\delta_{ll'} \delta_{nn'} + \delta_{l'n} \delta_{ln'} - \frac{2\nu}{1-\nu} \delta_{ln} \delta_{l'n'} \right) (\delta_{i'l'} \delta_{j'n'} - Q_{i'l'} Q_{j'n'}).$$

Appendix B

Details about calculations in Chap. 3

B.1 The mean-field elastic energy

In this section, the first three contributions of Eq. (3.20) are combined into a single expression in terms of Δ_{mf} , as defined in Eq. (3.21). To this end, the first three contributions of Eq. (3.20) are rewritten using the definitions in Eqs. (3.6) and (3.12)

$$\begin{aligned}
 & \frac{1}{2} \int dV \Delta_0 : \mathbb{C} : \Delta_0 + \frac{1}{2} \sum_{b,b'} \int dAdA' \rho_b(s) u_{b,b'}(s, s') \rho_{b'}(s') + \sum_b \int dA \rho_b(s) V_{b,0}(s) \\
 &= \frac{1}{2} \int dV \left(\Delta_0 + \left(\nabla \times \int dV' G_0(\mathbf{r}, \mathbf{r}') : \sum_b \hat{\xi} \otimes \mathbf{b} \rho_b(\mathbf{r}'_{2D}) \right) : \mathbb{S} \right) : \mathbb{C} : \\
 & \quad : \left(\Delta_0 + \left(\nabla \times \int dV' G_0(\mathbf{r}, \mathbf{r}'') : \sum_b \hat{\xi} \otimes \mathbf{b} \rho_b(\mathbf{r}''_{2D}) \right) : \mathbb{S} \right). \quad (\text{B.1})
 \end{aligned}$$

To rewrite this equation, it should be used that the following combination is divergence free and symmetric:

$$\mathbb{C} : \left(\Delta_0 + \left(\nabla \times \int dV' G_0(\mathbf{r}, \mathbf{r}') : \sum_b \hat{\xi} \otimes \mathbf{b} \rho_b(\mathbf{r}'_{2D}) \right) : \mathbb{S} \right). \quad (\text{B.2})$$

These two properties will first be shown. First, the divergence free character of $\mathbb{C} : \Delta_0$ follows immediately by Eq. (3.3), and $\nabla \times \int dV' G_0(\mathbf{r}, \mathbf{r}') : \sum_b \hat{\xi} \otimes \mathbf{b} \rho_b(\mathbf{r}'_{2D})$ is a rotation, and hence it is divergence free by definition.

Second, this combination is symmetric. For $\mathbb{C} : \Delta_0$, this is immediately clear. For $\nabla \times \int dV' G_0(\mathbf{r}, \mathbf{r}') : \sum_b \hat{\xi} \otimes \mathbf{b} \rho_b(\mathbf{r}'_{2D})$, this is more subtle. As mentioned below Eq. (3.13), $\int dV' G_0^{-1}(\mathbf{r}, \mathbf{r}') : \Psi(\mathbf{r}')$ is infinite if $\nabla \times \Psi(\mathbf{r})$ is not symmetric. Therefore, $\nabla \times G_0(\mathbf{r}, \mathbf{r}')$ should be symmetric in the first two indices. One can check that this is indeed the case for the infinite space solution for G_0 in Eq. (3.14).

From these two properties, the following relationship can be derived for any arbitrary

second order tensor field $\mathbf{h}(\mathbf{r})$ for which $\nabla \times \mathbf{h}(\mathbf{r})$ is symmetric:

$$\begin{aligned}
& \int dV \left(\mathbf{\Delta}_0 + \left(\nabla \times \int dV' G_0(\mathbf{r}, \mathbf{r}') : \sum_{\mathbf{b}} \hat{\xi} \otimes \mathbf{b} \rho_{\mathbf{b}}(\mathbf{r}'_{2D}) \right) : \mathbb{S} \right) : \nabla \times \mathbf{h}(\mathbf{r}) = \\
& = \int dV \left(\mathbf{\Delta}_0 : \nabla \times \mathbf{h}(\mathbf{r}) + \sum_{\mathbf{b}} \hat{\xi} \otimes \mathbf{b} \rho_{\mathbf{b}}(\mathbf{r}'_{2D}) : \mathbf{h}(\mathbf{r}) \right) \quad (\text{B.3}) \\
& = \int dV (\mathbf{\Delta}_0 : \nabla \times \mathbf{h}(\mathbf{r}) - \nabla \times \beta^p : \mathbf{h}(\mathbf{r})) \\
& = \int dV (\mathbf{\Delta}_0 : \nabla \times \mathbf{h}(\mathbf{r}) - (\beta^p)^s : \nabla \times \mathbf{h}(\mathbf{r})) = \int dV \mathbf{\Delta}_{\text{mf}} : \nabla \times \mathbf{h}(\mathbf{r})
\end{aligned}$$

where in the first step the definition of G_0^{-1} in Eq. (3.13) is used, in the second the definition of β^p in Eq. (3.21), in the third Gauss' theorem and the symmetry of $\nabla \times \mathbf{h}(\mathbf{r})$ and in the fourth step the definition of $\mathbf{\Delta}_{\text{mf}}$ in Eq. (3.21). By applying this identity twice in Eq. (B.1), it is found that

$$\begin{aligned}
& \frac{1}{2} \int dV \mathbf{\Delta}_0 : \mathbb{C} : \mathbf{\Delta}_0 + \frac{1}{2} \sum_{\mathbf{b}, \mathbf{b}'} \int dA dA' \rho_{\mathbf{b}}(\mathbf{s}) u_{\mathbf{b}, \mathbf{b}'}(\mathbf{s}, \mathbf{s}') \rho_{\mathbf{b}'}(\mathbf{s}') + \sum_{\mathbf{b}} \int dA \rho_{\mathbf{b}}(\mathbf{s}) V_{\mathbf{b}, 0}(\mathbf{s}) \\
& = \frac{1}{2} \int dV \mathbf{\Delta}_{\text{mf}} : \mathbb{C} : \mathbf{\Delta}_{\text{mf}}. \quad (\text{B.4})
\end{aligned}$$

This expression is used in Eq. (3.22).

B.2 The Gradient correction in the LDA

In this section, the gradient correction for the many body contribution is calculated using Eq. (3.28). To this end, the second derivative of the gradient correction with respect to the density profile is determined first:

$$\begin{aligned}
& \left. \frac{\delta^2 \mathcal{F}_{mb}[\rho_{\text{tot}}(\mathbf{s}'), T]}{\delta \rho_{\text{tot}}(\mathbf{0}) \delta \rho_{\text{tot}}(\mathbf{s})} \right|_{\rho_{\text{tot}}(\mathbf{s}) = \rho_{\text{tot}}} = -\text{Tr} \left[\left(\text{Id}(\mathbf{s}_1 - \mathbf{s}_2) + \frac{1}{k_B T} \int dz dz' G_0(\mathbf{s}_1 - \mathbf{s}_2, z - z') : \right. \right. \\
& \quad : \hat{\xi} \otimes \mathbf{b} \otimes \hat{\xi} \otimes \mathbf{b} \rho_{\text{tot}} \left. \right) : \frac{1}{k_B T} \int dz dz' G_0(\mathbf{s}_2 - \mathbf{s}_3, z - z') : \hat{\xi} \otimes \mathbf{b} \otimes \hat{\xi} \otimes \mathbf{b} : \\
& \quad : \left(\text{Id}(\mathbf{s}_3 - \mathbf{s}_4) + \frac{1}{k_B T} \int dz dz' G_0(\mathbf{s}_3 - \mathbf{s}_4, z - z') : \hat{\xi} \otimes \mathbf{b} \otimes \hat{\xi} \otimes \mathbf{b} \rho_{\text{tot}} \right) : \\
& \quad : \frac{1}{k_B T} \int dz dz' G_0(\mathbf{s}_4 - \mathbf{s}_1, z - z') : \hat{\xi} \otimes \mathbf{b} \otimes \hat{\xi} \otimes \mathbf{b} \left. \right] \delta(\mathbf{s}_1) \delta(\mathbf{s}_3 - \mathbf{s}). \quad (\text{B.5})
\end{aligned}$$

The convolution on the RHS can be written as a product in Fourier space. Therefore, this expression reads, using the eigenvalues $\tilde{\lambda}(\mathbf{q})$ in Eq. (3.34),

$$\left. \frac{\delta^2 \mathcal{F}_{mb}[\rho_{SSD}(\mathbf{s}), T]}{\rho_{SSD}(\mathbf{0}) \rho_{SSD}(\mathbf{s})} \right|_{\rho_{SSD}} = -\frac{1}{\rho_{SSD}^2} \frac{k_B T}{2} \frac{1}{(2\pi)^4} \int d^2 \mathbf{q} d^2 \mathbf{q}' e^{i(\mathbf{q}' - \mathbf{q}) \cdot \mathbf{s}} \frac{\tilde{\lambda}(\mathbf{q})}{1 + \tilde{\lambda}(\mathbf{q})} \frac{\tilde{\lambda}(\mathbf{q}')}{1 + \tilde{\lambda}(\mathbf{q}')}. \quad (\text{B.6})$$

The integrations over \mathbf{q} and \mathbf{q}' can be performed independently. The function $j(\mathbf{s})$ is used as shorthand notation for the integral over \mathbf{q} :

$$j(\mathbf{s}) \equiv -\frac{1}{(2\pi)^2} \int d^2\mathbf{q} e^{-i\mathbf{q}\cdot\mathbf{s}} \frac{\tilde{\lambda}(\mathbf{q})}{1 + \tilde{\lambda}(\mathbf{q})} = \frac{1}{\rho_{SSD}} \frac{1}{(2\pi)^2} \int d^2\mathbf{q} e^{-i\mathbf{q}\cdot\mathbf{s}} \frac{aq_y^2}{q^4 + aq_y^2} \quad (\text{B.7})$$

where, as in the main text, a is the shorthand notation for $a = \frac{\rho_{SSD} 2\mu b^2 L}{k_B T (1-\nu)}$. Eq. (B.6) can thus be written as

$$\left. \frac{\delta^2 \mathcal{F}_{mb}[\rho_{SSD}(\mathbf{s}), T]}{\delta \rho_{SSD}(\mathbf{0}) \delta \rho_{SSD}(\mathbf{s})} \right|_{\rho_{SSD}} = -\frac{k_B T}{2} j(\mathbf{s}) j(-\mathbf{s}) = -\frac{k_B T}{2} j(\mathbf{s})^2, \quad (\text{B.8})$$

where the symmetry of $j(\mathbf{s})$ was used. Hence the matrix $\mathbf{F}_{2,mB}(\rho_{SSD})$, as expressed in Eq. (3.28), reads

$$\mathbf{F}_{2,mB}(\rho_{SSD}, T) = \frac{k_B T}{8} \int dA \mathbf{s} \otimes \mathbf{s} j(\mathbf{s})^2. \quad (\text{B.9})$$

This can be rewritten as follows:

$$\begin{aligned} \mathbf{F}_{2,mB}(\rho_{SSD}, T) &= \left. \frac{k_B T}{8} \int dA \mathbf{s} \otimes \mathbf{s} j(\mathbf{s})^2 e^{i\mathbf{q}\cdot\mathbf{s}} \right|_{\mathbf{q}=0} \quad (\text{B.10}) \\ &= -\frac{k_B T}{8} \frac{d}{d\mathbf{q}} \otimes \frac{d}{d\mathbf{q}} \mathfrak{F} [j(\mathbf{s})^2] (\mathbf{q}) \Big|_{\mathbf{q}=0} = -\frac{k_B T}{8} \frac{d}{d\mathbf{q}} \otimes \frac{d}{d\mathbf{q}} \frac{1}{(2\pi)^2} \int d\mathbf{q}' \tilde{j}(\mathbf{q}') \tilde{j}(\mathbf{q} - \mathbf{q}') \Big|_{\mathbf{q}=0} \\ &= \frac{k_B T}{8} \frac{1}{(2\pi)^2} \frac{a^2}{\rho_{SSD}^2} \int d\mathbf{q}' \frac{d}{d\mathbf{q}'} \tilde{j}(\mathbf{q}') \otimes \frac{d}{d\mathbf{q}'} \tilde{j}(-\mathbf{q}') \\ &= \frac{k_B T}{8} \frac{1}{(2\pi)^2} \frac{a^2}{\rho_{SSD}^2} \int d\mathbf{q}' \left(\begin{array}{c} -4 \frac{q'_x q'_y{}^2 q'^2}{(q'^4 + a q_y'^2)^2} \\ 2 \frac{q'_y (q_x'^4 - q_y'^4)}{(q'^4 + a q_y'^2)^2} \end{array} \right) \otimes \left(\begin{array}{c} -4 \frac{q'_x q'_y{}^2 q'^2}{(q'^4 + a q_y'^2)^2} \\ 2 \frac{q'_y (q_x'^4 - q_y'^4)}{(q'^4 + a q_y'^2)^2} \end{array} \right), \end{aligned}$$

where in the third line, the inverse of the convolution theorem was used, and where for the last equality, the explicit form of $\tilde{j}(\mathbf{q})$ in Eq. (B.7) was used. These integrations can now be performed. Note that the q_x derivative is antisymmetric in q_x , and the q_y derivative is antisymmetric in q_y . Therefore, the off-diagonal terms in the matrix vanish. Using polar coordinates for the \mathbf{q}' -integral, this yields

$$\begin{aligned} \mathbf{F}_{2,mB}(\rho_{SSD}, T) &= \frac{k_B T}{8} \frac{1}{(2\pi)^2} \frac{4a^2}{\rho_{SSD}^2} \quad (\text{B.11}) \\ &= \int d\mathbf{q}' q' \int_0^{2\pi} d\phi \frac{q'^2 \cos^2 \phi}{(q'^2 + a \cos^2 \phi)^4} \begin{pmatrix} 4 \cos^2 \phi \sin^2 \phi & 0 \\ 0 & (\sin^4 \phi - \cos^4 \phi)^2 \end{pmatrix} \\ &= \frac{k_B T}{8} \frac{1}{(2\pi)^2} \frac{4a^2}{\rho_{SSD}^2} \int d\mathbf{q}' \begin{pmatrix} \frac{\pi}{2(q'^2 + a)^{5/2}} & 0 \\ 0 & \frac{\pi(4q'^2 + a^2)}{8q'^2 (q'^2 + a)^{7/2}} \end{pmatrix} \\ &= \frac{k_B T}{8} \frac{1}{(2\pi)^2} \frac{4a^2}{\rho_{SSD}^2} \begin{pmatrix} \frac{\pi}{3a^2} & 0 \\ 0 & -\frac{\pi}{3a^2} + \frac{\pi}{8a^{3/2} q_0} \end{pmatrix} \\ &= \frac{1}{24\pi} \frac{k_B T}{\rho_{SSD}^2} \begin{pmatrix} 1 & 0 \\ 0 & -1 + \frac{3\sqrt{\rho_{SSD}}}{8q_0} \sqrt{\frac{2\mu b^2 L}{k_B T (1-\nu)}} \end{pmatrix}, \end{aligned}$$

where q_0 is the lower bound of the q' -integral. The lower bound q_0 is inversely proportional to the largest length scale in the system, which is the system size R .

B.3 Summation over glide planes

In this appendix, the integrations over the y -coordinate and the summations over n in Eq. (3.48) are performed. First, the summation in the first term can be evaluated:

$$\int dy \sum_{n=-\infty}^{\infty} \delta(y - hn) = \sum_{n=-\infty}^{\infty} 1 \equiv N_y, \quad (\text{B.12})$$

where the latter equality is the definition of N_y . The number N_y can be interpreted as the number of glide planes. In the geometry considered here, this number is in principle infinite. However, it will be shown later that it is a common prefactor of all terms in Eq. (3.48).

Second, the summation in the second term can be evaluated using the explicit expression of the interaction potential in Eq. (3.14b):

$$\begin{aligned} \int dy \int dy' \sum_{n,n' \in \mathbb{N}} \delta(y - hn) \delta(y' - hn') u_{\text{edge}}(x - x', y - y') &= \quad (\text{B.13}) \\ &= \sum_{n=-\infty}^{\infty} \sum_{\Delta n=-\infty}^{\infty} u_{\text{edge}}(x - x', h\Delta n) \\ &= -N_y \frac{\mu b^2 L}{2\pi(1-\nu)} \sum_{\Delta n=-\infty}^{\infty} \left(\ln \left(\frac{\sqrt{(x-x')^2 + h^2 \Delta n^2}}{s_0} \right) + \frac{h^2 \Delta n^2}{(x-x')^2 + h^2 \Delta n^2} \right) \\ &= -N_y \frac{\mu b^2 L}{2\pi(1-\nu)} \left(2 \sum_{\Delta n=1}^{\infty} \left(\ln \left(\frac{\sqrt{(x-x')^2 + h^2 \Delta n^2}}{h|\Delta n|} \right) + \ln \left(\frac{h|\Delta n|}{s_0} \right) \right) \right) \\ &\quad + \ln \left(\frac{|x-x'|}{s_0} \right) - N_y \frac{\mu b^2 L}{2\pi(1-\nu)} \sum_{\Delta n=-\infty}^{\infty} \left(1 - \frac{(x-x')^2}{(x-x')^2 + h^2 \Delta n^2} \right), \end{aligned}$$

where in the first line Δn is shorthand notation for $n - n'$. To evaluate further, it is convenient to define A by

$$A \equiv 2 \sum_{\Delta n=1}^{\infty} \ln \left(\frac{h|\Delta n|}{s_0} \right), \quad (\text{B.14})$$

which is a constant independent of $x - x'$. The summation does not converge as the number of glide planes is infinite. However, it will be shown later that the dislocation density profile is independent of A . Furthermore, the following identities can be used:

$$\begin{aligned} 2 \sum_{\Delta n=1}^{\infty} \ln \left(\frac{\sqrt{\Delta x^2 + h^2 \Delta n^2}}{h|\Delta n|} \right) &= \ln \left(\frac{h}{\pi \Delta x} \sinh \left(\pi \frac{\Delta x}{h} \right) \right) \quad (\text{B.15}) \\ \sum_{\Delta n=-\infty}^{\infty} \frac{\Delta x^2}{\Delta x^2 + h^2 \Delta n^2} &= \pi \frac{\Delta x}{h} \coth \left(\pi \frac{\Delta x}{h} \right). \end{aligned}$$

This finally yields

$$\begin{aligned}
 \int dy \int dy' \sum_{n,n' \in \mathbb{N}} \delta(y - hn) \delta(y' - hn') u_{\text{edge}}(x - x', y - y') &= \quad (\text{B.16}) \\
 &= N_y \frac{\mu b^2 L}{2\pi(1-\nu)} \left(\pi \frac{\Delta x}{h} \coth \left(\pi \frac{\Delta x}{h} \right) - \ln \left(2 \sinh \left(\pi \frac{\Delta x}{h} \right) \right) \right) \\
 &\quad - N_y \frac{\mu b^2 L}{2\pi(1-\nu)} \left(N_y + A + \ln \left(\frac{h}{2\pi s_0} \right) \right),
 \end{aligned}$$

where the last line is a constant independent of $x - x'$. An additive constant in the interaction potential has no physical meaning. Therefore, it will be neglected further on. The interaction potential in the second line of Eq. (B.16) is equal to the interaction energy used in [99, 29] and will be denoted by $u_{\text{wall}}(\Delta x)$ further on.

Appendix C

Details about calculations in Chap. 5

C.1 Macroscopic entropy

The first aim of this appendix is to determine the macroscopic entropy in Eq. 5.16. Combining Eqs. (5.4a), (5.9), (5.13) and (5.15) yields for the macroscopic entropy

$$S_2(\mathbf{x}_2) = \frac{k_B T_B \ln [Z_B[T_B]] + \bar{E}_B}{T_B} \quad (\text{C.1})$$

$$+ \frac{k_B T_C \ln [Z_C[\mu_b(\mathbf{R}), T_C]] - \sum_b \int d\mathbf{R} \mu_b(\mathbf{R}) \rho_b(\mathbf{R}) + \bar{E}_C}{T_C}.$$

We now recognize $-k_B T_B \ln [Z_B[T_B]]$ as the free energy of the lattice, denoted by $F_B(T_B)$. Moreover, $-k_B T_C \ln [Z_C[\mu_b(\mathbf{R}), T_C]]$ is the grand potential of a dislocation system, controlled by the local chemical potential and the temperature. A Legendre transform to the dislocation density as a variable can be recognized in the above expression, see [23], such that we can identify

$$F_C[\rho_b(\mathbf{R}), T_C] = -k_B T_C \ln [Z_C[\mu_b(\mathbf{R}), T_C]] + \sum_b \int d\mathbf{R} \mu_b(\mathbf{R}) \rho_b(\mathbf{R}), \quad (\text{C.2})$$

where $F_C[\rho_b(\mathbf{R}), T_C]$ is the free energy at a given dislocation density profile and configurational temperature. This directly yields Eq. (5.16).

C.2 Derivation of Eq. (5.19)

The aim of this paragraph is to derive Eq. (5.19). To this end, we calculate

$$\begin{aligned} \nabla_{\mathbf{R}} (\rho_b(\mathbf{R})) &= \int d\mathbf{x}_1 \sum_{i, b(i)=b} \nabla_{\mathbf{R}} (\delta(\mathbf{R}(i) - \mathbf{R})) \rho_{\mathbf{x}_2}(\mathbf{x}_1) \\ &= \int d\mathbf{x}_1 \sum_{i, b(i)=b} \delta(\mathbf{R}(i) - \mathbf{R}) \nabla_{\mathbf{R}(i)} (\rho_{\mathbf{x}_2}(\mathbf{x}_1)) \\ &= \int d\mathbf{x}_1 \sum_{i, b(i)=b} \delta(\mathbf{R}(i) - \mathbf{R}) \frac{-\frac{\partial \Pi_{\bar{E}_C}}{\partial \mathbf{R}(i)} + \nabla_{\mathbf{R}} (\mu_b[\rho_b, T_C; \mathbf{R}])}{k_B T_C} \rho_{\mathbf{x}_2}(\mathbf{x}_1) \\ &= \frac{1}{k_B T_C} \left\langle \sum_{i, b(i)=b} \delta(\mathbf{R}(i) - \mathbf{R}) \mathbf{F}_{pk}(i) \right\rangle_{\mathbf{x}_2} + \frac{1}{k_B T_C} \rho_b(\mathbf{R}) \nabla_{\mathbf{R}} \left(\frac{\delta \mathcal{F}}{\delta \rho_b(\mathbf{R})} \right), \end{aligned}$$

where in the first equality, we used the definition of $\rho_{\mathbf{b}}$ in Eq. (5.15), in the second equality, we performed a partial integration, in the third equality, we used the expression for the phase space density in Eq. (5.13), and in the fourth that $\frac{\delta \mathcal{F}}{\delta \rho_{\mathbf{b}}(\mathbf{R})} = \mu_{\mathbf{b}}[\rho_{\mathbf{b}}, T_C; \mathbf{R}]$ and that $\frac{d\Pi_{\mathcal{E}_C}}{d\mathbf{R}(i)} = -\mathbf{F}_{pk}(i)$ as in Eq. (5.9). This is the identity in Eq. (5.19).

C.3 Macroscopic response function

To determine the second dynamical response function, \mathbf{K}_2 , the vector $D\Pi(\mathbf{x}_1)$ defined in Eq. (5.4c), is needed. Using Eqs. (5.9), (5.10) and (5.12), it is found that

$$\begin{aligned} \frac{\delta}{\delta \mathbf{x}_1} \cdot \mathbf{M}_1(\mathbf{x}_1) &= \left(\frac{d}{dS_{\text{lat}}} \left(\frac{1}{LB_{\mathbf{b}(i)}(T_{\text{lat}})} \right) \hat{\mathbf{s}}_{\mathbf{b}(i)} (\hat{\mathbf{s}}_{\mathbf{b}(i)} \cdot \mathbf{F}_{pk}(i)) \right), \\ &+ \sum_i \frac{\left(\hat{\mathbf{s}}_{\mathbf{b}(i)} \cdot \frac{d}{d\mathbf{R}(i)} \right) (\hat{\mathbf{s}}_{\mathbf{b}(i)} \cdot \mathbf{F}_{pk}(i))}{LB_{\mathbf{b}(i)}(T_{\text{lat}})} + \sum_i \frac{d}{dS_{\text{lat}}} \left(\frac{1}{T_{\text{lat}} LB_{\mathbf{b}(i)}(T_{\text{lat}})} \right) (\hat{\mathbf{s}}_{\mathbf{b}(i)} \cdot \mathbf{F}_{pk}(i))^2 \Big)^T \\ \mathbf{M}_1(\mathbf{x}_1) : \frac{\delta^2 \Pi}{\delta \mathbf{x}_1 \delta \mathbf{x}_1} &= \left(\begin{array}{c} \sum_{\mathbf{b}(i)=\mathbf{b}} \frac{T_{\text{lat}}}{LB_{\mathbf{b}(i)}(T_{\text{lat}})} (\hat{\mathbf{s}}_{\mathbf{b}(i)} \cdot \nabla)^2 \delta(\mathbf{R}(i) - \mathbf{R}) \\ \frac{dT_{\text{lat}}}{dS_{\text{lat}}} \sum_i \frac{1}{T_{\text{lat}} LB_{\mathbf{b}(i)}(T_{\text{lat}})} (\hat{\mathbf{s}}_{\mathbf{b}(i)} \cdot \mathbf{F}_{pk}(i))^2 \\ \sum_i \frac{T_{\text{lat}}}{LB_{\mathbf{b}(i)}(T_{\text{lat}})} \left(\hat{\mathbf{s}}_{\mathbf{b}(i)} \cdot \frac{d}{d\mathbf{R}(i)} \right) (\hat{\mathbf{s}}_{\mathbf{b}(i)} \cdot \mathbf{F}_{pk}(i)) \end{array} \right), \end{aligned}$$

which yields

$$D\Pi(\mathbf{x}_1) = (-\hat{\mathbf{s}}_{\mathbf{b}} \cdot \nabla (\mathcal{J}_{\mathbf{b}}), \mathcal{P}, -\mathcal{P})^T \quad (\text{C.3})$$

with

$$\begin{aligned} \frac{1}{\tilde{B}_{\mathbf{b}}(T_{\text{lat}})} &\equiv \frac{1}{B_{\mathbf{b}}(T_{\text{lat}})} + k_B \frac{d}{dS_{\text{lat}}} \left(\frac{1}{B_{\mathbf{b}}(T_{\text{lat}})} \right) \\ \mathcal{J}_{\mathbf{b}} &\equiv \frac{1}{L\tilde{B}_{\mathbf{b}}(T_{\text{lat}})} \left(\sum_{i, \mathbf{b}(i)=\mathbf{b}} \delta(\mathbf{R}(i) - \mathbf{R}) (\hat{\mathbf{s}}_{\mathbf{b}} \cdot \mathbf{F}_{pk}(i)) \right) - \frac{k_B T_{\text{lat}}}{LB_{\mathbf{b}}(T_{\text{lat}})} \hat{\mathbf{s}}_{\mathbf{b}} \cdot \nabla \Pi_{\rho_{\mathbf{b}}}(\mathbf{R}) \\ \mathcal{P} &\equiv \sum_i \frac{k_B T_{\text{lat}}}{LB_{\mathbf{b}(i)}(T_{\text{lat}})} \left(\hat{\mathbf{s}}_{\mathbf{b}(i)} \cdot \frac{d}{d\mathbf{R}(i)} \right) (\hat{\mathbf{s}}_{\mathbf{b}(i)} \cdot \mathbf{F}_{pk}(i)) + \sum_i \frac{1}{L\tilde{B}_{\mathbf{b}(i)}(T_{\text{lat}})} (\hat{\mathbf{s}}_{\mathbf{b}(i)} \cdot \mathbf{F}_{pk}(i))^2. \end{aligned}$$

$\tilde{B}_{\mathbf{b}}$ can be evaluated by using the good approximation that $B_{\mathbf{b}}(T_{\text{lat}})$ depends linearly on T_{lat} , and hence that

$$k_B \frac{d}{dS_{\text{lat}}} \left(\frac{1}{B_{\mathbf{b}}(T_{\text{lat}})} \right) \approx -k_B \frac{dT_{\text{lat}}}{dS_{\text{lat}}} \frac{1}{T_{\text{lat}} B_{\mathbf{b}}(T_{\text{lat}})} = -\frac{k_B}{C} \frac{1}{B_{\mathbf{b}}(T_{\text{lat}})}, \quad (\text{C.4})$$

where C is the heat capacity of the lattice. This was obtained using the thermodynamic definition $C \equiv T_{\text{lat}} \frac{dS_{\text{lat}}}{dT_{\text{lat}}}$. For aluminium at room temperature, $C = 24 \text{ J K}^{-1} \text{ mole}^{-1}$ [102], and hence $k_B/C = 5.8 \times 10^{-25}/R$, where R is the number of atoms in the lattice in mole. This implies that the difference between $B_{\mathbf{b}}$ and $\tilde{B}_{\mathbf{b}}$ is negligible.

It will turn out to be convenient to rewrite \mathcal{P} . To this end, we define $\mathbf{F}_{pk}(i) \equiv \delta \mathbf{F}_{pk}(i) + \left\langle \sum_{i, \mathbf{b}(i)=\mathbf{b}} \delta(\mathbf{R}(i) - \mathbf{R}) \mathbf{F}_{pk}(i) \right\rangle_{\mathbf{x}_2} / \rho_{\mathbf{b}}(\mathbf{R})$. Inserting this in the above expression for \mathcal{P} yields the expression in terms of \mathcal{Q} and $\mathcal{J}_{\mathbf{b}}$ in Eq. (5.20).

C.4 Energy evolution

The evolution equations for the energies that follow from Eqs. (5.17), (5.18) and (5.21) read

$$\frac{d\bar{E}_B}{dt} = \sum_b \int d\mathbf{R} \left(-\hat{s}_b \cdot \nabla_{\mathbf{R}} \left(\frac{\delta F_C}{\delta \rho_b(\mathbf{R})} - k_B T_C \log \left[\frac{\rho_b(\mathbf{R})}{\Lambda_b^2} \right] \right) \right) \quad (\text{C.5})$$

$$\begin{aligned} & \frac{\rho_b(\mathbf{R})}{LB_b(T_B)} \left(-\hat{s}_b \cdot \nabla_{\mathbf{R}} \left(\frac{\delta F_C}{\delta \rho_b(\mathbf{R})} \right) \right) \\ & - k_B (T_C - T_B) \sum_b \int d\mathbf{R} \frac{\hat{s}_b \cdot (\boldsymbol{\Sigma} \cdot \mathbf{b} \times \hat{\boldsymbol{\xi}})}{LB_b(T_{\text{lat}})} \hat{s}_b \cdot \nabla_{\mathbf{R}} \rho_b(\mathbf{R}) \\ & - k_B (T_C - T_B) \sum_{bb'} \int d\mathbf{R} d\mathbf{R}' \frac{\hat{s}_b \cdot \mathbf{F}_{\text{int}}^{bb'}(\mathbf{R}, \mathbf{R}')}{LB_b(T_{\text{lat}})} \hat{s}_b \cdot \nabla_{\mathbf{R}} \rho_{bb'}^{(2)}(\mathbf{R}, \mathbf{R}') \\ & + \frac{1}{k_B T_C} \sum_{b'} \int_0^{\tau'} d\Delta t \langle\langle \mathcal{P}(0), \mathcal{J}_{b'}(\mathbf{R}', \Delta t) \rangle\rangle \left(-\hat{s}_{b'} \cdot \nabla_{\mathbf{R}'} \left(\frac{\delta F_C(t - \Delta t)}{\delta \rho_{b'}(\mathbf{R}')} \right) \right) \\ & + \int_0^{\tau''} d\Delta t \langle\langle \mathcal{P}(0), \mathcal{P}(\Delta t) \rangle\rangle \left(\frac{1}{k_B T_B(t - \Delta t)} - \frac{1}{k_B T_C(t - \Delta t)} \right) \\ \frac{d\bar{E}_C}{dt} & = -\frac{d\bar{E}_B}{dt}, \end{aligned} \quad (\text{C.6})$$

where we have used the following identity to rewrite $\left\langle \sum_{i, b(i)=b} (\hat{s}_b \cdot \mathbf{F}_{pk}(i))^2 \right\rangle_{\mathbf{x}_2}$:

$$0 = (k_B T_C)^2 \int d\mathbf{x}_1 \sum_{i, b(i)=b} \left(\hat{s}_b \cdot \frac{\partial}{\partial \mathbf{R}(i)} \right)^2 \rho_{\mathbf{x}_2}(\mathbf{x}_1) \quad (\text{C.7})$$

$$\begin{aligned} & = \int d\mathbf{x}_1 \sum_{i, b(i)=b} \left(\hat{s}_b \cdot \mathbf{F}_{pk}(i) + \int d\mathbf{R} \hat{s}_b \cdot \nabla_{\mathbf{R}} (\mu_b(\mathbf{R})) \delta(\mathbf{R}(i) - \mathbf{R}) \right)^2 \rho_{\mathbf{x}_2}(\mathbf{x}_1) \\ & + k_B T_C \int d\mathbf{x}_1 \left(\sum_{i, b(i)=b} \hat{s}_b \cdot \frac{\partial}{\partial \mathbf{R}(i)} (\hat{s}_b \cdot \mathbf{F}_{pk}(i)) \right. \\ & \quad \left. - \int d\mathbf{R} \hat{s}_b \cdot \nabla_{\mathbf{R}} (\mu_b(\mathbf{R})) \hat{s}_b \cdot \nabla_{\mathbf{R}} \delta(\mathbf{R}(i) - \mathbf{R}) \right) \rho_{\mathbf{x}_2}(\mathbf{x}_1) \end{aligned} \quad (\text{C.8})$$

$$\begin{aligned} & = \left\langle \sum_{i, b(i)=b} (\hat{s}_b \cdot \mathbf{F}_{pk}(i))^2 \right\rangle_{\mathbf{x}_2} + \int d\mathbf{R} \hat{s}_b \cdot \nabla_{\mathbf{R}} (\mu_b(\mathbf{R})) \left\langle \sum_{i, b(i)=b} \delta(\mathbf{R}(i) - \mathbf{R}) \mathbf{F}_{pk}(i) \right\rangle_{\mathbf{x}_2} \\ & + k_B T_C \left\langle \sum_{i, b(i)=b} \hat{s}_b \cdot \frac{\partial}{\partial \mathbf{R}(i)} (\hat{s}_b \cdot \mathbf{F}_{pk}(i)) \right\rangle_{\mathbf{x}_2}. \end{aligned} \quad (\text{C.9})$$

For Eq. (C.8), we performed the derivative wrt. $\mathbf{R}(i)$ and for Eq. (C.9), we did the averaging and used Eq. (5.19). The last contribution can be rewritten further using a

split of the Peach-Koehler force into a part due to loading and a part due to interactions between dislocations. This yields

$$\begin{aligned}
& \left\langle \sum_{i, \mathbf{b}(i)=\mathbf{b}} \hat{\mathbf{s}}_{\mathbf{b}} \cdot \frac{\partial}{\partial \mathbf{R}(i)} (\hat{\mathbf{s}}_{\mathbf{b}} \cdot \mathbf{F}_{pk}(i)) \right\rangle_{\mathbf{x}_2} = \\
& \left\langle \sum_{i, \mathbf{b}(i)=\mathbf{b}} \hat{\mathbf{s}}_{\mathbf{b}} \cdot \frac{\partial}{\partial \mathbf{R}(i)} \left(\int d\mathbf{R} \delta(\mathbf{R}(i) - \mathbf{R}) \hat{\mathbf{s}}_{\mathbf{b}} \cdot (\boldsymbol{\Sigma} \cdot \mathbf{b} \times \hat{\boldsymbol{\xi}}) \right. \right. \\
& \quad \left. \left. + \sum_{\mathbf{b}'} \sum_{i', \mathbf{b}(i')=\mathbf{b}'} \int d\mathbf{R} d\mathbf{R}' \hat{\mathbf{s}}_{\mathbf{b}} \cdot \mathbf{F}_{int}^{bb'}(\mathbf{R}, \mathbf{R}') \delta(\mathbf{R}(i) - \mathbf{R}) \delta(\mathbf{R}(i') - \mathbf{R}') \right) \right\rangle_{\mathbf{x}_2} \\
& = - \int d\mathbf{R} \hat{\mathbf{s}}_{\mathbf{b}} \cdot (\boldsymbol{\Sigma} \cdot \mathbf{b} \times \hat{\boldsymbol{\xi}}) \hat{\mathbf{s}}_{\mathbf{b}} \cdot \nabla_{\mathbf{R}} \rho_{\mathbf{b}}(\mathbf{R}) \\
& \quad - \sum_{\mathbf{b}'} \int d\mathbf{R} d\mathbf{R}' \hat{\mathbf{s}}_{\mathbf{b}} \cdot \mathbf{F}_{int}^{bb'}(\mathbf{R}, \mathbf{R}') \hat{\mathbf{s}}_{\mathbf{b}} \cdot \nabla_{\mathbf{R}} \rho_{\mathbf{b}\mathbf{b}'}^{(2)}(\mathbf{R}, \mathbf{R}'),
\end{aligned}$$

where $\mathbf{F}_{int}^{bb'}(\mathbf{R}, \mathbf{R}')$ is the force of a dislocation with Burgers vector \mathbf{b}' at \mathbf{R}' , and where the two-point density is defined by $\rho_{\mathbf{b}\mathbf{b}'}^{(2)}(\mathbf{R}, \mathbf{R}') = \left\langle \sum_{i, i', i \neq i'} \delta(\mathbf{R}(i) - \mathbf{R}) \delta(\mathbf{R}(i') - \mathbf{R}') \right\rangle_{\mathbf{x}_2}$.

The different terms in Eq. (C.5) can be interpreted as follows: the first line is the average Peach-Koehler force times the flux due to free energy gradients. The second and third line reflect the correlation in driving force and flux. The fourth line is an emergent heat flux due to correlations in fluctuations of the heat- and dislocation flux, and the fifth line is the energy flux due to differences in inverse temperature between the two reservoirs.

C.5 A thermodynamic identity

The aim of this section is to show that $\left. \frac{\partial T_C}{\partial \rho_{\mathbf{b}}(\mathbf{R})} \right|_{\bar{E}_C}$ is large in the limit of weak fluctuations.

To this end, we write

$$\left. \frac{\partial T_C}{\partial \rho_{\mathbf{b}}(\mathbf{R})} \right|_{\bar{E}_C} = - \frac{\left. \frac{\partial \bar{E}_C}{\partial \rho_{\mathbf{b}}(\mathbf{R})} \right|_{T_C}}{\left. \frac{\partial \bar{E}_C}{\partial T_C} \right|_{\rho_{\mathbf{b}}(\mathbf{R})}} = - \int d\mathbf{R}' \frac{\left. \frac{\partial \bar{E}_C}{\partial \mu_{\mathbf{b}}(\mathbf{R}')} \right|_{T_C}}{\left. \frac{\partial \rho_{\mathbf{b}}(\mathbf{R})}{\partial \mu_{\mathbf{b}}(\mathbf{R}')} \right|_{T_C} \left. \frac{\partial \bar{E}_C}{\partial T_C} \right|_{\rho_{\mathbf{b}}(\mathbf{R})}}.$$

These three derivatives can be determined straightforwardly using Eqs. (5.13) and (5.15):

$$\begin{aligned}
\left. \frac{\partial \bar{E}_C}{\partial \mu_{\mathbf{b}}(\mathbf{R}')} \right|_{T_C} &= (\langle \Pi_{\bar{E}_C} \Pi_{\rho_{\mathbf{b}}}(\mathbf{R}') \rangle - \langle \Pi_{\bar{E}_C} \rangle \langle \Pi_{\rho_{\mathbf{b}}}(\mathbf{R}') \rangle) / k_B T_C \\
\left. \frac{\partial \rho_{\mathbf{b}}(\mathbf{R})}{\partial \mu_{\mathbf{b}}(\mathbf{R}')} \right|_{T_C} &= (\langle \Pi_{\rho_{\mathbf{b}}}(\mathbf{R}) \Pi_{\rho_{\mathbf{b}}}(\mathbf{R}') \rangle - \langle \Pi_{\rho_{\mathbf{b}}}(\mathbf{R}) \rangle \langle \Pi_{\rho_{\mathbf{b}}}(\mathbf{R}') \rangle) / k_B T_C \\
\left. \frac{\partial \bar{E}_C}{\partial T_C} \right|_{\rho_{\mathbf{b}}(\mathbf{R})} &= (\langle \Pi_{\bar{E}_C} \Pi_{\bar{E}_C} \rangle - \langle \Pi_{\bar{E}_C} \rangle \langle \Pi_{\bar{E}_C} \rangle) / k_B T_C^2.
\end{aligned}$$

When the correlations are weak, these three derivatives are all small, and hence $\left. \frac{\partial T_C}{\partial \rho_b(\mathbf{R})} \right|_{\bar{E}_C}$ is large.

Appendix D

Details about calculations in Chap. 6

D.1 Derivation of the density evolution equation

In this section, Eq. (6.2) is derived from the results in Chap. 5. In that work, the dominant contributions to the evolution equation of the dislocation density read, see Eq. (5.22)

$$\begin{aligned} \frac{\partial \rho_{\mathbf{b}}(\mathbf{R})}{\partial t} = & -\hat{\mathbf{s}}_{\mathbf{b}} \cdot \nabla_{\mathbf{R}} \int_0^{\tau_2} d\Delta t \left\{ \sum_{\mathbf{b}'} \int d\mathbf{R}' \frac{\langle\langle \mathcal{J}_{\mathbf{b}}(\mathbf{R}, 0), \mathcal{J}_{\mathbf{b}'}(\mathbf{R}', \Delta t) \rangle\rangle}{k_B T_C} \right. \\ & \left. \left(-\hat{\mathbf{s}}_{\mathbf{b}'} \cdot \nabla_{\mathbf{R}'} \frac{\delta F_C(t - \Delta t)}{\delta \rho_{\mathbf{b}'}(\mathbf{R}')} \Big|_{T_C} \right) \right. \\ & \left. + \langle\langle \mathcal{J}_{\mathbf{b}}(\mathbf{R}, 0), \mathcal{P}(\Delta t) \rangle\rangle \left(\frac{1}{k_B T_B(t - \Delta t)} - \frac{1}{k_B T_C(t - \Delta t)} \right) \right\}, \end{aligned} \quad (\text{D.1})$$

with $\mathcal{J}_{\mathbf{b}}(\mathbf{R}) = \sum_{i, \mathbf{b}(i)=\mathbf{b}} \delta(\mathbf{R}(i) - \mathbf{R})v(i)$ and $\mathcal{P} = \sum_{\mathbf{b}} \sum_{i, \mathbf{b}(i)=\mathbf{b}} \frac{(\hat{\mathbf{s}}_{\mathbf{b}} \cdot \mathbf{F}_{pk}(i))^2}{LB_{\mathbf{b}}(T_B)}$, where the double brackets $\langle\langle \dots, \dots \rangle\rangle$ denote the correlation of fluctuations; $\langle\langle A, B \rangle\rangle = \langle(A - \langle A \rangle), (B - \langle B \rangle)\rangle$. In Chap. 5, this equation was further simplified using a decomposition of \mathcal{P} . Here however a slightly different decomposition is chosen, which is more convenient in a numerical setting.

The first contribution in Eq. (D.1) can be simplified by using a local approximation, in which we write

$$\begin{aligned} \int d\mathbf{R}' \frac{\langle\langle \mathcal{J}_{\mathbf{b}}(\mathbf{R}, 0), \mathcal{J}_{\mathbf{b}'}(\mathbf{R}', \Delta t) \rangle\rangle}{k_B T_C} \left(-\hat{\mathbf{s}}_{\mathbf{b}'} \cdot \nabla_{\mathbf{R}'} \frac{\delta F_C(t - \Delta t)}{\delta \rho_{\mathbf{b}'}(\mathbf{R}')} \right) \\ \approx \frac{H_{\mathbf{b}\mathbf{b}'}^{(0)}(\Delta t)}{2k_B T_C} \left(-\hat{\mathbf{s}}_{\mathbf{b}} \cdot \nabla_{\mathbf{R}} \frac{\delta F_C(t - \Delta t)}{\delta \rho_{\mathbf{b}}(\mathbf{R})} \right) \end{aligned} \quad (\text{D.2})$$

with

$$H_{\mathbf{b}\mathbf{b}'}^{(0)}(\Delta t) \equiv 2 \int d\mathbf{R}' \langle\langle \mathcal{J}_{\mathbf{b}}(\mathbf{R}, 0), \mathcal{J}_{\mathbf{b}'}(\mathbf{R}', \Delta t) \rangle\rangle.$$

Furthermore, using translational invariance, $H_{\mathbf{b}\mathbf{b}'}^{(0)}(\Delta t)$ can be rewritten as

$$\begin{aligned} H_{\mathbf{b}\mathbf{b}'}^{(0)}(\Delta t) &= \frac{2}{\Omega} \int d\mathbf{R} \int d\mathbf{R}' \langle\langle \mathcal{J}_{\mathbf{b}}(\mathbf{R}, 0), \mathcal{J}_{\mathbf{b}'}(\mathbf{R}', \Delta t) \rangle\rangle \\ &= \frac{2}{\Omega} \left\langle\left\langle \sum_{i, \mathbf{b}(i)=\mathbf{b}} v(i, 0), \sum_{i', \mathbf{b}(i')=\mathbf{b}'} v(i', \Delta t) \right\rangle\right\rangle, \end{aligned}$$

which is equal to the definition in Eq. (6.3). To simplify $\langle\langle \mathcal{J}_b(\mathbf{R}, 0), \mathcal{P}(\Delta t) \rangle\rangle$, use is made of

$$\begin{aligned} \mathcal{P} - \langle \mathcal{P} \rangle &= 2 \sum_{\mathbf{b}} \langle \hat{\mathbf{s}}_{\mathbf{b}} \cdot \mathbf{F}_{pk} \rangle \sum_{i, \mathbf{b}(\hat{i})=\mathbf{b}} (v(i) - \langle v(i) \rangle) + \sum_{\mathbf{b}} \mathcal{R}_{\mathbf{b}} - \langle \mathcal{R}_{\mathbf{b}} \rangle \\ \text{with } \mathcal{R}_{\mathbf{b}} &= \sum_{i, \mathbf{b}(\hat{i})=\mathbf{b}} (v(i) - \langle v \rangle) (\hat{\mathbf{s}}_{\mathbf{b}} \cdot \mathbf{F}_{pk}(i) - \hat{\mathbf{s}}_{\mathbf{b}} \cdot \langle \mathbf{F}_{pk} \rangle). \end{aligned}$$

This implies, together with translational invariance, that

$$\langle\langle \mathcal{J}_b(\mathbf{R}, 0), \mathcal{P}(\Delta t) \rangle\rangle = \sum_{\mathbf{b}} H_{bb'}^{(0)}(\Delta t) \langle \hat{\mathbf{s}}_{\mathbf{b}} \cdot \mathbf{F}_{pk} \rangle + \frac{2}{\Omega} \sum_{\mathbf{b}} \left\langle \left\langle \sum_{i, \mathbf{b}(\hat{i})=\mathbf{b}} v(i, 0), \mathcal{R}_{\mathbf{b}}(\Delta t) \right\rangle \right\rangle. \quad (\text{D.3})$$

Note that $v(i) - \langle v \rangle$ is linear in the velocity fluctuations, while $\mathcal{R}_{\mathbf{b}} - \langle \mathcal{R}_{\mathbf{b}} \rangle$ is quadratic in these fluctuations. Therefore, the second contribution is odd in the fluctuations, and is expected to vanish. This has been verified numerically.

To simplify further, we use a relation between the expectation value of the Peach-Koehler force and the free energy derivative. By integrating Eq. 5.19 over space and by assuming that the system is translationally invariant, it is found that

$$\langle \hat{\mathbf{s}}_{\mathbf{b}} \cdot \mathbf{F}_{pk} \rangle = -\hat{\mathbf{s}}_{\mathbf{b}} \cdot \nabla_{\mathbf{R}} \left(\left. \frac{\delta F_C(t - \Delta t)}{\delta \rho_{\mathbf{b}}(\mathbf{R})} \right|_{T_C} - k_B T_C \log \left[\frac{\rho_{\mathbf{b}}(\mathbf{R})}{\Lambda_{\mathbf{b}}^2} \right] \right). \quad (\text{D.4})$$

Combining Eqs. (D.1,D.2,D.3) then yields

$$\begin{aligned} \frac{\partial \rho_{\mathbf{b}}(\mathbf{R})}{\partial t} &= -\hat{\mathbf{s}}_{\mathbf{b}} \cdot \nabla_{\mathbf{R}} \int_0^{\tau_2} d\Delta t \sum_{\mathbf{b}'} \int d\mathbf{R}' H_{bb'}^{(0)}(\Delta t) \\ &\left(-\hat{\mathbf{s}}_{\mathbf{b}} \cdot \nabla_{\mathbf{R}} \left(\left(\frac{1}{k_B T_B} - \frac{1}{2k_B T_C} \right) \left. \frac{\delta F_C(t - \Delta t)}{\delta \rho_{\mathbf{b}}(\mathbf{R})} \right|_{T_C} - k_B (T_C - T_B) \log \left[\frac{\rho_{\mathbf{b}}(\mathbf{R})}{\Lambda_{\mathbf{b}}^2} \right] \right) \right). \end{aligned} \quad (\text{D.5})$$

Accounting for $T_C \gg T_B$, and by defining $\frac{\delta \bar{F}}{\delta \rho_{\mathbf{b}}(\mathbf{R})} = \left. \frac{\delta F_C(t - \Delta t)}{\delta \rho_{\mathbf{b}}(\mathbf{R})} \right|_{T_C} - k_B (T_C - T_B) \log \left[\frac{\rho_{\mathbf{b}}(\mathbf{R})}{\Lambda_{\mathbf{b}}^2} \right]$, this yields Eq. (6.2).

D.2 Derivation of τ_{relax}

The aim of this section is to derive τ_{relax} in Eq. (6.9). To this end, the free energy expression for a single slip system as in Chap. 3 Eq. (4.17) is used. The density of dislocations with Burgers vector \mathbf{b} is $\rho_{\mathbf{b}}(\mathbf{R}) = \rho_0 + \delta \rho(\mathbf{R})$, and $\rho_{-\mathbf{b}}(\mathbf{R}) = \rho_0$. Then, the

driving force for dislocation dynamics reads

$$-\hat{s}_{\mathbf{b}} \cdot \nabla_{\mathbf{R}} \left(\frac{\delta \tilde{F}(t)}{\delta \rho_{\mathbf{b}}(\mathbf{R})} \right) = L \hat{s}_{\mathbf{b}} \cdot ((\boldsymbol{\Sigma} + \delta \boldsymbol{\sigma}(\mathbf{R})) \cdot \mathbf{b} \times \hat{z}) - \frac{\mu b^2 L}{(1-\nu) 2\rho_0} \hat{s}_{\mathbf{b}} \cdot \nabla_{\mathbf{R}} \delta \rho(\mathbf{R}) + \frac{k_B T_B}{\rho_0(\mathbf{R})} \hat{s}_{\mathbf{b}} \cdot \nabla_{\mathbf{R}} \delta \rho(\mathbf{R}) \quad (\text{D.6})$$

$$-\hat{s}_{-\mathbf{b}} \cdot \nabla_{\mathbf{R}} \left(\frac{\delta \tilde{F}(t)}{\delta \rho_{-\mathbf{b}}(\mathbf{R})} \right) = L \hat{s}_{\mathbf{b}} \cdot ((\boldsymbol{\Sigma} + \delta \boldsymbol{\sigma}(\mathbf{R})) \cdot \mathbf{b} \times \hat{z}) + \frac{\mu b^2 L}{(1-\nu) 2\rho_0} \hat{s}_{\mathbf{b}} \cdot \nabla_{\mathbf{R}} \delta \rho(\mathbf{R}),$$

where $\boldsymbol{\Sigma}$ is the macroscopically imposed stress field and $\delta \boldsymbol{\sigma}(\mathbf{R})$ is the stress field induced by $\delta \rho(\mathbf{R})$, and where it was used that $\hat{s}_{\mathbf{b}} = -\hat{s}_{-\mathbf{b}}$. Using this, the first order terms in $\delta \rho(\mathbf{R})$ in Eq. (6.7a) read

$$\begin{aligned} \frac{\partial \delta \rho(\mathbf{R})}{\partial t} &= -\hat{s}_{\mathbf{b}} \cdot \nabla_{\mathbf{R}} \left(\sum_{\mathbf{b}'} \frac{\Gamma_{\text{eff}, \mathbf{b}\mathbf{b}'}}{k_B T_B} \left(-\hat{s}_{\mathbf{b}'} \cdot \nabla_{\mathbf{R}} \left(\frac{\delta \tilde{F}(t)}{\delta \rho_{\mathbf{b}'}(\mathbf{R})} \right) \right) \right) \quad (\text{D.7}) \\ &= \frac{1}{k_B T_B} \frac{d\Gamma_{\text{eff}}}{d\rho_{\mathbf{b}}(\mathbf{R})} (-\hat{s}_{\mathbf{b}} \cdot \nabla_{\mathbf{R}} \delta \rho(\mathbf{R})) (2L \hat{s}_{\mathbf{b}} \cdot (\boldsymbol{\Sigma} \cdot \mathbf{b} \times \hat{z})) \\ &\quad + \frac{\Gamma_{\text{eff}}}{k_B T_B} \left(-\hat{s}_{\mathbf{b}} \cdot \nabla_{\mathbf{R}} (2L \hat{s}_{\mathbf{b}} \cdot \delta \boldsymbol{\sigma}(\mathbf{R}) \cdot \mathbf{b} \times \hat{z}) - \frac{k_B T_B}{\rho_0} (\hat{s}_{\mathbf{b}} \cdot \nabla_{\mathbf{R}})^2 \delta \rho(\mathbf{R}) \right), \end{aligned}$$

where we have used that $\Gamma_{\text{eff}, \mathbf{b}\mathbf{b}} = \Gamma_{\text{eff}, \mathbf{b}-\mathbf{b}}$. To proceed, we assume that $d\Gamma_{\text{eff}}/d\rho_{\mathbf{b}}(\mathbf{R})$ is of order $\Gamma_{\text{eff}}/\rho_{\mathbf{b}}(\mathbf{R})$, which is the case when Γ_{eff} depends on $\rho_{\mathbf{b}}(\mathbf{R})$ via a powerlaw. Furthermore, one could argue that the typical magnitude of $|\hat{s}_{\mathbf{b}} \cdot \nabla_{\mathbf{R}}(\boldsymbol{\sigma}(\mathbf{R}))| \approx 2\mu|\nabla \wedge \boldsymbol{\Delta}| = 2\mu b \delta \rho_{\mathbf{b}}(\mathbf{R})$, where $\boldsymbol{\Delta}$ is the elastic strain field. Finally, the typical length scale associated with the density fluctuation is denoted by κ^{-1} . This finally yields

$$\left| \frac{\partial \delta \rho(\mathbf{R})}{\partial t} \right| = \Gamma_{\text{eff}} \left(\frac{2bL\Sigma_{\text{res}}\kappa}{k_B T_B \rho_0} + \frac{2\mu b^2 L}{k_B T_B} + \frac{\kappa^2}{\rho_0} \right) |\delta \rho_{\mathbf{b}}(\mathbf{R})|. \quad (\text{D.8})$$

To estimate which of the three terms in the bracket on the RHS is dominant, we first note that $\kappa^{-1} > R$, as the dislocation density cannot vary on distances smaller than the dislocation spacing. The ratio between the first two terms is then $S\kappa R/(1-\nu)$, which is smaller than 1 (note that S is most likely of order 1, see discussion in Sec. 6.4.3). Moreover, one could estimate that $\mu b^2 L/k_B T_B > 2.4 \times 10^2$ (see Sec. 6.4.1), which implies that the second term is larger than the third. We thus conclude that the second term is dominant, and that $\tau_{\text{relax}}^{-1} = \Gamma_{\text{eff}} \frac{2\mu b^2 L}{k_B T_B}$.

D.3 Derivation of the force between dislocations

In this section, Eq. (D.10) is derived from [70]. To this end, the Peach-Koehler force on a dislocation resulting from an infinite array of dislocations as depicted in fig. D.1 is determined first. The stress field due to an infinite, horizontal array of tilted dislocations was determined in [70]. The Peach-Koehler force on the dislocation as a result of this

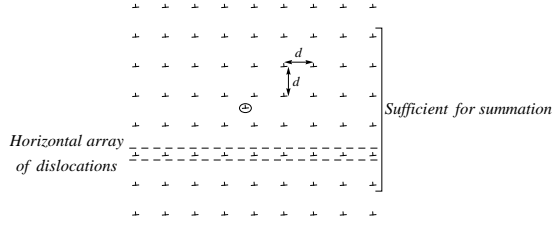


Figure D.1: Sketch of the grids of dislocations. Horizontal arrays of dislocations are indicated. The aim of this appendix is to determine the interaction force and energy between the marked dislocation and the infinite array of dislocations.

stress reads

$$\begin{aligned}
 \mathbf{F}_{\text{PK,array}}(\Delta\check{x}_{ii'}, \Delta\check{y}_{ii'}) = \mathbf{b}(i) \cdot \boldsymbol{\sigma}_{\text{array}}(\mathbf{R}(i)) \times \hat{\mathbf{z}} = \frac{\mu b(i)b(i')L}{2(1-\nu)d} & \left(\left(\frac{\sin(\Delta\check{x}_{ii'})}{\cosh(\Delta\check{y}_{ii'}) - \cos(\Delta\check{x}_{ii'})} \right) \right. \\
 + \cos(2\phi) & \left(-\frac{\Delta\check{y}_{ii'}(\cosh(\Delta\check{y}_{ii'})\cos(\Delta\check{x}_{ii'})-1)}{(\cosh(\Delta\check{y}_{ii'})-\cos(\Delta\check{x}_{ii'}))^2} + \frac{\sinh(\Delta\check{y}_{ii'})}{\cosh(\Delta\check{y}_{ii'})-\cos(\Delta\check{x}_{ii'})} \right) \\
 + \sin(2\phi) & \left(\frac{-\Delta\check{y}_{ii'}(\cosh(\Delta\check{y}_{ii'})\cos(\Delta\check{x}_{ii'})-1)}{(\cosh(\Delta\check{y}_{ii'})-\cos(\Delta\check{x}_{ii'}))^2} - \frac{\sin(\Delta\check{x}_{ii'})}{\cosh(\Delta\check{y}_{ii'})-\cos(\Delta\check{x}_{ii'})} \right) \Bigg) \quad (\text{D.9})
 \end{aligned}$$

where $\Delta\check{x}_{ii'} = \frac{2\pi(x_i - x'_i)}{d}$ and $\Delta\check{y}_{ii'} = \frac{2\pi(y_i - y'_i)}{d}$ are the position differences. Obviously, this function is periodic in $\Delta\check{x}_{ii'}$, as expected.

Now, to obtain the force due to the grid of dislocations, these forces are summed over multiple horizontal arrays with an equal number of arrays on the top and bottom side, as in fig. D.1. It was indicated by Kuykendall and Cai [70] that it is in practice therefore sufficient to sum over only three planes up and down.

The velocity in the glide plane due to this force is due to the component of the force in the slip direction $\hat{\mathbf{s}}_{\pm} = \pm(\cos(\phi), \sin(\phi))$. Hence the velocity of the i^{th} dislocation due to the applied load and the other dislocations reads:

$$\begin{aligned}
 v(i) = \frac{b\Sigma_{\text{res}}}{B_{\mathbf{b}(i)}(T_B)} & \quad (\text{D.10}) \\
 + \frac{\mu b^2}{2(1-\nu)dB_{\mathbf{b}(i)}(T_B)} \sum_{i'} \sum_{k=-\infty}^{\infty} \frac{b(i')}{|b(i')|} & \left(\frac{\sin(\Delta\check{x}_{ii'})}{\cosh(\Delta\check{y}_{ii'}^k) - \cos(\Delta\check{x}_{ii'})} \cos(\phi) \cos(2\phi) \right. \\
 - \frac{\Delta\check{y}_{ii'}^k \sinh(\Delta\check{y}_{ii'}^k) \sin(\Delta\check{x}_{ii'})}{(\cosh(\Delta\check{y}_{ii'}^k) - \cos(\Delta\check{x}_{ii'}))^2} \cos(3\phi) & + \frac{\sinh(\Delta\check{y}_{ii'}^k)}{\cosh(\Delta\check{y}_{ii'}^k) - \cos(\Delta\check{x}_{ii'})} \cos(\phi) \sin(2\phi) \\
 + \Delta\check{y}_{ii'}^k \frac{1 - \cosh(\Delta\check{y}_{ii'}^k) \cos(\Delta\check{x}_{ii'})}{(\cosh(\Delta\check{y}_{ii'}^k) - \cos(\Delta\check{x}_{ii'}))^2} & \left. \sin(\phi)(1 + 2\cos(2\phi)) \right),
 \end{aligned}$$

where $\Delta\check{y}_{ii'}^k = \frac{2\pi(y_i - y'_i + kd)}{d}$.

Appendix E

Details about the complete set of evolution equations

E.1 Temperature evolution

In this appendix, the evolution equations for the configurational temperature T_C will be derived to obtain the complete set of evolution equations as presented in 7.1. To this end, the decomposition proposed in Appendix D.1 is employed. First, we rewrite $\langle\langle \mathcal{P}(0), \mathcal{P}(\Delta t) \rangle\rangle$, which reads upon ignoring the odd terms in the fluctuations:

$$\langle\langle \mathcal{P}(0), \mathcal{P}(\Delta t) \rangle\rangle = 2\Omega \sum_{\mathbf{b}, \mathbf{b}'} \langle \hat{\mathbf{s}}_{\mathbf{b}} \cdot \mathbf{F}_{pk}(0) \rangle H_{\mathbf{b}\mathbf{b}'}^{(0)}(\Delta t) \langle \hat{\mathbf{s}}_{\mathbf{b}'} \cdot \mathbf{F}_{pk}(\Delta t) \rangle + K(\Delta t), \quad (\text{E.1})$$

where $K(\Delta t) \equiv \sum_{\mathbf{b}, \mathbf{b}'} \langle\langle \mathcal{R}_{\mathbf{b}}, \mathcal{R}_{\mathbf{b}'} \rangle\rangle$. The evolution equation for the configurational energy then follow by combining Eqs. (5.16-5.21) and D.3:

$$\begin{aligned} \frac{d\bar{E}_C}{dt} &= \frac{2}{T_B} \sum_{\mathbf{b}, \mathbf{b}'} \int d\mathbf{R} \langle \hat{\mathbf{s}}_{\mathbf{b}} \cdot \mathbf{F}_{pk}(t) \rangle H_{\mathbf{b}\mathbf{b}'}^{(0)}(\Delta t) \hat{\mathbf{s}}_{\mathbf{b}'} \cdot \nabla_{\mathbf{R}} \left(\frac{\delta \tilde{F}(t - \Delta t)}{\delta \rho_{\mathbf{b}'}(\mathbf{R})} \right) \\ &\quad - K(\Delta t) \left(\frac{1}{T_B} - \frac{1}{T_C} \right). \end{aligned} \quad (\text{E.2})$$

The evolution of T_C now follows from the chain rule:

$$\frac{dT_C}{dt} = \left. \frac{\partial T_C}{\partial \bar{E}_C} \right|_{\rho_{\mathbf{b}}} \frac{d\bar{E}_C}{dt} + \sum_{\mathbf{b}} \int d\mathbf{R} \left. \frac{\delta T_C}{\delta \rho_{\mathbf{b}}(\mathbf{R})} \right|_{\bar{E}_C} \frac{\partial \rho_{\mathbf{b}}(\mathbf{R})}{\partial t}. \quad (\text{E.3})$$

To proceed, we use $\left. \frac{\delta T_C}{\delta \rho_{\mathbf{b}}(\mathbf{R})} \right|_{\bar{E}_C} = - \left. \frac{\delta \bar{E}_C}{\delta \rho_{\mathbf{b}}(\mathbf{R})} \right|_{T_C} / \left. \frac{d\bar{E}_C}{dT_C} \right|_{\rho_{\mathbf{b}}(\mathbf{R})}$ and Eq. (6.2) to arrive at

$$\begin{aligned} \frac{dT_C}{dt} &= \left[\sum_{\mathbf{b}, \mathbf{b}'} \int d\mathbf{R} \left(2 \langle \hat{\mathbf{s}}_{\mathbf{b}} \cdot \mathbf{F}_{pk}(t) \rangle + \hat{\mathbf{s}}_{\mathbf{b}'} \cdot \nabla_{\mathbf{R}} \left(\left. \frac{\delta \bar{E}_C}{\delta \rho_{\mathbf{b}}(\mathbf{R})} \right|_{T_C} \right) \right) \frac{H_{\mathbf{b}\mathbf{b}'}^{(0)}(\Delta t)}{T_B} \right. \\ &\quad \left. \hat{\mathbf{s}}_{\mathbf{b}'} \cdot \nabla_{\mathbf{R}} \left(\frac{\delta \tilde{F}(t - \Delta t)}{\delta \rho_{\mathbf{b}'}(\mathbf{R})} \right) - K(\Delta t) \left(\frac{1}{T_B} - \frac{1}{T_C} \right) \right] / \left. \frac{\partial \bar{E}_C}{\partial T_C} \right|_{\rho_{\mathbf{b}}}. \end{aligned} \quad (\text{E.4})$$

Now, we can use the thermodynamic relation $\bar{E}_C = F_C[\rho_{\mathbf{b}}(\mathbf{R}), T_C] - T_C \left. \frac{dF_C}{dT_C} \right|_{\rho_{\mathbf{b}}(\mathbf{R})}$, the decomposition of the free energy in a mean-field, a statistical and a many-body contribution (see section 4.3), and the fact that the many-body contribution is almost independent of the temperature (see Eqs. (3.43) and (4.11)). First, this implies that the

configurational heat capacity is the heat capacity of the ideal gas in two dimensions, i.e. $\left. \frac{\partial \bar{E}_C}{\partial T_C} \right|_{\rho_b} = k_B \sum_b N_b$. Second, this can be used to derive

$$\begin{aligned} \hat{s}_{b'} \cdot \nabla_{\mathbf{R}} \left(\left. \frac{\delta \bar{E}_C}{\delta \rho_b(\mathbf{R})} \right|_{T_C} \right) &= \hat{s}_{b'} \cdot \nabla_{\mathbf{R}} \left(\left. \frac{\delta F_C}{\delta \rho_b(\mathbf{R})} \right|_{T_C} - k_B T_C \log \left[\frac{\rho_b(\mathbf{R})}{\rho_{b,0}} \right] \right) \\ &= - \langle \hat{s}_b \cdot \mathbf{F}_{pk}(t) \rangle. \end{aligned} \quad (\text{E.5})$$

Combining this finally yields the evolution equation for T_C presented in section 7.1.

Bibliography

- [1] D. Amit, Y. Goldschmidt, and G. Grinstein. Renormalisation group analysis of the phase transition in the 2D Coulomb gas, Sine-Gordon theory and XY-model. *Journal of Physics A: Mathematical and Theoretical*, 13:585-620, 1980.
- [2] C. Ayas and E. Van der Giessen. Stress relaxation in thin film/substrate systems by grain boundary diffusion: a discrete dislocation framework. *Modelling and Simulation in Materials Science and Engineering*, 17(6):064007, (2009).
- [3] D. J. Bammann. A model of crystal plasticity containing a natural length scale. *Materials Science and Engineering A*, 406-410 (2001).
- [4] S. Bargmann and B. Svendsen. Theoretical and algorithmic GND-based hardening in single crystals. *Journal for Multiscale Computational Engineering*, 10(6):551-565 (2012).
- [5] R. Baskaran, S. Akarapu, S. D. Mesarovic, and H. M. Zbib. Energies and distributions of dislocations in stacked pile-ups. *International Journal of Solids and Structures*, 47(9):1144-1153, (2010).
- [6] C. J. Bayley, W. A. M. Brekelmans, and M. G. D. Geers. A comparison of dislocation induced back stress formulations in strain gradient crystal plasticity. *International Journal of Solids and Structures*, 43:7268-7286, (2006).
- [7] C. J. Bayley, W. A. M. Brekelmans, and M. G. D. Geers. A three-dimensional dislocation field crystal plasticity approach applied to miniaturized structures. *Philosophical Magazine*, 87(8-9):1361-1378, (2007).
- [8] A. N. Beris and B. J. Edwards. *Thermodynamics of flowing systems*. Oxford, 1994.
- [9] E. Bouchbinder. Effective temperature dynamics in an athermal amorphous plasticity theory. *Physical Review E*, 77:051505, (2008).
- [10] E. Bouchbinder and J.S. Langer. Nonequilibrium thermodynamics of driven amorphous materials. II. Effective-temperature theory. *Physical Review E*, 80:031132, (2009).
- [11] L. Burakovsky, D.L. Preston, and R.R. Silbar. Melting as a dislocation-mediated phase transition. *Physical Review B*, 61(22):15011-15018, (2000).
- [12] D. Carlson. On the completeness of the Beltrami stress functions in continuum mechanics. *Journal of Mathematical Analysis and Applications*, 15:311-315, (1966).
- [13] P. Cermelli and G. Leoni. Renormalized Energy and Forces on Dislocations. *SIAM Journal on Mathematical Analysis*, 37(4):1131-1160, (2005).

- [14] P.M. Chaikin and T.C. Lubensky. *Principles of condensed matter physics*. Cambridge University Press, 1995.
- [15] L. F. Cugliandolo, J. Kurchan, and L. Peliti. Energy flow, partial equilibration, and effective temperatures in systems with slow dynamics. *Physical Review E*, 55(4):3898-3914, Apr. 1997.
- [16] J. Deng and A. El-Azab. Mathematical and computational modelling of correlations in dislocation dynamics. *Modelling and Simulation in Materials Science and Engineering*, 17(7):075010, (2009).
- [17] V.S. Deshpande, A. Needleman, and E. Van der Giessen. Discrete dislocation modeling of fatigue crack propagation. *Acta Materialia*, 50(4):831-846, (2002).
- [18] C. Du, PhD Student Eindhoven University of Technology, private communication
- [19] M. Ekh, M. Grymer, K. Runesson, and T. Svedberg. Gradient crystal plasticity as part of the computational modelling of polycrystals. *International Journal for Numerical Methods in Engineering*, 72:197-220, (2007).
- [20] A. El-Azab. Statistical mechanics treatment of the evolution of dislocation distributions in single crystals. *Physical Review B*, 61(18):11956-11966, (2000).
- [21] İ. Ertürk, J.A.W. van Dommelen, and M.G.D. Geers. Energetic dislocation interactions and thermodynamical aspects of strain gradient crystal plasticity theories. *Journal of the Mechanics and Physics of Solids*, 57(11):1801-1814, (2009).
- [22] P. Español and F. Vázquez. Coarse graining from coarse-grained descriptions. *Philosophical transactions of the Royal Society A*, 360:383-94, (2002).
- [23] R. Evans. The nature of the liquid-vapour interface and other topics in the statistical mechanics of non-uniform, classical fluids. *Advances in Physics*, 28(2):143-200, 1979.
- [24] L.P. Evers, W.A.M. Brekelmans, and M.G.D. Geers. Non-local crystal plasticity model with intrinsic SSD and GND effects. *Journal of the Mechanics and Physics of Solids*, 52:2379-2401, (2004).
- [25] L.P. Evers, W.A.M. Brekelmans, and M.G.D. Geers. Scale dependent crystal plasticity framework with dislocation density and grain boundary effects. *International Journal of Solids and Structures*, 41:5209-5230, (2004).
- [26] D. Frenkel, B. Smit. *Understanding Molecular Simulation*. Elsevier, 2002.
- [27] A. Garroni, P.J.P. van Meurs, M.A. Peletier, and L. Scardia. Boundary-layer analysis of a pile-up of walls of edge dislocations at a lock, ArXiv:1502.05805v1 (2015)
- [28] A. Garroni, P.J.P. van Meurs, M. A. Peletier, and L. Scardia. Upscaling of gradient flows describing dislocation dynamics in 2D. *In preparation*.

-
- [29] M. G. D. Geers, R. H. J. Peerlings, M. A. Peletier, and L. Scardia. Asymptotic behaviour of a pile-up of infinite Walls of Edge Dislocations. *Archive for Rational Mechanics and Analysis*, 209(2):495-539, 2013.
- [30] M. R. Gilbert, S. Queyreau, and J. Marian. Stress and temperature dependence of screw dislocation mobility in α -Fe by molecular dynamics. *Physical Review B*, 84(17):174103, (2011).
- [31] M. Grmela and H.C. Öttinger. Dynamics and thermodynamics of complex fluids. I. Development of a general formalism. *Physical Review E*, 56(6):6620-6632, 1997.
- [32] I. Groma. Link between the microscopic and mesoscopic length-scale description of the collective behavior of dislocations. *Physical Review B*, 56(10):5807-5813, 1997.
- [33] I. Groma and P. Balogh. Investigation of dislocation pattern formation in a two-dimensional self-consistent field approximation. *Acta Materialia*, 47(13):3647-3654, (1999).
- [34] I. Groma, F.F. Csikor, and M. Zaiser. Spatial correlations and higher-order gradient terms in a continuum description of dislocation dynamics. *Acta Materialia*, 51(5):1271-1281, (2003).
- [35] I. Groma, G. Györgyi, and B. Kocsis. Debye Screening of Dislocations. *Physical Review Letters*, 96:165503, (2006).
- [36] I. Groma, G. Györgyi, and B. Kocsis. Dynamics of coarse grained dislocation densities from an effective free energy. *Philosophical Magazine*, 87:1185-1199, (2007).
- [37] I. Groma, G. Györgyi, and P.D. Ispánovity. Variational approach in dislocation theory. *Philosophical Magazine*, 90:3679-3695, (2010).
- [38] I. Groma, Z. Vandrus, and P.D. Ispánovity. Scale-free phase field theory of dislocations. *Physical Review Letters*, 114:015503, (2015).
- [39] M. E. Gurtin. On the plasticity of single crystals: free energy, microforces, plastic-strain gradients. *Journal of the Mechanics and Physics of Solids*, 48:989-1036, (2000).
- [40] M. E. Gurtin. A gradient theory of single-crystal viscoplasticity that accounts for geometrically necessary dislocations. *Journal of the Mechanics and Physics of Solids*, 50:5-32, (2002).
- [41] M. E. Gurtin and L. Anand. A theory of strain-gradient plasticity for isotropic, plastically irrotational materials. Part I: Small deformations. *Journal of the Mechanics and Physics of Solids*, 53:1624-1649, (2005).
- [42] M. E. Gurtin, L. Anand, and S. P. Lele. Gradient single-crystal plasticity with free energy dependent on dislocation densities. *Journal of the Mechanics and Physics of Solids*, 55:1853-1878, (2007).

- [43] M. E. Gurtin. A finite-deformation, gradient theory of single-crystal plasticity with free energy dependent on densities of geometrically necessary dislocations. *International Journal of Plasticity*, 24:702-725, (2008).
- [44] M. Gurtin. A finite-deformation, gradient theory of single-crystal plasticity with free energy dependent on the accumulation of geometrically necessary dislocations. *International Journal of Plasticity*, 26:1073-1096, (2010).
- [45] C. L. Hall, S. J. Chapman, and J.R. Ockendon. Asymptotic analysis of a system of algebraic equations arising in dislocation theory *Society for Industrial and Applied Mathematics*, 70(7):2729-2749, (2010).
- [46] C. L. Hall. Asymptotic expressions for the nearest and furthest dislocations in a pile-up against a grain boundary. *Philosophical Magazine*, 90(29):3879-3890, (2010).
- [47] C. L. Hall. Asymptotic analysis of a pile-up of regular edge dislocation walls. *Materials Science and Engineering A*, 530:144-148, 2011.
- [48] J. Hilhorst and A. V. Petukhov. Variable Dislocation Widths in Colloidal Crystals of Soft Thermosensitive Spheres. *Physical Review Letters*, 107:095501, (2011).
- [49] J. P. Hirth and J. Lothe. *Theory of dislocations*. Krieger Publishing Company, Malabar, Florida, second edition, 1982.
- [50] T. Hochrainer, M. Zaiser, and P. Gumbsch. A three-dimensional continuum theory of dislocation systems: kinematics and mean-field formulation. *Philosophical Magazine*, 87:1261-1282, (2007).
- [51] T. Hochrainer, S. Sandfeld, M. Zaiser, and P. Gumbsch. Continuum dislocation dynamics: Towards a physical theory of crystal plasticity. *Journal of the Mechanics and Physics of Solids*, 63:167178, (2013).
- [52] C. Hoheisel, R. Vogelsang, and M. Schoen. Bulk viscosity of the Lennard-Jones fluid for a wide range of states computed by equilibrium molecular dynamics. *The Journal of Chemical Physics*, 87:7195, 1987.
- [53] C. Hoheisel and R. Vogelsang. Thermal transport coefficients for one-and two-component liquids from time correlation functions computed by molecular dynamics. *Computer Physics Reports*, 8(1):1-70, (1988).
- [54] P. Hohenberg and W. Kohn. Inhomogeneous Electron Gas. *Physical Review*, 136(3B), (1964).
- [55] D. Hull and D. J. Bacon. *Introduction to Dislocations*. Elsevier, 1965.
- [56] M. Hütter and T. A. Tervoort. Coarse Graining in Elasto-viscoplasticity : Bridging the Gap from Microscopic Fluctuations to Dissipation. *Advances in applied mechanics*, 42:253-318, (2008).
- [57] M. Hütter and T. A. Tervoort. Statistical-mechanics based modeling of anisotropic viscoplastic deformation. *Mechanics of Materials*, 80:37-51, (2015).

- [58] N. Irani, J.C.C. Remmers, and V.S. Deshpande. A discrete dislocation analysis of hydrogen-assisted mode I fracture. *submitted*, 2015.
- [59] P.D. Ispánovity, I. Groma, G. Györgyi, F.F. Csikor, and D. Weygand. Submicron Plasticity: Yield Stress, Dislocation Avalanches, and Velocity Distribution. *Physical Review Letters*, 105:085503, (2010).
- [60] B. Jouvét and R. Phythian. Quantum aspects of classical and statistical fields. *Physical Review A*, 19(3):1350-1355, (1979).
- [61] H. Kleinert. *Gauge fields in condensed matter*. World Scientific Publishing Co. Pte. Ltd., Singapore, 1989.
- [62] B. Klusemann, S. Bargmann, and B. Svendsen. Two models for gradient inelasticity based on non-convex energy. *Computational Material Science*, 64:96-100, (2012).
- [63] J. M. Kosterlitz and D. J. Thouless. Ordering , metastability and phase transitions in two-dimensional systems. *Journal of Physics C*, 6:1181-1203 (1973).
- [64] E. Kröner. Benefits and shortcomings of the continuous theory of dislocations. *International Journal of Solids and Structures*, 38:1115-1134, (2001).
- [65] L. P. Kubin, G. Canova, M. Condat, B. Devincere, V. Pontikis, and Y. Bréchet. Dislocation Microstructures and Plastic Flow: A 3D Simulation. *Solid State Phenomena*, 23-24:455-472, (1992).
- [66] R. Kubo, M. Toda, and N. Hashitsume. *Non-equilibrium Statistical mechanics, Vol II of Statistical Physics*. Springer, Berlin, second edition, 1991.
- [67] R. Kumar, L. Nicola, and E. Van der Giessen. Density of grain boundaries and plasticity size effects: A discrete dislocation dynamics study. *Materials Science and Engineering: A*, 527:7-15, (2009).
- [68] R. Kumar, F. Székely, and E. Van der Giessen. Modelling dislocation transmission across tilt grain boundaries in 2D. *Computational Materials Science*, 49:46-54, (2010).
- [69] M. Kuroda and V. Tvergaard. A finite deformation theory of higher-order gradient crystal plasticity. *Journal of the Mechanics and Physics of Solids*, 56:2573-2584, (2008).
- [70] W. P. Kuykendall and W. Cai. Conditional convergence in two-dimensional dislocation dynamics. *Modelling and Simulation in Materials Science and Engineering*, 21:055003, (2013).
- [71] L. D. Landau and E. M. Lifshitz. *The Classical Theory of Fields*. Elsevier, fourth rev edition, 1975.
- [72] J.S. Langer. Dynamics of shear-transformation zones in amorphous plasticity: Formulation in terms of an effective disorder temperature. *Physical Review E*, 70:041502, (2004).

- [73] S. Limkumnerd and E. Van der Giessen. Statistical approach to dislocation dynamics: From dislocation correlations to a multiple-slip continuum theory of plasticity. *Physical Review B*, 77:184111, (2008).
- [74] S. Limkumnerd and E. Van der Giessen. Study of size effects in thin films by means of a crystal plasticity theory based on DiFT. *Journal of the Mechanics and Physics of Solids*, 56: 3304-3314, (2008)
- [75] V.A. Lubarda, J.A. Blume, and A. Needleman. An analysis of equilibrium dislocation distributions. *Acta Metallurgica et Materialia*, 41(2):625-642, (1993).
- [76] S. Dj. Mesarovic. Energy, configurational forces and characteristic lengths associated with the continuum description of geometrically necessary dislocations. *International Journal of Plasticity*, 21:1855-1889, (2005).
- [77] S. Dj. Mesarovic, R. Baskaran, and A. Panchenko. Thermodynamic coarsening of dislocation mechanics and the size-dependent continuum crystal plasticity. *Journal of the Mechanics and Physics of Solids*, 58:311-329, (2010).
- [78] S. Mizushima. Dislocation Model of Liquid Structure. *Journal of the Physical Society of Japan*, 15(1):70-77, (1960).
- [79] D. Mordehai, E. Clouet, M. Fivel, and M. Verdier. Introducing dislocation climb by bulk diffusion in discrete dislocation dynamics. *Philosophical Magazine*, 88(6):899-925, 2008.
- [80] F. R. N. Nabarro. *Theory of Crystal Dislocations*. Oxford, 1967.
- [81] D. R. Nelson. Study of melting in two dimensions. *Physical Review B*, 18(5): 2318-2338, 1978.
- [82] D. R. Nelson and B. I. Halperin. Dislocation-mediated melting in two dimensions. *Physical Review B*, 19(5): 257-2484, (1979).
- [83] R. R. Netz. Electrostatics of counter-ions at and between planar charged walls : From Poisson-Boltzmann to the strong-coupling theory. *European Physical Journal E*, 5:557-574, (2001).
- [84] T. Ninomiya. Theory of Melting, Dislocation Model. I. *Journal of the Physical Society of Japan*, 44(1):263-268, 1978.
- [85] J. F. Nye. Some geometrical relations in dislocated crystals. *Acta Metallurgica*, 1:153-162, (1953).
- [86] D. L. Olmsted, L. G. Hector Jr, W. A. Curtin, and R. J. Clifton. Atomistic simulations of dislocation mobility in Al, Ni and Al/Mg alloys. *Modelling and Simulation in Material Science and Engineering*, 13:371-388, (2005).
- [87] H.C. Öttinger. General projection operator formalism for the dynamics and thermodynamics of complex fluids. *Physical Review E*, 57(2):1416-1420, (1998).
- [88] H.C. Öttinger. *Beyond Equilibrium Thermodynamics*. Wiley, 2005.

- [89] H.C. Öttinger and M. Grmela. Dynamics and thermodynamics of complex fluids. II. Illustrations of a general formalism. *Phys Rev E*, 56(6):6633-6655, (1997).
- [90] S. Panyukov and Y. Rabin. Statistical physics of interacting dislocation loops and their effect on the elastic moduli of isotropic solids. *Physical Review B*, 59(21):13657-13671, (1999).
- [91] M. Parrinello and A. Rahman. Strain fluctuations and elastic constants. *The Journal of Chemical Physics*, 76(5):2662-2666, 1982.
- [92] P. Pauš, J. Kratochvíl, and M. Beneš. A dislocation dynamics analysis of the critical cross-slip annihilation distance and the cyclic saturation stress in fcc single crystals at different temperatures. *Acta Materialia*, 61:7917-7923, (2013).
- [93] A. Pertsinidis and X. S. Ling. Diffusion of point defects in two-dimensional colloidal crystals. *Nature*, 413:147-50, (2001).
- [94] J. G. Powles, G. Rickayzen, and D. M. Heyes. Temperatures: old, new and middle aged. *Molecular Physics*, 103(10):1361-1373, (2005).
- [95] O. Punkkinen, A. Naji, R. Podgornik, I. Vattulainen, and P.-L. Hansen. Ionic cloud distribution close to a charged surface in the presence of salt. *Europhysics Letters*, 82:48001, (2008).
- [96] S. Queyreau, J. Marian, M. R. Gilbert, and B. D. Wirth. Edge dislocation mobilities in bcc Fe obtained by molecular dynamics. *Physical Review B*, 84:064106, (2011).
- [97] D. Raabe, F. Roters, F. Barlat, and L. Chen. *Continuum Scale Simulation of Engineering Materials*. Wiley, 2004.
- [98] A. Roy, R.H.J. Peerlings, M.G.D. Geers, and Y. Kasyanyuk. Continuum modeling of dislocation interactions: Why discreteness matters? *Materials Science and Engineering: A*, 486:653-661, (2008).
- [99] L. Scardia, R.H.J. Peerlings, M.A. Peletier, and M.G.D. Geers. Mechanics of dislocation pile-ups: A unification of scaling regimes. *Journal of the Mechanics and Physics of Solids*, 70:42-61, (2014).
- [100] P. Schall, I. Cohen, D. A. Weitz, and F. Spaepen. Visualization of dislocation dynamics in colloidal crystals. *Science*, 305:1944-19488, (2004).
- [101] R. Smallman and A. Ngan. *Physical Metallurgy and Advanced Materials*. Elsevier Science, 2011.
- [102] R. Smallman. *Modern Physical Metallurgy*. Elsevier, eight edition, 2014.
- [103] P. E. Smith and W. F. van Gunsteren. The viscosity of SPC and SPC/E water at 277 and 300 K. *Chemical Physics Letters*, 215(4):315-318, (1993).
- [104] H. T. C. Stoof, K. B. Gubbels, and D. B. M. Dickerscheid. *Ultracold Quantum Fields*. Springer, 2009.

- [105] B. Svendsen. Continuum thermodynamic models for crystal plasticity including the effects of geometrically-necessary dislocations. *Journal of the Mechanics and Physics of Solids*, 50:1297-1329, 2002.
- [106] B. Svendsen and S. Bargmann. On the continuum thermodynamic rate variational formulation of models for extended crystal plasticity at large deformation. *Journal of the Mechanics and Physics of Solids*, 58:1253-1271, (2010).
- [107] M. Tang and J. Marian. Temperature and high strain rate dependence of tensile deformation behavior in single-crystal iron from dislocation dynamics simulations. *Acta Materialia*, 70:123-129, (2014).
- [108] D. Ter Haar, editor. *Collected papers of L.D. Landau*. Pergamon, Oxford, 1965.
- [109] P.R.M. Van Beers. *Multiscale modelling of grain boundary plasticity*. PhD thesis, Eindhoven University of Technology, 2015.
- [110] E. Van der Giessen and A. Needleman. Discrete dislocation plasticity : a simple planar model. *Modelling and Simulation in Material Science and Engineering*, 3:689-735, (1995).
- [111] P. van Meurs and A. Muntean. Upscaling of the dynamics of dislocation walls. *Advances in Mathematical Sciences and Applications*, 24(2):401-414, (2014).
- [112] P. van Meurs, A. Muntean, and M. Peletier. Upscaling of dislocation walls in finite domains. *European Journal of Applied Mathematics*, 25:749-781, (2014).
- [113] V. Vinogradov and J.R. Willis. The pair distribution function for an array of screw dislocations. *International Journal of Solids and Structures*, 45:161-178, (2008).
- [114] L. Šamaj and I. Travenec. Thermodynamic Properties of the Two-Dimensional Two-Component Plasma. *Journal of Statistical Physics*, 101:713-730, (2000).
- [115] C. Walz and M. Fuchs. Displacement field and elastic constants in nonideal crystals. *Physical Review B*, 81:134110, (2010).
- [116] P.B. Wiegmann. One-dimensional Fermi system and plane xy model. *Journal of Physics C: Solid State Physics*, 11:1583-1598, (1978).
- [117] T. Yalcinkaya, W. A. M. Brekelmans, and M. G. D. Geers. Deformation patterning driven by rate dependent non-convex strain gradient plasticity. *Journal of the Mechanics and Physics of Solids*, 59:1-17, (2011).
- [118] T. Yamamoto and T. Izuyama. Statistical Mechanics of the Dislocation System in a Crystal. *Journal of the Physical Society of Japan*, 57(11):3742-3752, (1988).
- [119] S. Yefimov, I. Groma, and E. Van der Giessen. A comparison of a statistical-mechanics based plasticity model with discrete dislocation plasticity calculations. *Journal of the Mechanics and Physics of Solids*, 52:279-300, (2004).

-
- [120] M. Zaiser, M.-C. Miguel, and I. Groma. Statistical dynamics of dislocation systems: The influence of dislocation-dislocation correlations. *Physical Review B*, 64:224102, (2001).
- [121] A. Zee. *Quantum Field Theory*. Princeton University Press, 2003.

Samenvatting voor algemeen publiek

De collectieve dynamica van dislocaties

Staal wordt veel gebruikt in de wereld om ons heen: denk bijvoorbeeld aan bruggen, paperclips en onderdelen in een mobiele telefoon. Aan het staal in verschillende toepassingen worden heel verschillende eisen gesteld. Staal in gereedschap (bijvoorbeeld een boor) moet erg hard zijn en nauwelijks vervormen, terwijl staal voor blikjes sterk vervormd moet kunnen worden tijdens de productie zonder dat het kapot gaat. De verschillen tussen deze soorten staal zijn het resultaat van verschillen in de microstructuur van het staal: de manier waarop het staal is opgebouwd op het kleinste niveau.

Hoewel staal al lang gebruikt wordt, worden er nog steeds nieuwe soorten ontwikkeld. Nieuwe soorten staal hebben een andere microstructuur die zorgt voor een betere sterkte en/of verbeterde vervormingseigenschappen van het staal. Het zoeken naar een microstructuur die de gewenste sterkte en vervormingseigenschappen geeft, is helaas nog een kwestie van uitproberen. Het effect van de microstructuur op de vervormingseigenschappen van staal en andere metalen is nog onvoldoende begrepen om het effect vooraf te kunnen voorspellen. Daarom wordt er veel onderzoek gedaan naar de vervormingsmechanismen van metalen op microniveau.

Dislocaties en vervorming

De atomen in metalen zijn geordend in een rooster. Deze structuur ontstaat wanneer het metaal stolt. Vaak treden hierbij en bij de bewerking van het metaal imperfecties op, waardoor er onder andere lijnvormige defecten in het rooster ontstaan: de zogenoemde dislocaties (zie figuur 1). Een dislocatie wordt gekenmerkt door de lijnrichting en de vector die de vervorming van het rooster aangeeft: de Burgers' vector. Rondom dislocaties is het rooster vervormd.

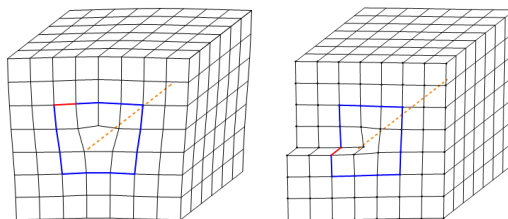


Figure 1: Twee voorbeelden van dislocaties. De oranje lijnen geven de lijnrichting van de dislocaties aan. De rode vectoren zijn de Burgers' vectoren. Dit zijn de vectoren die nodig zijn om de blauwe lus om de dislocatie heen te sluiten. Een dislocatie waarvan de Burgers' vector loodrecht staat op de lijnrichting heet een randdislocatie (links), en n waarvan de Burgers' vector parallel is aan de lijnrichting heet een schroefdislocatie (rechts).

Dislocaties spelen een belangrijke rol bij de vervorming van het metaal. Namelijk, wanneer er een kleine kracht op het materiaal wordt uitgeoefend, wordt het rooster wat opgerekt. We spreken van een elastische vervorming wanneer het materiaal terugvervormt zodra de kracht wordt losgelaten. De dislocatie blijft dan op z'n oorspronkelijke plaats.

Bij een wat grotere opgelegde vervorming kunnen dislocaties gaan bewegen, zich vermenvuldigen of samensmelten, zie bijvoorbeeld figuur 2. Dislocaties bewegen in dit geval vaak niet terug wanneer de opgelegde kracht wordt losgelaten. We spreken dan van een permanente vervorming.

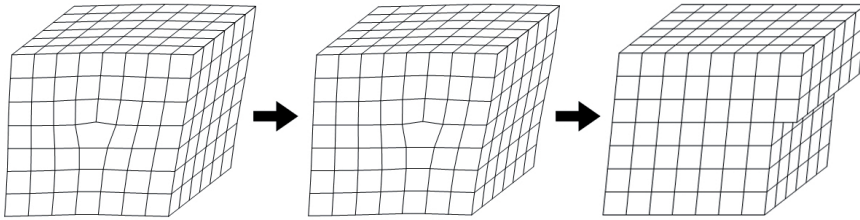


Figure 2: Een randdislocatie in een vervormd rooster. De dislocatie beweegt door de interne spanning in het rooster naar rechts, en bereikt uiteindelijk de rand van het rooster. De dislocatie zal niet terugbewegen, en dus is het materiaal permanent vervormd.

Emergentie

Het effect van een enkele dislocatie op de mechanische eigenschappen van een metaal (elastisch of permanent vervormen) is dus redelijk goed begrepen. Echter, metalen bevatten vaak veel dislocaties (tot wel 1000 kilometer dislocatie-lijn per kubieke millimeter), die elkaar bovendien sterk beïnvloeden. Een dislocatie vervormt namelijk het rooster, maar gaat ook bewegen als gevolg van vervormingen van het rooster, en dus beïnvloeden dislocaties elkaar. Het is daarom mogelijk dat het gezamenlijke gedrag van alle dislocaties samen kenmerken heeft die niet terug te voeren zijn op het gedrag van één geïsoleerde dislocatie. Dit is een voorbeeld van emergentie. Voor de start van dit onderzoek werd al vermoed dat emergente fenomenen belangrijk zijn. Daarom is de hypothese die onderzocht wordt in dit proefschrift:

“Emergente fenomenen in de dynamica van dislocaties bepalen de mechanische eigenschappen van een metaal, meer dan de dynamica van individuele dislocaties.”

Aanpak in dit proefschrift

Om deze hypothese te toetsen is in dit proefschrift de gezamenlijke beweging van alle dislocaties (de zogenoemde collectieve dynamica) afgeleid uit de bekende bewegingsvergelijkingen van individuele dislocaties, en bepaald in hoeverre emergente fenomenen een rol spelen. Voor de afleiding is de GENERIC-methode gebruikt (General Equation for the Non-Equilibrium Reversible-Irreversible Coupling: algemene vergelijking voor de

reversibele-irreversibele koppeling buiten evenwicht). Met deze methode kan op een systematische manier de collectieve dynamica afgeleid worden uit de beweging van de individuele deeltjes.

Het gebruik van de GENERIC-methode voor een specifiek systeem is geen sinecure. Daarom is er in dit proefschrift voor gekozen om te werken met een vereenvoudigd modelsysteem van oneindig lange, parallelle dislocaties. Enerzijds maakt dit de berekening wat makkelijker omdat de dislocatie beschreven kan worden als een punt in een tweedimensionale dwarsdoorsnede in plaats van een lijn in drie dimensies. Anderzijds blijkt uit computersimulaties van dit modelsysteem in de literatuur dat er, ondanks de vereenvoudiging, nog wel realistische resultaten te verwachten zijn. Het nadeel van een vereenvoudigd modelsysteem is echter dat er geen kwantitatieve, maar alleen kwalitatieve uitspraken gedaan kunnen worden over het collectieve gedrag van dislocaties. Met andere woorden: we kunnen alleen bepalen óf emergente fenomenen belangrijk zijn, en niet hoe die er precies uitzien.

Drijvende krachten

De eerste stap van een berekening binnen de GENERIC-methode is het bepalen van de verwachte energie en entropie (mate van wanorde) van alle dislocaties samen. Hiervoor kan gebruikgemaakt worden van statistische mechanica, waarin wordt gewerkt met kansen en verwachtingswaarden. Met behulp van de energie en entropie kan de drijvende kracht voor de dynamica bepaald worden. In dit proefschrift is deze kracht zowel analytisch (met pen en papier) uitgerekend als met een computersimulatie.

De drijvende kracht die hier is berekend voor het modelsysteem van dislocaties bestaat uit drie verschillende bijdragen. De eerste bijdrage is de zogenoemde gemiddelde-veldbijdrage. In deze bijdrage wordt alleen de gemiddelde kracht van alle andere dislocaties en de van buiten opgelegde kracht meegenomen. De tweede bijdrage is een statistische bijdrage, die voortkomt uit het tellen van toestanden. Deze beide bijdragen werden al gebruikt voor dislocaties in de literatuur. Uit de berekening in dit proefschrift blijkt echter dat de statistische bijdrage verwaarloosbaar klein is.

De derde bijdrage is de veeldeeltjes-bijdrage. Omdat dislocaties met tegenovergestelde Burgers' vectoren elkaar aantrekken, is het waarschijnlijk dat er vlakbij een dislocatie nog een dislocatie met tegenovergestelde Burgers' vector gevonden wordt. Dit beïnvloedt de krachten die de eerste dislocatie voelt, en dat wordt meegenomen in de veeldeeltjes-bijdrage. Deze bijdrage hangt af van de opgelegde kracht en de totale hoeveelheid dislocaties, en is in de literatuur nog niet eerder gevonden. Bovendien is deze bijdrage van dezelfde orde van grootte als de gemiddelde-veldbijdrage, en kan daarom niet verwaarloosd worden. Deze component in de kracht is niet terug te vinden als je alleen naar individuele dislocaties kijkt, en dus is dit een emergente bijdrage aan de kracht.

Transport van dislocaties

De tweede stap van de berekening bestaat uit het bepalen van het transport van dislocaties ten gevolge van de kracht. Hiervoor is een transportcoëfficiënt nodig, die de stroom van dislocaties relateert aan de drijvende kracht. Deze transportcoëfficiënt bestaat uit twee bijdragen: de transportcoëfficiënt van individuele deeltjes en een term als gevolg van

correlaties in fluctuaties van de snelheid van individuele dislocaties. Uit de berekeningen in dit proefschrift blijkt dat de tweede bijdrage veel groter is dan de eerste. Ook dit is een emergente bijdrage.

Resultaten en conclusies

We kunnen concluderen dat zowel voor de drijvende kracht als voor de transportcoëfficiënt emergente bijdragen belangrijk zijn. Dit bevestigt onze centrale hypothese.

Om het resultaat van de berekening te vergelijken met de literatuur, is in dit onderzoek gekeken naar de stroom van dislocaties voor verschillende waarden van de opgelegde kracht. Het model dat gebruikt is in dit proefschrift voorspelt dat het verband tussen de opgelegde kracht en de stroom van dislocaties sterker dan lineair is. Dat betekent dat de stroom veel meer dan twee keer zo groot wordt als de opgelegde kracht wordt verdubbeld. Dat betekent ook dat de permanente vervorming, die het gevolg is van de beweging van dislocaties, bij een kleine opgelegde kracht heel erg klein is en plotseling sterk toeneemt als de kracht toeneemt.

In de literatuur wordt zo'n sterk niet-lineair verband ook gebruikt in empirische modellen voor vervorming van metaal (de zogenoemde kristalplasticiteitsmodellen). Het resultaat van de berekening in dit proefschrift komt dus kwalitatief goed overeen met deze bestaande modellen, wat suggereert dat de GENERIC-methode een goede manier is om dynamica van dislocaties te beschrijven.

Er is wel een behoorlijk kwantitatief verschil met de empirische relaties uit de literatuur: de plotselinge toename van de dislocatiestroom is nog veel sterker in de empirische relaties. Dit verschil verandert vooral de tijdsafhankelijkheid van het materiaal (i.e. hoe snel het materiaal vervormt). Aan de ene kant kan het zo zijn dat een berekening met een meer realistische beschrijving van dislocaties een sterkere plotselinge toename oplevert dan het vereenvoudigde model dat we hier hebben gebruikt. Aan de andere kant zou het kunnen zijn dat de toename in de literatuur overschat wordt. De berekeningen die hier gepresenteerd worden kunnen dan helpen de tijdsafhankelijkheid van de kristalplasticiteitsmodellen uit de literatuur te verbeteren. Maar in ieder geval kan worden geconcludeerd dat emergente fenomenen cruciaal zijn om de vervorming van metaal goed te beschrijven.

Dankwoord

Een proefschrift schrijf je niet alleen, dat heb ik de afgelopen vier jaar wel ondervonden. Het past mij daarom hier een groot aantal mensen te bedanken.

Allereerst wil ik uiteraard mijn begeleiders bedanken voor de mogelijkheid om dit project te doen. Marc, bedankt voor je geduldige, leergierige en open houding in dit project. Bedankt ook voor de moeite die je je getroost hebt om een 'werktuigbouwkundig' probleem uit te leggen aan een (eigenwijze) natuurkundige en je betrokkenheid bij de vele aspecten van de promotie. Markus, bedankt voor je dagelijkse begeleiding, en in het bijzonder voor wat je me geleerd hebt over niet-evenwichts systemen, voor je begrip en geduld als ik, om wat voor reden dan ook, weer eens vast zat, en voor de hulp bij het begrijpen van de werktuigbouwers om ons heen.

I would like to thank the committee members for taking place in the committee, thoroughly reading the manuscript and their valuable comments.

I would like to thank NWO for the funding of this project within the COMPLEXITY-program.

Ik wil graag de wiskundigen bedanken die bij dit project betrokken waren. Mark, Adrian, Patrick en Lucia, bedankt voor de inspirerende dislocatie-bijeenkomsten en voor het beantwoorden van al mijn vragen.

Uiteraard wil ik hier mijn collega's bedanken. Alle MaTe-leden en in het bijzonder Jeroen, Francesco, Marc, Misha, Bart, Paul, Jan en natuurlijk Tom, bedankt voor alle gezellige koffie-, lunch-, taart- en fruitpauzes, voor de hulp op het cluster en bij de continuumsmechanica en -thermodynamica, en voor de vele waardevolle discussies, al dan niet over het werk. And to all the residents of room 4.09, thank you for the good working environment and the many room diners. And Lorenza and Andrés, thank you for the cultural exchange.

Op deze plaats wil ik ook graag alle docenten bedanken die ik ben tegengekomen op het Bonhoeffer College en aan de Universiteit Utrecht. Ik heb altijd met veel plezier geleerd en gestudeerd, en zonder dat was dit proefschrift er niet gekomen.

Daarnaast wil ik alle vrienden en kennissen bedanken die me de afgelopen jaren gesteund hebben, en in het bijzonder de leden en trainers van schaatsvereniging ISIS, de leden van Groep'78 zingt! en de Johannesgemeente voor het warme welkom in Eindhoven.

Heel veel dank gaat ook uit naar mijn ouders. Pap en mam, fijn dat jullie er altijd zijn en dat jullie zo geïnteresseerd zijn in waar ik mee bezig ben. Ook wil ik mijn broers Bram en Aart graag bedanken. Jullie zijn tof en ik ben er trots op dat jullie mijn paranimfen zijn. Ten slotte, Meilof, bedankt voor je liefde, je luisterend oor en je adviezen de afgelopen vier jaar. Het geeft me ongelooflijk veel rust, vreugde en vertrouwen om alle avonturen, goed en slecht, samen te kunnen beleven. Fijn dat je er bent.

Marleen

Eindhoven, september 2015

Curriculum Vitae

Marleen Kooiman was born on May 14, 1988 in Amsterdam. In 2006 she finished her secondary education at the Bonhoeffer College in Castricum. For her thesis *De stelling van Desargues in breder perspectief* (*Desargues' theorem in higher dimensions*), she received the UvA-werkstuklabprijs. Besides that, she participated in the Dutch National Physics Olympiad in 2005 and 2006, resulting in an eighth and ninth place respectively. In 2009, Marleen finished both bachelor programs Mathematics and Physics and Astronomy at the Utrecht University (both cum laude), after which she continued her education with the master program Theoretical Physics at the same university. Marleen wrote her thesis, entitled *Empowering Blue Energy*, in the group of dr. R. van Roij, and graduated in 2011 (cum laude). Motivated by her interest in dynamics of many-body systems, she started a PhD project at the Eindhoven University of Technology. During this research, she was supervised by prof.dr.ir. M.G.D. Geers and dr.sc.nat. M. Hütter. The results of this research are presented in this thesis.

Marleen Kooiman is geboren op 14 mei 1988 te Amsterdam. In 2006 rondde zij het Gymnasium af aan het Bonhoeffer College te Castricum. Voor haar profielwerkstuk *De stelling van Desargues in breder perspectief* ontving zij de UvA-werkstuklabprijs. Daarnaast nam zij deel aan de Nationale Natuurkunde Olympiade in 2005 en 2006, waar zij achtste en negende werd. In 2009 rondde Marleen beide bacheloropleidingen Wiskunde en Natuur- en Sterrenkunde cum laude af aan de Universiteit Utrecht, waarna zij haar opleiding vervolgde met de master Theoretische Natuurkunde aan dezelfde universiteit. Marleen schreef haar afstudeerscriptie *Empowering Blue Energy* in de groep van dr. R. van Roij, en studeerde hiermee in 2011 cum laude af. Ingegeven door haar interesse in de dynamica van veeldeeltjessystemen, begon zij daarna aan een promotieproject aan de Technische Universiteit Eindhoven. Tijdens dit onderzoek werd ze begeleid door prof.dr.ir. M.G.D. Geers en dr.sc.nat. M. Hütter. De resultaten van dit onderzoek worden gepresenteerd in dit proefschrift.



